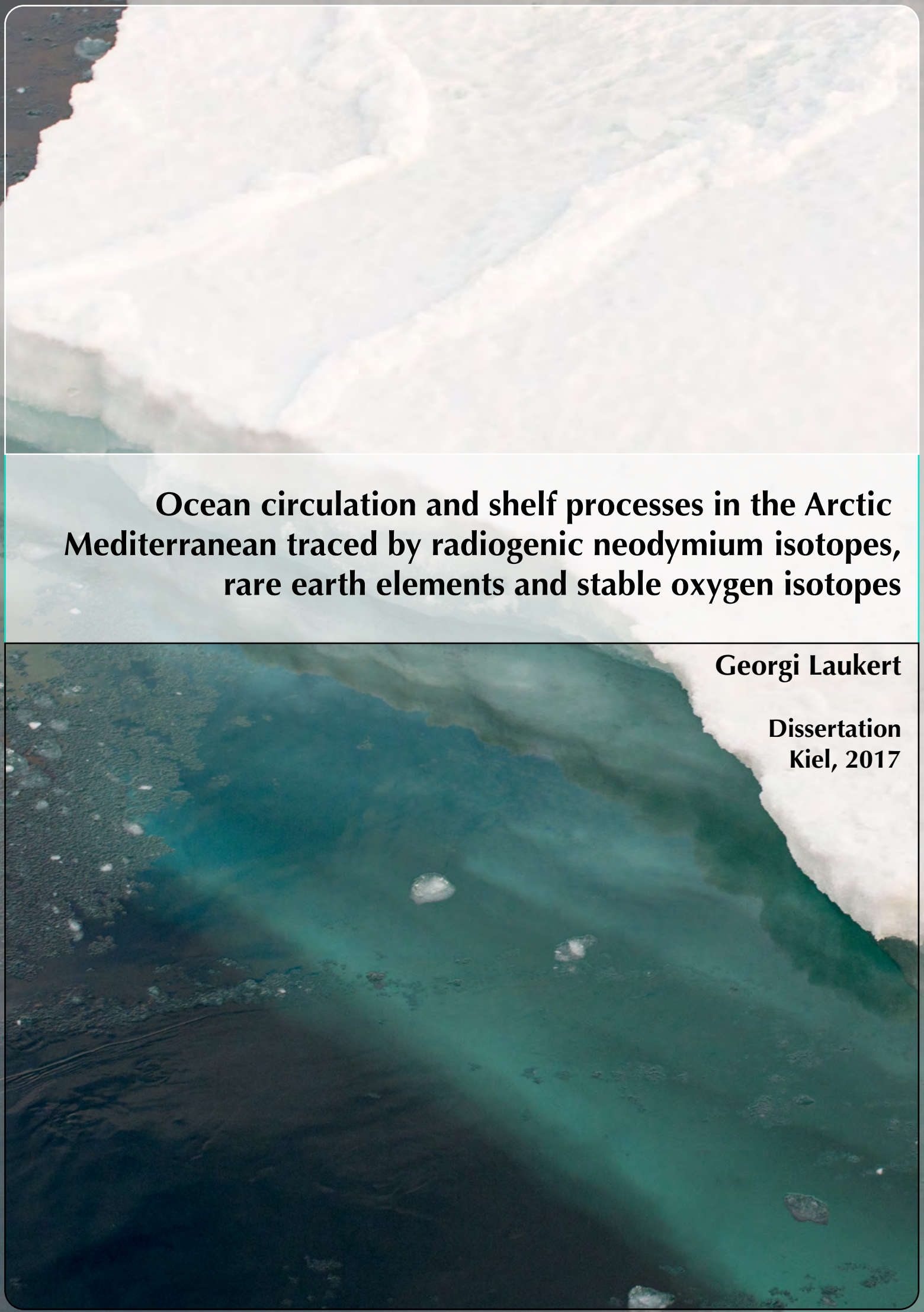

Ocean circulation and shelf processes in the Arctic Mediterranean traced by radiogenic neodymium isotopes, rare earth elements and stable oxygen isotopes

Georgi Laukert

Dissertation
Kiel, 2017

Ocean circulation and shelf processes in the Arctic Mediterranean traced by radiogenic neodymium isotopes, rare earth elements and stable oxygen isotopes

Dissertation zur Erlangung des Doktorgrades

Dr. rer. nat.

der Mathematisch-Naturwissenschaftlichen Fakultät

der Christian-Albrechts-Universität zu Kiel

vorgelegt von

Georgi Laukert

Kiel, 2017

1. **Gutachter und Betreuer:** Prof. Dr. Martin Frank
2. **Gutachter:** Prof. Dr. Don Porcelli

Eingereicht am: 26. Januar 2017

Tag der Disputation: 20. Februar 2017

Zum Druck genehmigt: 20. Februar 2017

Gez. Prof. Dr. Natascha Oppelt, Dekanin

Erklärung

Hiermit erkläre ich an Eides statt, dass ich die vorliegende Abhandlung, abgesehen von der Beratung durch meinen Betreuer, nach Inhalt und Form selbstständig erarbeitet habe und keine anderen, als die von mir aufgeführten Quellen und Hilfsmittel, verwendet wurden.

Diese Arbeit ist unter Einhaltung der Regeln guter wissenschaftlicher Praxis der Deutschen Forschungsgemeinschaft entstanden und wurde weder in Auszügen noch in ganzer Form an einer anderen Stelle im Rahmen eines Prüfungsverfahrens eingereicht.

Teile dieser Arbeit sind bereits in einer Fachzeitschrift veröffentlicht, wurden zur Veröffentlichung eingereicht oder sind in Vorbereitung eingereicht zu werden.

Kiel, den 26. Januar 2017

Georgi Laukert

CONTENTS

ABSTRACT **1**

KURZFASSUNG **3**

1. INTRODUCTION **6**
1.1 The changing Arctic Mediterranean 6
1.2 Bathymetry, hydrography and ocean circulation in the Arctic Mediterranean 7
1.3 Annual hydrographic variability of the Siberian shelf seas 10
1.4 Principles and application of neodymium isotopes as water mass tracer 11
1.5 Principles and application of REEs in seawater 14
1.6 REE sources in the Arctic Mediterranean and their ε_{Nd} signatures 17
1.7 Stable oxygen isotope systematics and source-defined components 21
1.8 Objectives and outline of the thesis and contributions to the chapters 22

2. METHODS **25**
2.1 Sample collection and pre-concentration 25
2.2 Chemical procedures including chromatographic purification 26
2.3 Neodymium isotope and ID concentration measurements via MC-ICP-MS 28
2.4 Rare earth element concentration measurements 28
2.5 Oxygen isotope, nutrient and sample salinity measurements 29
2.6 Binary and ternary mixing based on salinity, Nd isotopes and [Nd] 29

3. PUBLICATION AND MANUSCRIPTS **31**

CHAPTER I: Ocean circulation and freshwater pathways in the Arctic Mediterranean based on a combined Nd isotope, REE and oxygen isotope section across Fram Strait 31

CHAPTER II: Transport and transformation of riverine Nd isotope and rare earth element signatures in high latitude estuaries: A case study from the Laptev Sea 63

CHAPTER III: Propagation of Greenland freshwater in the western Fram Strait - Evidence from dissolved Nd isotopes and REEs **89**

4. SUMMARY, CONCLUSIONS AND OUTLOOK **100**
4.1 Summary and Conclusions 100
4.2 Outlook 103

DANKSAGUNG **105**

REFERENCES **106**

DATA TABLES **127**

ABSTRACT

The warming of the Arctic region in the recent past has proceeded at rates double that of the global average and has been accompanied by rapid sea ice retreat and increased heat and freshwater fluxes to the Arctic Mediterranean (i.e. the Arctic Ocean and the Nordic Seas, AM). Further warming will have strong impacts on ocean circulation, freshwater pathways, and marine ecosystems in the AM. Disentangling the sources, distribution and mixing of water masses involved in the transport and transfer of heat and freshwater is therefore critical for the understanding of present and future hydrological changes in the high-latitude and polar regions and their consequences. This study refines the knowledge of water mass circulation and mixing in the AM and provides new insights into the processes occurring on the Arctic shelves and in high-latitude estuaries. A multi-proxy approach is used combining dissolved radiogenic Nd isotopes (ε_{Nd}), rare earth elements (REEs) and stable oxygen isotopes ($\delta^{18}O$) together with standard hydrographic tracers.

The sources, distribution and mixing of water masses that circulate in the AM and pass the Fram Strait are assessed through evaluation of dissolved ε_{Nd} and REE, and $\delta^{18}O$ data obtained from samples recovered in 2012 along a full water depth section extending between Svalbard and Greenland at ~79 °N, and through a compilation and reassessment of literature Nd isotope and concentration data previously reported for other sites within the AM. The Nd isotope and REE distribution in the central Fram Strait and the open AM primarily reflects the lateral advection of water masses and their mixing, whereas seawater-particle interactions exert important control only above the shelf regions. For example, on the NE Greenland Shelf, remineralization of biogenic and/or release from detrital particles is recorded in bottom waters. Advection of warm Atlantic Water (AW) in the upper water column of the eastern and central Fram Strait is clearly reflected by an ε_{Nd} signature of -11.7 and a Nd concentration ([Nd]) of 16 pmol/kg. Freshening and cooling of the AW on its way through the AM are accompanied by a continuous change towards more radiogenic Nd isotope compositions (e.g. -10.4 of dense Arctic Atlantic Water). This change results from mixing with intermediate waters but also mirrors the admixture of dense Kara Sea waters and Pacific-derived waters. Exchange with basaltic formations of Iceland and southeastern Greenland is suggested to impart the intermediate and deep waters of the AM with more radiogenic ε_{Nd} signatures, which reach -9.5 in the Fram Strait. Significant inputs of Nd from Svalbard are not observed and surface waters and Nd on the western Svalbard Shelf originate in the Barents Sea. Shallow (< 200 m) waters of Arctic origin form the core of the East Greenland Current above the Greenland slope and have relatively radiogenic ε_{Nd} (reaching -8.8) and elevated [Nd] (21-29 pmol/kg), which together with $\delta^{18}O$ and standard hydrographic tracers are used to determine the proportions of Pacific-derived (< 30 % based on Nd isotopes) and Atlantic-derived seawater, as well as of river waters (< 8 %). A change in the Nd isotope compositions to less radiogenic values (-12.4) and an increase in [Nd] (38 pmol/kg) are observed at water depths above 100 m near the Greenland coast documenting addition of Greenland-sourced freshwater (GFW). The

amount of GFW contained in the upper water column on the NE Greenland Shelf reached 6 % in 2012. Data obtained for the years 2014 and 2015 for the northern and southern NE Greenland Shelf suggest similar fractions of GFW for shallow waters in the Norske Trough and east of Ob Bank, indicating southward and northward propagation of GFW along the Greenland coast assuming that the NE Greenland Ice Stream is the freshwater source. The Nd isotope compositions of Arctic-derived waters (ε_{Nd} ~ -9) and other water masses were essentially constant over the time period 2012-2015, which provides a solid basis for quantitative estimates of GFW admixture. The GFW distribution suggests that future increased GFW supply forced by global warming will lead to additional freshening of shallow Arctic waters, which, once these waters have traversed the Nordic Seas, may ultimately affect overturning strength in the northern Labrador Sea. Overall, the results obtained from the Fram Strait demonstrate that the pronounced gradients in ε_{Nd} and REE contents in the upper water column provide a reliable basis for assessments of short-term shallow hydrological changes within the AM.

New insights into the processes occurring in high latitude estuaries are provided by dissolved Nd isotope and REE compositions together with $\delta^{18}O$ data for the Laptev Sea based on filtered samples collected during two summers (2013 + 2014) and one winter (2012). The Laptev Sea is a Siberian Shelf sea characterized by extensive river-runoff, sea-ice production and ice transport into the Arctic Ocean. The broad range in ε_{Nd} (-6 to -17), REE concentrations (16 to 600 pmol/kg for Nd) and REE patterns found in the frame of this study is attributed to freshwater supply from the Siberian rivers and advection of open ocean Arctic Atlantic Water. Strikingly and contrary to expectations, there is no evidence for significant release of Nd from particulate phases and Nd isotopes can thus be used to assess water mass mixing together with the salinity after correction for variations in the salinity caused by sea-ice formation and melting. High fractions of riverine contributions from the Lena River (up to 75 %) are determined for the surface layer of the eastern Laptev Sea with significant interannual variations, while the less variable advection of Yenisei and Ob freshwater (up to ~20 %) is restricted to the western Laptev Sea. Essentially all Laptev shelf waters are depleted in light (L)REEs, while the distribution of the heavy (H)REEs shows a deficiency at the surface and an excess in the bottom layer. A combination of REE removal through coagulation of nanoparticles and colloids and REE redistribution within the water column through formation and melting of sea ice and river ice is suggested to account for the distribution of all REEs. Estuarine removal of riverine REEs starts at salinities close to 10 and after a drop of all REEs by about 30 % transfers into preferential LREE removal, which for Nd reaches 75 % at salinities near 34. Although the delayed onset of dissolved REE removal contrasts with observations from most other estuarine environments, the distributions coincide remarkably well with results from recent experiments simulating estuarine mixing with organic-rich river waters. The melting and formation of sea ice and river ice lead to further REE depletion at the surface and enrichments in the bottom water layer as a function of ice melting and brine transfer, respectively. The ice-related processes contribute to the redistribution of other elements and may also affect macronutrient distribution and primary productivity in high latitude estuaries.

KURZFASSUNG

In der jüngsten Vergangenheit erwärmte sich die arktischen Region doppelt so schnell wie der Rest der Erde, was von einem schnellen Rückgang des Meereises sowie von erhöhten Süßwasser- und Wärmeflüssen in das arktische Mittelmeer (AM) begleitet wurde (dies umfasst das Nordpolarmeer, das Europäische Nordmeer sowie die Grönlandsee und die Islandsee). Die fortschreitende Erderwärmung wird starke Auswirkungen auf die Ozeanzirkulation, die Süßwassertransportwege und die Meeresökosysteme im AM haben. Die Bestimmung der Herkunft, Verteilung und Mischung von Wassermassen, die an der Lieferung und Transformation von Wärme und Süßwasser im AM beteiligt sind, ist für das Verständnis der gegenwärtigen und zukünftigen hydrologischen Veränderungen im AM und den damit verbundenen Konsequenzen daher von entscheidender Bedeutung. Diese Studie vertieft das Wissen über die Wassermassenzirkulation und -mischung im AM und liefert neue Einblicke in Prozesse, die in den arktischen Schelfmeeren und in den Flussmündungen der hohen nördlichen Breiten ablaufen. Hierzu wurde eine kombinierte Untersuchung gelöster radiogener Neodymisotope (ε_{Nd}), gelöster Seltenerdelemente (REEs), stabiler Sauerstoffisotope ($\delta^{18}O$) und herkömmlicher hydrographischer Tracer angewandt.

Die Herkunft, Verteilung und Mischung von Wassermassen, die Teil der Zirkulation innerhalb des AM sind und die Framstraße passieren, wird durch die Auswertung der oben genannten Parameter an Proben bestimmt, die in der gesamten Wassersäule im Jahr 2012 entlang eines 79°N-Schnittes zwischen Svalbard und Grönland entnommen wurden. Eine Zusammenstellung und Neubewertung von Literaturdaten, die Nd-Isotopensignaturen und Nd-Konzentrationen aus anderen Gebieten innerhalb des AM einschließen, wird ebenfalls herangezogen. Die Verteilung von gelösten Nd-Isotopensignaturen und REE-Konzentrationen in der zentralen Framstraße und im offenen AM spiegelt primär die laterale Advektion von Wassermassen und deren Mischung wider, wohingegen Meerwasser-Partikel-Wechselwirkungen nur auf den arktischen Schelfen eine wichtige Rolle spielen. So ist auf dem nordöstlichen (NE) Grönland-Schelf die Freisetzung von Nd durch Remineralisation von biogenen und/oder Auflösung von detritischen Partikeln im bodennahen Bereich zu beobachten. Die Advektion des warmen atlantischen Wassers (AW) innerhalb der oberen Wassersäule der östlichen und zentralen Framstraße wird deutlich durch eine ε_{Nd}-Signatur von -11.7 und eine Nd-Konzentration ([Nd]) von 16 pmol/kg angezeigt. Während der Zirkulation von AW innerhalb des AM wird dessen Abkühlung und Abnahme des Salzgehaltes durch eine kontinuierliche Veränderung hin zu radiogeneren Nd-Isotopensignaturen begleitet (beispielsweise hat dichtes Arktisches Atlantisches Wasser eine Signatur von -10.4). Diese Veränderung resultiert einerseits aus der Mischung mit tieferen Wassermassen, aber auch aus der Beimischung von dichtem Schelfwasser aus der Karasee und Meerwasser pazifischen Ursprungs. Die radiogeneren ε_{Nd}-Signaturen von Zwischen- und Tiefenwässern (bis zu -9.5) werden durch den Austausch mit basaltischen Formationen von Island und Südostgrönland erklärt. Signifikante Einträge von Nd aus Svalbard werden nicht beobachtet und Oberflächenwasser und Nd auf dem westlichen Svalbard-

Schelf stammen aus der Barentssee. Oberflächennahe (< 200 m) Wässer arktischen Ursprungs bilden den Kern des Ostgrönlandstroms über dem Kontinentalrand Grönlands und haben ebenfalls relativ radiogene ε_{Nd}-Signaturen (bis zu -8,8) und erhöhte [Nd] (21-29 pmol/kg), die zusammen mit $\delta^{18}O$ und herkömmlichen hydrographischen Tracern verwendet werden, um die Anteile von Wässern pazifischen (< 30 % basierend auf Nd-Isotopen) und atlantischen Ursprungs sowie von Flusswasser (< 8 %) zu bestimmen. Eine Änderung hin zu niedrigeren ε_{Nd}-Werten (-12.4) und eine Zunahme von [Nd] (bis zu 38 pmol/kg) zur Grönländischen Küste hin wird in Wassertiefen bis 100 m beobachtet und dokumentiert die Zumischung von Süßwasser grönländischen Ursprungs (GFW). Die in der oberen Wassersäule auf dem NE Grönlandschelf enthaltene Menge an GFW erreichte im Jahr 2012 ca. 6 %. Die Daten für die Jahre 2014 und 2015 deuten auf ähnliche Anteile von GFW für die oberflächennahen Wasserschichten im untermeerischen Norske-Tal (südliche Teil des NE Grönlandschelfs) und östlich der Ob Bank (nördlicher Teil des NE Grönlandschelfs) hin, was die südliche und nördliche Ausbreitung von GFW entlang der Küste Grönlands dokumentiert, vorausgesetzt dass die Herkunft des GFW der NE-Grönland-Eisstrom ist. Die Nd-Isotopenzusammensetzungen von oberflächennahen Wässern arktischen Ursprungs (ε_{Nd} ~ -9) und anderen Wassermassen im AM waren im Zeitraum 2012-2015 im Wesentlichen konstant, was eine solide Grundlage für die quantitative Bestimmung der GFW-Zumischung zur oberen Wassersäule darstellt. Die GFW-Verteilung legt nahe, dass der durch die globale Erderwärmung künftig erhöhte GFW-Eintrag in den Ozean zu einer zusätzlichen Aussüßung der oberflächennahen arktischen Wässer führen wird und nach ihrer Advektion in den Nordatlantik die Tiefenkonvektion im der nördlichen Labradorsee beeinflussen könnte. Die Ergebnisse aus der Framstraße zeigen insgesamt, dass die ausgeprägten Gradienten der ε_{Nd}-Signaturen und REE-Konzentrationen in der oberen Wassersäule eine zuverlässige Grundlage für die Beurteilung kurzfristiger oberflächennaher hydrologischer Veränderungen innerhalb des AM liefern.

Neue Einblicke in die Prozesse, die innerhalb von Flussmündungen der hohen nördlichen Breiten vorherrschen, liefern gelöste Nd-Isotopensignaturen und REE-Zusammensetzungen sowie $\delta^{18}O$-Daten aus der Laptewsee, die an gefilterten Wasserproben bestimmt wurden, die während zweier arktischer Sommer (2013 + 2014) und eines Winters (2012) genommen wurden. Die Laptewsee ist eines der sibirischen Schelfmeere, das durch einen sehr hohen Flusswassereintrag, sowie durch starke Meereisproduktion und den Export von Meereis in den Arktischen Ozean gekennzeichnet ist. Die im Rahmen dieser Studie gefundenen große Variabilität in ε_{Nd}-Signaturen (-6 bis -17), REE-Konzentrationen (16 bis 600 pmol/kg für Nd) und REE-Muster werden der Süßwasserzufuhr aus den verschiedenen sibirischen Flüssen sowie der Advektion von modifiziertem AW zugeschrieben. Bemerkenswerterweise, und entgegen den Erwartungen, gibt es keinen Nachweis für eine signifikante Freisetzung von Nd aus partikulärem Material und die Nd-Isotopensignaturen können somit zusammen mit dem Salzgehalt verwendet werden um die Wassermassenmischung zu bestimmen. Dieser wurde auf Änderungen korrigiert, die durch den Salztransfer während der Bildung und Schmelze des Meereises verursacht wurden. Für die

Oberflächenwässer der östlichen Laptewsee werden hohe Anteile von Flusswasser der Lena (bis zu 75 %) bestimmt, wobei signifikante zwischenjährliche Variationen der Flusswasser-Verteilung innerhalb der Laptewsee beobachtet wurden. Die Advektion von Süßwasser des Jenissej und Ob (bis zu 20 %) hingegen zeigt eine geringere zwischenjährliche Variabilität und deren Vorkommen beschränkt sich auf die westliche Laptewsee. Alle Schelfwässer in der Laptewsee sind generell abgereichert an leichten (L)REEs, während die Verteilung der schweren (H)REEs ein Defizit an der Oberfläche und einen Überschuss in Bodennähe zeigt. Als Erklärung für diese REE Verteilung wird eine Kombination aus zwei Prozessen vorgeschlagen: Einerseits findet eine Ausfällung gelöster REEs durch Koagulation von REE-reichen und durch Flüsse eingetragene Nanopartikel und Kolloide statt und andererseits werden die REEs innerhalb der Wassersäule durch die Bildung und das Schmelzen von Meereis und Flusseis umverteilt. Die Ausfällung aller eingetragenen REEs innerhalb der Lenamündung um etwa 30 % beginnt bei Salzgehalten nahe 10 und wird gefolgt von einer bevorzugten LREE-Ausfällung, die für Nd mindestens 75 % beträgt und bis zu Salzgehalten von 34 anhält. Der verzögerte Beginn der Ausfällung steht im Widerspruch zu bisherigen Beobachtungen aus anderen Flussmündungsgebieten, stimmt jedoch bemerkenswert gut überein mit neueren Experimenten, die die Mischung von Meerwasser und Flusswasser, das reich an organischen Verbindungen ist, simulieren. Das Schmelzen und die Bildung von Meereis und Flusseis führen zu einem weiteren Defizit der REEs in der oberflächennahen Wasserschicht und zu Anreicherungen in der Bodenwasserschicht als Funktion des Eisschmelzens durch Verdünnung bzw. der Eisbildung und der dadurch verursachten Laugenbildung. Die Eisprozesse haben auch Auswirkungen auf die Verteilung von anderen Metallen und von Nährsoffen, und damit auch auf die Primärproduktivität in eisbeeinflussten Regionen.

1. INTRODUCTION

1.1 The changing Arctic Mediterranean

The Arctic region has warmed more than twice as fast as the global average in the recent past, a robust feature known as Arctic amplification (e.g. Cohen et al., 2014; Serreze et al., 2009; Serreze and Barry, 2011). The concurrent rapid sea ice retreat is projected to result in an ice-free Arctic summer before the middle of the 21st century (e.g. Holland et al., 2006; Wang and Overland, 2009). Both warming and sea ice loss significantly contribute to an intensification of the hydrological cycle in the Arctic region, which is evidenced by increasing precipitation (Kattsov et al., 2007) and river runoff (Peterson et al., 2002) and accompanied by accelerated mass loss of the Greenland ice sheet (Bamber et al., 2012). The observed increased freshwater supply is of global significance, as it contributes to the freshening of the North Atlantic and thus may cause global climatic feedbacks through weakening of the Atlantic Meridional Overturning Circulation (e.g. Rahmstorf et al., 2015; Yang and Haley, 2016).

The warming also significantly affects oceanic conditions in the Arctic Mediterranean (i.e. the Arctic Ocean and the Nordic Seas, AM). In addition to the freshening, the AM undergoes substantial warming by increasing poleward transport of oceanic heat, which is regarded to be another facet of the Arctic amplification (Spielhagen et al., 2011 and references therein). Most of the oceanic heat is supplied by advection of warm and saline waters of Atlantic origin that enter the AM across the Greenland-Scotland Ridge (e.g. Aagaard et al., 1987; Rudels et al., 2004). These waters have in recent decades exhibited unprecedented temperatures compared to the last two millennia (Spielhagen et al., 2011), with a maximum temperature so far reached in 2006 (Schauer et al., 2008). Their advection was also shown to have a significant impact on the Arctic sea-ice cover through upward heat loss (Dmitrenko et al., 2014; Polyakov et al., 2010).

Both phenomena, the freshening and the warming of the AM, cause a clearly discernable alteration of Arctic marine ecosystems (Wassmann et al., 2011 and references therein) and affect various physical and chemical processes occurring in the open AM and on the wide Arctic shelves (e.g. Bauch et al., 2010; Dmitrenko et al., 2014; Hölemann et al., 2011; Janout et al., 2016; Moore et al., 2015; Polyakov et al., 2010; Rippeth et al., 2015; Semiletov et al., 2016; Shakhova et al., 2010). The water masses involved in the transport and transfer of heat and freshwater within the AM therefore not only play a key role in regulating the heat and freshwater budget of the AM, but also significantly contribute to the alteration of the marine ecosystems and to changes of various chemical and physical processes. A detailed investigation of their sources, distribution and circulation is therefore critical for the understanding of present and potential near-future hydrological, biological and biogeochemical changes in this highly dynamic and climatically sensitive region.

1.2 Bathymetry, hydrography and ocean circulation in the Arctic Mediterranean

The AM is a semi-enclosed ocean that comprises the Nordic Seas (i.e. the Greenland Sea, the Iceland Sea and the Norwegian Sea, NS) and the Arctic Ocean (AO) (Rudels et al., 1999b and references therein), which are connected through the Fram Strait gateway (sill depth of ~2545 m) and the Barents Sea (average depth of ~230 m) (Fig. 1). The AO itself consists of ~50 % shallow shelf seas and ~50 % deep basins and is divided by the Lomonosov Ridge (sill depth of ~1870 m) into the Eurasian and the Canadian (or Amerasian) Basins. The Eurasian Basin is further subdivided by the Nansen-Gakkel Ridge (sill depth of ~3000 m) into the Nansen Basin (~4000 m deep) and the Amundsen Basin (~4500 m deep) and the Canadian Basin is separated into the Canada Basin and the Makarov Basin (both ~4000 m deep) by the Alpha-Mendeleev Ridge (sill depths of ~2400 m) (Jones, 2001; Mauritzen et al., 2013). Exchange between the AM and the North Atlantic is maintained across the Greenland-Scotland Ridge (sill depth of ~840 m in the Faroe Bank Channel and ~640 m in the Denmark Strait) and the Canadian Archipelago (major gateways are the Nares Strait, the Lancaster Sound, and the Jones Sound, with maximum sill depths of ~220 m), while communication with the Pacific is restricted to the ~50 m deep and ~50 km wide Bering Strait.

The water column of the AO is highly stratified (Aagaard et al., 1985; Carmack, 1990; Jones, 2001). The upper water column is dominated by riverine runoff from the Arctic Rivers, which constitutes ~10 % of the world's river discharge (Aagaard and Carmack, 1989). The riverine freshwater is mainly transported or stored within the Polar Mixed Layer (PML), which occupies the uppermost water column (< ~50 m) and is isolated from the Atlantic Layer by a cold and almost isothermal halocline (Jones, 2001). The latter is maintained by the admixture of dense brine-enriched shelf waters (Aagaard et al., 1981; Melling and Lewis, 1982) and historically has been divided into the upper and the lower halocline, which were suggested to mainly comprise waters of Pacific and Atlantic origin, respectively (Jones and Anderson, 1986). In contrast to the nutrient-poor lower halocline (salinities of 34.2-34.4), the upper halocline (salinities of 32.8-33.2) is characterized by high nutrient concentrations, as well as low oxygen and pH values, in agreement with its Chukchi and East Siberian seas origin, where remineralization of organic matter and release of decay products occur in brine-enriched shelf bottom waters (Anderson et al., 2013). While the upper halocline is limited to the Canadian Basin of the AO and only rarely reaches the Amundsen Basin where it merges with the PML, the lower halocline can be found throughout the entire AO. According to Rudels et al. (2005), the ~150 m thick Arctic halocline is a distinct water mass and not just an indication of a sharp salinity gradient. Waters spreading within the Arctic halocline and the PML have been classified as Polar Surface Water (PSW) or Polar Water (Rudels et al., 2012; 2005). The composition of the PSW that exits the AO through the western Fram Strait via the southward flowing East Greenland Current (EGC) has been the focus of numerous studies that tried to decipher the different Arctic derived components and documented seasonal and interannual variations of their relative fractions (e.g. Dodd et

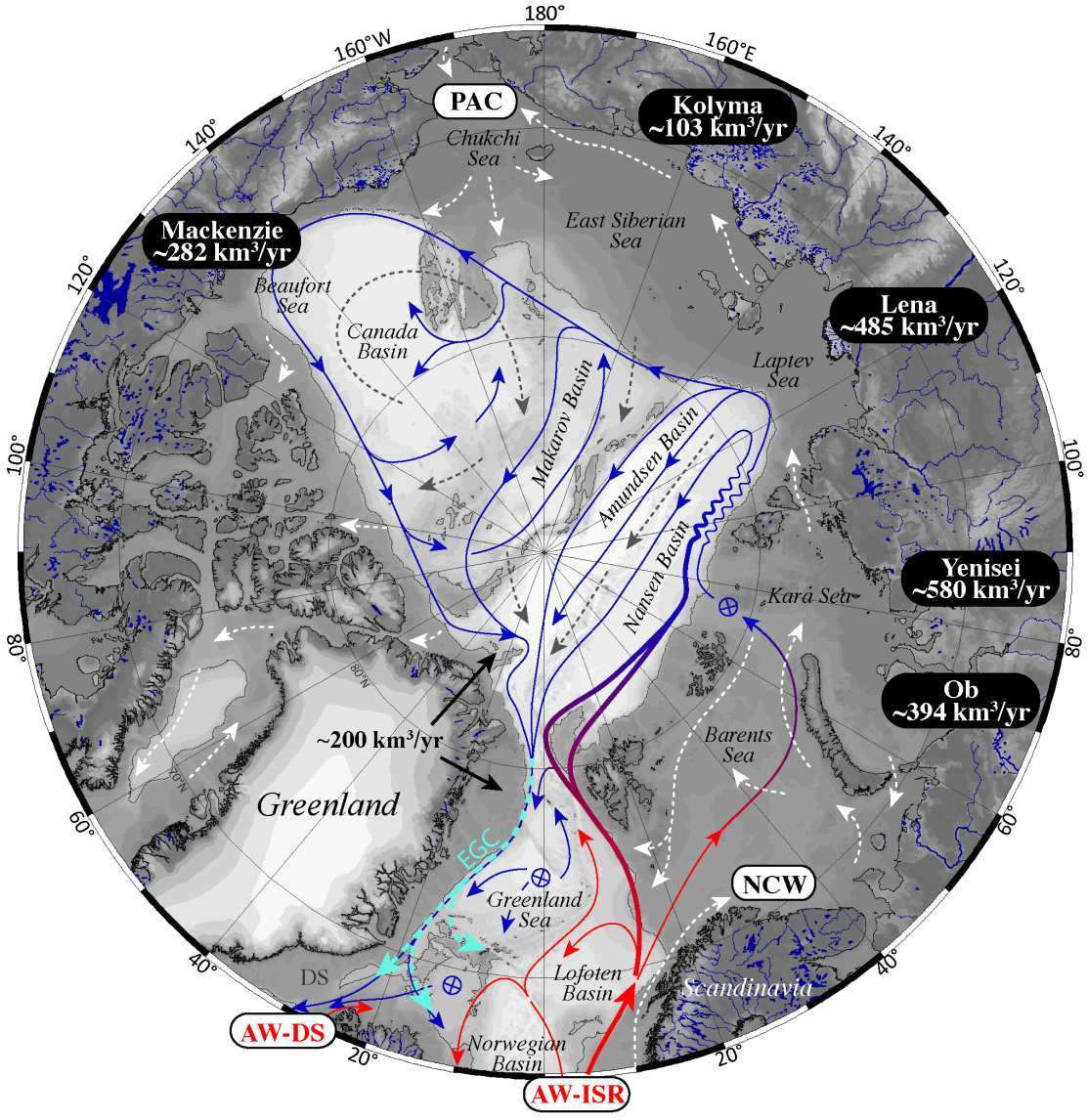

Figure 1: Bathymetric map of the AM (IBCAO; Jakobsson et al., 2012) with circulation scheme of the upper layers (dashed white and gray lines) and the subsurface Atlantic and intermediate layers (solid red and blue lines; change in color represents transformation of Atlantic Water) (modified after Rudels et al., 2012). Flow of the East Greenland Current (EGC) is indicated in addition (dashed cyan lines). Circled crosses indicate sites of convection or sinking from intermediate and AW layers to deeper levels. Water masses and major Arctic rivers that contribute to the AM are provided in white and black rounded boxes, respectively. Water masses are labeled as follows: Atlantic Water at the Iceland-Scotland Ridge – AW-ISR, Atlantic Water at the Denmark Strait – AW-DS, Pacific-derived water – PAC. Mean annual discharge of the rivers (R-Arctic-NET, http://www.r-arcticnet.sr.unh.edu/) and from Greenland (for 2010, Bamber et al., 2012) to the AM is given in km³/yr. The figure was produced using Ocean Data View (Schlitzer, 2016) and modified manually.

al., 2009; Dodd et al., 2012; Falck, 2001; Falck et al., 2005; Jones et al., 2008b; Laukert et al., 2017; Rabe et al., 2013; Taylor et al., 2003).

The relatively warm and saline Atlantic-derived waters form the Atlantic Layer of the AM below the Arctic halocline (Aagaard and Carmack, 1989; Aagaard et al., 1985) and reach depths of ~750 m within the AO (Rudels et al., 2004). It is common practice to refer to these waters as “Atlantic Water” (AW). The AW not only is the major source

of oceanic heat to the AM but also dominates the circulation within the AM (Fig. 1). It enters the AM across the Greenland-Scotland Ridge and is transported northward via the Norwegian Atlantic Current (Aagaard et al., 1987), which further north is transferred into the West Spitsbergen Current (WSC) (e.g. Rudels et al., 1999b; 2004). While one part of the AW returns to the Nordic Seas within the Fram Strait or slightly north of it and is termed Recirculating Atlantic Water (RAW), the other part enters the AO as the Fram Strait Branch Water (FSBW), and, after subdivision into the Yermak and the Svalbard streams and their recombination north of Svalbard, continues to flow eastward as the Arctic Circumpolar Boundary Current along the continental margins of the AO (Aksenov et al., 2011; Rudels et al., 1999b). While the circulation of the FSBW is mainly restricted to the Nansen Basin, AW entering the AO through the Barents Sea continues to flow along the continental slope and ultimately enters the Makarov and Canada Basins (Rudels et al., 2015). During its transport through the AO, AW of both branches loses heat due to ice melting and exchange with the atmosphere and/or mixing with colder waters from the Barents Sea, the Bering Strait, and with river runoff (e.g. Rudels et al., 2015). This transformation results in the formation of the Atlantic-derived halocline water (i.e. mostly the lower Arctic halocline, see above) and the cooler ($\theta \leq 2$ °C) Arctic Atlantic Water (AAW), which north of the Fram Strait acquires a bi-modal structure due to the recombination of the two branches (Rudels et al., 2012). Together with the RAW, the AAW exits the AO through the western part of Fram Strait via the EGC and forms one of the major sources of the Denmark Strait Overflow Water (Havik et al., 2016).

Below the Atlantic Layer, the Upper Polar Deep Water (UPDW) and the Arctic Intermediate Water (AIW) occupy most of the intermediate depths in the AO and the NS, respectively. While the UPDW consists of Arctic intermediate waters prevailing below the AAW and above the Lomonosov Ridge (~1700 m) (Rudels et al., 2000) and has a similarly bi-modal structure compared to the AAW, the AIW is formed through cooling and convection of AAW and RAW after their detachment from the EGC in the northern NS (Rudels et al., 2012). There, the AIW spreads below the AW and also re-enters the AO as part of the WSC. The UPDW is mainly ventilated by boundary convection processes, which are thought to transfer shelf waters with high amounts of brines to deeper depths (e.g. Aagaard and Carmack, 1989). The ventilation of this intermediate layer in the Eurasian Basin is faster (~200 years) than that in the Canadian Basin (~300 years) (Tanhua et al., 2009).

The Eurasian Basin Deep Water (EBDW) and Canadian Basin Deep Water (CBDW) are found below the intermediate depths (> ~1700 m) and are confined to the major basins of the AO, but also exit the AO along the East Greenland margin (e.g. Rudels et al., 2000). Due to the deep ocean circulation of the AM being isolated from the world ocean below ~840 m depth (i.e. this is the deepest sill depth of the Greenland-Scotland Ridge), the EBDW and the CBDW have relatively long ventilation times of ~250-300 and ~360-800 years, respectively (Tanhua et al., 2009 and references therein). The deep waters from the Nordic Seas are commonly summarized as the Nordic Seas Deep Water (NDW) and include the Greenland Sea Deep Water (GSDW), the Iceland Sea Deep Water (ISDW) and the Norwegian Sea Deep Water (NSDW) (e.g. Rudels et al.,

2012; 2005). The stratification in the NS in general is less well defined compared to that of the AO due to the strong advection of Arctic- and Atlantic-derived water masses, but also due to the transformation of the latter to deeper levels at sites of deep convection (Aagaard, 1989).

In contrast to the generally cyclonic movement of AW and other subsurface water masses within the AO (Fig. 1), the movement of sea ice is mainly anticyclonic and is controlled by the Beaufort Gyre and the Transpolar Drift Stream. Both wind-driven currents not only govern sea-ice transport within the AO but also control the freshwater movements in the uppermost water column (Fig. 1), causing freshwater accumulation in the Canadian Basin (e.g. Giles et al., 2012). The exact flow paths of sea ice and freshwater and their changes are regulated by the North Atlantic Oscillation and the Arctic Oscillation (Ambaum et al., 2001), which influence transport in a similar fashion (e.g. Steele et al., 2004).

1.3 Annual hydrographic variability of the Siberian shelf seas

The hydrography of the vast and shallow Siberian shelf seas is strongly influenced by river discharge, sea-ice formation and melting, tides, wind mixing and episodic advection of Arctic basin waters (e.g. Janout et al., 2016), and thus differs significantly from that of the open AM. As an example, the annual hydrographic variability of the Laptev Sea is illustrated in Fig. 2 as a schematic drawing (Janout et al., 2016) and discussed in the following.

During winter (i.e. November to April), the near-coast regions of the shelf seas are covered by landfast ice (i.e. ice that is fastened to the coast), while mobile pack ice dominates the central and outer regions (e.g. Bareiss and Görgen, 2005). So-called polynyas (i.e. openings in the ice cover) frequently form along the landfast-ice edges due to southerly winds (e.g. Bareiss and Görgen, 2005) leading to extreme air-sea heat fluxes and persistent sea-ice formation, as well as salinification of the water column due to brine rejection. Increasing solar radiation during spring and early summer (i.e. April to July) induces fast-ice breakup and sea-ice melt, which coincide with maximum river discharge rates that are several times higher than their annual mean (R-Arctic-NET, see http://www.r-arcticnet.sr.unh.edu/). The freshwater addition from rivers and sea-ice melt results in the formation of a fresh and warm surface layer, which is separated from the marine and brine enriched near-bottom waters by a strong vertical density and salinity gradient (i.e. seasonal pycnocline) throughout summer (i.e. August and September). Increased storm activity and a decrease in river discharge in late summer and fall (i.e. late September and October) decrease stratification again and allow cooling and mixing of the water column (e.g. Hölemann et al., 2011; Janout et al., 2016; Janout and Lenn, 2014). This generally leads to a nearly homogeneous water column during winter, except when summer stratification was anomalously strong before, winter mixing was weak (e.g. Dmitrenko et al., 2012 and references therein) or in areas where

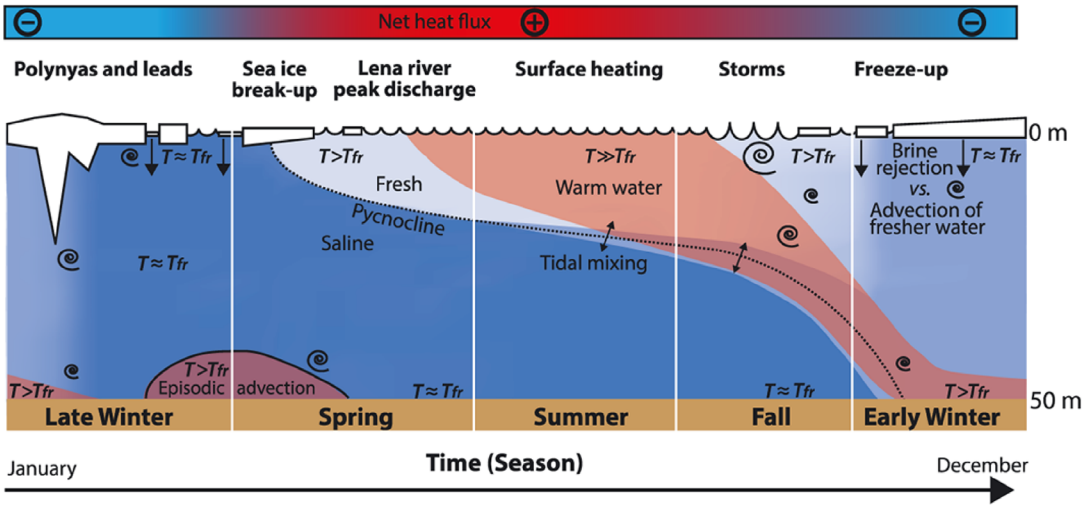

Figure 2: Schematic drawing of the annual hydrographic variability on the Laptev Sea shelf showing the dominant processes that control the structure of the water column. The density within the water column is indicated by the colors, with lighter colors representing less dense waters. The red area shows the spatiotemporal transformation of the warmed surface water to deeper levels. Water temperatures are expressed as "near freezing" ($T \approx T_{fr}$), "above freezing" ($T > T_{fr}$), and "significantly above freezing" ($T \gg T_{fr}$). The color bar indicates air-sea heat fluxes. Figure adopted from Janout et al. (2016).

freshwater is supplied beneath the fast-ice (e.g. close to the Lena Delta in the Laptev Sea).

Strong riverine runoff and the resulting lateral salinity gradients are among the most important factors that affect the complex water column structure and thus the physical as well as the biogeochemical environment in the shelf seas. The freshwater distribution on the shelves is mainly controlled by the atmospheric pressure conditions. For example, the spreading and distribution of the Lena River plume has been linked to larger-scale atmospheric indices (e.g. Morison et al., 2012; Thibodeau et al., 2014) and to regional wind fields during summer (e.g. Dmitrenko et al., 2008; Janout et al., 2015), which either push the freshwater northwards across the shelf or eastwards into the East Siberian Sea.

1.4 Principles and application of neodymium isotopes as water mass tracer

Neodymium is a rare earth element and has seven naturally occurring stable isotopes (^{142}Nd, ^{143}Nd, ^{144}Nd, ^{145}Nd, ^{146}Nd, ^{148}Nd, and ^{150}Nd). A fraction of the isotope ^{143}Nd (abundance ~12.2 %) has been produced via α-decay of the samarium (Sm) isotope ^{147}Sm (abundance ~15 %), which has a shorter half-life (~1.06 x 10^{11} y) than that of ^{148}Sm, which has also been confirmed to be radioactive (half life of ~7 x 10^{15} y). The decay of ^{147}Sm is thus short enough to produce small but measurable changes in the abundance of the daughter isotope ^{143}Nd over time, while the decay of ^{148}Sm does not produce measurable

changes in the abundance of its daughter ^{144}Nd. Commonly, the radiogenic ^{143}Nd isotope is normalized to the primordial isotope ^{144}Nd, and the ^{143}Nd/^{144}Nd ratio typically is expressed in the ε_{Nd} notation, which denotes the deviation of a measured ^{143}Nd/^{144}Nd ratio from the Chondritic Uniform Reservoir (CHUR) in parts per 10000, with CHUR having a modern ^{143}Nd/^{144}Nd value of 0.512638 (Jacobsen and Wasserburg, 1980). The ε_{Nd} notation thus is defined by the following equation:

$$\varepsilon Nd = \left[\frac{\left(\frac{^{143}Nd}{^{144}Nd}\right) SAMPLE}{\left(\frac{^{143}Nd}{^{144}Nd}\right) CHUR} - 1 \right] \times 10{,}000$$

Given that Nd is more incompatible than Sm in solid-liquid magmatic systems, it preferentially accumulates in the melt during partial melting or fractional crystallization over Sm. This produces lower Sm/Nd ratios in the melt than in the residue, ultimately yielding higher ^{143}Nd/^{144}Nd ratios in the mantle (i.e. the residue fraction) compared to those in the crust (i.e. the melt fraction). Consequently, young mantle-derived rocks formed at mid-ocean ridges or at hotspots (e.g. basalts, diorites, gabbros) exhibit higher ^{143}Nd/^{144}Nd ratios compared to the old continental rocks (e.g. granites, metamorphic rocks) and thus have higher, more radiogenic ε_{Nd} values than old continental rocks, which typically have more negative (i.e. unradiogenic) ε_{Nd} values. The rock ε_{Nd} signatures do not only vary as a function of the age of the rocks, but also as a function of the Sm/Nd ratio of the rocks, which causes distinct ε_{Nd} signatures for different continental regions and geological formations.

During physical and chemical weathering of the continental crustal material Nd isotopes are generally not affected significantly by isotopic fractionation (Frank, 2002 and references therein) and thus the characteristic Nd isotope compositions of the rocks are transferred to the rivers and subsequently to the oceans. The quasi-conservative behavior of Nd in the open ocean (Frank, 2002; Goldstein and Hemming, 2003) and its intermediate oceanic residence time of several hundred years (Arsouze et al., 2009; Rempfer et al., 2011; Tachikawa et al., 2003) then imparts water masses with distinct ε_{Nd} signatures at the ocean boundaries and allows tracing of these water masses and their mixing in the open ocean. However, the Nd isotope distribution in the oceans is not only controlled by the ε_{Nd} signatures of the source material and the advection and mixing of water masses, but also depends on various criteria that govern the marine distribution of the rare earth elements (see section 1.5). While biological processes or evaporation do not fractionate Nd isotopes (e.g. Frank, 2002) and they are also not affected by hydrothermal contributions (e.g. German et al., 1990; Halliday et al., 1992), the preformed Nd isotope distribution can be changed significantly through particle-seawater interactions (see also section 1.5). In the open oceans, alterations of the seawater Nd isotope composition without significant changes in the Nd concentration were globally observed in intermediate and deep waters at ocean margins, and the responsible mechanism was termed “boundary exchange” (Lacan and Jeandel, 2005).

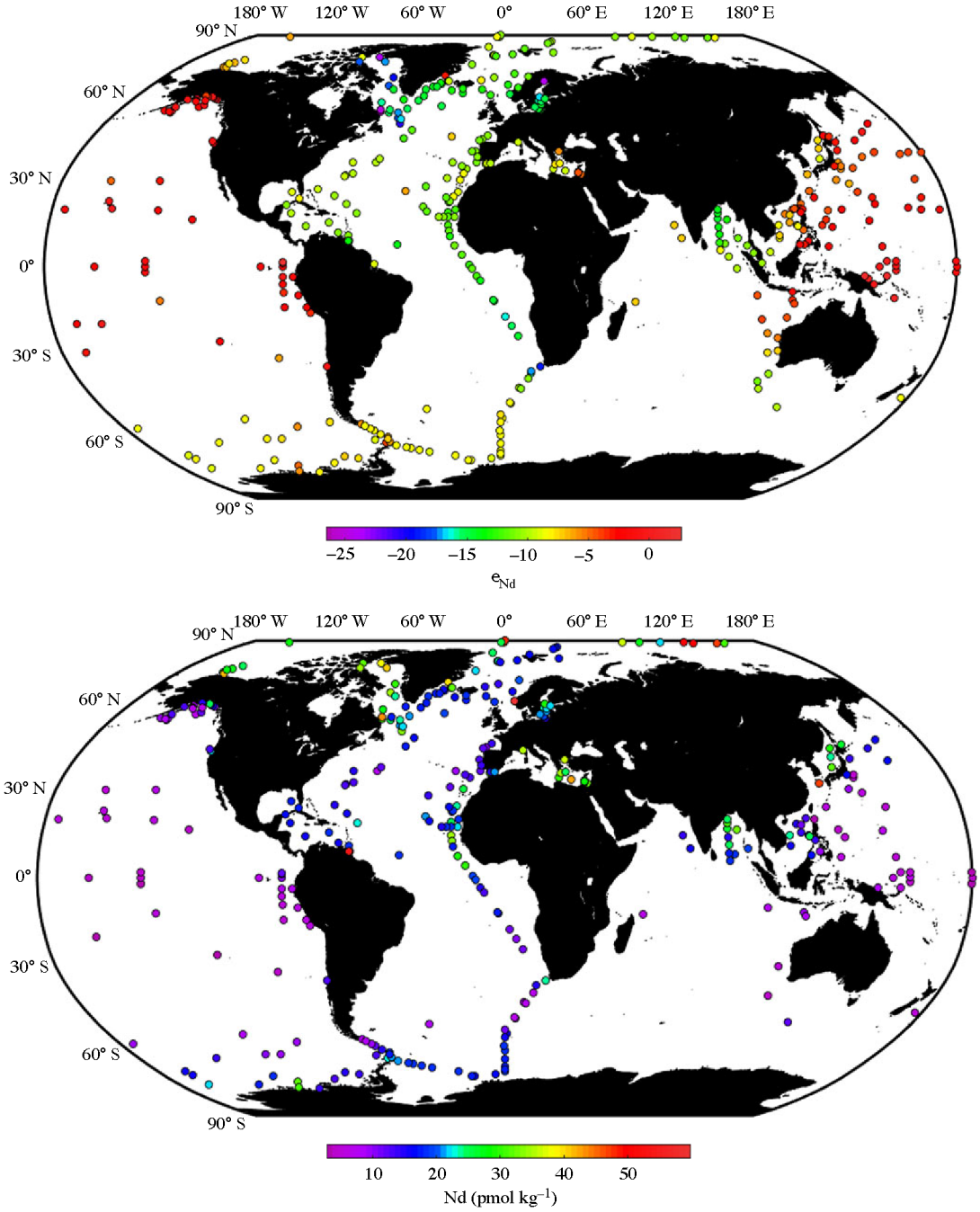

Figure 3: Map of surface seawater Nd isotopic compositions (upper panel) and Nd concentrations (lower panel). Only seawater samples from depths shallower than 100 m are shown and samples with Nd concentrations > 60 pmol/kg are not shown in order to visualize the main features of the Nd distribution in the open ocean. Modified after van de Flierdt et al., 2016).

According to Jeandel (2016) the processes and locations contributing to boundary exchange are discharge of large amounts of freshly weathered particles at the river mouths, submarine weathering of deposited sediments along the margins, submarine groundwater discharges and release via subterranean estuaries. The constant Nd concentrations are likely maintained during this process because release of Nd through

dissolution, desorption or remineralization competes with Nd removal through precipitation and adsorption. Another observation that complicates the applicability of Nd isotopes as a water mass tracer is that the Nd concentration profiles within the open water column are mostly decoupled from profiles of Nd isotopes (e.g. Goldstein and Hemming, 2003), a phenomenon summarized under the term "Nd paradox" (Siddall et al., 2008). The Nd paradox was suggested to result from "reversible scavenging" (Nozaki and Alibo, 2003; Siddall et al., 2008), a process that involves vertical transport of the REEs through a combination of formation and remineralization of organic particles or scavenging and release from inorganic particles. These processes for example have been recently confirmed to contribute to the REE distribution observed in the North Atlantic (e.g. Lambelet et al., 2016; Stichel et al., 2015).

Still, the modern marine Nd isotope distribution, in particular in near surface waters, can to a large extent be attributed to the ε_{Nd} signatures supplied by the continental sources, which can be seen in Fig. 3, in which global surface seawater Nd isotopic compositions and Nd concentrations are plotted (van de Flierdt et al., 2016). While the Pacific is characterized by relatively radiogenic ε_{Nd} signatures in agreement with the young mantle-derived lithologies that surround this ocean basin (cf. circum-Pacific belt), the North Atlantic exhibits less radiogenic seawater ε_{Nd} values consistent with Nd input from the old rocks of North America and Greenland. The upper water column Nd isotope distribution of the AM is also mainly controlled by the riverine and marine sources (see Fig. 4 and chapter I). This overall illustrates that Nd isotopes are a powerful tool to study modern water mass provenance and their mixing. In addition, as indicated above, the Nd isotopes are also a useful tool to investigate processes that change their distribution beyond what can be expected from water mass advection and mixing (e.g. Lambelet et al., 2016; Stichel et al., 2015). They are also widely applied in paleoceanography as a tracer for change of past water mass provenance and ocean circulation on different timescales (e.g. Böhm et al., 2015; Chen et al., 2012; Dausmann et al., 2015; Fagel and Mattielli, 2011; Fagel et al., 2014; Haley and Polyak, 2013; Teschner et al., 2016; Werner et al., 2014).

1.5 Principles and application of REEs in seawater

The rare earth elements (REEs) are defined as a group of transition metals that include all lanthanides (i.e. lanthanum, La, cerium, Ce, praseodymium, Pr, neodymium, Nd, samarium, Sm, europium, Eu, gadolinium, Gd, terbium, Tb, dysprosium, Dy, holmium, Ho, erbium, Er, thulium, Tm, ytterbium, Yb and lutetium, Lu), as well as yttrium (Y) and scandium (Sc). The latter has historically been classified as a REE but typically is not considered due to its small ionic radius. A subdivision into light (L)REEs (from La up to and including Eu), middle (M)REEs (from Gd up to and including Dy) and heavy (H)REEs (from Ho up to and including Lu) is often applied to cluster REEs of similar behavior. The REEs behave coherently in nature but a gradual decrease in ionic radius and an increase in covalent character with increasing atomic number due to the filling of

the 4f-orbital (i.e. the lanthanide contraction) lead to small but systematic changes in the geochemical behavior across the group. While the LREEs are highly incompatible in a magmatic solid-liquid system and thus prefer the liquid phase (i.e. the melt), the HREEs are more compatible and thus prefer to stay in the solid phase (i.e. the mantle). The fractionation of elements during partial melting and fractional crystallization of igneous minerals and rocks in the past has led to the chemical differentiation of the Earth's interior (Hofmann, 1988), and means for the modern REE distributions that different minerals and lithologies are imparted with distinct REE concentrations and distribution patterns.

Once the minerals and rocks are exposed at the Earth's surface, they are physically and chemically weathered and the mobilized REEs are introduced into the oceans mainly via rivers (e.g. Byrne and Sholkovitz, 1996; Goldstein et al., 1984) and through atmospheric inputs (e.g. de Baar, 1983; Elderfield and Greaves, 1982; Frank, 2002; Sholkovitz, 1993; Tachikawa et al., 1999). The mobilization and fractionation of lithogenic REEs during weathering has been suggested to depend on (i) the chemistry of the waters involved, soil pH and the concentration of dissolved organic matter, (ii) the abundance and weathering pattern of the weathered minerals and (iii) the formation of secondary phases in soils that sequester the REEs (Baskaran, 2011 and references therein). This complex interplay of parameters and processes makes it almost impossible to predict the exact concentrations of the mobilized REEs. Assessments of the REE budget and distribution in the oceans therefore require observational data from the land-ocean interface, which ideally include REE end-member concentrations of the individual sources of weathered material. Due to the lithogenic origin of the REEs, it is common practice to normalize their concentrations to those of a continental reference material, for example to those of the Post Archean Australian Shale (PAAS, McLennan, 2001). This approach not only allows tracking changes after the REEs have been introduced into the oceans but also provides the basis for detecting subtle differences in the REE patterns.

The rivers are assumed to be the main primary source of lithogenic REEs to the oceans. The REEs supplied via the riverine loads span a wide range of concentrations (e.g. Elderfield et al., 1990; Goldstein and Jacobsen, 1987), which generally are higher (Nd > ~100 pmol/kg) than those determined in open ocean seawater (up to ~50 pmol/kg for Nd, see Fig. 3 which presents the updated global Nd database provided by van de Flierdt et al. (2016). Similar to the heterogeneity in REE concentrations observed for the rivers, the relative REE distribution patterns differ between most rivers and partly exhibit distinct anomalies for individual REEs (e.g. Elderfield et al., 1990; Sholkovitz, 1992, 1995). However, compared to the REE distributions in seawater, most riverine REE distributions are characterized by lower HREE to LREE ratios (e.g. Elderfield et al., 1990), resulting in overall flat or slightly HREE-enriched PAAS-normalized REE patterns (Goldstein and Jacobsen, 1988a, b). Rivers that are enriched in the MREEs are less common and exhibit hump-shaped PAAS-normalized REE patterns (e.g. Tepe and Bau, 2014).

The riverine REEs are supplied to the oceans within different size pools. The REEs carried in the suspended load (> 0.2 or 0.45 μm) are quickly removed from the water column and thus likely have no significant influence on the REE distribution in the open oceans, in contrast to REEs supplied by the dissolved load. While early investigations considered everything that passes the 0.2 (or 0.45) μm filter membrane to be dissolved (e.g. Elderfield et al., 1990), recent investigations differentiate between the truly dissolved pool (< 1 or 10 kDa) and the colloidal pool (1 or 10 kDa < REE < 0.2 or 0.45 μm) (e.g. Merschel et al., 2017; Rousseau et al., 2015; Tepe and Bau, 2015). The latter hosts different REE-bearing nanoparticles and colloids (NPCs), which are composed either of organic (e.g. humic and vulvic acids) or inorganic (e.g. mineral particles and volcanic ash, including Fe and Mn (oxyhydr)oxides) material. As the river water mixes with seawater, the seawater cations induce coagulation of the NPCs, which are then removed from the water column as they settle to the seafloor (Boyle et al., 1977). This process has often been indirectly documented by a sharp decrease of the dissolved REE concentrations in the low-salinity zone of several global estuaries together with concurrent preferential removal of LREEs over HREEs (e.g. Åström et al., 2012; Elderfield et al., 1990; Lawrence and Kamber, 2006; Nozaki et al., 2000; Pokrovsky et al., 2014; Rousseau et al., 2015; Sholkovitz and Szymczak, 2000; Sholkovitz, 1995). The fractionation between LREEs and HREEs has been attributed to the combined effects of HREEs preferentially staying in solution and the general affinity of all REEs to attach to surfaces of organic or inorganic NPCs (Lee and Byrne, 1993). The removal of REEs in estuaries globally amounts to ~70 % for Nd, but differs between rivers (Rousseau et al., 2015). Recent experiments simulating estuarine mixing show that the composition of the rivers and in particular the riverine NPCs plays a major role in estuarine REE behavior (Merschel et al., 2016; Tepe and Bau, 2016). While large amounts of organic NPCs contained in river water inhibit the aggregation of REEs until salinities of ~10 are reached, the presence of large amounts of inorganic NPCs favors fast and strong REE removal (Merschel et al., 2016). River chemistry also controls estuarine release of NPC-bound REEs at higher salinities (e.g. Tepe and Bau, 2016). Arctic estuarine mixing experiments of Tepe and Bau (2016) show that this process likely only occurs when the riverine end-member is rich in inorganic NPCs and poor in organic NPCs. In addition to release of NPC-bound REEs, the release of REEs from suspended or deposited lithogenic particles was suggested to occur in estuaries, but to date was only demonstrated for the Amazon River (Rousseau et al., 2015).

All above-mentioned estuarine processes (i.e. REE removal through coagulation of NPCs, remobilization of REEs from aggregated NPCs and release of REEs from suspended or deposited lithogenic particles) also play an important role in the development of the seawater pattern (Hoyle et al., 1984; Nozaki et al., 2000; Rousseau et al., 2015; Sholkovitz, 1995). However, the distribution of the REEs in the oceans also highly depends on their residence times (close to the oceanic overturning time of ~1000 years; Broecker and Peng, 1982), their oxidation state (+3 for all REEs, except for Ce and Eu that also can occur in +2 and +4 oxidation states, respectively; e.g. Brookins, 1989) and seawater-particle interactions either occurring at the more widely defined land-

ocean interface including the margins (i.e. processes summarized under the term "boundary exchange", see section 1.4) or within the water column of the open ocean (e.g. vertical redistribution of the REEs through combined formation and remineralization of organic particles or scavenging and release from inorganic particles, a process summarized as "reversible scavenging", see section 1.4). Lateral advection of water masses that have a distinct REE distribution pattern depending on their age and their source region also significantly contribute to the distribution of the REEs within the oceans (often called "preformed" distribution; e.g. Zheng et al., 2016). All these criteria contribute differently in different oceanic settings and regions, resulting in distinct REE distributions observed within the oceans. In general, the water column in the Pacific and the Atlantic oceans is depleted in REEs at the surface and enriched at depth, while the concentrations are higher in the deep Pacific than in the deep Atlantic, likely as a function of water mass ages (Goldstein and Hemming, 2003). The REE distribution within the AM differs fundamentally from those of the Pacific and Atlantic oceans, given its REE enrichment in the upper water column due to high riverine inputs and almost constant REE concentrations at greater depths (Andersson et al., 2008; Porcelli et al., 2009; Westerlund and Öhman, 1992; Yang and Haley, 2016). The latter can likely be explained by the circulation pattern of the AM and the low primary productivity, which both inhibit strong vertical transport of REEs from the upper water column to deeper levels (see chapter I).

The PAAS-normalized seawater REE patterns are globally depleted in LREEs and have a pronounced Ce anomaly (e.g. Elderfield and Greaves, 1982), which forms due to the oxidation of Ce^{3+} to insoluble Ce^{4+}. Yttrium develops a positive anomaly and may decouple from Ho during estuarine mixing although it is its geochemical twin (e.g. Bau et al., 1995; Lawrence and Kamber, 2006). Thus, while the Ce anomaly provides valuable information on the oxidation state of seawater and sediments and the age of the water masses, the Y/Ho ratio mainly provides information on estuarine processes. Several studies have shown that the dissolved REE concentrations and their distribution patterns can provide valuable information on the composition of the source rocks and input pathways, the amount of time that passed since the last exposure of waters to weathering inputs, and particle adsorption and desorption processes (e.g. Garcia-Solsona et al., 2014; Haley et al., 2014; Hathorne et al., 2015; Molina-Kescher et al., 2014; Osborne et al., 2015; Rousseau et al., 2015; Wilson et al., 2013; Zheng et al., 2016).

1.6 REE sources in the Arctic Mediterranean and their ε_{Nd} signatures

While the amount of Nd data globally has doubled between 2011 and 2015 (van de Flierdt et al., 2016), no dissolved Nd data from the AM have been published during this period of time. Observations from pioneering studies performed in the 2000s (Andersson et al., 2008; Lacan and Jeandel, 2004a, b; Porcelli et al., 2009; Zimmermann et al., 2009), however, still allow a holistic evaluation of the major Nd sources (see below and Fig. 4).

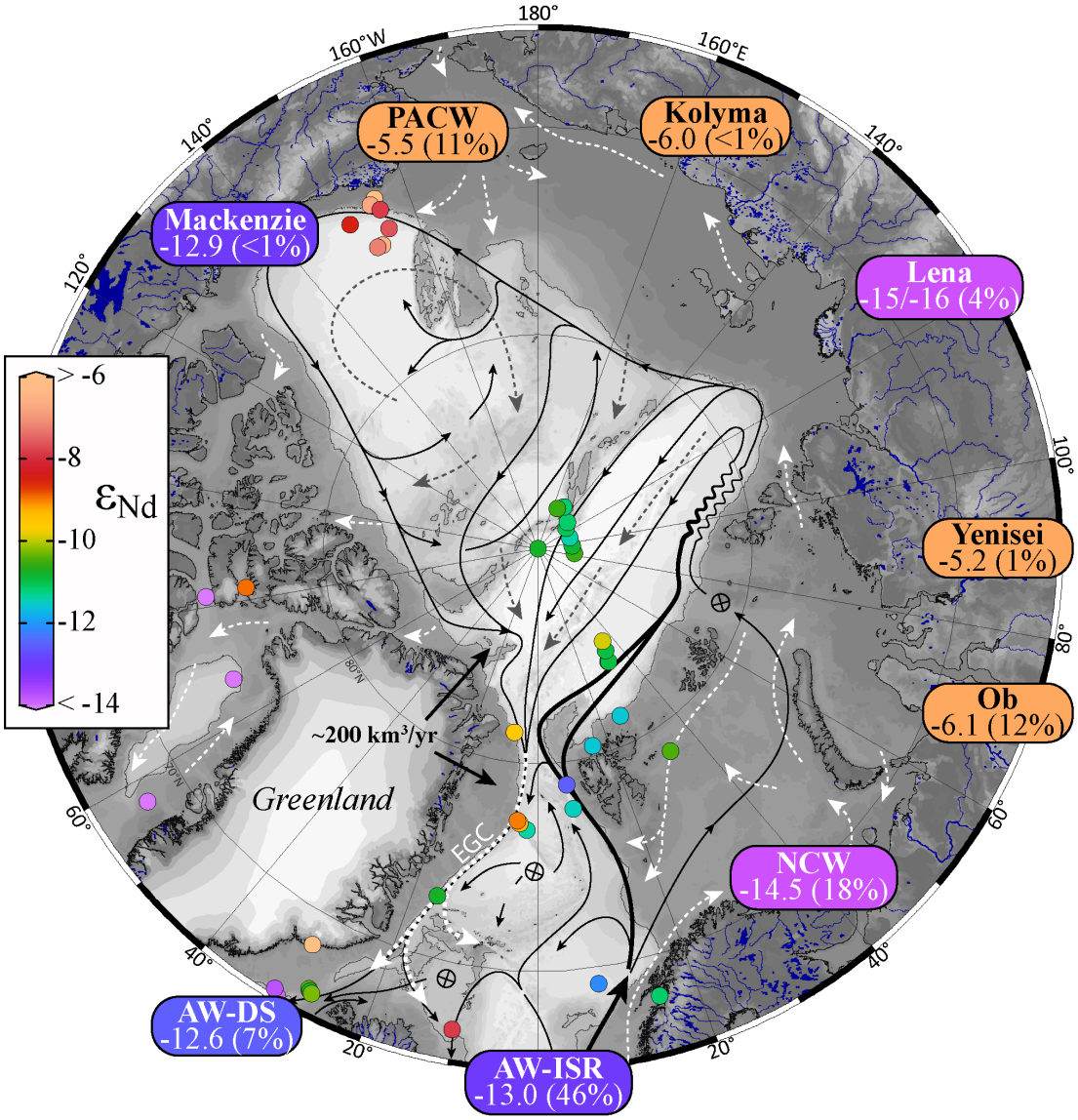

Figure 4: Map of the AM (Fig. 1) showing the ε_{Nd} distribution, which is color-coded and provided for REE sources (color-coded rounded boxes with ε_{Nd} values) and shallow seawater samples compiled from literature (color-coded circles) (Andersson et al., 2008; Lacan and Jeandel, 2004a, b; Piepgras and Wasserburg, 1987; Porcelli et al., 2009; Werner et al., 2014; Zimmermann et al., 2009). Only seawater data from water depths shallower than 60 m and uncertainties (2σ) better than 0.7 are shown. Rare earth element sources with known ε_{Nd} values and [Nd] are Atlantic Water (AW) entering through the Iceland-Scotland Ridge (AW-ISR) and the Denmark Strait (AW-DS) (Lacan and Jeandel, 2004a,b), Norwegian Coastal Water (NCW; Petrova, 2015), modified Pacific-derived water emerging from the Chukchi Sea (PACW; Dahlqvist et al., 2007; Porcelli et al., 2009) and major Arctic rivers (Persson et al., 2011; Porcelli et al., 2009; Zimmermann et al., 2009). Bold black arrows indicate mean freshwater flux from Greenland into the Arctic Ocean and the Nordic Seas for the year 2010 (Bamber et al., 2012). The estimated Nd inputs of the corresponding sources are given as percentage of the total Nd input into the AM taking into account volume transport and [Nd] of the sources (only rivers with discharges >100 km³/yr are considered). Further information on the REE sources of the AM is provided in the text. The figure was produced using Ocean Data View (Schlitzer, 2016) and modified manually.

The AW is clearly the major marine source of Nd (~53 % of Nd input to the AM; estimated here by taking into account volume transport (for mean volume transport of water masses see Mauritzen et al., 2013; for mean discharge of the Arctic rivers see R-Arctic-NET, http://www.r-arcticnet.sr.unh.edu/) and [Nd] (Lacan and Jeandel, 2004a, b; Persson et al., 2011; Petrova, 2015; Porcelli et al., 2009; Zimmermann et al., 2009) of all known Nd sources) and is characterized by an average ε_{Nd} signature of -13.0 (1 SD = 0.6, n = 7) and an average Nd concentration ([Nd]) of 16.2 pmol/kg (1 SD = 2.1) at the Iceland-Scotland Ridge (AW/ISR; data from Lacan and Jeandel, 2004b) and average ε_{Nd} = -12.6 (1 SD = 0.8, n = 2) and [Nd] = 19.1 pmol/kg (1 SD = 0.5) at the Denmark Strait (AW/DS; data from Lacan and Jeandel, 2004a). As discussed in chapter I, the AW which enters the AO through the eastern Fram Strait carries an ε_{Nd} signature of -11.7 (1 SD = 0.4, n = 11) and [Nd] = 15.9 pmol/kg (1 SD = 0.5). The AW that enters the AO through the Barents Sea has an ε_{Nd} signature of -12.4 (1 SD = 0.4, n = 5) and [Nd] = 16.7 pmol/kg (1 SD = 1.3) in the western Barents Sea (Petrova, 2015). There is also clear evidence that the Nd isotopic composition of AW gradually changes during transport across the AM due to admixture of other water masses (see chapter I).

The second largest marine REE source (~18 % of the Nd input into the AM) is the Norwegian Coastal Water (NCW) that enters the AM from the North Sea. It flows along the western and northern coast of Norway (i.e. Norwegian Coastal Current) and is characterized by S < 34.7 in the Barents Sea (Loeng, 1991). These waters mainly originate from the Baltic Sea (Gascard et al., 2004), where the dissolved Nd isotopic compositions are relatively unradiogenic (ε_{Nd} < -13) and an ε_{Nd} signature of -15.6 is reported for the surface sample closest to the Danish Straits (Chen et al., 2013). Water mass data from the western Barents Sea that resemble NCW characteristics also show a relatively unradiogenic ε_{Nd} composition of -14.5 and [Nd] = 22.5 pmol/kg (Petrova, 2015).

In contrast to these relatively unradiogenic Nd sources, Pacific-derived waters entering the AO through the Bering Strait have more radiogenic ε_{Nd} values between -4 and -6 (Dahlqvist et al., 2007). These waters are modified towards less radiogenic values through water-shelf interaction in the Chukchi Sea, which results in ε_{Nd} values of ~ -5.5 and Nd concentrations of up to ~30 pmol/kg (PACW; see Porcelli et al., 2009) for waters leaving the shelf. These waters are the third largest REE source (~11 % of Nd input to the AM) and the largest source with radiogenic Nd isotopic compositions.

The Siberian and North American Rivers draining into the Arctic Ocean have a wide range of Nd concentrations and isotopic compositions (see Persson et al., 2011; Porcelli et al., 2009; Zimmermann et al., 2009), and their Nd input to the AM is estimated to be ~19 % (here, only rivers with known [Nd] and discharge rate > 100 km^3/yr are considered). Their initial Nd concentrations can be a hundred times higher than those of typical seawater, but a considerable fraction is removed in estuaries and on the Arctic shelves (Porcelli et al., 2009). The major rivers (Mackenzie, Lena, Yenisei, Ob and Kolyma) have been sampled in 2003 (Zimmermann et al., 2009), and only the Lena River was re-sampled in 2004 (Porcelli et al., 2009) and in 2008 (Persson et al., 2011). No shift in the isotopic composition (ε_{Nd} = -14.2±0.3 for 2003; ε_{Nd} = -13.6±0.4 for 2004) but large differences in Nd concentrations (826 pmol/kg for 2003; 477 pmol/kg for

2004) have been observed between 2003 and 2004, and seasonal variations in weathering inputs and precipitation were suggested to account for this change (Porcelli et al., 2009). However, the ε_{Nd} and [Nd] values from 2003 and 2004 (Porcelli et al., 2009; Zimmermann et al., 2009) reported for the Lena River do not exactly represent the Nd isotopic composition of freshwater at the Lena Delta, since they were obtained from samples collected ~500 km upstream (Zhigansk, Russian Federation; see Zimmermann et al., 2009, for further information). Additionally, the sample from 2003 was only filtered a few days after collection (Zimmermann et al., 2009). Persson et al. (2011) reported a less radiogenic ε_{Nd} of -15 and [Nd] ~600 pmol/kg for the Lena River water at the river mouth. Seawater data close to the Lena Delta from September 2013 indicate a slightly less radiogenic signature of the Lena River water with ε_{Nd} ~ -16 and [Nd] ~550 pmol/kg (see chapters I and II). The change in the Nd isotopic composition from -14 (~500 km upstream) to -15/-16 (Lena Delta) most likely results from the different compositions of the geological formations within the Lena River catchment combined with seasonal variations in river runoff.

Additional contributions of Nd via glacial meltwater and runoff are also likely. Dissolved REE concentrations in glacial waters from the Kangerlussuaq area in western Greenland were for example shown to be ~60 times higher (for [Nd]) than those of typical seawater and indicate significant input of REEs from the Greenland Ice Sheet to the North Atlantic (Tepe and Bau, 2015). Tepe and Bau (2015) suggested local Archean basement as well as Asian dust to be the main sources of REEs, which indicates a mixture of different Nd isotopic compositions to be released to the North Atlantic. For shelf waters ($30.5 < S < \sim 33$) close to the Nansen Fjord on the east side of Greenland, Lacan and Jeandel (2004a) also reported high [Nd] (~100 pmol/kg) with a distinct Nd isotopic signature (ε_{Nd} ~ -3.5), suggesting that this enrichment is caused by lithogenic input from the basaltic Fjord area. The input of Greenland-sourced Nd to the AM is also evidenced by seawater Nd data from the Fram Strait (see chapter I).

A direct release of REEs from aeolian dust to the sea surface was shown to occur worldwide (e.g. Goswami et al., 2014; Greaves et al., 1999; Rickli et al., 2010). However, in the polar region the low temperatures and the sea-ice cover largely prevent a direct release of REEs from the atmosphere to the Arctic Ocean in winter and year-round in the central Arctic. Instead, the REEs are most likely scavenged by snow, deposited on the sea ice and only released during snow and sea-ice melting. No REE concentrations have been reported as yet for Arctic snow deposited on the Arctic sea-ice cover and the contribution of REE inputs through snow melting is thus unknown.

Similarly, no observational evidence is available for significant Nd fluxes during sea-ice formation or melting. Sea-ice production is accompanied by salt rejection into the underlying water with the remaining salt in the ice being trapped in liquid interstitial brines (e.g. Notz and Worster, 2009). No dissolved REE concentrations have been reported for Arctic fast or pack ice to date, but it is reasonable to assume that the distribution of the dissolved REEs will be consistent with the salinity changes. The salinity of Arctic sea ice mainly ranges from close-to-zero to ~10 (e.g. Vancoppenolle et al., 2009 and references therein), with an overall average salinity of ~4 (Bauch et al.,

2011). This indicates potentially significant changes of the Nd budget through 1.) passive Nd enrichment due to freshwater removal through wind driven surface currents (e.g. Transpolar Drift Stream) in areas where sea ice is formed and 2.) dilution of Nd (or enrichment; depending on difference in seawater [Nd] between source area and melting area) in areas where sea-ice melting prevails. The ε_{Nd} signatures are likely affected only through the latter process, provided that the sea ice is exported from its formation area and melted in areas with different ε_{Nd} signatures of seawater. These theoretical considerations are supported by a detailed investigation of the REE and Nd isotope distribution in the Laptev Sea, where REEs are redistributed due to formation and melting of sea ice and river ice, while the Nd isotope distribution is not changed significantly (see chapter II).

1.7 Stable oxygen isotope systematics and source-defined components

The proportion of $H_2{}^{18}O$ in seawater is a tracer of water mass origin (Craig and Gordon, 1965; Epstein and Mayeda, 1953), with the $^{18}O/^{16}O$ ratio commonly being expressed in the δ notation, which denotes the deviation of a measured $^{18}O/^{16}O$ ratio from the Vienna Standard Mean Ocean Water (VSMOW; Craig, 1961) as follows:

$$\delta^{18}O = \left[\frac{\left(\frac{^{18}O}{^{16}O}\right) SAMPLE}{\left(\frac{^{18}O}{^{16}O}\right) VSMOW} - 1 \right] \times 1000$$

During evaporation of water, fractionation between the heavier and lighter oxygen isotopes occurs whereby the vapor is isotopically lighter (i.e. the $\delta^{18}O$ value of the vapor becomes more negative). The atmospheric water vapor undergoes several modifications by evaporation, precipitation and air/sea exchange during its transport towards the north, resulting in Arctic vapor and precipitation $\delta^{18}O$ values ranging between -10 and -30 ‰ (Östlund and Hut, 1984). Conclusively, the Arctic rivers also exhibit a significant depletion of ^{18}O relative to VSMOW (e.g. $\delta^{18}O$ = -20 ‰ for the Lena River), while the Arctic marine $\delta^{18}O$ values are significantly higher (e.g. ~ 0.3 ‰ for AW) (Ekwurzel et al., 2001; Östlund and Hut, 1984). This difference allows tracing riverine discharge in the AO. In addition, in combination with salinity, stable oxygen isotopes also provide information on sea-ice formation and melting, as these processes cause deviations from the seawater-river water mixing line in $\delta^{18}O$-salinity space (e.g. Östlund and Hut, 1984).

The seawater of the AO may be assumed to consist of the following source-defined components: Meteoric water (MW), sea-ice meltwater (SIM), Pacific-derived water (PAC) and Atlantic-derived water (ATL). Several studies focused on the calculation of their fractions (f_{MW}, f_{SIM}, f_{PAC}, f_{ATL}) within the Arctic halocline (Bauch et al., 2011; 1995; Ekwurzel et al., 2001; Newton et al., 2013; Östlund and Hut, 1984; Yamamoto-Kawai et

al., 2008). While f_{MW}, f_{SIM} and a marine component can be calculated based on the salinity and the $\delta^{18}O$ alone (see above), a third parameter is necessary to distinguish between PAC and ATL. For deep waters, Broecker et al. (1985) defined a quasi-conservative phosphate-oxygen relationship ($PO^* = PO_4^{3-} + O_2/175 - 1.95$ in µmol/kg) where the calculated initial phosphate concentration accounts for production and aerobic respiration of organic matter changing phosphate and dissolved oxygen concentrations according to the Redfield relationships. The PO* may be used to estimate f_{PAC} and f_{ATL} (Ekwurzel et al., 2001), even though exchange of oxygen at the surface in ice free regions introduces uncertainties of this method. Although an attempt has been made by Newton et al. (2013) to improve this tracer by adjustments of the empirical relationships of phosphate and oxygen concentrations below and above the halocline (S ~34.5) based on observations made in the Arctic Ocean, the changes in the oxygen concentration during air-sea exchange still restrict the application of this tracer to subsurface waters or to areas with a permanent sea-ice cover and reduced oxygen atmospheric exchange.

A different approach based on different nitrate-phosphate (N/P) relationships between Atlantic and Pacific derived waters (Jones et al., 1998) can also be used to estimate f_{PAC} and f_{ATL} (Yamamoto-Kawai et al., 2008). Sedimentary denitrification on the Bering and Chukchi shelves decreases inorganic nitrogen concentrations in the Pacific-derived waters entering the AO, causing a phosphate surplus and therefore a change in the N/P ratio between the PAC and the ATL. However, Bauch et al. (2011) find evidence that denitrification on the shallow East Siberian (Anderson et al., 2013) and Laptev Sea shelves (Nitishinsky et al., 2007) can result in overestimation of the fraction of PAC of up to 50 %. A further comparatively small uncertainty is introduced because the N/P relationships for MW and SIM are unknown and are typically adopted from ATL (Jones et al., 1998; 2003).

Alkire et al. (2015) recently compared six common methods to estimate fractions of PAC and ATL by using identical samples and end-member values between all methods. Their calculations show that large discrepancies can be observed for calculated fractions between the N/P and the PO* methods. Particularly, the calculation of f_{PAC} can cause differences of up to 60% between these methods. Larger discrepancies can also be observed in the f_{MW} calculated with both methods, while the sea-ice melt fractions remain relatively constant. A Monte Carlo approach applied by Alkire et al. (2015) to examine uncertainties in the water mass fractions yield median standard deviations for f_{MW}, f_{SIM} and f_{PAC} of 1 %, 0.6 % and 13 %, respectively, outlining the high uncertainties of the Pacific-derived water component.

1.8 Objectives and outline of the thesis and contributions to the chapters

The work of this thesis was embedded in the framework of the joint Russian-German bilateral research network "*Laptev Sea System*" and was performed within the subproject

TP1A of the project "*The Transpolar System of the Arctic Ocean*", which was coordinated by Heidemarie Kassens and funded by the *German Federal Ministry of Education and Research* (BMBF) and the *Ministry of Education and Science of the Russian Federation* during the time period 2013-2016 (BMBF grant 03G0833). While the overall goal of the project was to assess how climate change will affect the highly sensitive Arctic environment and in which way changes will have consequences for European climate, the sub-project TP1A (designed by Martin Frank and Carolyn Wegner) more specifically focused on the variability of water masses and transport of matter within the Transpolar Drift System from the Laptev Sea (Siberian Arctic) to the Fram Strait.

This thesis mainly aims at improving the understanding of the ocean circulation of the entire AM (including water mass transport within the Transpolar Drift System) and provides new insight into the processes occurring on the Arctic shelves. This is achieved through a multi-proxy geochemical inventory including dissolved Nd isotopes, dissolved REEs, seawater $\delta^{18}O$ and standard hydrographic tracers (e.g. T, S, NO_3, PO_4, Si). A second aim of this thesis is to improve the understanding of the behavior of REEs and Nd isotopes in the modern AM and in freshwater and ice-dominated regions. A fundamental question is whether the distribution of Nd isotopes and REEs is changed beyond what can be expected from water mass advection and mixing, for example through seawater-particle interactions or processes related to ice formation and melting. The study areas are the Fram Strait as the major gateway between the Arctic Ocean and the Nordic Seas and the Laptev Sea as one of the Siberian shelf seas. Data from multiple years allow studying interannual variability of water mass advection and mixing.

The following chapters provide the main results and discussion of the thesis. Chapters I, II and III are presented in the form of separate articles, with chapter I being published, chapter II being in review and chapter III being in preparation for submission in a peer-reviewed journal.

Chapter I presents a refinement of the water mass distribution in the Fram Strait based on a detailed geochemical tracer inventory including seawater Nd isotope, REE and $\delta^{18}O$ data from the Fram Strait and the North-East Greenland Shelf. It provides new insights into the sources, the distribution and mixing of the water masses passing Fram Strait and together with a compilation and reassessment of literature seawater Nd data investigates the ocean circulation and freshwater pathways in the entire AM. This study also evaluates if the pronounced gradients in Nd isotope compositions and REE characteristics in the upper water column provide a reliable basis for assessments of shallow hydrological changes within the AM.

This chapter was already published in the journal *Geochimica et Cosmochimica Acta (GCA)*, authored by Georgi Laukert, Martin Frank, Dorothea Bauch, Ed C. Hathorne, Benjamin Rabe, Wilken-Jon von Appen, Carolyn Wegner, Moritz Zieringer and Heidemarie Kassens under the title: **Ocean circulation and freshwater pathways in the Arctic Mediterranean based on a combined Nd isotope, REE and oxygen isotope section across Fram Strait** (http://dx.doi.org/10.1016/j.gca.2016.12.028).

My and the co-authors contributions to the article are as follows: I prepared all samples in the laboratory, measured the Nd isotope and concentration data as well as the REE concentrations, and wrote the manuscript. Martin Frank proposed the study. Moritz Zieringer and Jutta Heinze collected the samples during the expedition ARK-XXVII/1 (PS80, 2012). Dorothea Bauch provided the oxygen isotope data. Ed C. Hathorne assisted in the analyses of the REE data. All co-authors contributed to the discussions and improved the text of the manuscript. The manuscript was also improved by the contributions of three reviewers and the associate editor of GCA, Tina van de Flierdt.

Chapter II assesses the general behavior of Nd isotopes and REEs in a high latitude estuary. In particular, it is addressed if changes in the seawater Nd isotope and REE distribution - apart from those caused by water mass advection and mixing - occur, for example through particle-seawater interactions or through ice formation and melting. In addition, this study investigates the spatial and temporal variation of water mass advection and mixing in the Laptev Sea.

This chapter has recently been submitted to the journal *Earth and Planetary Science Letters (EPSL)*, authored by Georgi Laukert, Martin Frank, Dorothea Bauch, Ed C. Hathorne, Marcus Gutjahr, Markus Janout, Jens Hölemann and Leonid Timokhov under the title: **Transport and transformation of riverine Nd isotope and rare earth element signatures in the high latitude estuaries: A case study from the Laptev Sea**.

My and the co-authors contributions to the manuscript are as follows: I collected the samples during the summer expeditions TD-XXI (2013) and TD-XXII (2014) and prepared all samples in the laboratory, measured the Nd isotope and REE data, measured the in-situ salinity and wrote the manuscript. Martin Frank proposed the study. Leonid Timokhov organized the expeditions. Jens Hölemann collected samples during the winter expedition TD-XX (2012). Dorothea Bauch provided the oxygen isotope data. Ed C. Hathorne assisted in the analyses of the REE data. All co-authors contributed to the discussions and improved the text of the manuscript.

Chapter III examines the propagation of North-East Greenland Ice Sheet sourced freshwater on the North-East Greenland Shelf and assesses the interannual variability of the water masses passing Fram Strait. Furthermore, this study examines if Nd isotopes are suitable to trace Greenland freshwater without the application of stable oxygen isotopes.

This chapter will be prepared for submission to the journal *Geophysical Research Letters (GRL)* in the following months and will be authored by Georgi Laukert, Martin Frank, Ed C. Hathorne, Benjamin Rabe, Wilken-Jon von Appen, Dorothea Bauch, Antje Wildau, Kristin Werner and Heidemarie Kassens under the title: **Propagation of Greenland freshwater in the western Fram Strait – Evidence from dissolved Nd isotopes and REEs.**

My and the co-authors contributions to the manuscript are as follows: I proposed the study, prepared all samples in the laboratory, measured the Nd isotope and REE

data, and wrote the manuscript. Antje Wildau and Kirsten Werner collected the samples during the expeditions ARK-XXVIII/2 (PS85, 2014) and ARK-XXIX/2.1 (PS93.1, 2015). Ed C. Hathorne assisted in the analyses of the REE data. Martin Frank contributed to the discussions and improved the text of the chapter.

2. METHODS

The methods used in this study are based on well-established techniques and thus only a brief overview of the methodologies applied is given. They are similarly but not as extensively presented in chapters I, II and III together with detailed information on sampling campaigns, sampling locations and sample recovery. Thus, the focus of this Methods chapter is on sample collection and pre-concentration, chemical procedures including chromatographic purification, mass spectrometric measurements, and the mixing calculations used in all chapters. The entire pre-concentration, purification and measurement techniques for REE concentrations and Nd isotope compositions reported here followed approved GEOTRACES protocols, which were confirmed through participation of the GEOMAR clean laboratory facilities in the international GEOTRACES inter-calibration study (van de Flierdt et al., 2012). The methodologies applied to determine oxygen isotope and nutrient data are also briefly presented below.

2.1 Sample collection and pre-concentration

Seawater samples were collected with 12L (samples presented in chapters I and III) or 2.5 L (samples presented in chapter II) Niskin-type sample bottles mounted to a SBE32 Carousel Water Sampler (Sea-Bird Electronics, Inc.) including a CTD (conductivity, temperature, depth) system for CTD data acquisition. Under-ice seawater samples (presented in chapter II) were collected through an ice hole with a 2 L Niskin-type sample bottle. Seawater samples at the sediment-water interface (presented in chapter II) were collected with a multicorer device (MuC).

Samples for Nd isotope analyses were collected in 20 L (samples presented in chapters I and III) or 10 L (samples presented in chapters II and III) acid-cleaned LDPE-cubitainers and filtered through 0.45 µm Millipore® cellulose acetate filters using a peristaltic pump (samples presented in chapter I) or filtered through AcroPak™500 Capsules containing Supor Membrane (pore size: 0.8/0.2 µm) filter cartridges (samples presented in chapters II and III) and were acidified to pH ~2.2 with distilled concentrated hydrochloric acid within ~2 hours after sampling (samples presented in chapters I and III) or after transport to the Otto-Schmidt Laboratory in St. Petersburg, Russia (samples presented in chapters II). An aliquot of ~2 L of each sample was separated into an acid-cleaned LDPE-bottle for concentration analyses. About 100 mg of Fe was added to the remaining sample as purified $FeCl_3$ solution (~1 g $Fe(III)Cl_3$/mL in 3 M HCl) and sufficient time for equilibration was given (1-2 days). Subsequently, the pH

was adjusted to ~8 by addition of ammonia solution (25 %, Merck Suprapur®), which led to co-precipitation of the dissolved REEs together with the iron hydroxides (FeOOH). After settling of the precipitate (> 3 days), most of the supernatant was discarded and the Fe-precipitate was transferred into a 2 L acid-cleaned LDPE-bottle, which was returned to the home laboratory at GEOMAR, Kiel.

2.2 Chemical procedures including chromatographic purification

For the extraction and isolation of dissolved Nd the procedure outlined in Stichel et al. (2012) was applied (sample treatment performed for chapters II and III) or a slightly modified version of it (sample treatment performed for chapter I), for which during the cation exchange chromatography (see below) instead of a mixture of HCl and HF only HCl was used as a reagent (see also table 1). The Fe-precipitates were centrifuged (3 x 10 minutes at 3500 rpm) and rinsed with deionized (18.2 MΩ cm, Milli-Q system) water first to remove major seawater ions (e.g. Na, Mg). Subsequently, the precipitates were re-dissolved in 6 M HCl and transferred into 60 mL Teflon vials. After drying, the samples were treated with aqua regia at 110 °C for at least 24 h to destroy organic components. Subsequently, precleaned diethyl ether was used to separate the Fe from the samples (liquid-liquid extraction). This back-extraction method (see Stichel, 2010) involves Fe extraction of the acid phase through multiple addition and removal steps of 3 mL of the ether, and has been applied for each large volume sample to prevent the columns of the following chromatographic separation step from overloading with Fe. After back-extraction, the samples were dried, re-dissolved in 0.5 mL 1 M HCl and transferred into 7 mL Teflon vials.

After a second single centrifugation step (5 minutes at 13000 rpm), further separation of the major element cations and high field strength elements from the REEs was achieved through cation exchange chromatography (BIORAD® AG50W-X8 resin, 200-400 µm mesh-size, 1.4 mL resin bed) following the slightly modified separation scheme of Stichel (2010) and Barrat et al. (1996) (table 1). After the cuts of the samples containing the REEs had been collected in 7 mL Teflon vials, they were dried and re-dissolved in 0.5 mL 0.1 M HCl. Neodymium separation from the other REEs then was achieved by a second column chemistry step using Eichchrom® LN-Spec resin (50-100 µm mesh size, 2 mL resin bed) and a modified separation scheme from Le Fèvre and Pin (2005) and Pin and Zalduegui (1997) (table 2).

The preparation of samples for a more precise determination of Nd concentrations (chapter I) based on an isotope dilution (ID) method (Rickli et al., 2009) included the addition of a pre-weighed ^{150}Nd spike to a ~0.5 L aliquot of each sample. After equilibration and addition of the purified $FeCl_3$ solution (see above), co-precipitation was achieved at pH ~8. Pre-concentration was then performed identically to that of the large volume samples (i.e. the samples used for Nd isotope determination). Similarly, the REE separation for the ID samples was identical to that for the isotope

measurements (i.e. the large volume samples), except that only the cation exchange chromatography (BIORAD® AG50W-X8 resin, 200-400 µm mesh-size, 1.4 mL resin bed) was applied.

After collection of the Nd cuts and subsequent drying, the samples were treated with 100 µL H_2O_2 (~30 wt.%) for at least 2 hours and then dried again to avoid possible contamination by traces of resin and to prevent disturbing matrix effects. Dissolution in 0.5 M HNO_3 was the final chemical treatment before the samples were measured on the MC-ICP-MS. Due to the weakness of the acid dissolution, the samples needed up to 48 hours at ~100 °C. In difficult cases, the samples were put into an ultrasonic bath for ~5 minutes. After complete dissolution, the samples were transferred to 1.5 mL safe-lock tubes and stored for measurement.

Table 1: AG50W-X8 (200-400 µm mesh-size, 1.4 mL resin bed) column chemistry.

stage	volume	reagent
pre-clean	10 mL	6 M HCl (+0.5 M HF*)
pre-condition	0.5 mL	1 M HCl (+0.05 M HF*)
condition	1 mL	1 M HCl (+0.05 M HF*)
load sample (+ collect Hf)	0.5 mL	1 M HCl (+0.05 M HF*)
wash in (+ collect Hf)	1.5 mL	1 M HCl (0.05 M HF*)
elute Fe/Sr	5 mL	3 M HCl
change acid	2 x 1 mL	MQ
elute Ba	10 mL	2 M HNO_3
collect REE (including Nd)	6.5 mL	6 M HNO_3
clean	2 mL	6 M HNO_3
change acid	2 x 1 mL	MQ
clean	10 mL	6 M HCl (+0.5 M HF*)
pass and store	2 + 3 mL	MQ

* acid containing HF was used for sample treatment performed for chapters II and III.

Table 2: LN-Spec resin (50-100 µm mesh size, 2 mL resin bed) column chemistry.

stage	volume	reagent
pre-clean	8 mL	6 M HCl
pre-condition	0.5 mL	0.1 M HCl
pre-condition	1 mL	0.1 M HCl
load sample	0.5 mL	0.1 M HCl
wash in and elute Ba	0.5 mL	0.1 M HCl
elute LREE	8 mL	0.25 M HCl
collect Nd	6.5 mL	0.25 M HCl
clean	8 mL	6 M HCl
pass and store	1 + 1 mL	MQ

2.3 Neodymium isotope and ID concentration measurements via MC-ICP-MS

Neodymium isotope compositions and the ID-based Nd concentrations were measured on a Nu Plasma (Nu Instruments Limited) (chapters I, II and III) and a Neptune Plus (Thermo Scientific) (chapter II) MC-ICP-MS at GEOMAR, Kiel. Gain calibration for the Faraday cup was performed on the same day before the samples were measured. As mentioned above, the samples were introduced into the mass spectrometers dissolved in 0.5 M HNO_3.

Prior to the Nd isotope measurements, the sample concentrations were tested by diluting a small fraction of the sample in 0.5 M HNO_3 and by measuring it together with a standard calibration curve of different concentrations. This allowed similar beam intensity for both the samples and the standards during each measurement session. For the Nd isotope measurements, an exponential mass fractionation law was applied for correction of instrumental mass bias using a $^{146}Nd/^{144}Nd$ ratio of 0.7219. The measured $^{143}Nd/^{144}Nd$ ratios of all samples were normalized to the value of 0.512115 for the JNdi-1 standard (Tanaka et al., 2000). Based on repeated measurements (every two samples) of JNdi-1 and in-house standards with concentrations similar to those of the samples (see above), the 2σ external reproducibility ranged between 0.1 and 0.4 ε_{Nd} units for all individual measurement runs presented in chapters I, II and III. Duplicate analyses (n = 16, for the entire thesis) resulted in identical Nd isotopic compositions within these uncertainties.

The principle and detailed calculations of the ID method are provided in Stichel (2010) and in Chen (2013). Replicates of the isotope dilution measurements (n = 13) yielded an external reproducibility of 1.5 % (2σ) on average.

2.4 Rare earth element concentration measurements

The REE concentrations (chapters I, II and III) were measured using an online pre-concentration (OP) ICP-MS technique at GEOMAR, Kiel by directly coupling a "seaFAST" system (Elemental Scientific Inc., Nebraska, USA) to an ICP-MS (Agilent 7500ce) following Hathorne et al. (2012). This method was improved by using an 8 mL sample loop and by preparation of calibration standards with a mixed REE solution of a seawater-like composition in a natural seawater matrix (Osborne et al., 2015). Trace metals including REEs were quantitatively removed from the seawater matrix through FeOOH co-precipitation yielding REE concentrations (generally < 0.2 pmol/kg for Ce and lower for all other REEs) in the resulting emptied seawater indistinguishable from distilled 0.1 % HCl. Repeated measurements of GEOTRACES inter-calibration samples BATS 15 m and BATS 2000 m from the Bermuda Atlantic Time-Series (van de Flierdt et al., 2012) were used to monitor the external reproducibility.

2.5 Oxygen isotope, nutrient and sample salinity measurements

For oxygen isotope analyses (chapters I and II) a CO_2-water isotope equilibration technique (Epstein and Mayeda, 1953) on a DeltaPlusXL instrument was applied to at least two subsamples of each water sample at the Leibniz Laboratory for Radiometric Dating and Stable Isotope Research in Kiel (chapter I) or at the Stable Isotope Laboratory of the College of Earth, Ocean, and Atmospheric Sciences at Oregon State University in Corvallis (chapter II) with an external reproducibility of ±0.04 ‰ or better. Nutrient samples (chapter I) were collected in plastic bottles and directly frozen at –80 °C and stored at –20 °C. Silicate, phosphate, nitrate and nitrite were analyzed at GEOMAR Helmholtz Centre for Ocean Research Kiel following standard procedures (Grasshoff et al., 2009). Salinities (chapter II) were determined with an AutoSal 8400A salinometer at a precision of ±0.003 and an accuracy better than ±0.005.

2.6 Binary and ternary mixing based on salinity, Nd isotopes and [Nd]

Two-component mixing can be calculated based on salinity (S), the Nd isotope composition (ε_{Nd}) and the Nd concentration ([Nd]) following

$$\varepsilon Nd_{MIX} = \frac{\varepsilon Nd_1 * [Nd]_1 * S_1 * f_1 + \varepsilon Nd_2 * [Nd]_2 * S_2 * f_2}{[Nd]_1 * S_1 * f_1 + * [Nd]_2 * S_2 * f_2} \quad (1)$$

and

$$1 = f_1 + f_2 \quad (2)$$

where f_1 and f_2 denote the mass fractions of end-member 1 and 2 in the sample, respectively, and $\varepsilon_{Nd\text{-}MIX}$ is the ε_{Nd} value of the mixture of the two end-members in each sample.

Mixing between three components can also be calculated based on ε_{Nd} and [Nd] following

$$f_1 = 1 - f_2 - f_3 \quad (3)$$

$$f_2 = \frac{[Nd]_m - [Nd]_3 - f_1 * ([Nd]_1 - [Nd]_3)}{[Nd]_2 - [Nd]_3} \quad (4)$$

$$f_3 = \frac{\varepsilon Nd_m * [Nd]_m - \varepsilon Nd_2 * [Nd]_2 - f_1 * (\varepsilon Nd_1 * [Nd]_1 - \varepsilon Nd_2 * [Nd]_2)}{\varepsilon Nd_3 * [Nd]_3 - \varepsilon Nd_2 * [Nd]_2} \quad (5)$$

where $\varepsilon_{Nd\text{-}1}$, $\varepsilon_{Nd\text{-}2}$ and $\varepsilon_{Nd\text{-}3}$ are the end-member Nd isotopic compositions and $[Nd]_1$, $[Nd]_2$ and $[Nd]_3$ are the end-member concentrations, respectively, while $\varepsilon_{Nd\text{-}m}$ and $[Nd]_m$ denote the Nd isotopic composition and concentration of the sample, respectively, for which the fractions of the three end-members can be calculated by iteratively solving the equations (3), (4) and (5). The calculation was performed on a spreadsheet program through a goal-seek subroutine.

The fractions of the three components for the sample can also be calculated for the case that the $[Nd]_m$ does not represent the [Nd] expected from conservative mixing and thus cannot be used for the calculations (i.e. the Nd does not behave conservatively, e.g. due to removal from the water column through particle-seawater interactions; release of particulate Nd may change the dissolved Nd isotope composition and thus has to be excluded). This, however, requires an additional conservative parameter, i.e. the salinity, and two of the three components to have identical end-member values for the salinity. This special case is suggested for the Laptev Sea (see chapter II). There, Nd isotopes seem to behave conservatively, while a significant fraction of Nd is clearly removed from the water column. The three end-members suggested to contribute to Laptev Sea waters represent a marine component and two riverine components with S = 0. In this case, the fraction of the marine component (f_{SW}) can be calculated as

$$f_{SW} = \frac{S_m}{S_{SW}} \tag{6}$$

where S_m is the salinity of the sample and S_{SW} the salinity of the marine end-member. The initial fractions of the two freshwater components (f_{RI} and f_{R2}) are then calculated by iteratively solving the following equations:

$$f_{R1} = 1 - f_{R2} - f_{SW} \tag{7}$$

$$f_{R2} = \frac{[Nd]_m - [Nd]_{SW} - \mathrm{f}_{R1} * ([Nd]_{R1} - [Nd]_{SW})}{[Nd]_{R2} - [Nd]_{SW}} \tag{8}$$

$$f_{SW} = \frac{\varepsilon Nd_m * [Nd]_m - \varepsilon Nd_{R2} * [Nd]_{R2} - \mathrm{f}_{R1} * (\varepsilon Nd_{R1} * [Nd]_{R1} - \varepsilon Nd_{R2} * [Nd]_{R2})}{\varepsilon Nd_{SW} * [Nd]_{SW} - \varepsilon Nd_{R2} * [Nd]_{R2}} \tag{9}$$

where $\varepsilon_{Nd\text{-}SW}$, $\varepsilon_{Nd\text{-}RI}$ and $\varepsilon_{Nd\text{-}R2}$ are the Nd isotopic compositions and $[Nd]_{SW}$, $[Nd]_{RI}$ and $[Nd]_{R2}$ are the Nd concentrations of the marine end-member and the riverine end-member 1 and 2, respectively. The $[Nd]_m$ is calculated during the iteration process and requires to meet the additional condition

$$[Nd]_m \; of \; equation \; (8) = [Nd]_m \text{ of equation (9)} \tag{10}$$

which was also achieved through a goal-seek subroutine on a spreadsheet program.

The setting in the Laptev Sea is further complicated by formation and melting of sea ice (see chapter II), which requires distinguishing between the initial salinity (S_0) and the initial [Nd] ($[Nd]_0$) that represent the salinity and [Nd] expected without alterations through sea-ice formation or melting, respectively, and S_m and $[Nd]_m$ that reflect water mass mixing and sea-ice processes.

3. PUBLICATION AND MANUSCRIPTS

CHAPTER I

Ocean circulation and freshwater pathways in the Arctic Mediterranean based on a combined Nd isotope, REE and oxygen isotope section across Fram Strait

***Published as**: Laukert, G., Frank, M., Bauch, D., Hathorne, E. C., Rabe, B., von Appen, W. J., Wegner, C., Zieringer, M. and Kassens, H. (2017): Ocean circulation and freshwater pathways in the Arctic Mediterranean based on a combined Nd isotope, REE and oxygen isotope section across Fram Strait. Geochimica et Cosmochimica Acta, 202. pp. 285-309. DOI: 10.1016/j.gca.2016.12.028.*

Abstract

The water masses passing the Fram Strait are mainly responsible for the exchange of heat and freshwater between the Nordic Seas and the Arctic Ocean (the Arctic Mediterranean, AM). Disentangling their exact sources, distribution and mixing, however, is complex. This work provides new insights based on a detailed geochemical tracer inventory including dissolved Nd isotope (ε_{Nd}), rare earth element (REE) and stable oxygen isotope ($\delta^{18}O$) data along a full water depth section across Fram Strait.

We find that Nd isotope and REE distributions in the open AM primarily reflect lateral advection of water masses and their mixing. Seawater-particle interactions exert important control only above the shelf regions, as observed above the NE Greenland Shelf. Advection of northward flowing warm Atlantic Water (AW) is clearly reflected by an ε_{Nd} signature of -11.7 and a Nd concentration ([Nd]) of 16 pmol/kg in the upper ~500 m of the eastern and central Fram Strait. Freshening and cooling of the AW on its way trough the AM are accompanied by a continuous change towards more radiogenic ε_{Nd} signatures (e.g. -10.4 of dense Arctic Atlantic Water). This mainly reflects mixing with intermediate waters but also admixture of dense Kara Sea waters and Pacific-derived waters. The more radiogenic ε_{Nd} signatures of the intermediate and deep waters (reaching -9.5) are mainly acquired in the SW Nordic Seas through exchange with basaltic formations of Iceland and CE Greenland. Inputs of Nd from Svalbard are not observed and surface waters and Nd on the Svalbard shelf originate from the Barents Sea. Shallow southward flowing Arctic-derived waters (< 200 m) form the core of the East Greenland Current above the Greenland slope and can be traced by their relatively

radiogenic ε_{Nd} (reaching -8.8) and elevated [Nd] (21-29 pmol/kg). These properties are used together with $\delta^{18}O$ and standard hydrographic tracers to define the proportions of Pacific-derived (< ~30 % based on Nd isotopes) and Atlantic-derived waters, as well as of river waters (< ~8 %). Shallow waters (< 150 m) on the NE Greenland Shelf share some characteristics of Arctic-derived waters, but exhibit less radiogenic ε_{Nd} values (reaching -12.4) and higher [Nd] (up to 38 pmol/kg) in the upper ~100 m. This suggests local addition of Greenland freshwater of up to ~6 %. In addition to these observations, this study shows that the pronounced gradients in ε_{Nd} signatures and REE characteristics in the upper water column provide a reliable basis for assessments of shallow hydrological changes within the AM.

1. Introduction

The oceanic heat and freshwater budget of the Arctic Mediterranean (i.e. the Arctic Ocean and Nordic Seas, AM) is highly sensitive to climate forcing and in turn has a major impact on global climate variability (cf. Anisimov et al., 2007). A thorough assessment of sources, distribution and circulation of water masses involved in the transport and transfer of heat and freshwater within the AM is therefore critical for our understanding of present and potential future hydrological changes in the high-latitude and polar regions.

Together with the shallow Barents Sea (average depth of ~230 m), the deep (sill depth of 2545 m) and wide (~500 km) Fram Strait acts as a fundamental gateway through which water masses, and therefore heat and freshwater, exchange between the Arctic Ocean (AO) and the Nordic Seas (NS). Mixing processes upstream, downstream and within the Strait thus exert significant influence on climate (e.g. Aagaard et al., 1985; Rudels, 2009). Warm and saline Atlantic-derived waters, cold and fresh Arctic-derived waters and intermediate and deep waters from the AM deep basins meet and interact in the Fram Strait (e.g. Rudels et al., 1999b), which results in a complex hydrography involving a large number of distinct water masses that have been tracked by their temperature, salinity and potential density characteristics (e.g. Rudels et al., 2005; Schlichtholz and Houssais, 2002). Enhanced melting of the Greenland ice sheet additionally affects the upper water column of the western Fram Strait through increasing admixture of Greenland freshwater (e.g. Stedmon et al., 2015). The fate of the latter in the NS and its potential influence on the circulation pathways is not well known, which emphasizes the demand of a detailed geochemical inventory of water masses in this region.

Assessments of the fractional contributions to Arctic water masses have been carried out in previous studies but results based on different methodologies show significant discrepancies, in particular with regard to the contribution of Pacific-derived waters (Alkire et al., 2015). Here we use a novel combination of dissolved neodymium (Nd) isotope, rare earth element (REE) and stable oxygen isotope ($\delta^{18}O$) measurements with standard hydrographic tracers (T, S, NO_3, PO_4, Si) to refine the characterization of

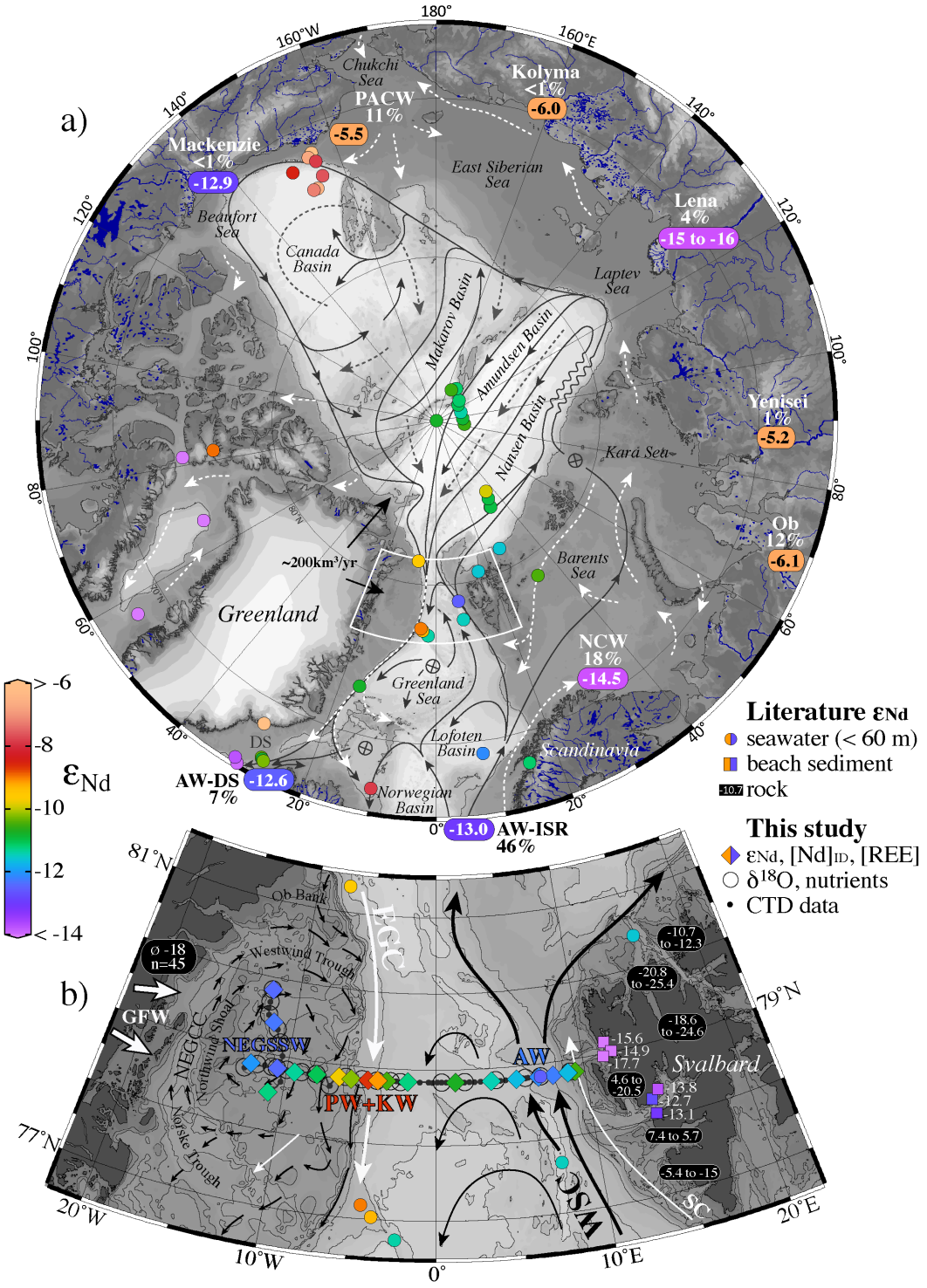

Figure 1: Bathymetric map of the AM with an inset representing the Fram Strait region (IBCAO; Jakobsson et al., 2012). a) Map of the AM with circulation scheme of the upper layers (dashed white and grey lines) and the subsurface Atlantic and intermediate layers (solid black lines) (modified after Rudels et al., 2012). Circled crosses indicate sites of convection or sinking from intermediate and AW layers to deeper levels. The ε_{Nd} distribution is color-coded and shown for REE sources (colored rounded boxes with ε_{Nd} values) and shallow seawater samples compiled from literature (colored circles) (Andersson et al., 2008; Lacan and Jeandel, 2004a, b; Piepgras and Wasserburg, 1987; Porcelli et al., 2009; Werner et al., 2014; Zimmermann et al., 2009).

Figure 1 (continued): Only seawater samples from depths shallower than 60 m and uncertainties (2σ) better than 0.7 are shown. REE sources with known ε_{Nd} values and [Nd] are Atlantic Water (AW) entering through the Iceland-Scotland Ridge (AW-ISR) and the Denmark Strait (AW-DS) (Lacan and Jeandel, 2004a, b), Norwegian Coastal Water (NCW; Petrova, 2015), Pacific-derived water (PACW; Dahlqvist et al., 2007; Porcelli et al., 2009) and major Arctic rivers (Persson et al., 2011; Porcelli et al., 2009; Zimmermann et al., 2009). Bold black arrows indicate mean freshwater flux from Greenland into the AO and the NS for the year 2010 (Bamber et al., 2012). The estimated Nd inputs of the corresponding sources are given as percentage of the total Nd input into the AM taking into account volume transport and [Nd] of the sources (only rivers with discharges > 100 km³/yr are considered). Further information on the REE sources of the AM is provided in the data tables (A1-A2). b) Fram Strait region with the four major currents (WSC, West Spitsbergen Current; EGC: East Greenland Current; NEGCC: North-East Greenland Coastal Current; SC, Sørkapp Current) and ε_{Nd} data from literature (seawater: circles; rocks: black rounded boxes, see data table A4) and this study (colored diamonds). The near-surface baroclinic circulation on the NE Greenland Shelf (bathymetry nomenclature after Arndt et al., 2015) is shown as black arrows with the length of the arrows indicating flow speed (Bourke et al., 1987). A clear distinction in the Nd isotopic signature is seen between AW (mean ε_{Nd} = -11.7, ISD = 0.4, n = 11), Arctic-derived waters (Polar Water, PW and Knee Water, KW; most radiogenic ε_{Nd} = -8.8) and locally formed NE Greenland Shelf Shallow Water (NEGSSW; mean ε_{Nd} = -11.7, 1 SD = 0.5, n = 13). More radiogenic ε_{Nd} signatures on the western shelf of Svalbard document Arctic-derived cold and less saline waters transported northward with the SC, which is an extension of the East Spitsbergen Current (Walczowski, 2013 and references therein). White arrows indicate marine outlets of the NE Greenland Ice Stream with Nioghalvfjerdsbræ (79° N Glacier; north arrow) and Zachariæ Isstrøm (south arrow) indicating the major source areas of Greenland freshwater (GFW) on the NE Greenland Shelf. The figures were produced using Ocean Data View (Schlitzer, 2016) and modified manually.

water masses along a zonal section crossing Fram Strait between Svalbard and Greenland.

The combination of standard hydrographic properties and $\delta^{18}O$ allows distinguishing between meteoric waters, sea-ice meltwater and Atlantic-derived and Pacific-derived waters within the Arctic halocline (e.g. Ekwurzel et al., 2001; Jones et al., 2008a; 1998; Newton et al., 2013; Yamamoto-Kawai et al., 2008). The fractions of these source-defined components have previously been determined for waters in the Fram Strait region and further south applying different sets of mass balance calculations and end-members (e.g. de Steur et al., 2015; Dodd et al., 2009; 2012; Falck, 2001; Falck et al., 2005; Jones et al., 2008b; Rabe et al., 2013; Stedmon et al., 2015; Sutherland et al., 2009; Taylor et al., 2003). However, besides the uncertainties mentioned above, these assessments lack a distinction of the different meteoric waters and their sources. Here radiogenic Nd isotopes provide important information given that water masses acquire their dissolved signatures mainly through particulate and dissolved riverine inputs of weathered continental crustal material, as well as exchange with the ocean margin sediments (Lacan and Jeandel, 2001, 2005), for which the Nd isotopic compositions vary as a function of the age and the Sm/Nd ratio of the source rocks (Frank, 2002). The quasi-conservative behavior of Nd in the open ocean (Frank, 2002; Goldstein and Hemming, 2003) and its intermediate average oceanic residence time of several hundred years (Arsouze et al., 2009; Rempfer et al., 2011; Tachikawa et al., 2003) then allows the tracking of these water masses and their mixing in the open ocean. The dissolved REE concentrations and their relative distribution patterns provide complementary information on the composition of the source material, the amount of time since the last contact with weathering inputs, and adsorption and desorption processes (e.g. Garcia-

Solsona et al., 2014; Haley et al., 2014; Hathorne et al., 2015; Molina-Kescher et al., 2014). This is possible because of systematic changes in the particle-reactivity of the REEs across the group caused by decreasing ionic radii and increasing covalent character with increasing atomic number.

The combination of dissolved Nd isotope compositions, REE distributions, $\delta^{18}O$ and hydrographic properties in the Fram Strait applied in this study for the first time allows a detailed evaluation of the suitability of Nd isotopes as a water mass tracer in the AM and an assessment of the origin and mixing of water masses in the AM based on geochemical properties.

2. Arctic Mediterranean REE and Nd isotope characteristics

Figure 1a shows the major potential REE sources and their Nd isotopic compositions (i.e. the radiogenic Nd isotope ratio $^{143}Nd/^{144}Nd$, commonly expressed as $\varepsilon_{Nd} = [(^{143}Nd/^{144}Nd)_{sample}/(^{143}Nd/^{144}Nd)_{CHUR} -1] \times 10^4$ with CHUR = 0.512638 and referring to a 'CHondritic Uniform Reservoir'; Jacobsen and Wasserburg, 1980) in the AM based on previously reported and new data from this study. Atlantic Water (AW) that enters the AM is characterized by an average ε_{Nd} signature of -13.0 (1 SD = 0.6, n = 7) and -12.6 (1 SD = 0.8, n = 2) and an average Nd concentration ([Nd]) of 16.2 and 19.1 pmol/kg (1 SD = 2.1 and 0.5, respectively) at the Iceland-Scotland Ridge and the Denmark Strait, respectively (data from Lacan and Jeandel, 2004a, b). The Pacific-derived waters entering the AO through the Bering Strait have ε_{Nd} values between -4 and -6 (Dahlqvist et al., 2007). These waters are likely modified towards less radiogenic compositions through water-shelf interaction in the Chukchi Sea, which results in ε_{Nd} values of ~ -5.5 and Nd concentrations of up to ~30 pmol/kg for waters leaving the shelf (PACW; Porcelli et al., 2009). The Norwegian Coastal Water (NCW) is another marine REE source that originates from the Baltic Sea (Gascard et al., 2004) and enters the AM from the North Sea flowing along the western and northern coast of Norway into the Barents Sea (Loeng, 1991). In the western Barents Sea it is characterized by ε_{Nd} = -14.5 and [Nd] = 22.5 pmol/kg (Petrova, 2015) consistent with its Baltic Sea origin (i.e. ε_{Nd} = -15.6 close to the Danish Straits, Chen et al., 2013). The Siberian and North American Rivers draining into the AO have a wide range of Nd concentrations and isotopic compositions (Persson et al., 2011; Porcelli et al., 2009; Zimmermann et al., 2009). Their initial Nd concentrations can be 100 times higher than those of typical seawater, but a considerable fraction is removed in estuaries and on the Arctic shelves (Porcelli et al., 2009), preventing most of the riverine Nd to reach the open AO. The potential for additional input of REEs and/or modification of the Nd isotopic composition through other weathering sources and processes, including release from particles and sediments, sea-ice formation and melting, glacial meltwater/runoff, and aeolian dust remains to be investigated in detail.

The seawater Nd isotope distribution in the AM has been attributed to weathering inputs, water mass circulation and mixing, but also to seawater-sediment exchange processes occurring on the wide Siberian shelves and the shelf slopes (e.g.

Andersson et al., 2008; Porcelli et al., 2009). The unknown impact of the latter and the scarcity of Nd data available so far prevented exploring the full potential of Nd isotopes as a water mass tracer in the AM. Moreover, the majority of the previous studies focusing on the distribution of Nd isotopes only reported the concentrations of Nd (Andersson et al., 2008; Lacan and Jeandel, 2004a; Piepgras and Wasserburg, 1987; Porcelli et al., 2009; Werner et al., 2014; Zimmermann et al., 2009). Despite their potential as a source tracer, there are only two studies that so far reported distributions of all REEs for unfiltered seawater in the AM (Lacan and Jeandel, 2004b; Westerlund and Öhman, 1992), and one providing dissolved REEs for the Canada Basin (Yang and Haley, 2016).

Table 1: Summary of salinity and Nd characteristics of REE sources in the AM and water masses observed in Fram Strait in 2012. All samples used to determine the compositions of REE sources are listed in the data tables (A1-A3).

REE sources in the Arctic Mediterranean*	Abbreviation	salinity	ε_{Nd}	ε_{Nd} 1SD**/n***	[Nd] (pmol/kg)
Atlantic Water at the Iceland-Scotland Ridge	AW-ISR	35.27	-13.0	0.6/7	16.2
Atlantic Water at the Denmark Strait	AW-DS	35.10	-12.6	0.8/2	19.1
Pacific Water emerging from Chuckchi Sea	PACW	32.70	-5.5	-	30.0
Norwegian Coastal Water in the western Barents Sea	NCW	34.52	-14.5	0.4/2	22.5
Ob River freshwater	Ob	0	-6.1	0.3/1	2152
Lena River freshwater	Lena	0	-15 to -15.7	>0.2/2	~600
Yenisei River freshwater	Yenisei	0	-5.2	0.3/1	154
Kolyma River freshwater	Kolyma	0	-6.0	0.4/1	129
Mackenzie River freshwater	Mackenzie	0	-12.9	0.3/1	111

Water mass compositions - Fram Strait (summer 2012)	Abbreviation	salinity	ε_{Nd}	ε_{Nd} 1SD*/n**	[Nd] (pmol/kg)
Atlantic-derived waters					
Atlantic Water	AW	35.09	-11.7	0.4/11	15.9
Recirculating Atlantic Water	RAW	35.01	-11.6	0.1/3	16.3
dense Arctic Atlantic Water	dAAW	34.91	-10.4	0.2/5	16.3
Arctic-derived waters					
Polar Water (most radiogenic sample)	PW*εNd-max*	32.30	-8.8	0.2/1	26.3
Polar Water (all samples)	PW	33.01	-9.9	0.7/7	27.1
Knee Water	KW	33.98	-9.6	0.2/3	22.3
Locally modified waters					
NE Greenland Shelf Shallow Water	NEGSSW	31.41	-11.7	0.5/13	36.6
NE Greenland Shelf Bottom Water	NEGSBW	34.28	-11.8	0.2/4	24.0
Intermediate and deep waters					
Arctic Intermediate Water	AIW	34.91	-10.1	0.2/4	15.5
Upper Polar Deep Water	UPDW	34.90	-10.2	0.4/5	15.7
Nordic Seas Deep Water	NDW	34.91	-10.0	0.2/3	16.1
Eurasian Basin Deep Water / Greenland Sea Deep Water	EBDW/GSDW	34.92	-10.5	0.2/6	15.8
Canadian Basin Deep Water	CBDW	34.92	-10.1	0.5/3	15.4

* references are provided in the main text

** standard deviation of sample mean; the measurement uncertainty (2 SD) is shown instead if 1 SD of mean is zero or only one sample was used

*** number of samples used to calculate ε_{Nd} mean

3. Methods

3.1 General information and oceanographic data

All samples presented in this study were acquired during the first leg of the 27th expedition of the German research vessel FS Polarstern between 15 June and 15 July 2012 (PS80, ARKXXVII/1). Details about the cruise track, sea-ice conditions and other information can be found in the expedition report (Beszczynska-Möller, 2013).

CTD (conductivity, temperature, depth) profiles were obtained along a latitudinal transect between 9.3° E and 12.5° W at approximately 78.8° N and on the NE Greenland Shelf along the fast ice edge, between 78.5° N and 79.8° N (Fig. 1b; Beszczynska-Möller and Wisotzki, 2012). Seawater samples were collected along the meridional section at 78.8° N covering the entire Fram Strait and continuing on the NE Greenland Shelf in the inter-trough area east of the Northwind Shoal. A SBE32 rosette water sampler equipped with 24 Niskin-type sample bottles (12 L) was used for recovery of all samples. Samples for Nd isotope and REE analyses were recovered from the full water column of the central Fram Strait down to a maximum depth of 2668 m, while the sampling depth on the NE Greenland Shelf and the western Svalbard Shelf reached 395 and 197 m, respectively. Samples for oxygen isotope and nutrient analyses were taken at different stations and depths along the cruise track due to limited sampling time and capabilities onboard, but the geographical distribution of these stations fully cover the distribution of the Nd and REE stations with maximum meridional and zonal distances between the data points of less than ~10 km and ~14 km, respectively. Sampling locations for all parameters are shown in Fig. 1b.

In addition, we report the Nd isotopic composition and concentration of one sample from the Laptev Sea margin (~200 m depth) and one surface sample from the SE Laptev Sea close to the Lena River delta acquired during the Transdrift-22 (September 2014) and Transdrift-21 (September 2013) expeditions, respectively.

3.2 Nd isotopic composition, $[Nd]_{ID}$ and [REE]

The entire pre-concentration, purification and measurement techniques reported here strictly followed approved GEOTRACES protocols and were confirmed through participation in the international GEOTRACES inter-calibration study (van de Flierdt et al., 2012). Samples for Nd isotopic analyses were collected in 20 L (Fram Strait samples) or 10 L (Laptev Sea samples) acid-cleaned LDPE-cubitainers and immediately filtered through 0.45 µm Millipore® cellulose acetate filters using a peristaltic pump (Fram Strait samples) or through AcroPak™500 Capsules with Supor Membrane (pore size: 0.8/0.2 µm) filter cartridges (Laptev Sea samples) and subsequently acidified to pH ~2.2 with ultra-pure concentrated hydrochloric acid within 2 hours after sampling (Fram Strait samples) or after transport to the Otto-Schmidt Laboratory in St. Petersburg, Russia (Laptev Sea samples). An aliquot of 2 L of each sample was separated into an acid-cleaned LDPE-bottle for concentration analyses. About ~100 mg of Fe was added to the

remaining large sample as purified $FeCl_3$ solution (~1 g $Fe(III)Cl_3$/mL) and at least 48 hours for equilibration was given before the pH was adjusted to ~8 using ammonia solution (25%, Merck Suprapur®) leading to co-precipitation of the dissolved REEs together with the iron hydroxides (FeOOH). Most of the supernatant was discarded and the Fe-precipitate transferred into a 2 L acid-cleaned LDPE-bottle and returned to the home laboratory at GEOMAR, Kiel.

For the extraction and isolation of dissolved Nd a procedure similar to that described by Stichel et al. (2012) was applied: The Fe-precipitates were centrifuged and rinsed with deionized (18.2 MΩ cm, Milli-Q system) water to remove major seawater ions. Organic components were then destroyed by treatment with concentrated aqua regia (heated for at least 24 h at 110°C). Afterwards, clean diethyl ether was used to separate Fe from the samples (liquid-liquid extraction). Major element cations were separated from the REEs through cation exchange chromatography (BIORAD® AG50W-X8 resin, 200-400 µm mesh-size, 1.4 mL resin bed) with a slightly modified separation scheme of Stichel et al. (2012), where instead of a mixture of HCl and HF acids only HCl was used as a reagent. Neodymium separation from the other REEs was achieved by a second column chemistry step using Eichchrom® Ln Spec resin (50-100 µm mesh size, 2 mL resin bed) and the separation scheme from Le Fèvre and Pin (2005). Nd concentrations ([Nd]) were determined using an isotope dilution (ID) method (i.e. $[Nd]_{ID}$) after Rickli et al. (2009). A pre-weighed ^{150}Nd spike was added to a 0.5 L aliquot of each sample and after equilibration and addition of Fe-hydroxide co-precipitation was achieved at pH ~8. For REE separation the same method as for the isotope measurements was used but only the cation exchange chromatography was applied.

Neodymium isotope compositions and $[Nd]_{ID}$ were measured on a Nu plasma MC-ICP-MS at GEOMAR, Kiel. An exponential mass fractionation law was applied for correction of instrumental mass bias using a $^{146}Nd/^{144}Nd$ ratio of 0.7219. The measured $^{143}Nd/^{144}Nd$ ratios of all samples were normalized to the value of 0.512115 for the JNdi-1 standard (Tanaka et al., 2000). Based on repeated measurements (every two samples) of JNdi-1 and in-house standards with concentrations similar to those of the samples, the 2σ external reproducibility ranged between 0.2 and 0.3 ε_{Nd} units for the individual measurement runs. Duplicate analyses (n = 10) resulted in identical Nd isotopic compositions within these uncertainties. Replicates of the isotope dilution measurements (n = 13) yielded an external reproducibility of 1.5 % (2σ) on average.

REE concentrations were measured using an online pre-concentration (OP) ICP-MS technique at GEOMAR, Kiel by directly coupling a "seaFAST" system (Elemental Scientific Inc., Nebraska, USA) to an ICP-MS (Agilent 7500ce) (Hathorne et al., 2012). The method of Hathorne et al. (2012) was further improved by using 8 mL sample loop and by preparation of calibration standards with a mixed REE solution of a seawater-like composition in a natural seawater matrix (Osborne et al., 2015). Trace metals including REEs were quantitatively removed from the seawater matrix through FeOOH co-precipitation yielding REE concentrations (generally < 0.2 pmol/kg for Ce and lower for all other REEs) in the resulting emptied seawater indistinguishable from distilled 0.1 % HCl. Repeated measurements of GEOTRACES inter-calibration samples BATS 15 m and

BATS 2000 m from the Bermuda Atlantic Time-Series (van de Flierdt et al., 2012) were used to monitor the external reproducibility (see data table A3).

3.3 Oxygen isotopes and nutrient analyses

For oxygen isotope analyses a CO_2-water isotope equilibration technique (Epstein and Mayeda, 1953) on a Finnigan gas bench II unit coupled to a Finnigan DeltaPlusXL was applied to at least two subsamples of the same water sample at the Leibniz Laboratory for Radiometric Dating and Stable Isotope Research, Kiel. The external reproducibility for all $\delta^{18}O$ measurements is ±0.04 ‰ or smaller and the measured $^{18}O/^{16}O$ ratio is provided as a deviation from Vienna Standard Mean Ocean Water in the δ-notation (Craig, 1961).

Nutrient samples were collected in plastic bottles and directly frozen at -80 °C and stored at -20 °C. Silicate, phosphate, nitrate and nitrite were analyzed at GEOMAR Helmholtz Centre for Ocean Research Kiel following standard procedures (Grasshoff et al., 2009).

3.4 Water mass classification, PO* and N/P methods and Nd-based mixing

We assigned water masses to most samples presented in this study and literature Nd data from the entire AM based on the classification of Rudels et al. (2012; 2005). This classification is based on constant θ-S end-member definitions and therefore does not take into account changes in the end-member properties, such as the warming of deep-water masses observed at Fram Strait over the last two decades (von Appen et al., 2015). To address the latter observation at least in a way that prevents misinterpretation, we do not distinguish between Eurasian Basin Deep Water and Greenland Sea Deep Water. The classification also broadly defines waters with σ_θ < ~27.7 as Polar Surface Water (PSW), thus not considering studies that pointed to contributions of locally formed waters on the NE Greenland Shelf (Bignami and Hopkins, 1997; Budéus and Schneider, 1995; Budéus et al., 1997). Consequently, for waters with σ_θ < ~27.7, we instead combine findings of Bignami and Hopkins (1997) and Budéus et al. (1997) and ascribe particular recurring θ-S properties and silicate concentrations to distinct water masses. We refer to these water masses as NE Greenland Shelf Shallow Water (NEGSSW, S ≤ ~31.8) and NE Greenland Shelf Bottom Water (NEGSBW, S ~34.4), as well as silicate-rich Polar Water (PW, [Si] > ~6 to ~8 µmol/kg, ~32 < S < ~33.5) and silicate-poor Knee Water (KW, [Si] < ~5 µmol/kg, S ~34, T near freezing point).

For shallow samples recovered from the western Fram Strait (i.e. mostly NEGSSW, NEGSBW, PW or KW), fractions of the source-defined components (i.e. meteoric water, MW, sea-ice meltwater, SIM, Atlantic-derived water, ATL, and Pacific-derived water, PAC) were calculated based on different empirical nutrient ratios (referred to as N/P method) and a phosphate-oxygen relationship (referred to as PO* method) following Bauch et al. (2011), who also provide the end-member compositions. Due to insignificantly small quantities of PAC combined with the inaccuracies in end-members and measurements, some of the calculated PAC fractions may be negative and

have no physical meaning. In these cases, a three-component system of equations is applied instead and the fraction of PAC set to zero. For mixing between Arctic-derived waters and Greenland freshwater, the interpolated $\delta^{18}O$ value (-1.5 ‰) of the PW sample with the most radiogenic ε_{Nd} signature was used as the marine $\delta^{18}O$ end-member, while for salinity, [Nd] and Nd isotopes the average composition of PW was used to account for modification of this water mass on the NE Greenland Shelf. For the Greenland freshwater end-member, the $\delta^{18}O$ was set to -23.4 ‰ (Stedmon et al., 2015).

Binary mixing based on S, Nd isotopes and [Nd] was calculated following

$$\varepsilon\mathrm{Nd}_{MIX} = \frac{\varepsilon\mathrm{Nd}_1 * [Nd]_1 * S_1 * f_1 + \varepsilon\mathrm{Nd}_2 * [Nd]_2 * S_2 * f_2}{[Nd]_1 * S_1 * f_1 + * [Nd]_2 * S_2 * f_2}$$

and

$$1 = f_1 + f_2$$

where f_1 and f_2 denote the mass fractions of end-member 1 and 2, respectively, and εNd_{MIX} is the ε_{Nd} value of the mixture of the two end-members. Note that we do not use an optimum multiparameter analysis here due to the poorly defined end-member compositions of most of the water masses of the AM. In addition, significant seasonal and interannual variations of the upper water column and longer-term changes in hydrographic properties of the intermediate and deep waters render such a steady-state approach unsuitable in the study area.

4. Results

All CTD data including temperature, salinity, oxygen concentration, O_2-saturation and attenuation were reported previously by Beszczynska-Möller and Wisotzki (2012) and are available through the PANGEA database (https://doi.pangaea.de/10.1594/PANGAEA.801791). Neodymium isotopic compositions, [Nd] obtained from the isotope dilution method, and REE concentrations measured with OP-ICP-MS are reported in the data tables (A3) together with corresponding S, T, O_2 concentrations and attenuation. Nutrient concentrations and $\delta^{18}O$ values are reported in the same way. All data are in addition accessible through the PANGEA database. The average Nd isotope and REE characteristics of all water masses resulting from our study are also listed in table 1 together with salinity and are reported in the data tables (A1-A2). where also a compilation of the composition of all water masses of the AM is provided.

4.1 Hydrography, water mass distribution and water mass components

The θ-S distribution of the waters of our study is presented in Fig. 2 (black dots) and is within the typical θ-S range at Fram Strait and the NE Greenland Shelf (e.g. Budéus et al., 1997; Schlichtholz and Houssais, 2002). Waters confined to the NE Greenland Shelf

and the upper water column (~300 m) above the Greenland continental margin (density σ_θ < ~27.7) exhibit recurring θ-S features (i.e. the sharp inflection at S ~34 and data tightly clustering at S ~31.8 before showing a larger scatter at lower salinities) and salinities reaching values as low as ~30. In contrast, the waters occupying most of the Fram Strait section (σ_θ > ~27.7, including AW, intermediate and deep waters, insets A and B in Fig. 2) show only limited variations in S, but a pronounced increase in temperatures towards the surface.

The distribution of water masses in 2012 overall matches earlier observations very well (e.g. Rudels et al., 2000). As shown in Fig. 3, the main core of AW is located shallower than ~500 m depth at the eastern side of Fram Strait and exhibits S_{max} = 35.14 and T_{max} = 5.36 °C in 2012. The AW comprises surface and intermediate waters that are transported northward into the AO along the Svalbard continental margin via the West Spitsbergen Current (WSC; e.g. Rudels et al., 2004), which is the northernmost extension of the Norwegian Atlantic Current (NAC; Aagaard et al., 1987) (Fig. 1). The surface front between inflowing AW that has never interacted with sea ice and the outflowing PSW is located near the Greenwich meridian. Patches of Recirculating Atlantic Water (RAW), which return to the NS within the Fram Strait or slightly north of it, are found near the front in the western Fram Strait below the surface. All water masses constituting PSW are located in the upper water column (~300 m) between this front and the coast of Greenland, with PW and KW forming the core of the EGC and NEGSSW and NEGSBW occupying the water column west of the EGC on the NE Greenland Shelf. Below RAW, dense Arctic Atlantic Water (dAAW) is found in the western Fram Strait at depths of ~400 to ~900 m. According to the θ-S-based classification, Arctic Intermediate Water (AIW) prevails below the AW/RAW/dAAW layer on both sides of Fram Strait, while Upper Polar Deep Water (UPDW) is mainly distributed above the continental slope of Greenland. Similarly, Eurasian Basin Deep Water (EBDW) or Greenland Sea Deep Water (GSDW) and Canada Basin Deep Water (CBDW) prevail on both sides of Fram Strait, while Nordic Seas Deep Water (NDW) is mostly confined to the Svalbard continental slope. For further information on the water mass distribution and characteristics in 2012, as well as the long-term variability, the reader is referred to Beszczynska-Möller (2013).

Similar fractions of MW (f_{MW}) and SIM (f_{SIM}) were computed with the PO* and N/P methods for PSW (the N/P based distributions are shown in Fig. 4), with the values of f_{MW} calculated with the PO* approach being somewhat higher compared to the N/P-based values (up to ~2 %) as a response to different consideration of marine fractions. Discrepancies to a far greater extent (up to ~40 %) are observed for the fractions of PAC (f_{PAC}) and ATL (f_{ATL}) between both methods, with the N/P method computing higher f_{PAC} and thus lower f_{ATL} compared to the PO* method (Fig. 4). A Monte Carlo approach applied by Alkire et al. (2015) to examine uncertainties in the different fractions yields median standard deviations for f_{MW}, f_{SIM} and f_{PAC} of 1%, 0.6% and 13%, respectively, outlining the high uncertainties of the calculated fractions of PAC. Therefore, we adopt f_{MW} and f_{SIM} from the PO* and N/P methods, but show f_{PAC} of both methods for comparison with Nd-based estimates only.

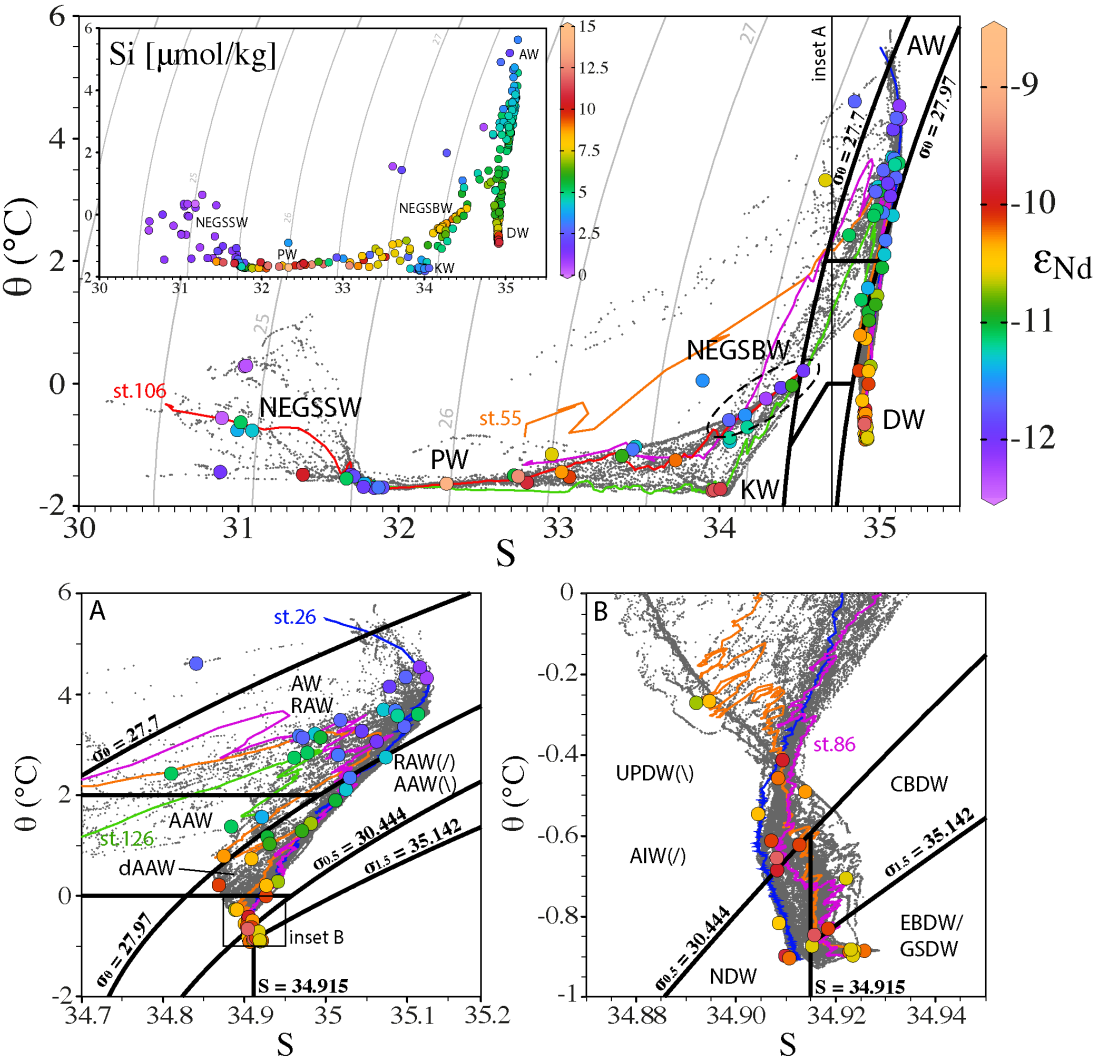

Figure 2: Potential temperature (°C) versus salinity plots with potential density isopycnals (solid back lines; σ_θ, $\sigma_{0.5}$ and $\sigma_{1.5}$ = potential density at reference pressures 0 m, 500 m and 1500 m, respectively), together with ε_{Nd} values (main plot, insets A and B) and [Si] (inset in main plot representing identical S and θ ranges) shown as color-coded circles. Additionally shown are all CTD data from the cruise with highlighted selected stations (26, 55, 86, 106 and 126). Waters with σ_θ > ~27.7 are classified based on the basis of constant θ-S end-member definitions (after Rudels et al., 2012; 2005) and for waters with σ_θ < ~27.7 (confined to the NE Greenland Shelf and the upper water column above the Greenland continental margin), we applied a classification based on findings of Bignami and Hopkins (1997) and Budéus et al. (1997). Water masses are labeled as follows: Polar Water – PW, Knee Water - KW, NE Greenland Shelf Shallow Water – NEGSSW, NE Greenland Shelf Bottom Water – NEGSBW, Atlantic Water – AW, Recirculating Atlantic Water – RAW, Arctic Atlantic Water – AAW, dense Arctic Atlantic Water – dAAW, Upper Polar Deep Water – UPDW, Arctic Intermediate Water – AIW and deep waters – DW. DW is further subdivided in inset B to Nordic Seas Deep Water – NDW, Canada Basin Deep Water – CBDW, Eurasian Basin Deep Water – EBDW and Greenland Sea Deep Water – GSDW. (/) indicates unstable stratification in salinity or temperature, (\) indicates stable stratification in both salinity and temperature (Rudels et al., 2005). Plots produced using Ocean Data View (Schlitzer, 2016) and modified manually.

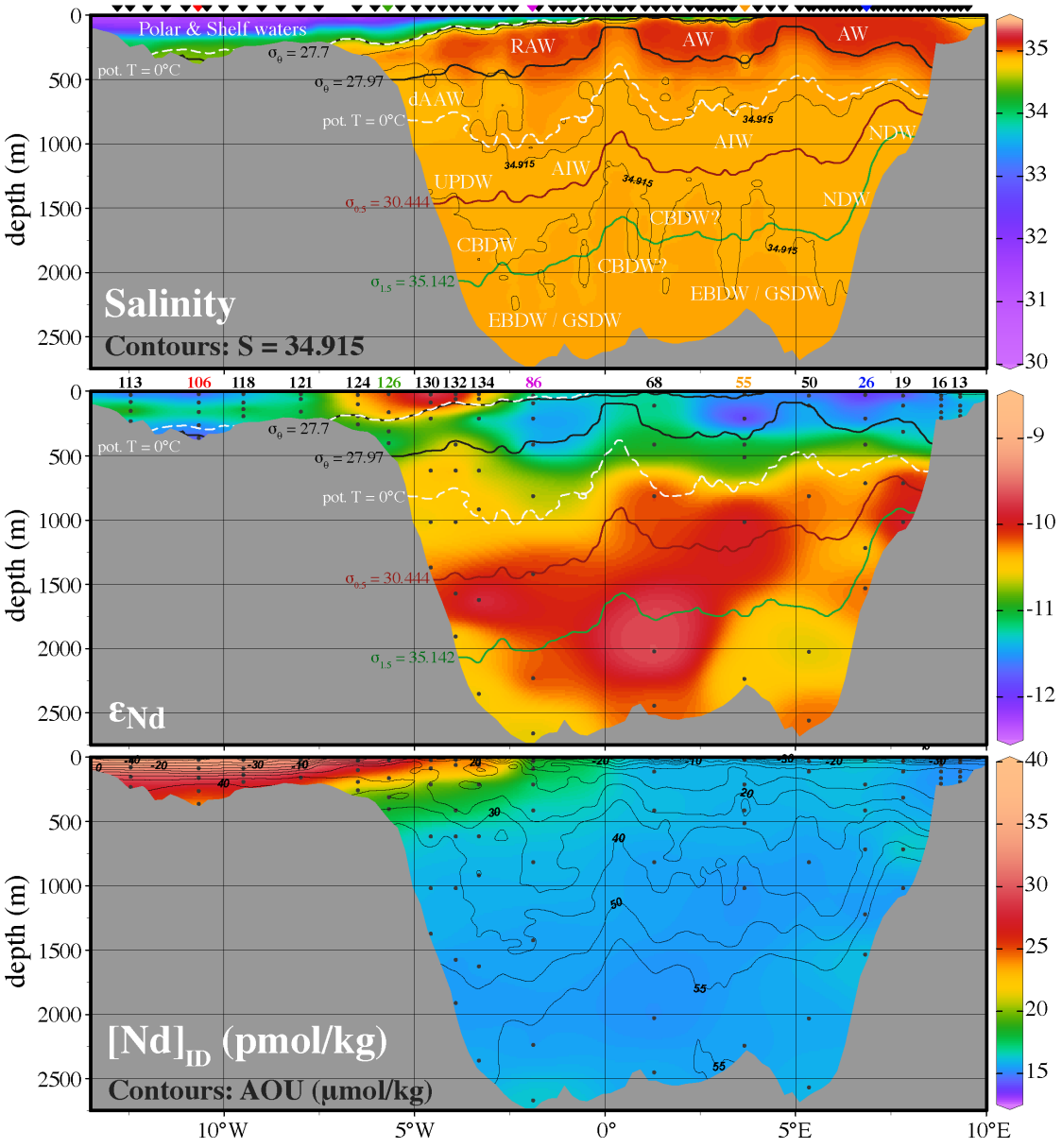

Figure 3: Distribution of the salinity (all CTD data), the Nd isotopic composition (ε_{Nd}) and the Nd concentration measured with the isotope dilution method ($[Nd]_{ID}$, in pmol/kg) along the latitudinal section at 78.8° N. On the salinity and ε_{Nd} sections, distinct potential density (black, red and green solid lines) and potential temperature (0 °C, white dashed lines) isopycnals are also shown (see Rudels et al., 2012; 2005). On the salinity plot S = 34.915 is also shown as thin black contour lines. For $[Nd]_{ID}$, the apparent oxygen utilization (AOU, in µmol/kg) is shown as thin black contour lines. The distribution of water masses as defined in the text and in figure 2 is indicated in the salinity plot. The numbers of the stations where Nd isotope samples were taken are given above the ε_{Nd} plot. Similarly, the locations of stations with salinity profiles are shown as inverted triangles above the salinity plot. The selected stations shown in figure 2 are highlighted with the same color. Sections produced using Ocean Data View (Schlitzer, 2016) and modified manually.

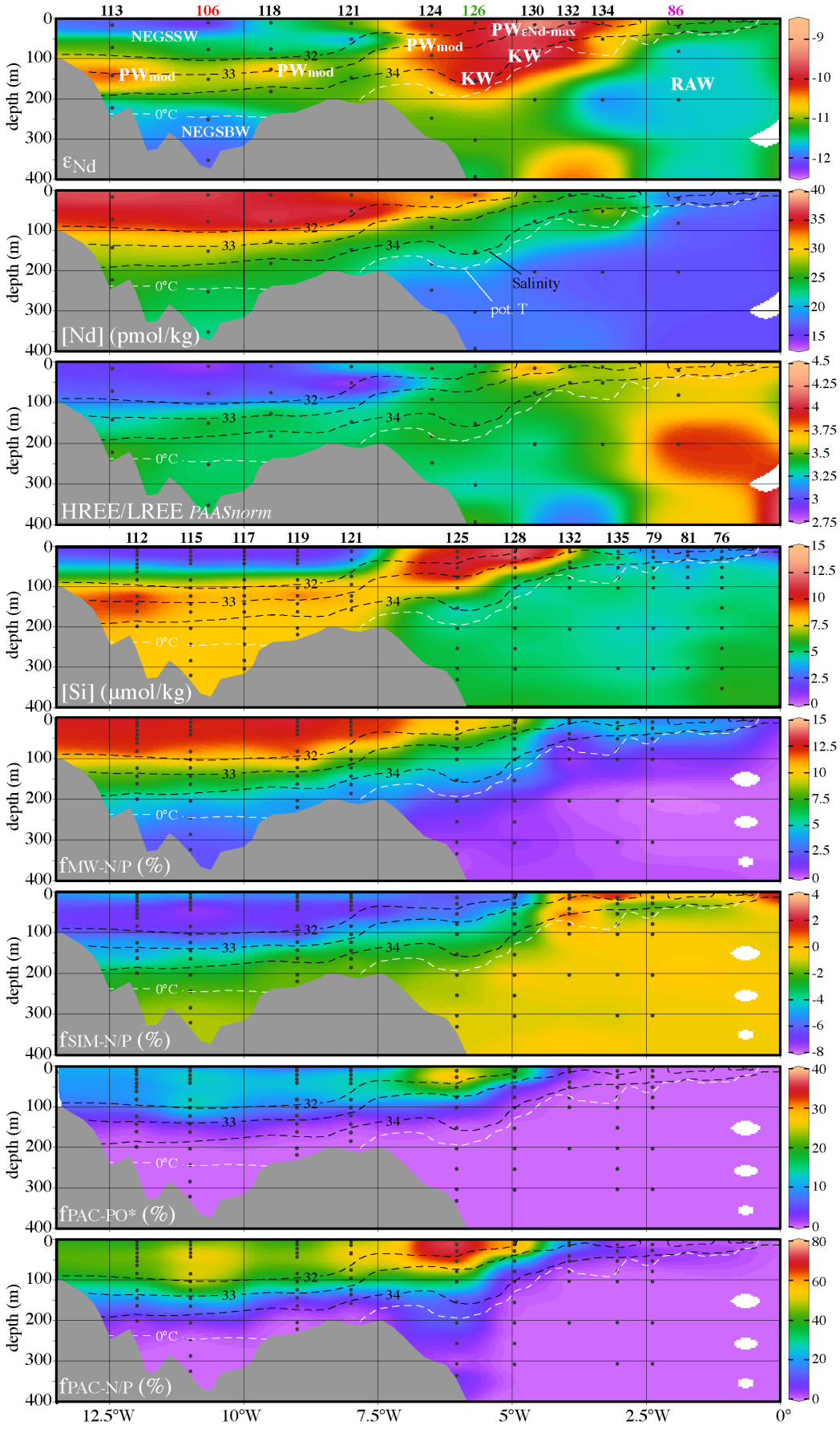
113 106 118 121 124 126 130 132 134 86
NEGSSW
PWmod
PWmod
PWmod
PWεNd-max
KW
KW
RAW
0°C
NEGSBW
εNd
Salinity
pot. T
[Nd] (pmol/kg)
HREE/LREE PAASnorm
112 115 117 119 121 125 128 132 135 79 81 76
[Si] (µmol/kg)
fMW-N/P (%)
fSIM-N/P (%)
fPAC-PO* (%)
fPAC-N/P (%)
depth (m)
12.5°W 10°W 7.5°W 5°W 2.5°W 0°

Figure 4 (previous page): Distribution of distinct measured and calculated parameters of the uppermost 400 m on the NE Greenland Shelf and above the Greenland margin. Fractions computed with the N/P and PO* methods (Bauch et al., 2011) are: Meteoric water – $f_{MW-N/P}$, sea-ice meltwater – $f_{SIM-N/P}$, Pacific-derived Water – $f_{PAC-N/P}$ and f_{PAC-PO^*}. Water masses as defined in the text and in figure 2 are schematically indicated on the ε_{Nd} plot. Here, distinction between PW samples modified through admixture of NEGSBW (PW_{mod}) and the most radiogenic PW sample ($PW_{\varepsilon Nd-max}$) is made. Contour lines of salinity (32, 33 and 34) and potential temperature (0 °C) are shown as black dashed and white lines, respectively. Names of stations with Nd samples are given above the ε_{Nd} plot (selected stations shown in figure 2 are highlighted with the same color) and for stations with nutrient and $\delta^{18}O$ samples above [Si]. Sections produced using Ocean Data View (Schlitzer, 2016) and modified manually.

4.2 Nd isotopes, $[Nd]_{ID}$ and [REE]

The Nd isotope and REE data set obtained covers the entire θ-S-range of the CTD data and includes all water masses present (Fig. 2). Neodymium concentrations obtained by isotope dilution range between 14.8 and 38.1 pmol/kg (Figs. 3 and 4), with lowest and highest $[Nd]_{ID}$ values observed above the western Svalbard Shelf and the NE Greenland Shelf, respectively. Waters with σ_θ > ~27.7 show only limited variations in $[Nd]_{ID}$ (average = 15.9 pmol/kg, 1 SD = 0.7, n = 58), while waters with σ_θ < ~27.7 show an inverse gradient with highest $[Nd]_{ID}$ values observed for NEGSSW. Two samples (station 68, 15.3 m; station 132, 202.6 m) exhibited anomalously high $[Nd]_{ID}$ (38.1 pmol/kg and 27.0 pmol/kg, respectively), neither consistent with Nd concentrations of adjacent samples nor with oceanographic properties. The REE patterns of these samples indicate that only the light REEs are anomalously enriched. Since we cannot completely rule out contamination during sampling, we report the $[Nd]_{ID}$ values of these two samples but exclude them from the figures and the following discussion.

Neodymium concentrations obtained by OP-ICP-MS are identical to the $[Nd]_{ID}$ data within the 95 % confidence limits of the OP-ICP-MS technique (see Hathorne et al., 2012 for more details), with the maximum difference between the two methods being ~15 % (sample 130-200). Similar to $[Nd]_{ID}$, all REE and Y concentrations are nearly constant throughout the whole water column for waters with σ_θ > ~27.7, in agreement with unfiltered REE data from Lacan and Jeandel (2004b) from the NS. Waters with σ_θ < ~27.7 show inverse gradients in the water column that slightly differ for each REE. Figure 5 shows REE concentrations normalized to Post-Archean Australian Sedimentary rocks (PAAS; McLennan, 2001) and to the sample BATS 15 m from the Bermuda Atlantic Time-Series (van de Flierdt et al., 2012), revealing typical patterns for open ocean seawater with a progressive enrichment from light REEs (LREEs) to heavy REEs (HREEs). The HREE to LREE ratios (here: $([Tm]_N+[Yb]_N+[Lu]_N)/([La]_N+[Pr]_N+[Nd]_N)$, whereby "N" refers to PAAS-normalized concentrations) are constant in waters with σ_θ > ~27.7 (4.3, 1 SD = 0.3, n = 58), and overall lower in waters with σ_θ < ~27.7 (3.8, 1 SD = 0.3, n = 44), with lowest ratios determined in NEGSSW (3.5, 1 SD 0.2, n = 13). A negative cerium anomaly is observed for all samples, and the Ce/Ce* ratio (defined as the $[Ce]_N/([(La]_N+[Pr]_N)/2])$ varies between ~0.10 (PW) and ~0.25 (mostly AW) at the

surface with most samples having ~0.2. A slight decrease in Ce/Ce* from ~0.2 to ~0.1 is observed with depth.

The Nd isotopic compositions range between ε_{Nd} = -12.4 and -8.8 for all samples (Figs. 2-4 and 6). Waters with σ_θ > ~27.7 and shallower than ~500 m (mostly classified as AW/RAW) have relatively unradiogenic compositions (least radiogenic ε_{Nd} = -12.2±0.2) compared to intermediate and deep waters deeper than ~500 m depth (most radiogenic ε_{Nd} = -9.5±0.2), with the exception of station 68 that shows more radiogenic signatures in the upper ~500 m of the water column even if the potentially contaminated surface sample is not considered (Fig. 3). On the western Svalbard Shelf, a slightly more radiogenic Nd isotopic composition is also observed for surface waters (ε_{Nd} = -10.6±0.2). Waters with σ_θ < ~27.7 have different Nd isotopic compositions, largely following the distribution of the water masses defined by θ-S and nutrient properties. The NEGSSW

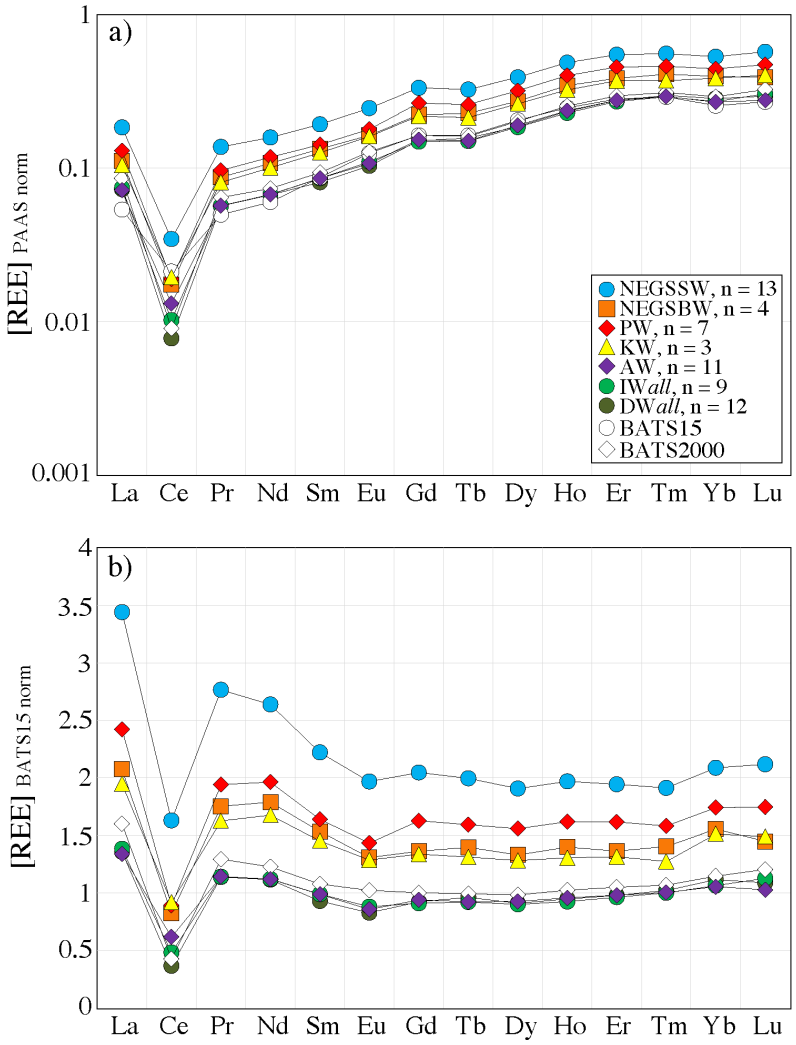

Figure 5: a) Post-Archean Australian Shale (PAAS; McLennan, 2001) normalized REEs (plotted on log scale). Averages of selected water masses (as introduced in figure 2 and IWall = all intermediate waters, DWall = all deep waters) are plotted together with Bermuda surface water (BATS15) and Bermuda deep water (BATS2000) (van de Flierdt et al., 2012). b) Bermuda surface water (BATS15) normalized REEs.

has less radiogenic signatures (ε_{Nd} = -11.7, 1 SD = 0.5, n = 13), similar to AW/RAW samples. In contrast, PW and KW have more radiogenic εNd signatures including the most radiogenic sample of the data set (ε_{Nd} = -8.8±0.2). Such signatures are dominant in surface waters near ~5° W, but also can be found on the NE Greenland Shelf at ~150 m depth following the isoline of S ≈ 33 (Fig. 4). Deeper than this depth less radiogenic signatures with ε_{Nd} = -11.8 (1 SD = 0.2, n = 4) characterize NEGSBW.

At the Laptev Sea margin, water with typical θ-S characteristics of AAW has [Nd] = 16.4 pmol/kg and ε_{Nd} = -10.0±0.1 at ~200 m depth. Surface seawater (S ≈ 7) close to the Lena River delta has [Nd] = 556 pmol/kg and ε_{Nd} = -15.7±0.2.

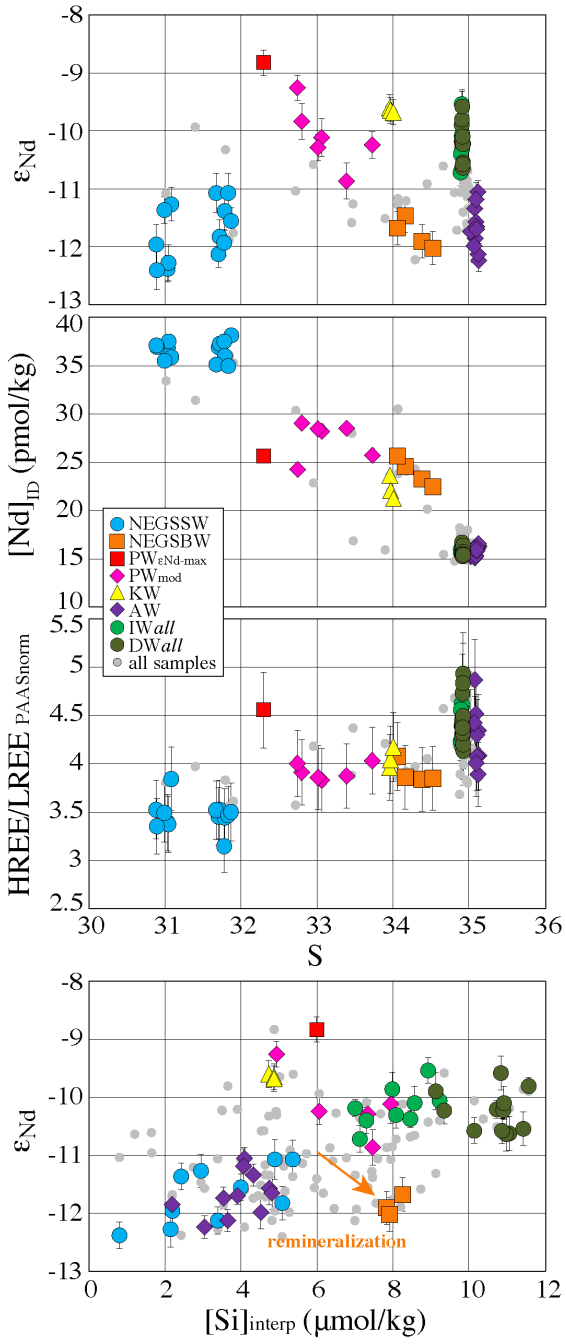

Figure 6: Salinity versus ε_{Nd}, $[Nd]_{ID}$ and HREE/LREE (PAAS-normalized), as well as interpolated silicate concentrations ($[Si]_{interp}$, in µmol/kg) versus εNd plots for all samples (grey dots) and distinct water masses (see legend) as defined in text. The composition of NEGSBW does not correspond to what can be expected from mixing between AW/RAW and PW or KW, but rather suggests that local remineralization occurred and resulted in an increase of [Si] and a shift towards less radiogenic ε_{Nd} signatures (orange arrow).

5. Discussion

5.1 Transport and modification of Nd isotopes in the Fram Strait

The waters occupying most of the Fram Strait water column (σ_θ > ~27.7) show no significant variations in dissolved [REE], in contrast to the dissolved Nd isotopic composition that changes from relatively unradiogenic values at shallow depths (< ~500 m) to more radiogenic values in intermediate and deep layers (Figs. 2, 3 and 6). The absence of vertical gradients in $[Nd]_{ID}$ (Fig. 3) and REE patterns (Fig. 5) between shallow, intermediate and deep waters and the differences in ε_{Nd} signatures between waters of the upper and the deeper water column together clearly demonstrate that significant REE release from sinking organic or inorganic particles does not occur in the open Fram Strait, given that this would result in increasing [REE] and a change of the ε_{Nd} signatures of the intermediate and deep water masses towards the less radiogenic signatures of the upper waters. In contrast, the apparent oxygen utilization (AOU) increases with depth (contour lines in [Nd] plot of Fig. 3), which points to decomposition of organic matter that may result in REE release and a change of the ambient dissolved Nd isotope compositions. In the North Atlantic an increase in AOU is accompanied by either increasing [Nd] that is attributed to remineralization of organic particles below productive waters (Stichel et al., 2015) or constant [Nd] in regions of strong lateral advection (Lambelet et al., 2016). The latter scenario may be conceivable for the Fram Strait region, but almost constant [REE] are observed throughout the water column of the entire open AM (Andersson et al, 2008; Porcelli et al., 2009; Yang and Haley, 2016), indicating that remineralization of organic particles does not control the Nd isotope and REE distributions, not even in regions characterized by weak lateral advection (e.g. the deep central Canada Basin, Yang and Haley, 2016).

The most likely explanation for the absence of particulate REE release in the AM is the overall low primary productivity in the upper central AO due to the light limitation caused by a permanent sea-ice cover (Fernández-Méndez et al., 2015 and references therein), which results in low particle fluxes and in the suppression of significant vertical REE transport to intermediate and deeper layers. While the largest direct source of terrestrial REEs to the AM is the Arctic rivers (Fig. 1a), their impact on the vertical distribution of REEs in the open AM is limited, too. Recent experiments simulating Arctic estuarine mixing have shown that most of the particle-reactive riverine REEs are bound to inorganic nanoparticles and colloids that are removed from the water column through coagulation in the low-salinity range (Tepe and Bau, 2016). Most of the coagulated REE-bearing colloids are thus likely confined to the shelves, suggesting that potential remobilization of the REEs mainly occurs in proximity to the coast. Their transport to the open AM is also inhibited by the Arctic Circumpolar Boundary Current (e.g. Aksenov et al., 2011) that transports AW and other waters along the Arctic margins (see also Fig. 1a) and thus prohibits direct advection of significant amounts of particles to the open AM. A limited amount of dissolved REEs is advected with the riverine freshwaters (Porcelli et al., 2009), which does, however, not affect the deeper waters below. Supported by the lack of significant vertical fluxes, the dissolved Nd isotope and

REE distributions in the open AM mainly reflect lateral water mass advection and mixing, in agreement with recent findings by Yang and Haley (2016). Our data thus provides further evidence that the REEs exhibit conservative behavior in the entire open AM (in the NS at least down to ~2600 m depth) and that the dissolved Nd isotope distribution is dominantly controlled by lateral advection of water masses and their mixing.

In contrast, the Arctic shelf regions are clearly affected by particle-seawater interactions causing non-conservative REE and Nd isotope behavior (e.g. Dahlqvist et al., 2007; Porcelli et al., 2009). In the Fram Strait region, modification of [Nd] and the Nd isotope signature through remineralization of biogenic particles, remobilization of REEs from coagulated inorganic nanoparticles and colloids and/or REE release from detrital particles clearly occurs in bottom waters on the NE Greenland Shelf (i.e. NEGSBW). The NEGSBW was suggested to be ultimately of AW or RAW origin due to its relatively high temperatures (e.g. Budéus et al., 1997), the advection of AW or RAW on the NE Greenland Shelf from any direction, would however, also result in mixing with PW or KW and cause a shift in the Nd isotopic composition of AW (ε_{Nd} = -11.7, 1 SD = 0.4, n = 11, see section 5.2) towards more positive ε_{Nd} values. Yet, NEGSBW has ε_{Nd} values identical to AW (ε_{Nd} = -11.8, 1 SD = 0.2, n = 4) but significantly higher [Nd] (24.0 pmol/kg, 1 SD = 1.4) than that of AW (15.9 pmol/kg). These Nd characteristics neither reflect pure AW nor can they be explained through pure mixing between AW/RAW and PW or KW (see Fig. 8c and d). Positive AOU values (up to ~50 µmol/kg) and elevated Si concentrations ([Si] ≈ 8 µmol/kg, Fig. 6) instead point to remineralization of biogenic particles formed in the unradiogenic NEGSSW to mostly account for the modification of the ε_{Nd} signatures towards less radiogenic values and higher [Nd] compared to the composition expected from mixing of AW with PW or KW. Remineralization processes have been previously suggested to be common for the area east of the Northwind Shoal (Budéus et al., 1997). The Nd isotopic composition of NE Greenland Shelf particles and surface sediments is unknown, but is likely similar to the highly unradiogenic composition of rocks from NE Greenland (ε_{Nd} ≈ -18, 1 SD = 9.5, n = 45, all samples including references are reported in the data table A4). Relatively long residence times (10-20 years) of NEGSBW on the shelf are evident from transient tracer data obtained during the same cruise (Stöven et al., 2016) and are in agreement with previous studies (Budéus et al., 1997; Top et al., 1997) thus promoting seawater-particle interactions and remineralization processes.

5.2 Origin and fate of Atlantic Water

5.2.1 Composition and distribution of AW and RAW at Fram Strait

The unradiogenic ε_{Nd} values of the upper water column in the eastern and central Fram Strait clearly correlate with the distribution of warm and saline AW entering the AO via the WSC (Fig. 3). Representative AW samples (S > 35.0; θ > 3 °C; 27.70 < σ_θ ≤ 27.97) have an average ε_{Nd} of -11.7 (1 SD = 0.4, n = 11) and [Nd] = 15.9 pmol/kg (1 SD = 0.5), similar to an AW sample collected in 2011 at the same latitude (ε_{Nd} = -11.9±0.27 and [Nd] = 16.8 at

150 m depth; Werner et al., 2014) and three AW samples collected in 2001 in the upper water column north of Svalbard (average ε_{Nd} = -11.8 with 1 SD = 0.5 and [Nd] = 16.6 with 1 SD = 0.2; Andersson et al., 2008). These data are also identical to two unfiltered samples from the upper water column collected in 1999 at ~77.7° N and ~7.7° E (average ε_{Nd} of -11.5 with 1 SD = 0.4; data from station 29, Lacan, 2002). Our high resolution data also show that the least radiogenic ε_{Nd} signatures within the AW layer are observed at stations 19, 26 and 55 (Fig. 3) and seperated through waters with slightly more radiogenic signatures and lower salinities at ~5° E. This distribution might either reflect the cores of the Yermak (at ~3.7° E) and Svalbard (at ~7° E) branches of the AW (e.g. Rudels et al., 2000; Walczowski et al., 2005), or document the eddy activity in the region (e.g. Hattermann et al., 2016; von Appen et al., 2016a).

The identification of a distinct AW signature with an ε_{Nd} = -11.7 in the Fram Strait is not consistent with the previous assumption that all waters entering the AO have a homogeneous ε_{Nd} signature of -10.8 (cf. Andersson et al., 2008; Porcelli et al., 2009). This misconception was mainly a result of the lack of data with typical θ-S characteristics of AW (e.g. no Nd samples were collected in depths < ~600 m in the eastern Fram Strait before 2011). Instead, inputs from Svalbard shelf sediments were invoked to account for the less radiogenic compositions of samples collected in 2001 north of Svalbard (Andersson et al., 2008), which is in agreement with relatively high [Nd] (up to 30 pmol/kg) determined in samples shallower than ~100 m depth but not consistent with the low [Nd] of the three above-mentioned AW samples recovered below ~100 m in 2001. This suggests that either inputs from Svalbard shelf sediments increase [Nd] in waters without significantly affecting the Nd isotopic composition or that waters with relatively high [Nd] but similar ε_{Nd} signatures are admixed to the upper water column north of Svalbard. The samples with the relatively high [Nd] exhibit slightly lower salinities compared to the three AW samples, which is consistent with admixture of small quantities of freshwater and argues against lithogenic Nd input from Svalbard.

Our surface samples recovered on the Svalbard continental shelf in addition argue against any Nd input from western Svalbard to the Fram Strait region. The shift towards more radiogenic ε_{Nd} values (-10.6±0.19 in near surface sample next to the ship) and lower [Nd] (~15 pmol/kg) and S (~34.5) in comparison to AW points to contribution of surface waters with sea-ice meltwater, provided that less Nd is released from the sea ice during melting than initially present in the water of the melting area (i.e. resulting in dilution of Nd). Input of Nd from Svalbard would likely result in an increase in [Nd] and yield a shift towards less radiogenic Nd isotopic compositions, as indicated by the relatively unradiogenic ε_{Nd} signatures of beach deposits of western Spitsbergen (Fig. 1b). The latter are relatively uniform with an average ε_{Nd} of -14.6 (1 SD = 1.84, n = 6) and perhaps more suitable to evaluate Nd input from Svalbard than the variable ε_{Nd} signatures of Svalbard rocks (the range in rock ε_{Nd} values for particular Svalbard areas is shown in Fig. 1b; rock and beach deposit samples including references are provided in the data table A4). The small mean annual discharge (~20 km^3 for entire Svalbard) also argues against significant contributions of freshwater and Nd from Svalbard (Beszczynska-Möller et al., 1997 and references therein). We therefore instead suggest

that the Nd isotope characteristics observed on the western Svalbard Shelf reflect the advection of Arctic-derived cold and less saline Polar Water with relatively high sea-ice meltwater fractions. These waters most likely originated in the Barents Sea and have been transported northward within the Sørkapp Current, an extension of the East Spitsbergen Current (Walczowski, 2013 and references therein).

Three shallow and intermediate samples of station 86 have ε_{Nd} values identical to AW (-11.6, 1 SD = 0.1), but most likely correspond to RAW as they are clearly separated from AW by more radiogenic ε_{Nd} signatures at ~1° E (station 68) (Fig. 3). This distribution indicates admixture of more radiogenic intermediate waters to shallower depths, which is consistent with lowered S and T at ~0.5° E. Mesoscale eddies generated in the WSC (von Appen et al., 2016a) have been shown to be involved in the westward and subsequent southward transport of the Yermak Branch, with the most intensive recirculation occurring between 78° N and 81° N (e.g. Hattermann et al., 2016; Walczowski, 2013). These eddies might induce upwelling and thus perhaps were responsible for the vertical mixing of the more radiogenic Nd isotope signatures observed at station 68 in 2012. About half of the northward transport returns back into the NS without significant changes in θ-S characteristics (de Steur et al., 2014; Marnela et al., 2013). The ε_{Nd} data also argue for little transformation of the returning waters and confirm that RAW returns immediately north of the Strait without significantly mixing with other waters. The Nd isotopes further suggest that modified RAW extends as far as the Greenland continental margin at depths between ~200 and ~400 m (below PW and KW), consistent with relatively high T and S observed at these depths (Fig. 3).

5.2.2 Modification of AW within the AM

Our new data and the compilation and reassessment of literature seawater Nd data collected at different locations within the AM provide evidence that the Nd isotopic composition of AW gradually changes during transport across the AM from unradiogenic signatures ($\varepsilon_{Nd} \approx -13$) at the Greenland-Scotland Ridge (GSR) towards more radiogenic signatures ($\varepsilon_{Nd} \approx -9$) in the Canada Basin (Fig. 7). Changes in θ, S and potential density characteristics within the AW layer were previously assigned to heat loss due to ice melting and exchange with the atmosphere and/or mixing with colder waters from the Barents Sea, the Bering Strait and with river runoff, resulting in the formation of the Atlantic-derived halocline water and a cooler ($\theta \leq 2$ °C) AAW (e.g. Rudels et al., 2015). The continuous change in θ, S and potential density in Nd samples compiled from different years implies that they can be used to assess general trends in Nd isotope characteristics and the processes causing them. In contrast to elevated [Nd] in AW samples from the Denmark Strait and the eastern Norwegian Sea/Lofoten Basin (> 19 pmol/kg), the [Nd] of most AW samples from other locations is uniform at ~16 pmol/kg (except Canada Basin), including the AW at the Iceland-Scotland Ridge (i.e. the main inflow area of AW, [Nd] = 16.2 pmol/kg, 1 SD = 2.1, n = 7) (Fig. 7b). This implies that local modification of Nd characteristics in AW samples from the Denmark Strait

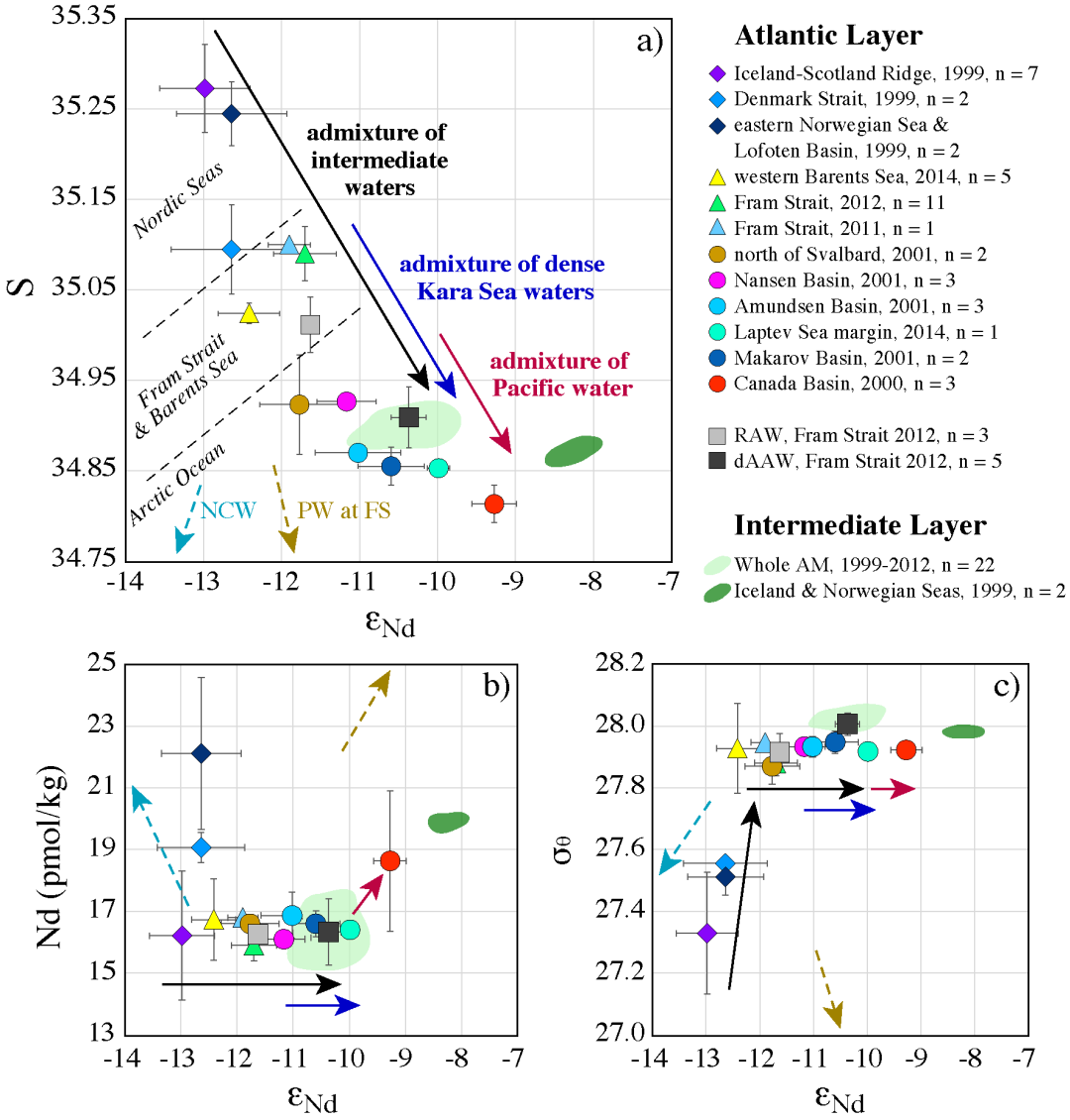

Figure 7: Assessment of the composition of AW within the AM. Only samples with θ > 0 °C (all) and 27.70 < σ_θ ≤ 27.97 (AW and AAW within the Arctic Ocean) have been used. Atlantic-derived water entering the AM through the Iceland-Scotland Ridge is modified subsequently towards more radiogenic compositions through admixture of intermediate waters, dense Kara Sea waters and Pacific-derived waters. Admixture of Norwegian Coastal Water (NCW) or Polar Water (PW) cannot account for the observed compositions of AW samples. Light and dark green areas are the compositional fields of intermediate waters from the entire AM and the Iceland and Norwegian Seas, respectively.

and the eastern Norwegian Sea/Lofoten Basin must have occurred and we consequently exclude these from further discussion of water mass mixing.

A change in the Nd isotopic composition without significant changes in [Nd] can be attributed to either admixture of other water masses with similar [Nd] or by seawater-particle exchange (i.e. boundary exchange; Jeandel and Oelkers, 2015). Intermediate waters below the AW layer in the whole AM have more positive ε_{Nd} values but [Nd] overall identical to AW except in the Iceland and Norwegian Seas (Fig. 7b). Admixture of

such waters could explain the change in ε_{Nd} as well as T, S and potential density (Fig. 7c) as far as the Laptev Sea continental slope (in particular in the Nordic Seas, where deep water convection involves conversion of inflowing warm AW to deep cold water). Further north and east, admixture of old and dense Kara Sea shelf waters may cause additional shifts towards radiogenic ε_{Nd} without significantly affecting [Nd]. These waters may have acquired the ε_{Nd} signature of Yenisei and/or Ob freshwater but at the same time have low [Nd], since most of the riverine Nd may have likely been removed through coagulation of REE-bearing nanoparticles and colloids from the water column in the Kara Sea. In the Canada Basin, deep-water ventilation with involvement of relatively radiogenic PACW evolving from the Chukchi Sea with [Nd] around 30 pmol/kg could result in further modification towards more radiogenic ε_{Nd}, but also result in a slight increase in [Nd] (Porcelli et al., 2009).

Clearly, most of the compositions observed in the AW layer of the AM can be explained by admixture of the above-mentioned waters, which overall agrees with previous observations based on θ, S and potential density characteristics (e.g. Rudels et al., 2015) and which suggests that consideration of significant seawater-particle exchange is not required. Admixture of significant amounts of relatively radiogenic PW or KW that leaves the AO through Fram Strait would result in a strong increase in [Nd] and a decrease in S and thus cannot account for the observed change (Fig. 7a and b). Significant admixture of NCW is also unlikely, as this water mass has a less radiogenic ε_{Nd} (-14.5) than AW.

After transport through the AO, AW ultimately leaves the AO via the EGC as cold, modified AAW (e.g. Rudels et al., 2005). Our Nd data does not provide evidence for a distinct AAW layer in 2012, but instead points to a water body that exhibits θ-S and potential density characteristics of dense AAW (dAAW). This water mass is observed in the western Fram Strait between ~3 and 5° W and between ~400 and ~900 m depth characterized by a homogeneous ε_{Nd} value of -10.4 (1 SD = 0.2, n = 5) and [Nd] = 16.3 (1 SD = 1.1). Based on our comparison with other AW samples from the AO, most of the dAAW observed at Fram Strait must have recirculated within the Eurasian part of the AO (see Fig. 7). This is also in agreement with the relatively low ventilation ages of dAAW (~30 years) based on transient tracer data (Stöven et al., 2016), which suggests that these waters took the short loop within the AO (cf. Tanhua et al., 2009). The fate of dAAW in the NS is unknown although its flow within the EGC at intermediate depths and its similar Nd isotopic composition to the precursor of Denmark Strait Overflow Water (Lacan and Jeandel, 2004a; in the data tables A1 and A2 referred to as AIW/GS) indicates that a part of it leaves the NS within the Denmark Strait Overflow Water. Indeed, about half of the overflow water supplied from the AM to North Atlantic Deep Water has passed the AO (Rudels, 2009), which argues for a significant contribution of dAAW to the overflow.

5.2.3 AW as precursor of intermediate and deep waters

The AW/RAW and dAAW are the main precursors of intermediate and deep waters within the AM. Their mixture with other intermediate waters is not only reflected in a change of the composition of the AW layer, but also reflected in the gradual ε_{Nd} change of intermediate and deep waters from radiogenic signatures in the Iceland and Norwegian Seas and the Lofoten Basin (~ -8.1 to ~ -10.1; Lacan and Jeandel, 2004b) towards less radiogenic signatures in the AO ($\varepsilon_{Nd} \approx$ -10.7; Andersson et al., 2008; Porcelli et al., 2009; Zimmermann et al., 2009). However, conversion of AW/RAW and dAAW to intermediate and deep waters cannot account for the observed radiogenic ε_{Nd} values of the latter, reaching -9.5 in the Fram Strait. The source of these signatures is likely located in the Iceland and Norwegian Seas where the most radiogenic ε_{Nd} signatures within the entire AM were observed in previous studies (i.e. ~ -8.1). Neodymium release from or boundary exchange with the basaltic formations of Iceland and Central-East Greenland is the most likely explanation for the more radiogenic intermediate and deep-water signatures (e.g. Lacan and Jeandel, 2004a), in good agreement with the slightly elevated [Nd] in intermediate waters of these regions (Fig. 7b). Andersson et al. (2008) also suggested boundary exchange along the Canadian archipelago to account for relatively unradiogenic ε_{Nd} signatures (~ -9.8) of intermediate waters northwest of the Fram Strait, as the limited data available for the Arctic inflow area at the time indicated a homogeneous ε_{Nd} composition of ~ -10.8 throughout the water column. Our new data clearly document that ε_{Nd} values around ~ -10 are present in the eastern and western Fram Strait below ~500 m, thus there is no evidence for such a process. The small ε_{Nd} variations below ~500 m do not clearly reflect the water masses defined by their hydrographic properties, which suggests that the intermediate and deep water masses in the AM are well mixed in terms of their Nd distribution.

5.2.4 Origin of AW prior to its entrance into the AM

The relatively unradiogenic ε_{Nd} signature of AW at the GSR most likely originates from contributions of modified Gulf Stream water and Labrador Current water from the North Atlantic. Waters with characteristics similar to AW at the GSR have been recently reported in the region around the Grand Banks and have been attributed to mixing between the Gulf Stream and the Labrador Current (Lambelet et al., 2016). The relatively unradiogenic ε_{Nd} signature observed in Labrador Sea waters thus most likely not only affects the Nd isotope distribution in the subpolar gyre, but is also responsible for modification of shallower waters within the North Atlantic Current that ultimately enter the AM. This is also in agreement with previous studies based on θ-S properties that identified cooler and slightly fresher Modified North Atlantic Water (MNAW) at the GSR in addition to North Atlantic Water (Hansen and Østerhus, 2000 and references therein). A high contribution of MNAW in AW is further supported by the REE distribution of AW in the Fram Strait, which is characterized by [MREE] and [HREE] and slightly enriched [LREE] (except Ce) similar to the NW Atlantic Ocean (BATS 15 m and

BATS 2000 m; van de Flierdt et al., 2012) and indicates that admixture of Labrador Sea waters mainly results in an increase of [LREE] (Fig. 5b).

5.3 Distribution, composition and fate of Arctic-derived waters

Despite several attempts to decipher the different fractional components within the Arctic-derived waters (e.g. Dodd et al., 2012; Falck, 2001; Falck et al., 2005; Jones et al., 2008b; Rabe et al., 2013; Taylor et al., 2003), a clear picture of the distribution, composition and fate of these waters is still missing, particularly because observations of the above mentioned studies do not agree with earlier results suggesting the contribution of locally formed waters in the western Fram Strait (Bignami and Hopkins, 1997; Budéus and Schneider, 1995; Budéus et al., 1997). The Arctic-derived waters discussed here (i.e. PW and KW) were defined based on findings of Budéus et al. (1997) and Bignami and Hopkins (1997), who used recurring θ-S features and silicate concentrations ([Si]) to distinguish between locally formed and imported water masses. However, the [Si] can be affected through biological production and remineralization processes, which in 2012 most likely caused low to zero [Si] in NEGSSW (Fig. 4) and elevated [Si] ≈ 8 µmol/kg in NEGSBW (Figs. 4 and section 5.1), respectively. Hence, the [Si] distribution reliably traces PW and KW only in areas where direct advection from the AO is evident. The general current distribution in Fram Strait and over NE Greenland Shelf (e.g. Beszczynska-Möller et al., 2012; Bourke et al., 1987; Woodgate et al., 1999) suggests that PW and KW are directly advected above the Greenland continental slope where they significantly contribute to the formation of the core of the EGC. The elevated [Si] at ~5 °W thus clearly can be attributed to PW imported from the AO and the associated relatively radiogenic ε_{Nd} signatures (including the most radiogenic value of the Fram Strait section with ε_{Nd} = -8.8±0.2, $PW_{\varepsilon Nd\text{-}max}$) and elevated $[Nd]_{ID}$ (Fig. 1b, 3 and 4) also must have been directly imported from the AO and likely represent undiluted compositions of PW and KW. The relatively radiogenic values follow salinities of ~33 and [Si] > ~8 µmol/kg on the NE Greenland Shelf, pointing to the presence of PW on the shelf down to ~150 m depth and confirming that [Si] on the shelf can either be formed through local remineralization or can be imported from the AO (Budéus et al., 1997).

Neodymium isotope based mixing calculations show that most PW and KW samples lie close to the mixing line between AW that enters the AO through Fram Strait and modified Pacific Water leaving the Chukchi Sea shelf (PACW) (Fig. 8a and b). All PW and KW samples have too high [Nd] and too low S for their ε_{Nd} to directly plot on the mixing line and thus require contributions from a third end-member or a process to explain this offset. Arctic rivers constitute the second largest REE source in the AM (Fig. 1a and data table A1) and dominate the Nd in the shallow waters (e.g. Porcelli et al., 2009). Their contribution is thus most likely responsible for the offset from the mixing line towards higher [Nd] and lower S (see also Andersson et al., 2008), which inhibits a quantitative assessment of the three end-members based on Nd isotopes alone since contributions of riverine Nd may originate from any of the major Arctic rivers and would

result in differing increases in [Nd] and changes in ε_{Nd}. The mass balance calculations based on $\delta^{18}O$, S and nutrients (N/P and PO* methods) however provide further information on the composition and provide quantitative fractions for meteoric water. The amount of f_{MW} for the $PW_{\varepsilon Nd\text{-}max}$ sample that represents pure PW is ~6 to ~8 %, and for KW samples is even lower (< ~5 %), which documents a small amount of river water being present in the Arctic-derived waters in the Fram Strait. Although the initial [Nd] in rivers can be 100 times as high as in seawater most of the riverine Nd is removed in estuaries and on the Siberian shelves (Porcelli et al., 2009), which together with the low f_{MW} implies a relatively low contribution of riverine Nd to these waters and suggests that the shift of the ε_{Nd} signature caused by addition of riverine Nd was overall small. The ratio between PACW and AW of $PW_{\varepsilon Nd\text{-}max}$ thus likely is close to ~ 2:3, and results in Nd-based PACW fractions (f_{PACW}) as high as ~30 % for Arctic-derived waters (Fig. 8a and b). This Nd-based maximum f_{PACW} matches the maximum f_{PAC} (up to ~30 %) determined with the PO* method, but does not agree with the maximum f_{PAC} (up to ~70%) determined with the N/P method (see Fig. 4), pointing to uncertainties in end-member definitions for the calculation of the PAC fractions. In particular denitrification on the Siberian Shelves can result in overestimation of the N/P-based f_{PAC} (Anderson et al., 2013; Bauch et al., 2011), suggesting that the "Pacific-derived Water" end-member used in the N/P method does not represent a pure water mass composition. Despite these uncertainties, the contribution of PACW/PAC is supported by low Ce to Ce* ratios ("Ce anomaly") seen in PW samples that overall have the strongest Ce anomalies in surface waters of the entire Fram Strait section. A strong Ce anomaly can be attributed to continuous removal of $Ce(IV)O_2$ and may be indicative of the time a water mass was isolated from fresh, unfractionated continental inputs (Hathorne et al., 2015), which is in agreement with the age and the flow path of Pacific-derived water that must have traveled across the entire AO.

The origin of PW can be attributed to the Pacific-derived upper halocline (Jones and Anderson, 1986) and more shallow waters of the Canada Basin for S < 33 based on its [Si] and the salinity properties. Comparison with literature Nd data in addition suggests that PW is advected through the Amundsen and Makarov Basins (Fig. 8a and b), indicating transport of the Pacific-derived component of PW along the continental slope of the East Siberian Sea into the Transpolar Drift and the western Fram Strait (cf. Aksenov et al., 2016). An Atlantic origin was suggested for KW by previous studies due to the distinct θ-S properties and low [Si] (e.g. Budéus et al., 1997), as well as f_{PAC} close to 0 % (Falck, 2001). Rudels et al. (2005) have shown that waters with such θ-S properties form north of Svalbard, where melting of sea ice above the AW creates a less saline upper layer. Although f_{SIM} of our KW samples is negative or close to zero and therefore rather indicates addition of brine waters instead of sea-ice melt, this does not contradict the formation process mentioned above given that freezing and melting may occur simultaneously during this process (Rudels et al., 1999a) and will result in different f_{SIM}. Furthermore, addition of SIM would most likely cause a decrease in Nd concentration (i.e. through dilution) without significantly affecting the Nd isotopic composition, the PACW to AW ratio thus would mostly remain unaffected. According to our Nd isotope

mixing calculations the PACW to AW ratio of KW is about 1:4, which confirms a high contribution of AW (~80 %) (Fig. 8a and b). The comparison with literature Nd data from the AM shows that KW shares characteristics with shallow samples from the Nansen Basin (Fig. 8a and b), and thus further supports the origin of these waters to be located north of Svalbard.

South of Fram Strait both PW and KW can be traced along the Greenland continental slope as far as the Denmark Strait. While shallow waters of the southern and western NS only show minor amounts of these waters, most of the Nd isotope

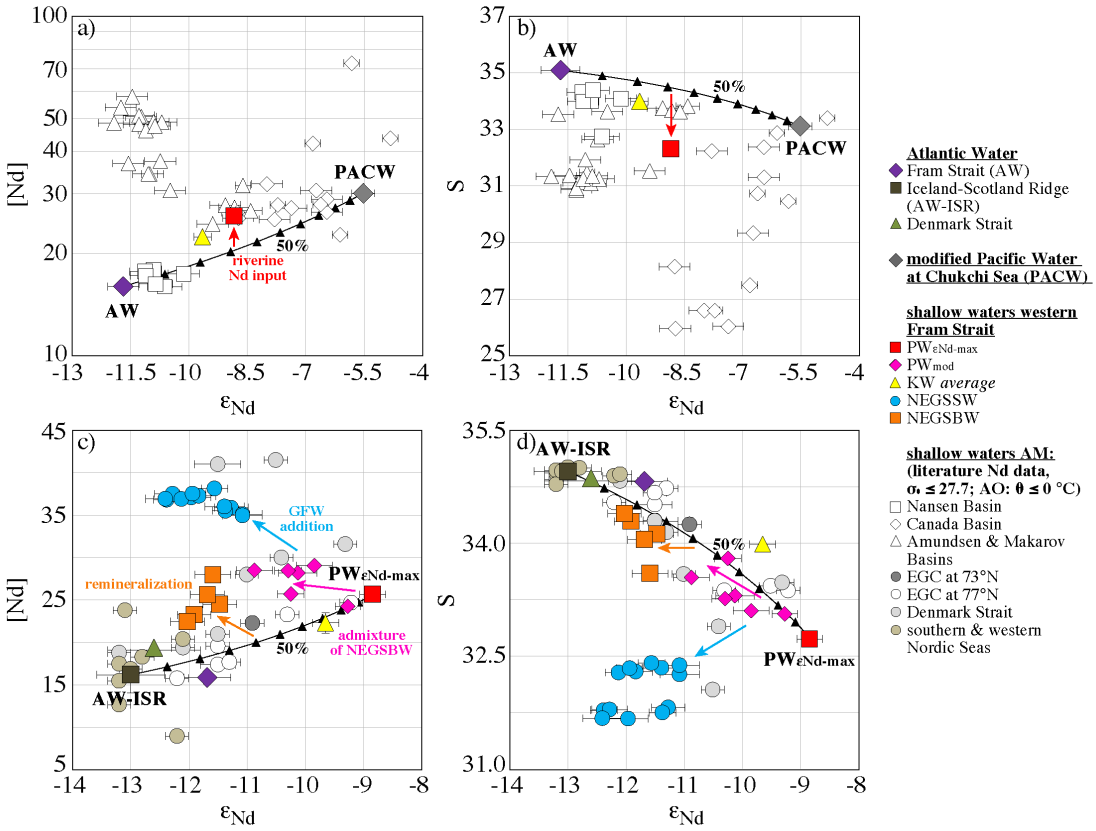

Figure 8: a) and b) Assessment of the Arctic source of PW and KW. The most radiogenic PW sample ($PW_{\varepsilon Nd\text{-}max}$) can be explained by admixture of mainly AW and PACW and a small amount (6-8 %) of river water (red arrows). The AW to PACW ratio for $PW_{\varepsilon Nd\text{-}max}$ is about 3:2, while it is for KW 4:1, with less amount of river water (< 5 %). $PW_{\varepsilon Nd\text{-}max}$ shares characteristics with shallow samples ($\sigma_\theta \leq 27.7$, $\theta \leq 0$ °C) from the Amundsen and Makarov Basins, while characteristics of KW more closely match those of shallow samples from the Nansen Basin. c) and d) Assessment of the fate of PW and KW in the Nordic Seas. Shallow waters in the Nordic Seas ($\sigma_\theta \leq 27.7$) can be mostly explained as a mixture of Polar Water exiting the AO through the western Fram Strait (here represented as $PW_{\varepsilon Nd\text{-}max}$ and KW) and Atlantic-derived water from the Iceland-Scotland Ridge (AW-ISR), the Denmark Strait or the Fram Strait. Modified PW samples (PW_{mod}) show an increase in [Nd] and S, which can be attributed to admixture of NEGSBW (pink arrows). Modification through Greenland shelf sediments is observed in NEGSBW towards higher [Nd] and less radiogenic ε_{Nd} signatures at constant salinities (orange arrows). In contrast, addition of Greenland freshwater (GFW) is documented in NEGSSW with a strong increase in [Nd] and a decrease in salinities (blue arrows). Most of the samples within the EGC and the Denmark Strait show either modification through Greenland shelf sediments or addition of GFW. Samples from the southern and western Nordic Seas do not show significant contribution of Arctic-derived PW and KW.

characteristics of shallow waters of the EGC at 73 and 77° N and the Denmark Strait can be explained by their advection and admixture of AW from the ISR, the Denmark Strait or the Fram Strait (Fig. 8c and d). An increase in [Nd] and S in PW samples that have less radiogenic ε_{Nd} values compared to $PW_{\varepsilon Nd\text{-}max}$ (resulting in modified PW, PW_{mod}) indicates local admixture of NEGSBW (Fig. 8c and d) after its interaction with Greenland shelf sediments (section 5.1), which results in an increase in [Nd] and a shift towards lower ε_{Nd} at constant S. In contrast, addition of Greenland freshwater (GFW) causes an increase in [Nd] and a decrease in salinity, while the ε_{Nd} signature is shifted towards less radiogenic values (section 5.4). Both processes could also account for the composition of samples obtained from the Denmark Strait, while samples from the EGC at 73 and 77° N do not show such a pronounced interaction with GFW or NEGSBW.

We point out that the composition of PW and KW presented in this study represents only a snapshot of the water mass distribution in the Fram Strait (i.e. summer 2012). Several studies have shown that the f_{MW}, f_{SIM} and f_{PAC} of PSW that leaves the AO through the western Fram Strait exhibit seasonal as well as interannual variability (e.g. Dodd et al., 2012; Falck, 2001; Falck et al., 2005; Jones et al., 2008b; Rabe et al., 2013; Taylor et al., 2003). Future multi-year surveys that include Nd isotope and REE measurements will test the promising sensitivity of Nd isotopes and REEs to reflect and quantify these changes.

5.4 Admixture of Greenland freshwater

Studies carried out in the mid-1990s pointed to contribution of locally formed waters on the NE Greenland Shelf (Bignami and Hopkins, 1997; Budéus and Schneider, 1995; Budéus et al., 1997). Bignami and Hopkins (1997) in particular suggested that shelf surface waters that show a "fanning out" of the temperature below S ~32 in the θ-S field can be attributed to local runoff and modification by local heating and ice melting, while shelf intermediate waters (S ~32) form convectively through loss of buoyancy to the atmosphere with the surface waters as the source waters. These findings are supported by a substantial change from ε_{Nd} = -8.8 ($PW_{\varepsilon Nd\text{-}max}$) to $\varepsilon_{Nd} \approx$ -12 (NEGSSW) observed on the shelf of Greenland, which is accompanied by an increase in [Nd] and a slight decrease in HREE/LREE and S (Figs. 4 and 8). A concurrent increase in f_{MW} from ~6-8 % to ~13 % at first glance would in combination with the shift in ε_{Nd} suggest additional contribution from an Arctic river with relatively unradiogenic Nd isotopic composition (e.g. Mackenzie or Lena River, Fig. 1a). Surface samples obtained from the Amundsen and Makarov Basins with likely high fractions of riverine Nd indeed document characteristics similar to NEGSSW and may thus be the origin of NE Greenland Shelf waters. However, it is unlikely that the relatively unradiogenic ε_{Nd} signatures observed in shallow waters of the central AO would be preserved during their transport to the NE Greenland Shelf, as admixture of PW and KW would modify these signatures towards more positive ε_{Nd} values. We therefore suggest that the source of the Nd and the isotopic composition of NEGSSW is local and located west of the EGC.

The freshwater flux from Greenland to the AM was ~200 km^3/yr in 2010, with a general trend towards increasing fluxes in the last few decades (Bamber et al., 2012). Contribution of GFW (precipitation and Greenland Ice Sheet melt) to coastal and shelf waters off Greenland was recently investigated by Stedmon et al. (2015). Their data from the same year as our cruise (September) and the same location indicate GFW fractions (f_{GFW}) as high as ~4 % for waters with θ-S properties similar to NEGSSW, which clearly points to significant changes of the Nd characteristics, in agreement with the shift observed between PW/KW and NEGSSW. Dissolved [REE] in glacial-derived waters from western Greenland for example are ~60 times higher (for [Nd]) than those of typical seawater and indicate significant input of REEs from Greenland to the North Atlantic (Tepe and Bau, 2015). Similarly, high [Nd] (~100 pmol/kg) and $\varepsilon_{Nd} \approx -3.5$ have been reported for East Greenland Shelf waters ($30.5 < S < \sim 33$) at 68° N and were suggested to derive from lithogenic inputs from Greenland (Lacan and Jeandel, 2004a).

For our study area, we assume that all river water (this is f_{MW} if precipitation is neglected) contained within PW is derived from the AO and that the difference between f_{MW} of PW and NEGSSW was caused by GFW addition. The resulting $\delta^{18}O$ and salinity based mixing calculation shows that f_{GFW} reaches ~6 % in NEGSSW (Fig. 9a), which is similar to estimates of Stedmon et al. (2015) based on calculations involving $\delta^{18}O$ and colored dissolved organic matter. The presence of brines ($f_{SIM} < 0$) and sea-ice melt ($f_{SIM} > 0$) results in small offsets from our mixing line. The Nd isotopic composition of the GFW end-member is unknown, but is assumed to be relatively unradiogenic based on Nd isotopic compositions of rocks from NE Greenland (samples including references are reported in the data table A4). We used the average rock Nd isotopic composition ($\varepsilon_{Nd} \approx -18$, 1 SD = 9.5, n = 45) and adjusted the Nd concentration of the GFW end-member until the mixing line matched the f_{GFW} of the surface sample with the highest [Nd], resulting in [Nd] = 210 pmol/kg, which is within the range of concentrations reported for glacier-derived waters from other sites (e.g. Lacan and Jeandel, 2004a; Tepe and Bau, 2015) and supports our hypothesis that the admixture of GFW is the cause of changes in Nd isotopes and REEs. Note, however, that the calculation of [Nd] does not account for any REE removal during salt-induced coagulation of REE-bearing nanoparticles and colloids in the low-salinity range (e.g. Tepe and Bau, 2016), which contrasts with REE release assumed to be significant only in NEGSBW, i.e. after the aggregated nanoparticles and colloids reached the depth of remineralization (~200 m, see section 5.1).

Strikingly, as seen in Fig. 9b, the expanded Nd isotope mixing calculation also reveals that the sea-ice related changes observed for $\delta^{18}O$ and salinity likely are also mirrored by the [Nd], resulting in too low [Nd] in NEGSSW surface samples (~10 m depth) and too high [Nd] in NEGSSW intermediate depth samples (~60 m) for their f_{GFW}. This supports that sea-ice melting may account for the decrease in [Nd] (i.e. through dilution), while sea-ice formation results in a brine signal that may account for excess [Nd]. The ε_{Nd} signature changes towards higher values for all samples (Fig. 9c), suggesting either that the Nd isotopic composition changes during addition of both brine and sea-ice meltwater, or indicating that the GFW end-member Nd isotopic composition is slightly more radiogenic than we assumed (e.g. $\varepsilon_{Nd} = -14$, Fig. 9c).

Nevertheless, all REEs of NEGSSW samples are enriched in comparison to PW and resemble REE characteristics of glacially fed rivers from western Greenland characterized by relative enrichments of LREEs compared to HREEs (Tepe and Bau, 2015), further supporting GFW addition.

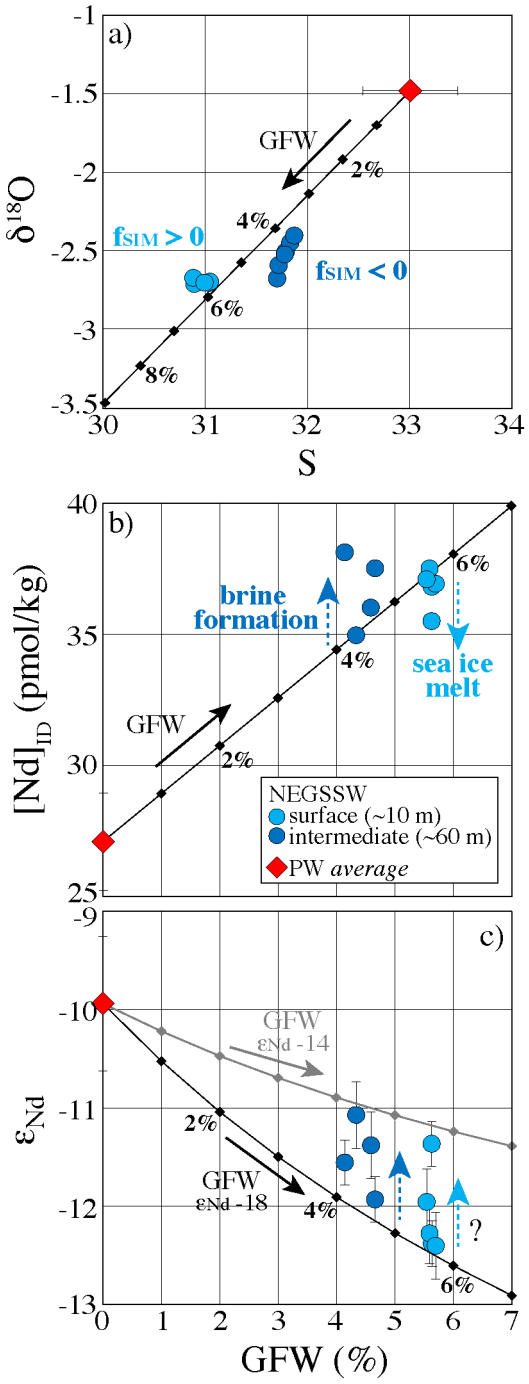

Figure 9: Mixing between Greenland freshwater (GFW; $\delta^{18}O$ = -23.4 ‰; ε_{Nd} = -18; [Nd] = 210 pmol/kg; S = 0) and Polar Water (PW *average*; $\delta^{18}O$ = -1.5 ‰; ε_{Nd} = -9.9; [Nd] = 27.1 pmol/kg; S = 33.01) on the NE Greenland Shelf. a) $\delta^{18}O$ against salinity, b) and c) $[Nd]_{ID}$ and ε_{Nd} against GFW in percent, respectively. The composition of NEGSSW can be explained by up to ~6 % addition of GFW, but offsets from the mixing line indicate that sea-ice melting and brine formation also affect $\delta^{18}O$ and salinity, as well as [Nd] and Nd isotopes. An alternative mixing line (grey) is shown in c) representing admixture of GFW with a more radiogenic ε_{Nd} signature (ε_{Nd} = -14).

The distribution of GFW on the NE Greenland Shelf and the near-surface anticyclonic circulation scheme (e.g. Budéus et al., 1997; Rabe et al., 2009) both argue for a local source of GFW (e.g. the NE Greenland Ice Stream and its ice tongues Nioghalvfjerdsbræ/79° N Glacier and the Zachariæ Isstrøm) and provide further evidence for the GFW distribution to be restricted to the Greenland Shelf area (e.g. Hopwood et al., 2015). The strong EGC most likely also plays a major role for the entrapment of GFW on the Greenland Shelf. Future potential changes of its strength and eddy variability might regulate the advection of GFW to the central NS and therefore to sites of open-ocean deep convection.

6. Summary and conclusion

This work presents seawater Nd isotope (ε_{Nd}), rare earth element (REE) and stable oxygen isotope ($\delta^{18}O$) data from the Fram Strait and the NE Greenland Shelf obtained on samples collected during the ARKXXVII/1 expedition (June-July 2012). A comparison with hydrographic parameters, biogeochemical data and fractions of different water masses calculated with $\delta^{18}O$, salinity and nutrient based methods allows a comprehensive evaluation of prevailing water masses with implications for the understanding of the circulation within the Arctic Mediterranean (AM).

- Neodymium isotope and REE distributions in the open Fram Strait primarily reflect lateral advection of water masses and their mixing, while any significant influence of vertical processes is not observed. This is likely valid for the entire open AM (in the Nordic Seas at least down to 2600 m) and has implications for paleoceanographic reconstructions.
- Remineralization of biogenic and/or release from detrital particles is recorded in bottom waters on the NE Greenland Shelf and results in a shift towards less radiogenic ε_{Nd} signatures and elevated silicate concentrations. Silicate is either released locally or advected from the Arctic Ocean (AO).
- Atlantic Water (AW) enters the AO through the eastern Fram Strait and is characterized by ε_{Nd} = -11.7 and [Nd] ≈ 16 pmol/kg. This Nd isotope composition of AW is less radiogenic than previously reported and should be used for future oceanographic and paleoceanographic studies. The admixture of intermediate waters, dense Kara Sea waters and Pacific-derived waters to AW within the AM is documented by a continuous change towards more radiogenic ε_{Nd} signatures and decreasing temperatures and salinities. Based on these changes, we confirm that Recirculating Atlantic Water and dense Arctic Atlantic Water (dAAW) return to the Nordic Seas (NS) within the Fram Strait and the Eurasian Basin of the AO, respectively. These waters then significantly contribute to the East Greenland Current (EGC) and part of the dAAW leaves the NS within the Denmark Strait Overflow Water. Significant inputs of Nd from Svalbard to the AW layer are not observed and surface waters on the Svalbard shelf are attributed to Polar Water from the Barents Sea with minor contributions of sea-ice meltwater.

- Intermediate and deep waters have relatively radiogenic ε_{Nd} signatures (reaching -9.5) that were acquired in the SW Nordic Seas (i.e. close to sites of deep water convection) and likely result from Nd inputs from basaltic formations of Iceland and Central-East Greenland. In terms of their Nd distribution, the intermediate and deep-water masses in the AM are well mixed.
- Arctic-derived shallow waters (Polar Water, PW and Knee Water, KW) are found in the western Fram Strait and are characterized by relatively radiogenic ε_{Nd} signatures (reaching -8.8) and variable [Nd] (21 to 29 pmol/kg). Both Nd characteristics and assessments based on S, ^{18}O and nutrients suggest that PW and KW were mostly composed of different proportions of Pacific- (< ~30 %, based on Nd isotopes) and Atlantic-derived waters, as well as of river waters (< ~8 %) in 2012. The fraction of Pacific-derived waters estimated by our approach based on Nd isotopes is in line with that computed with the PO* method, but differs significantly from that computed with the N/P method likely due to end-member uncertainties of the latter. While the PW composition resembles that of the Pacific-derived upper halocline and is most likely advected through the Amundsen and Makarov Basins, higher fractions of AW are evident in the KW, which shares characteristics of previously published Nd data from the Nansen Basin and most likely formed through mixing between AW and sea-ice meltwater. After PW and KW pass the Fram Strait and enter the NS, they mix with AW and constitute a significant fraction of shallow waters of the EGC.
- The admixture of locally discharged Greenland freshwater (GFW) to PW is traced by Nd characteristics and an elevated meteoric water fraction and results in newly formed NE Greenland Shelf Shallow Water (NEGSSW). The amount of GFW in NEGSSW is estimated to be ~6 %. Due to the near-surface anticyclonic circulation on the shelf, this water mass is distributed and accumulated above the shelf and most likely does not enter the central NS directly, which may change in the future due to increasing meltwater inputs and may then have implications for deep convection in the NS.
- The pronounced gradients in ε_{Nd} signatures and REE characteristics in the upper water column of the AM together with $\delta^{18}O$ and standard hydrographic tracers provide a new basis to determine shallow hydrological changes within the AM.

Acknowledgements

We thank the Captain and Crew of RV Polarstern for help in collecting the samples and Toste Tanhua (GEOMAR) for support with the nutrient measurements. We also acknowledge Jutta Heinze (GEOMAR) for laboratory assistance and the editor Tina van de Flierdt and three reviewers for their constructive comments. Benoit Thibodeau is also acknowledged for comments. Furthermore, we thank the German Federal Ministry of Education and Research (BMBF) and the Ministry of Education and Science of the Russian Federation for support of the "Laptev Sea System" project (BMBF grant 03G0833). Dorothea Bauch acknowledges financial support from DFG project BA1689.

CHAPTER II

Transport and transformation of riverine Nd isotope and rare earth element signatures in high latitude estuaries: A case study from the Laptev Sea

***Submitted to EPSL as**: Laukert, G., Frank, M., Bauch, D., Hathorne, E. C., Gutjahr, M., Janout, M., Hölemann, J. and Timokhov, L.: Transport and transformation of riverine Nd isotope and rare earth element signatures in high latitude estuaries: A case study from the Laptev Sea.*

Abstract

Marine neodymium (Nd) isotope and rare earth element (REE) compositions are valuable tracers for present and past ocean circulation and continental inputs. Yet their supply via high latitude estuaries is largely unknown. Here we present a comprehensive dissolved Nd isotope (expressed as ε_{Nd} values) and REE data set together with seawater stable oxygen isotope ($\delta^{18}O$) compositions of samples from the Laptev Sea recovered in two Arctic summers and one winter.

The Laptev Sea is a Siberian Shelf sea characterized by extensive river-runoff, sea-ice production and ice transport into the Arctic Ocean. The large variability in ε_{Nd} (~ -6 to ~ -17), REE concentrations (~16 to ~600 pmol/kg for Nd) and REE patterns is controlled by freshwater supply from distinct riverine sources and open ocean Arctic Atlantic Water. Strikingly and contrary to expectations, no evidence for significant release of REEs from particulate phases was found. Essentially all shelf waters are depleted in light (L)REEs, while the distribution of the heavy (H)REEs shows a deficiency at the surface and an excess in the bottom layer. This distribution documents REE removal through coagulation of riverine nanoparticles and colloids. Removal of riverine REEs starts at salinities near 10 and after a drop of all REE concentrations by ~30 % transfers into preferential LREE removal that for Nd reaches ~75 % at a salinity of 34. Although the delayed onset of dissolved REE removal contrasts with previous observations from most other estuarine environments, it agrees remarkably well with results from recent experiments simulating estuarine mixing with organic-rich river waters. The melting and formation of sea ice and river ice lead to further REE depletion at the surface and enrichment in the bottom water layer as a function of ice melting and brine transfer, respectively. The ice-related processes contribute to the redistribution of other elements and may also affect macronutrient distribution and primary productivity in high latitude estuaries.

1. Introduction

The radiogenic neodymium (Nd) isotopes (the $^{143}Nd/^{144}Nd$ ratio, expressed as $\varepsilon_{Nd} = [(^{143}Nd/^{144}Nd)_{sample}/(^{143}Nd/^{144}Nd)_{CHUR} -1] \times 10^4$ with CHUR = 0.512638 referring to the

'CHondritic Uniform Reservoir', Jacobsen and Wasserburg, 1980) have been widely used to trace modern and past ocean circulation (cf. Frank, 2002, van de Flierdt et al., 2016; van de Flierdt and Frank, 2010). In addition to Nd isotopes, the complete set of dissolved rare earth elements (REEs, here including yttrium) has been shown to provide constraints on the composition of the source areas, on the time that passed since last contact of a water mass with weathering inputs, as well as on particle adsorption and desorption processes (e.g. Garcia-Solsona et al., 2014; Haley et al., 2014; Molina-Kescher et al., 2014; Rousseau et al., 2015). The Nd isotope and REE distribution in the open Arctic Ocean reflects the lateral advection of water masses and their mixing (Andersson et al., 2008; Laukert et al., 2017; Porcelli et al., 2009) but fluxes and behavior of these tracers in Arctic estuarine regions, such as the freshwater-dominated Siberian Shelf seas, are largely unknown. This has so far prevented the utilization of their full potential to determine water mass sources and mixing in high latitudes and to provide information on inputs and ice related processes beyond what is provided by classical hydrographic parameters.

The Laptev Sea is a wide and shallow Siberian Shelf sea characterized by extensive river runoff, strong sea-ice formation and sea-ice transport into the open Arctic Ocean (Fig. 1). It is ice-covered from October to June with mobile pack ice on the deeper shelf and immobile landfast ice across the vast shallower near-shore regions (Bareiss and Görgen, 2005). Southerly winter and spring winds frequently open polynyas (i.e. regions of open water in ice covered regions) north of the landfast ice edge, causing intense heat loss that favors formation of sea-ice and associated dense brines. The latter contribute to the Arctic halocline, which separates the Arctic ice cover from the warm Atlantic-derived waters underneath (Aagaard et al., 1981). The upper water column of the central and eastern Laptev Sea is dominated by variable freshwater contributions from the Lena River. The maximum freshwater runoff in May and June coincides with the onset of sea-ice melting and induces a strong stratification that separates the fresher surface waters from the more saline basin-derived waters. In fall and winter, different processes (e.g. storms, brine transfer, tidal mixing) slowly erode this stratification, leading to a generally well-mixed water column by late winter or spring (Janout et al., 2016). In the northwestern (NW) Laptev Sea, riverine (Ob and Yenisei) waters from the Kara Sea are advected via the Vilkitsky Strait Current (VSC; Janout et al., 2015). In contrast to the Lena River freshwater that exerts important control on the physical and biogeochemical processes on the entire shelf, the flow and influence of the Kara Sea waters has been suggested to be mostly restricted to the outer shelf (cf. Janout et al., 2015).

Here we report the first comprehensive dissolved water column Nd isotope compositions and REE contents for the entire Laptev Sea combined with seawater stable oxygen isotope data obtained from samples recovered during Septembers of 2013 and 2014. This data set is complemented by data obtained from seawater sampled near the Lena Delta during late winter 2012. The results of this study improve the understanding of the general behavior of REEs and Nd isotopes in a freshwater and ice dominated shallow sea.

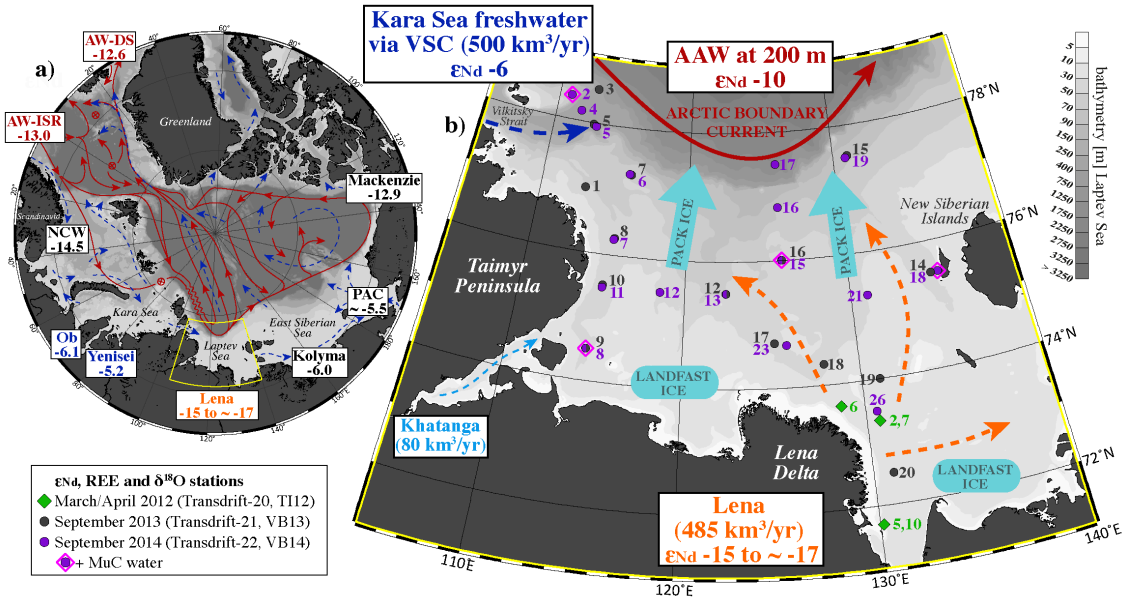

Figure 1: Bathymetric map of the Arctic Mediterranean with the inset representing the Laptev Sea area (IBCAO, Jakobsson et al., 2012). a) Map of the Arctic Mediterranean (i.e. Nordic Seas and Arctic Ocean) with circulation scheme of the upper layers (dashed blue lines) and subsurface Atlantic and intermediate layers (solid red lines) (modified after Rudels et al., 2012). REE sources with known ε_{Nd} values and [Nd] are Atlantic-derived water entering through the Iceland-Scotland Ridge (AW-ISR) and the Denmark Strait (AW-DS), Norwegian Coastal Water (NCW), Pacific-derived water (PAC), major Siberian Rivers (Ob, Yenisei, Lena, Kolyma), and the Mackenzie River. Further information on the Nd sources of the AM including references is provided in Laukert et al. (2017). b) Laptev Sea region with the Arctic boundary current and potential freshwater pathways. REE sources are shown together with their ε_{Nd} values (except for the Khatanga River). In addition, the mean annual freshwater transport is reported for freshwater REE sources (R-Arctic-NET: http://www.r-arcticnet.sr.unh.edu/; Janout et al., 2015). Arctic Atlantic Water (AAW) is modified AW at ~200 m depth. Stations of this study are shown as color-coded symbols along with station numbers. The samples presented in this study were obtained during expeditions Transdrift-20 (TI12, 19 March to 23 April 2012), Transdrift-21 (VB13, 22 August to 21 September 2013) and Transdrift-22 (VB14, 3 September to 10 October 2014) in the frame of the "Laptev Sea System" project. Figures were produced using Ocean Data View (Schlitzer, 2016) and modified manually.

2. REE sources and their Nd isotope characteristics

Figure 1 illustrates the major potential REE sources and their Nd isotope compositions in the Arctic Ocean and the Nordic Seas (Fig. 1a, see Laukert et al., 2017 and references therein) and in detail in the Laptev Sea (Fig. 1b). The end-member compositions used in this study are listed in Table 1.

The major riverine source to the Laptev Sea is the Lena River, which supplies freshwater with Nd concentrations ([Nd]) between ~600 and ~750 pmol/kg and ε_{Nd} signatures between ~ -15 and ~ -16 during Arctic summer and ~ -17 during winter (Persson et al., 2011; this study). More variable [Nd] (~500 to ~800 pmol/kg) and more radiogenic ε_{Nd} signatures (~ -14) have been reported for Lena River water obtained 500 km upstream (Porcelli et al., 2009; Zimmermann et al., 2009). The range in [Nd] and ε_{Nd}

signatures results from the compositions of the geological formations within the Lena River catchment and seasonal variations in river runoff (cf. Porcelli et al., 2009).

The freshwater component of Kara Sea waters that enter the NW Laptev Sea via the VSC (here defined as Kara Sea freshwater) consists of Yenisei and Ob freshwater and has an ε_{Nd} signature of ~ -6 and [Nd] ≈ 1000 pmol/kg based on a mixing calculation applying the [Nd] and ε_{Nd} signature of the two rivers and their mean annual discharge (Zimmermann et al., 2009). The REE characteristics of the Khatanga River are unknown, but given the hinterland geology (e.g. Sharma et al., 1992) an ε_{Nd} signature similar to the Ob and Yenisei Rivers is expected. However, in view of the relatively small mean annual discharge of only ~80 km^3/yr (R-Arctic-NET, http://www.r-arcticnet.sr.unh.edu/), its impact on the REE budget of the Laptev Sea will be small and locally restricted.

The basin-derived Arctic Atlantic Water (AAW) is the only open ocean marine REE source and is characterized by ε_{Nd} ≈ -10 and [Nd] = 16.7 pmol/kg at the Laptev Sea slope at ~200 m depth (Laukert et al., 2017 and this study). The AAW forms through cooling and freshening of Atlantic-derived waters that enter the Arctic Ocean through the Fram Strait and the Barents Sea and flow along the Eurasian continental slope as part of the Arctic boundary current (e.g. Rudels et al., 1999b).

Table. 1: End-member compositions of the REE sources applied in this study.

End-member compositions used in this study	Salinity	ε_{Nd}	[Nd]	[Yb]	HREE/LREE[a]	$\delta^{18}O$
Arctic Atlantic Water – AAW	34.85[b]	-9.9[b]	16.7[b]	4.6[b]	4.0[b]	0.2[b]
Kara Sea freshwater – KS	0	-6.0[c]	956[c]	96[e]	1.5[f]	-20[h]
Lena River summer end-member – L_S	0	-15.7[d]	744[d]	66[e]	1.3[g]	-20[h]
Lena River winter end-member – L_W	0	-16.7[d]	679[d]	60[e]	1.3[g]	-20[h]
Sea-ice	4	-	-	-	-	-2[h]

(a) PAAS-normalized Yb/Nd. (b) average of samples VB14/17/1/5 and VB13/03/6/190. (c) calculated based on a mixing calculation applying the [Nd] and εNd signature of the Yenisei and Ob rivers (Zimmermann et al., 2009) and their mean annual discharge (R-Arctic-NET). (d) calculated based on a mixing calculation applying the [Nd] and εNd signature of the low-salinity samples (VB13/19/03/4 for the summer end-member, TI12/10/03 for the winter end-member) and AAW. The mixing composition is calculated for the salinity 0. The computed compositions are within the range of concentrations reported for pure freshwater from the Lena River (Persson et al., 2011; Zimmermann et al., 2009; Porcelli et al., 2009). (e) calculated from the HREE/LREE ratio and the [Nd]. (f) calculated based on 13 freshwater samples from the Yenisei River (personal communication Pokrovsky, data from 2012 and 2015) and two freshwater samples from the Ob River (Strizhevoy station, Pokrovsky et al., 2016). Note, this value is identical to the average value calculated for all samples (n = 64) obtained by Pokrovsky et al. (2016) from the Western Siberian Lowland, which is drained by the rivers Ob, Pur Nadym, Taz and partly also by the Yenisei River. (g) values taken from the low-salinity samples, see (d). (h) values taken from Bauch et al. (2011).

3. Methods

The samples presented were obtained during Transdrift expeditions 20-22 in late winter 2012 and the summers of 2013 and 2014 (Fig. 1). The helicopter-based Transdrift-20 expedition in late Arctic winter comprised the installation of three ice camps in the fast-ice area east and northeast of the Lena Delta and sampling was conducted with 2 L Niskin-type bottles. The Transdrift-21 and Transdrift-22 expeditions were performed under ice-free conditions onboard the Russian research vessel RV Viktor Buynitskiy in Arctic summer, which allowed to recover samples and obtain CTD (conductivity, temperature, depth) profiles on the entire Laptev Sea shelf and above the shelf slope (down to ~310 m depth) with a SBE 32 rosette water sampler equipped with 12 Niskin

bottles (2.5 L). Selected stations of the 2013 expedition were resampled in 2014 (Fig. 1) and enable direct interannual comparison. Where possible, one surface sample (between 2 and 7 m water depth) and one near-bottom sample (few meters above ground) were recovered at each station. In addition, bottom water samples immediately above the undisturbed sediment-water interface were recovered at four stations in 2014 (Fig. 1) by a multicorer device (MuC).

Sampling, preconcentration, chemical purification and analysis of Nd isotopes by MC-ICPMS and of REE concentrations by online preconcentration (OP) ICP-MS (Hathorne et al., 2012) followed approved GEOTRACES protocols and were confirmed through participation in the international GEOTRACES inter-calibration study (van de Flierdt et al., 2012) (see supplementary information A for details). Each Nd isotope and [REE] sample was subsampled for $\delta^{18}O$ and salinity analyses. Oxygen isotopes were analyzed by applying a CO_2-water isotope equilibration technique (Epstein and Mayeda, 1953) and dual inlet mass spectrometry on a DeltaPlusXL instrument at the Stable Isotope Laboratory of the College of Earth, Ocean, and Atmospheric Sciences at Oregon State University (Corvallis, USA) with an external reproducibility of ±0.04 ‰ or better. The measured $^{18}O/^{16}O$ ratios are provided as deviation from Vienna Standard Mean Ocean Water in the δ-notation (Craig, 1961). Salinity was determined with an AutoSal 8400A salinometer and a precision of ±0.003 and accuracy better than ±0.005. Salinity and $\delta^{18}O$ data were combined to determine the fractions (f) of meteoric water (neglecting precipitation this constitutes river water, RW), sea-ice meltwater (SIM; negative values are proportional to the subsequent addition of brines to the water column) and marine water (SW) by applying a mass balance calculation (Östlund and Hut, 1984). Calculations and end-members (see also table 1) were conducted following (Bauch et al., 2011).

4. Results

All data are reported in the data table A1 and in the PANGEA database.

4.1 Hydrography and origin of waters based on salinity and $\delta^{18}O$

Hydrographic measurements in March/April 2012 (Transdrift-20) revealed near-freezing temperatures and a wide range of surface salinities (S) over a comparatively small area ranging from S ≈ 6 east of the Lena Delta (station TI12/5,10) to S ≈ 20 further northeast (stations TI12/6 and TI12/2,7). A sharp pycnocline between 6 and 15 m depth separated the surface waters from the well-mixed bottom water layer beneath characterized by intermediate salinities (S ≈ 30).

In September 2013, the Lena River freshwater plume occupied large parts of the shelf, with minimum surface salinities of ~5 in the east, and ~18 on the central shelf (Fig. 2). In contrast to that, salinities in 2014 were significantly higher (S > 20) and only a small area in the eastern Laptev Sea indicated the presence of a diminished Lena River

plume (Fig. 2). Surface temperatures on the central shelf in both years reached maximum values at ~4.5 °C. Contrary to the central shelf, the generally colder NW Laptev Sea near Vilkitsky Strait featured higher surface salinities in 2013 (S ~28) than in 2014 (S ~22). The depth of the seasonal pycnocline was generally shallower in the southeastern Laptev Sea and deepened (10-35 m) with distance from the Lena River Delta. Maximum salinities were < 33.5 in 2013 and > 34.5 in 2014 near the bottom at near-freezing temperatures (~ -1.8 °C). The waters below 100 m depth at the Laptev Sea shelf break had salinities near 34.85 in both years and temperatures ranging between -1.7 and 1.7 °C, with warmest waters found in the core of AAW at ~200 m depth. More information on the circulation in the NW Laptev Sea is provided in Janout et al. (2015).

The highest fractions of RW (f_{RW}) were found in the surface layer of the central and southeastern Laptev Sea reaching 85 % in 2012 and 75 % in 2013. In 2014, f_{RW} was overall lower and < 45 % in surface waters of the eastern Laptev Sea. Lowest f_{RW} (10 % in 2013 and 6 % in 2014) were observed in the NW Laptev Sea north of the VSC, the presence of which is reflected by higher f_{RW} at the southern slope of the Vilkitsky Trough in both years (reaching 20 % in 2014). Positive SIM fractions (f_{SIM}) were encountered in surface waters of the NW Laptev Sea in 2013 and 2014 (up to 11 %), while negative f_{SIM} (reaching -12 %) dominated the central and eastern Laptev Sea in both years (except in the easternmost Laptev Sea in 2013). Almost all near-bottom waters exhibit negative f_{SIM} in both years (reaching -11 % in 2014). The fraction of marine water (f_{SW}, essentially AAW) was consistently higher in the bottom layer than in the surface layer.

4.2 REE concentrations and distributions

All REE concentrations increase with decreasing salinity, albeit with different gradients for each REE. Highest concentrations (here reported for Nd concentrations, $[Nd]_m$) are observed for winter 2012 (up to 570 pmol/kg) and summer 2013 (556 pmol/kg) at the surface near the Lena Delta, while $[Nd]_m$ was much lower in the summer of 2014 (108 pmol/kg) in the same region (Fig. 3). The lowest surface $[Nd]_m$ are encountered in the NW Laptev Sea north of the VSC reaching only 25 and 28 pmol/kg for 2013 and 2014, respectively. Below the seasonal pycnocline, the highest $[Nd]_m$ in near-bottom shelf waters is observed close to the Lena Delta (215 pmol/kg, 145 pmol/kg and 80 pmol/kg for 2012, 2013 and 2014, respectively), while samples with the lowest $[Nd]_m$ of the entire data set of 16 pmol/kg were collected off the shallow shelf at 200 m depth in the Vilkitsky Trough (2013 and 2014) and above the slope of the central Laptev Sea (2014) (Fig. 4b).

Most samples exhibit typical seawater REE patterns with a progressive enrichment from light (L)REEs to heavy (H)REEs after normalization to Post-Archean Australian Shale (PAAS, McLennan, 2001) (see supplementary information B). The HREE/LREE ratios (here: $[Yb]_N/[Nd]_N$, whereby "N" refers to PAAS-normalized concentrations) are lowest (reaching 1.2 and 1.3 for 2012 and 2013, respectively) for surface samples with high $[Nd]_m$ and low salinities close to the Lena Delta (Figs. 3, 5a and b). The ratio increases with decreasing $[Nd]_m$ and increasing salinity reaching

highest HREE/LREE ≈ 5.5 for near-bottom shelf waters in the NW Laptev Sea. Waters at the shelf slope (below 100 m, including AAW) have HREE/LREE ratios of around 4 (Fig. 4c). The MREE/MREE* ratios (here $([Gd]_N+[Dy]_N)/([Yb]_N+[Nd]_N)$) generally increase with decreasing HREE/LREE ratios from 0.9 to 1.3 (Fig. 5c). A negative cerium anomaly is present in all samples, and the Ce/Ce* (defined as the $[Ce]_N/([[La]_N+[Pr]_N)/2]$) ranges between 0.1 and 0.6 with lowest Ce/Ce* observed in samples with the highest HREE/LREE ratios (Fig. 5d).

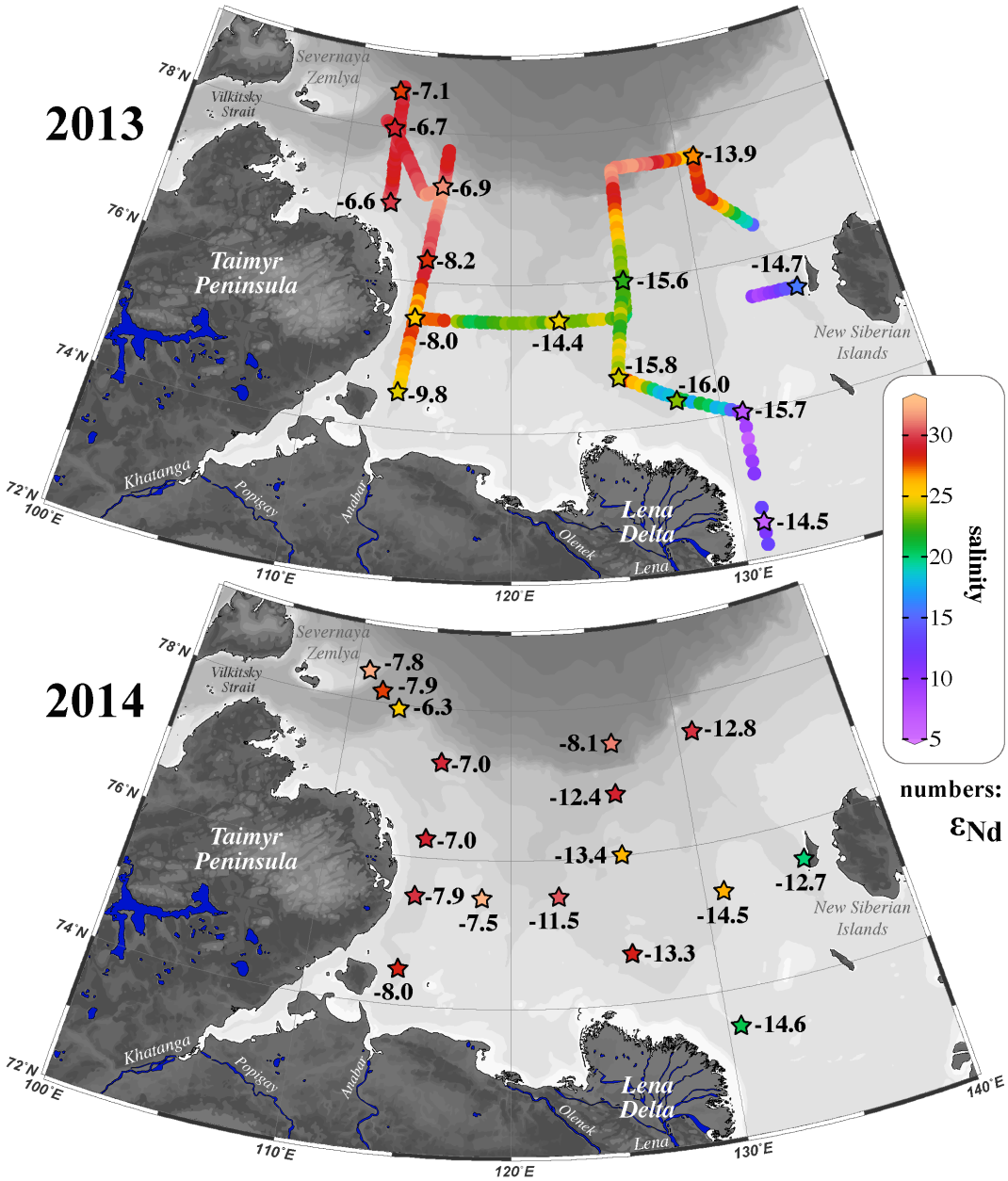

Figure 2: Surface distribution of ε_{Nd} data for the summer of 2013 and 2014 together with sample salinities for both years (color-coded stars) and UCTD-salinity (average 0-10 m) for 2013 (Janout et al., 2015). Figures were produced using Ocean Data View (Schlitzer, 2016) and modified manually.

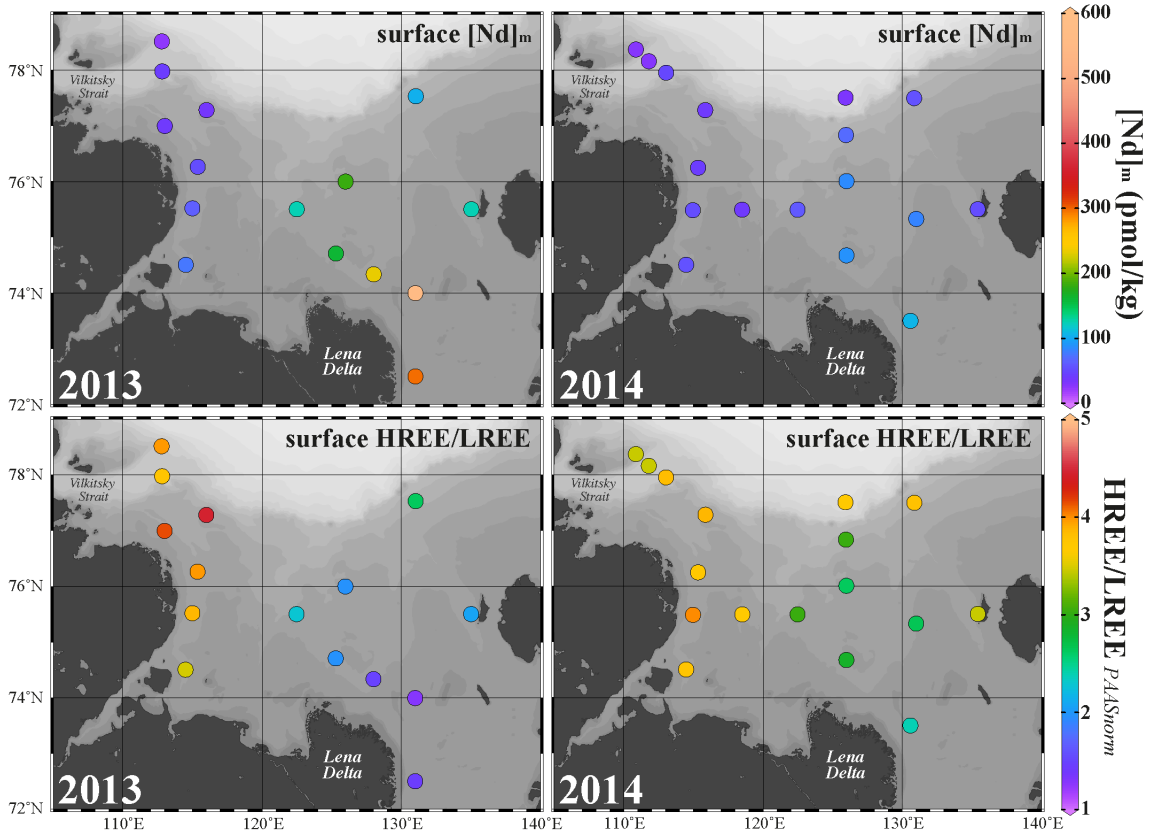

Figure 3: Surface distribution of measured Nd concentrations ($[Nd]_m$) and the PAAS normalized HREE/LREE ratios for the summer of 2013 and 2014. A negative correlation between $[Nd]_m$ and the HREE/LREE ratios is observed in both years, with highest $[Nd]_m$ and lowest HREE/LREE ratios observed in the central and eastern Laptev Sea close to the Lena Delta. Figures were produced using Ocean Data View (Schlitzer, 2016) and modified manually.

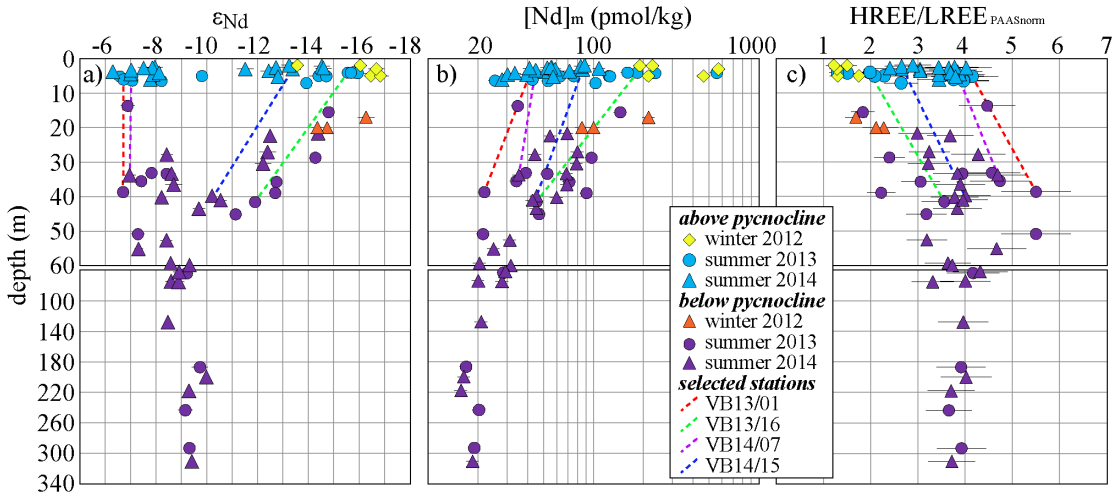

Figure 4: a) ε_{Nd}, b) $[Nd]_m$ and c) HREE/LREE ratios against depth for all samples. Note the logarithmic scale for $[Nd]_m$ and the different depth scaling of the upper 60 m and the 60 to 340 m depth range. Representative stations of the western (VB13/01 and VB14/07) and the central (VB13/16 and VB14/15) Laptev Sea are shown for both summer field campaigns. Error bars represent the external 2-sigma errors.

4.3 Nd isotopes

The Nd isotope compositions show a large range between ε_{Nd} = -16.8 and -6.3 (Figs. 2, 4a and 6). The least radiogenic ε_{Nd} signatures are found in surface waters with the highest [REE] and the lowest salinities in the vicinity of the Lena Delta. In contrast, surface waters of the western and northwestern Laptev Sea have the most radiogenic ε_{Nd} signatures reaching maximum values in surface waters within the VSC (ε_{Nd} = -6.6 ± 0.4 at station 1 in 2013 and ε_{Nd} = -6.3 ± 0.1 at station 5 in 2014) (Fig. 2). North of the VSC, a small shift towards less radiogenic Nd isotope compositions ($\varepsilon_{Nd} \approx$ -8) is observed for surface samples from 2014.

Near-bottom shelf waters from the central and eastern Laptev Sea (i.e. stations with relatively unradiogenic ε_{Nd} signatures in the surface layer) in all years show up to 4 ε_{Nd} units more radiogenic ε_{Nd} signatures than the surface samples from the same stations (Fig. 4a). In contrast, shelf waters from the NW Laptev Sea exhibit no significant differences in ε_{Nd} signatures between near-bottom waters and the surface layer (Figs. 4a). Waters above the slope (including the Vilkitsky Trough) have $\varepsilon_{Nd} \approx$ -8.5 at ~50 m depth and $\varepsilon_{Nd} \approx$ -9 below 200 m depth. Two samples at ~200 m depth with typical θ-S characteristics of AAW (θ > 0 °C and S ≈ 34.85) display slightly less radiogenic ε_{Nd} = -9.9 (1 SD = 0.2, n = 2) (Fig. 4a). The bottom water samples recovered with the MuC have ε_{Nd} signatures and REE concentrations within error identical to the near-bottom samples obtained from the same stations.

5. Discussion

5.1 Tracing water mass mixing with Nd isotopes

In freshwater influenced areas, changes in the seawater Nd isotope composition apart from those caused by water mass advection and mixing have been shown to occur via REE release from the dissolution of riverine lithogenic material (Rousseau et al., 2015) or remobilization of REEs from previously coagulated riverine nanoparticles and colloids (NPCs) (Tepe and Bau, 2016). Any significant REE input via groundwater discharge (Kim and Kim, 2014) can be excluded in the Laptev Sea due to the presence of submarine and terrestrial permafrost (Nicolsky et al., 2012). Hence, the only process capable of significantly altering the seawater ε_{Nd} signatures apart from mixing in the Laptev Sea is particle-seawater interaction.

All four MuC water samples taken directly above the sediment seawater interface in the Laptev Sea in 2014 have typical PAAS-normalized open ocean patterns, REE concentrations, and Nd isotope compositions essentially identical to corresponding CTD-rosette samples at comparable salinities taken with the CTD-rosette few meters above ground at the same stations. These observations suggest that neither significant release of lithogenic or NPC-bound REEs nor exchange (cf. Jeandel, 2016 and references therein) between surface sediments hosting the particulate REEs (cf. Abbott et al., 2015 and references therein) and seawater occurred on the Laptev shelf in 2014. The only

exception is [Ce], which is slightly higher in the MuC water samples than in the CTD-rosette near-bottom samples. Similar observations were made for MuC samples from the western (Molina-Kescher et al., 2014) and eastern South Pacific (Haley et al., 2004) and were ascribed to release of Ce^{+3} from reduced sediments (Haley et al., 2004).

In order to further constrain the potential release of Nd from deposited or suspended material we performed conservative mixing calculations (supplementary information C) based on the salinity and Nd isotope end-member compositions listed in table 1. In ε_{Nd}-salinity space, all samples of this study within error either plot on the two end-member mixing lines between AAW on the one hand and Lena or Kara Sea freshwater on the other or fall within the ternary mixing field defined by these three end-members (Fig. 6a). Note that only calculated S_0 instead of S_m is considered in order to remove variations in the salinity caused by sea-ice formation and melting (see below). Although this observation does not unambiguously rule out exchange with Nd of solid phases (samples with altered ε_{Nd} signatures may still plot within this mixing field), it indicates that such a process does not result in significant changes of the dissolved ε_{Nd} signatures beyond what is expected from mixing of the water mass end-members.

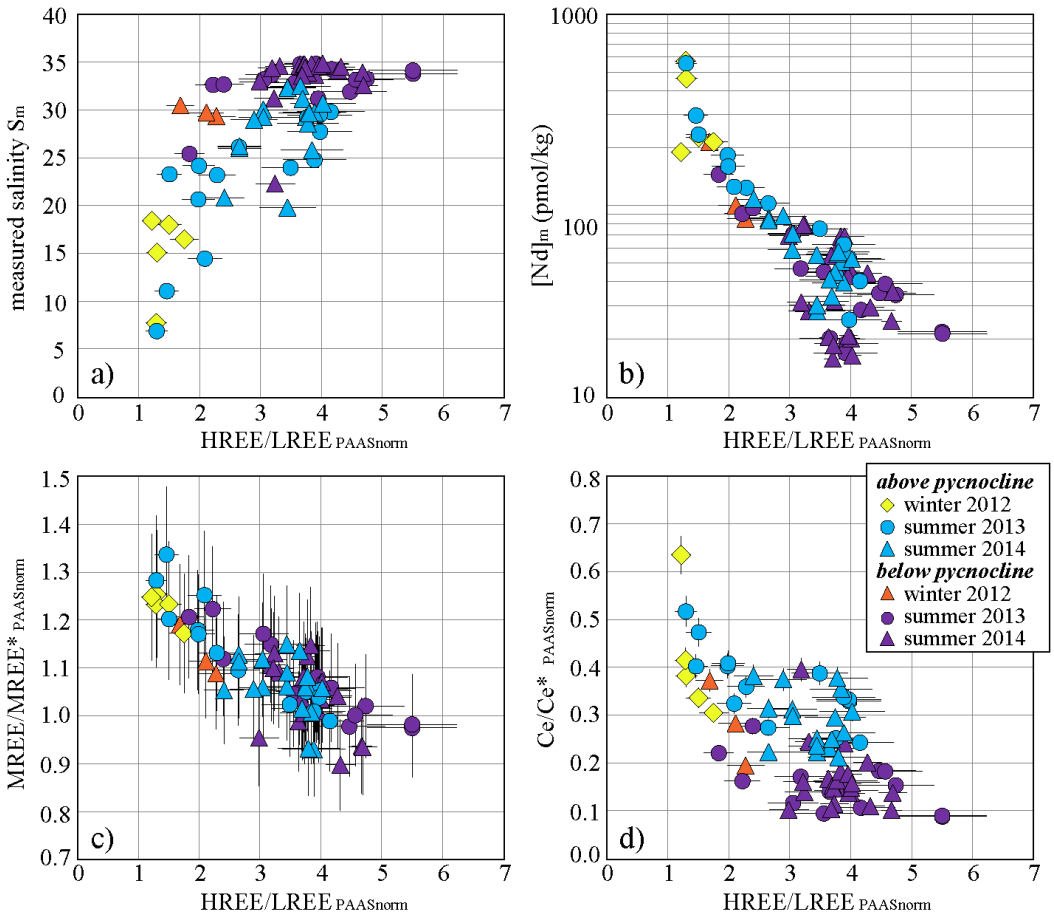

Figure 5: The HREE/LREE ratio against a) measured salinity S_m, b) $[Nd]_m$, c) the MREE/MREE* ratio and d) the Ce/Ce* ratio. Error bars represent the external 2-sigma error for repeat measurements of calibration standards (see main text for further information). Note the logarithmic scale for $[Nd]_m$.

More information from the mixing calculations is only provided regarding the behavior of riverine Nd from Yenisei and Ob. Based on the circulation pattern and the salinity distribution in 2014 (Figs. 1 and 2), the surface sample of station VB14/05 recovered in the NW Laptev Sea represents the freshest Kara Sea waters directly advected through the Vilkitsky Strait, thus reflecting an essentially pure mixture of AAW and Kara Sea freshwater (f_{RW} ~20 %). Its location about 1000 km away from the Yenisei and Ob estuaries and its relatively high salinity (S = 25.80) both imply that sufficient time had passed during transport to allow for potential interactions between suspended riverine material of Yenisei and Ob and the dissolved phase. As shown in Fig. 6, this sample falls exactly on the mixing line between the AAW and the Kara Sea freshwater end-members in ε_{Nd}-salinity space and in ε_{Nd}-[Nd] space, after correction of $[Nd]_m$ for Nd removal (see below and section 5.2). This supports that no significant particulate (lithogenic or NPC-bound) Nd release from the suspended load of the Yenisei and Ob rivers occurred. The release of Nd from the suspended load of the Lena River at mid to high salinities cannot be assessed based on the mixing calculations but appears to be insignificant given that the seawater ε_{Nd} signatures in the eastern and central Laptev Sea become more radiogenic with increasing salinities, which clearly reflects admixture of AAW rather than release of particulate riverine Nd, as the Lena riverbed surface sediment ε_{Nd} signature is -14.6 to -16.7 (Schmitt, 2007) and the dissolved load is -15 to -17 (this study; Persson et al., 2011).

Release of Nd from riverine sediments was invoked to explain variations of Nd data in shallow waters in the central Arctic Ocean (Porcelli et al., 2009), but unambiguous evidence for this process was not provided due to absence of estuarine data. As shown in section 5.2.1, interaction of seawater and riverine freshwater in the Laptev Sea drives coagulation of NPCs resulting in Nd removal from the dissolved phase until salinities of about 34 are reached, similar to observations in the Severnaya Dvina River estuary (Pokrovsky et al., 2014). There, although this process was shown to be limited to the zone of the initial salinity increase, no increase of REE concentrations at higher salinities was observed. This contrasts with observations from other estuaries where REE removal at low salinities is accompanied by a pronounced rebound of REE concentrations in the mid to high salinity zone (e.g. Elderfield et al., 1990; Lawrence and Kamber, 2006; Nozaki et al., 2000; Rousseau et al., 2015; Sholkovitz and Szymczak, 2000; Sholkovitz, 1995), but supports our observation that release of particulate Nd does not occur in the Laptev Sea. In addition, experiments simulating Arctic estuarine mixing recently showed that release of NPC-bound REEs likely only occurs when the riverine end-member is rich in inorganic and poor in organic NPCs (Tepe and Bau, 2016), which is not the case for most Siberian rivers including Lena, Yenisei and Ob (Dittmar and Kattner, 2003 and references therein).

These observations overall suggest that a pronounced alteration of the dissolved ε_{Nd} signatures through REE release or exchange with particles in the Laptev Sea does not occur. Combined with salinity, Nd isotopes can thus be used directly to trace water mass distribution and mixing and to provide information on the behavior of REEs in the Laptev Sea. Formation and melting of sea ice and river ice likely change the distribution

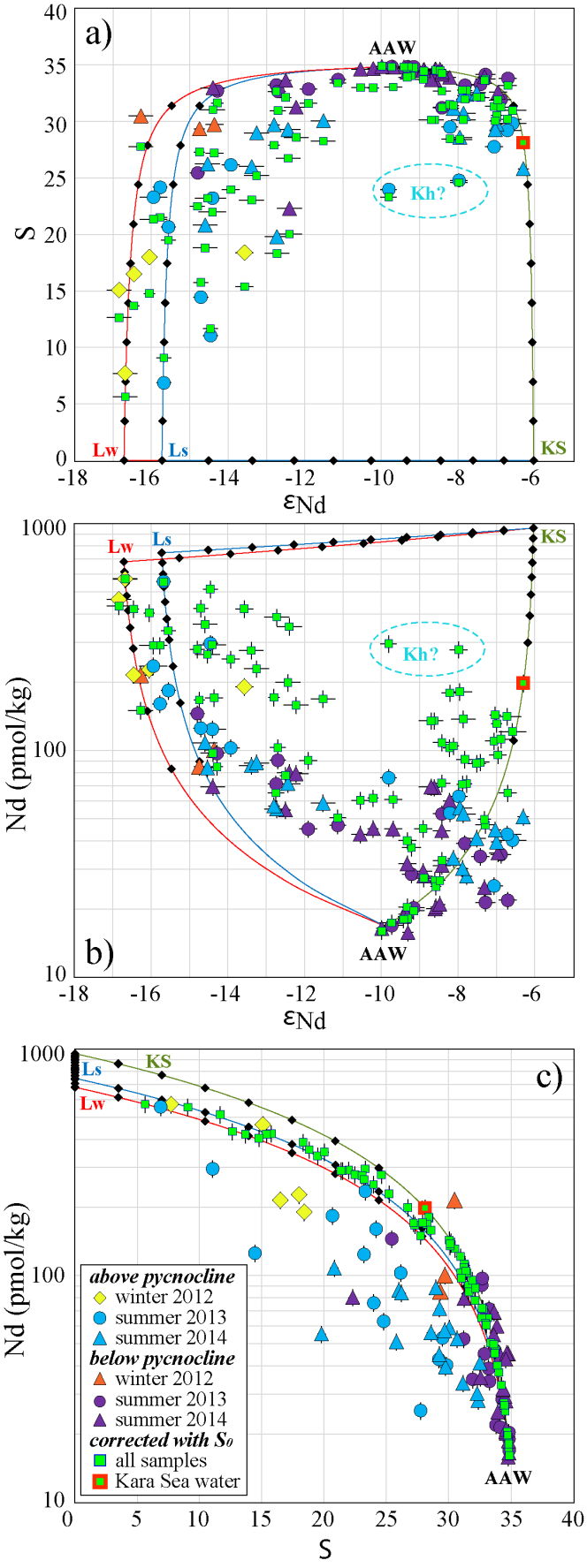

Figure 6: a) salinity vs. ε_{Nd}; b) [Nd] vs. ε_{Nd}; c) [Nd] vs. salinity. Shown are end-member mixing lines between the Lena River (summer: L_S, winter: L_W), the Kara Sea freshwater (KS) and Arctic Atlantic Water (AAW), divided into 10 % steps (black symbols). The values of the end-members correspond to the values given in table 1. The measured data are given by the same symbols as in Figs. 4 and 5, while the green squares represent data determined with the end-member mixing calculation (i.e. based on ε_{Nd} and the initial salinity S_0). Only two samples indicate high riverine contributions from the Khatanga River (Kh). The surface sample of station VB14/05 (Kara Sea water) represents the freshest Kara Sea waters (f_{RW} ~20 %, S = 25.80) that entered the Laptev Sea through the Vilkitsky Strait and thus reflects essentially pure mixing of AAW and KS not containing any riverine contributions from the Lena River. After correction with S_0, this sample falls on the mixing line between AAW and KS, indicating that no significant particulate Nd release from the suspended load of the Yenisei and Ob rivers occurred. Error bars represent the external 2-sigma error.

of salinity and Nd isotopes and thus affect the assessment of the water composition, which, however, can either be corrected for or the effects are relatively small (see supplementary information D), resulting in an estimated uncertainty of 5 % for the accuracy of the calculated water mass fractions (provided in supplementary information E).

The water mass distribution based on our conservative mixing calculations shows a clear dominance of the Lena River freshwater in the eastern Laptev Sea with higher contributions for 2013 (up to ~75 %) than for 2014 (up to ~45 %). Even though the advection of Kara Sea freshwater to the NW Laptev Sea based on our calculations was higher in 2014 (up to ~20 %) compared to 2013 (up to 13 %), similarly low Kara Sea freshwater fractions were determined for surface waters further south for both years (up to ~10 % in 2013 and ~12 % in 2014), confirming that most of the Kara Sea waters that enter the Laptev Sea via the VSC do not flow south onto the shelf (see also Janout et al., 2015). The apparently higher fractions of Kara Sea freshwater in some surface samples of the SW Laptev Sea in 2013 (up to ~23 %) likely can be attributed to riverine discharge from the Khatanga River, which is indicated by their specific compositions that deviate in ε_{Nd}-salinity space (circled in Fig. 6). Our results further demonstrate that near-bottom waters are primarily composed of AAW (> 90 % in samples below 40 m depth).

5.2 Processes controlling the REE distribution

To evaluate the role of estuarine and ice related processes in the Laptev Sea, the measured REE concentrations ($[REE]_m$) of each sample are compared to the calculated concentrations expected from water mass mixing only ($[REE]_0$, equivalent to S_0) and to those expected from water mass mixing and REE redistribution due to sea-ice formation and melting ($[REE]_{SIM}$, equivalent to S_m). Information on the calculation of $[REE]_0$ and $[REE]_{SIM}$ is provided in supplementary information C. In the following we compare the difference between $[REE]_0$ and $[REE]_m$ (i.e. $\Delta[REE]_{0\text{-}m}$, in %) to the difference between $[REE]_0$ and $[REE]_{SIM}$ (i.e. $\Delta[REE]_{0\text{-}SIM}$, in %). An uncertainty of 10 % is assumed for both differences due to the small alterations of Nd isotopes and salinity through sea-ice formation and melting. For better illustration, we use Nd and Yb as the representative elements of the LREEs and the HREEs, respectively.

The distribution of Nd and Yb at the Laptev shelf slope (below 100 m depth) is mainly controlled by water mass advection and mixing ($\Delta[Nd;Yb]_{0\text{-}m} \approx 0$) (Fig. 7). On the Laptev shelf (i.e. the upper ~60 m), the Nd and Yb distributions can neither be entirely explained by water mass mixing ($\Delta[Nd;Yb]_{0\text{-}m} \neq 0$) nor by water mass mixing and sea-ice formation or melting ($\Delta[Nd;Yb]_{0\text{-}m} \neq \Delta[Nd;Yb]_{0\text{-}SIM}$). Instead, a large Nd deficiency (i.e. negative $\Delta[Nd]_{0\text{-}m}$ values) is observed in most samples, reaching -85 % at the surface and decreasing (i.e. higher $\Delta[Nd]_{0\text{-}m}$ values) with depth (Fig. 7a). Only the near-bottom samples of stations characterized by high Lena River contributions (e.g. close to the Lena Delta) exhibit significant Nd excess (one of these stations is winter station TI12/06, highlighted in Fig. 7). In contrast to Nd, the distribution of Yb features two distinct trends (Fig. 7b). While all surface samples exhibit an Yb deficiency reaching -65 %, most

of the bottom layer samples are characterized by a pronounced Yb excess reaching 80 %. Comparison between $\Delta[Nd]_{0\text{-}m}$ and $\Delta[Yb]_{0\text{-}m}$ reveals that $\Delta[Nd]_{0\text{-}m}$ is generally identical or lower than $\Delta[Yb]_{0\text{-}m}$ (Fig. 7c).

We suggest that two combined processes account for the observed distributions of LREEs and HREEs on the Laptev Shelf. Coagulation of NPCs preferentially removes all the LREEs over HREEs in the mid to high salinity zone, whereas formation and melting of sea ice and river ice result in redistribution of the REEs within the water column, causing REE deficiency at the surface and REE excess in the bottom layer (Fig. 7d). Even though these processes may occur simultaneously they are discussed separately below.

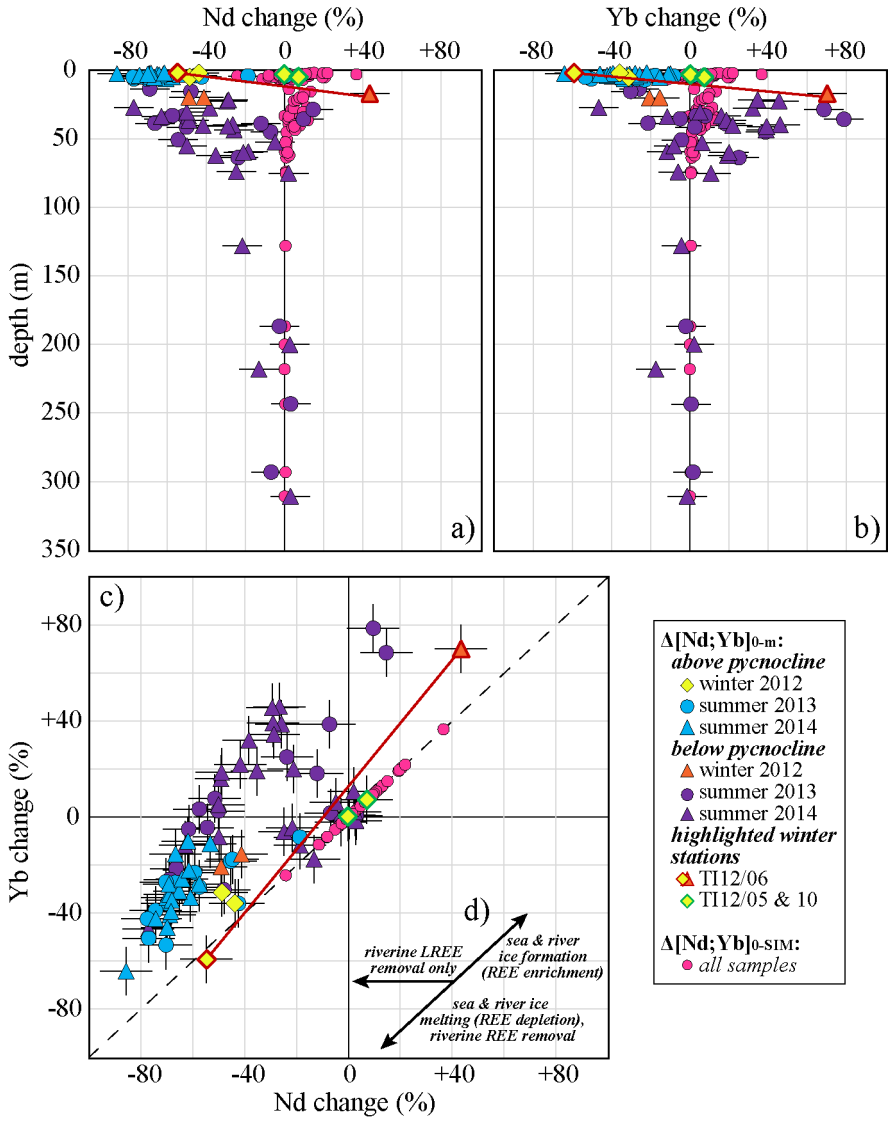

Figure 7: a) Percent changes of $[Nd]_0$ to $[Nd]_m$ ($\Delta[Nd]_{0\text{-}m}$) and $[Nd]_{SIM}$ ($\Delta[Nd]_{0\text{-}SIM}$). b) Percent changes of $[Yb]_0$ to $[Yb]_m$ ($\Delta[Yb]_{0\text{-}m}$) and $[Yb]_{SIM}$ ($\Delta[Yb]_{0\text{-}SIM}$). c) Comparison of Nd and Yb changes. d) Scheme indicating the direction of changes in Nd and Yb through formation and melting of sea ice and river ice and through riverine REE removal. Zero percent changes in Nd and Yb correspond to values expected from water mass advection and mixing, which also is the starting point in d).

5.2.1 Removal of riverine REEs

Removal of REEs has been documented for the low-salinity range of estuaries and regions influenced by riverine runoff, and has been attributed to salt-induced coagulation of REE-carrying NPCs with preferential removal of LREEs over HREEs (e.g. Åström et al., 2012; Elderfield et al., 1990; Lawrence et al., 2006; Nozaki et al., 2000; Pokrovsky et al., 2014; Rousseau et al., 2015; Sholkovitz et al., 1995; Sholkovitz and Szymczak, 2000). The fractionation between LREEs and HREEs is attributed to the combined effects of HREEs preferentially staying in solution and the general affinity of all REEs to attach to surfaces of Fe and Mn (oxyhydr)oxides or organic NPCs (cf. Lee and Byrne, 1993). This process is resolvable in the Laptev Sea via increasing HREE/LREE ratios with increasing salinity and decreasing $[Nd]_m$ (Fig. 5a,b). The removal of REEs transforms the riverine REE patterns into typical LREE-depleted open ocean seawater patterns (supplementary information B). The riverine REE patterns are slightly concave and thus have relatively high MREE/MREE* ratios, which decrease with increasing HREE/LREE ratios (Fig. 5c) in addition suggesting that the removal efficiency follows LREEs > MREEs > HREEs (e.g. Lawrence and Kamber, 2006; Sholkovitz and Szymczak, 2000; Sholkovitz, 1995).

It is clear that admixture of AAW also contributes to changes in the REE characteristics. However, we observe that the REE distribution at mid to high salinities (< ~34) mostly reflects removal of riverine REEs. This is evident from some near-bottom water samples (S ~34) that have higher HREE/LREE ratios (~5.5) than AAW (~4), suggesting that preferential removal of LREEs occurs up to salinities of ~34 and produces REE patterns that exhibit an enhanced fractionation of LREEs over HREEs. Moreover, the efficient removal results in Ce concentrations falling below the Ce concentration of AAW. This is also recorded in the Ce anomaly (i.e. Ce/Ce*), which is commonly used to assess the time since water masses last were in contact with continental input due to the preferential removal of highly insoluble Ce^{+4} over time (Hathorne et al., 2015 and references therein). The Ce anomalies show that the "young" waters supplied by the Lena River have the highest Ce/Ce* ratios (~0.4 to ~0.6) compared to those of "older" Kara Sea waters (~0.35) and to those of the AAW (~0.15), which is the "oldest" water mass in the study area (Fig. 5). The above-mentioned near-bottom samples have even lower Ce/Ce* ratios (~0.1) than AAW, which is attributed to very efficient removal of Ce.

To account for the changes caused by admixture of AAW, we normalized the $[Nd]_m$ and $[Yb]_m$ to the riverine end-member, which was calculated for each sample individually based on the proportions between freshwater from the Lena River and from the Kara Sea. As can be seen in Fig. 8a and b, the river-normalized concentrations of Nd and Yb reflect water mass mixing in the low salinity range (i.e. S < ~10), but both drop by about 30 % at S ~10. For higher salinities, an increase in HREE/LREE ratios is observed in agreement with preferential removal of LREEs over HREEs (Fig. 8c). The delayed onset of REE removal contrasts with observations from other estuaries, where REE removal often was reported to be most intense in the lowest salinity range (e.g. Åström et al., 2012; Elderfield et al., 1990; Lawrence et al., 2006; Nozaki et al., 2000; Pokrovsky et al.,

2014; Rousseau et al., 2015; Sholkovitz et al., 1995; Sholkovitz and Szymczak, 2000). For example, in the Amazon estuary most of the riverine REEs are removed already below salinities of 2 (shown for comparison in Fig. 8; Rousseau et al. 2015). In addition, multiple studies observed increasing REE concentrations at intermediate salinities (e.g. Lawrence et al., 2006; Nozaki et al., 2000; Rousseau et al., 2015; Sholkovitz et al., 1995) likely resulting from dissolution of lithogenic suspended sediments (Rousseau et al., 2015). We do, however, not see any evidence for release of particulate (lithogenic or NPC-bound) REEs at mid to high salinities (section 5.1), which is in agreement with observations from the Severnaya Dvina River estuary (Pokrovsky et al. 2014) and with the absence of NPC-bound release (Merschel et al., 2017; Tepe and Bau, 2016). These experiments further show that the composition of riverine NPCs plays a major role in estuarine REE behavior, with large amounts of *organic* NPCs contained in river water inhibiting the aggregation of REEs until mid salinities of ~10 are reached (Merschel et al., 2016). This is confirmed by our field observations showing a similarly delayed onset of REE removal in the Laptev Sea, which is characterized by riverine runoff mostly from the Lena River, which is rich in dissolved organic carbon (cf. Dittmar and Kattner, 2003).

We determined the REE concentrations expected prior to REE removal by adding 30 % of riverine Yb to the $[Yb]_m$ of each sample with S > 10 (except for the winter sample with S ~13) and by adjusting the $[Nd]_m$ to the removal-corrected Yb concentration to account for the preferential removal of LREEs. Note that the corrected data are closer to the mixing line but some samples still exhibit significant offsets (Fig. 8), which likely are related to formation and melting of sea ice and river ice (see section 5.2.2 below). The calculated removal of Nd amounts to ~75 % (Fig. 9), which is similar to the mean Nd removal of ~70 % calculated for investigated estuaries globally (Rousseau et al., 2015). Since we do not correct for any HREE removal beyond the initial 30 % drop, our calculated Nd removal represents the minimum fraction of Nd removed. This amount is still significantly higher than that observed in mixing experiments with a similar riverine end-member (Merschel et al., 2016). However, these experiments do not consider removal related to the presence of the suspended riverine load (> 0.2 µm). Apart from this, the experiments show that fast and strong REE removal essentially only occurs when high contents of *inorganic* and low contents of *organic* NPCs are present. This also explains the overall lower removal of REEs in the Laptev Sea compared to that in the Amazon estuary (Fig. 9), as less *inorganic* NPCs in Siberian rivers are present than in the Amazon River. In addition, our winter samples show less removal at similar salinities compared to most of our summer samples (Fig. 9a), which might reflect seasonal variations of the composition of Lena River freshwater. Moreover we note that the preferential LREE removal increases until maximum removal is reached (Fig. 9b), which indicates that increasing salinities favor the HREEs to preferentially stay in solution.

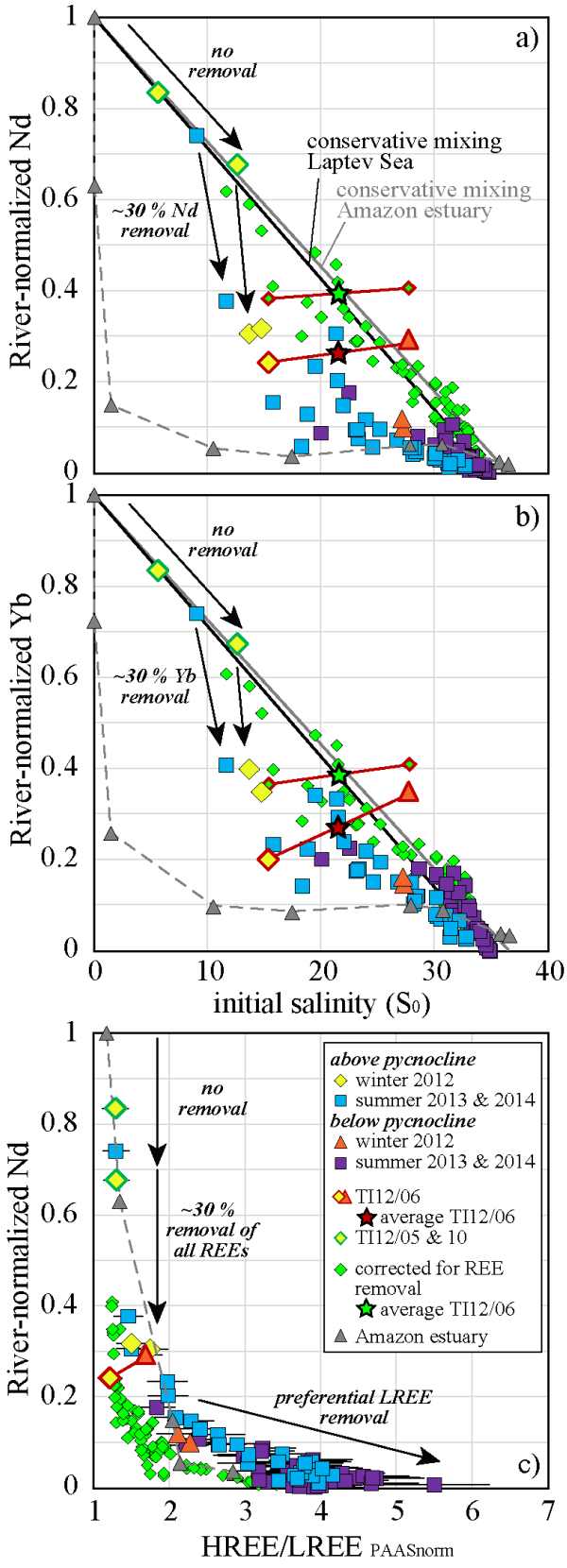

Figure 8: a) and b) river-normalized Nd and Yb concentrations against the initial salinity S_0. c) River-normalized Nd concentration against the PAAS-normalized HREE/LREE ratios. No REE removal is observed in the low salinity range. At S ~10, REE concentrations drop by ~30 %. After this drop, the LREEs are preferentially removed from the water column, which is evidenced by increasing HREE/LREE ratios. REE behavior in the Amazon estuary is shown for comparison (Rousseau et al., 2015). Note that the green diamonds correspond to the river-normalized values corrected for REE removal and do not correspond to the green squares shown in Figure 6.

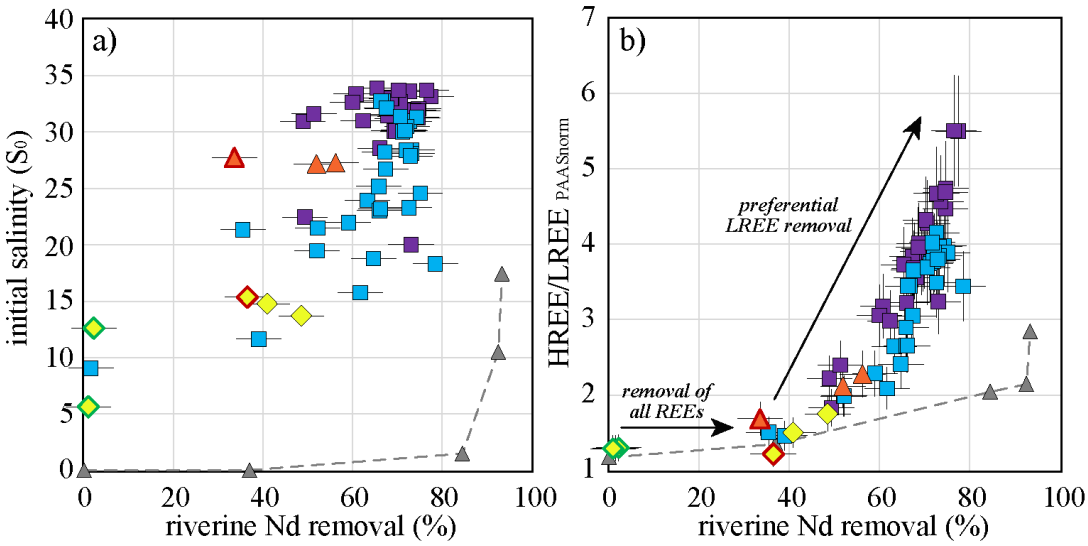

Figure 9: a) Riverine Nd removal vs. the initial salinity S_0. b) Nd removal vs. the HREE/LREE ratios. Nd removal starts at S ~10 and proceeds until S ~34. Changes in the HREE/LREE ratios show that LREEs are preferentially removed over HREEs with increasing salinities. The maximum Nd removal reached (~75 %) corresponds to the values determined from other studies globally (Rousseau et al., 2015). Neodymium removal in the Amazon estuary is shown for comparison. Symbols are the same as in Figure 8.

In contrast to our observations, Porcelli et al. (2009) concluded that freshwaters from the Siberian rivers do not loose substantial amounts of Nd on the shelf. However, they also pointed out that significant contributions of Ob freshwater to the investigated shallow waters from the central Arctic Ocean would require significant losses of riverine Nd prior to entering the Arctic Ocean. Our mixing calculations with the riverine end-members provided here (including Ob freshwater) and AW from the Fram Strait (Laukert et al., 2017) as the marine end-member for these waters reveal similar riverine fractions (up to 10 %) to those reported by Porcelli et al. (2009) but as a result of a significant deficiency of Nd (up to -75 %), which agrees with our observations from the Laptev Sea and supports that REE removal is common to Siberian rivers.

5.2.2 REE redistribution through formation of sea ice and river ice

It has long been known that some major and trace elements preferentially stay in the liquid phase when ice crystals form (e.g. Nebbia and Menozzi, 1968 and references therein; Fournier et al., 1974 and references therein). This process is also observed during natural sea-ice formation, when a significant fraction of salt is rejected into the underlying water and only a small fraction remains trapped in the interstitial brine (Notz and Worster, 2009). The behavior of REEs during sea-ice formation is unknown to date but can be expected to be proportional to salinity changes, resulting in REE enrichment in the remaining brine-enriched water, which should be reflected by REE excess compared to expected concentrations from water mass advection and mixing. Conversely, melting of REE-poor sea-ice will dilute the REEs in the surface layer of the melting region and will be evident by REE deficiencies. The Nd isotope distribution in

contrast should not significantly change by these ice-related processes (see supplementary information D).

The distribution of REEs in the Laptev Sea cannot be explained by REE removal throughout the water column alone. Even though this process partly accounts for the deficiency of Nd and Yb (see section 5.2.1), it does not explain the pronounced excess of Yb observed in most samples of the bottom layer on the shelf (Fig. 7b). An even stronger excess of Yb and Nd is observed if the REE concentrations are corrected for REE removal (see supplementary information F). The redistribution of REEs via brine rejection during sea-ice formation and melting of REE-depleted sea-ice might be a reasonable explanation here, which is supported by the fact that stations with the strongest Yb deficiency in the surface layer exhibit the strongest Yb excess in the bottom layer for all years (e.g. station TI12/06 highlighted in Fig. 7). During winter, the REE-enriched waters generated through sea-ice formation are transported to the shelf bottom layer through brine sinking and winter convective mixing. During freshening in spring, the formation of the seasonal pycnocline separates this REE-enriched 'winter water' from the freshwater-rich surface layer depleted in REEs due to melting of REE-poor sea-ice.

Striking evidence for this scenario is provided by the winter samples in particular. Two surface winter samples were recovered close to the main Lena River outflow (stations TI12/5,10) and represent unaffected winter freshwater of the Lena River (highlighted in Figs. 7, 8 and 9). These samples have $\Delta[Nd,Yb]_{0\text{-}m} \approx 0$ %, which indicates that neither freezing nor REE removal occurred. In contrast, winter samples recovered north of the Lena Delta close to an active polynya (station TI12/06) represent older waters, which in addition to ~30 % estuarine REE removal, were strongly affected by formation and melting of sea ice and river ice. This agrees with the calculated strong deficiency of Yb at the surface ($\Delta[Yb]_{0\text{-}m} \approx$ -60 %) and the similarly strong Yb excess in the bottom layer ($\Delta[Yb]_{0\text{-}m} \approx$ 70 %). The average river-normalized Nd and Yb concentrations at this station should reflect REE removal only (assuming that no significant mixing with other waters occurred), which is confirmed by the removal-corrected average concentrations that plot directly on the mixing line (green stars in Fig. 8). Surface melting during late winter may be unexpected, but likely was induced by northward-directed runoff of Lena River freshwater (f_{RW} ~60 % in the surface sample) that acted as a heat source (cf. Janout et al., 2016).

After being corrected for estuarine REE removal, the excess of Nd and Yb in the bottom layer reaches 100 %, while their deficiency at the surface reaches -40 % only (see supplementary information F). The excess of REEs in the bottom layer is thus higher than expected from REE redistribution via formation and melting of sea-ice. In freshwater-influenced shelf regions, formation and melting of river ice has to be considered, which has the potential to transfer very high REE concentrations. River-ice formation has been observed in Arctic estuarine regions before. For example, Macdonald et al. (1995) have estimated that 15 % of the winter discharge of the Mackenzie River was incorporated into the landfast-ice during winter 1990/1991, which resulted in landfast-ice that on average consisted of 40 % of river ice. Even offshore pack ice was shown to still contain 10 % of river ice. No direct information exists on REE behavior during river-ice

formation, but it is reasonable to assume that the dissolved REEs entirely remain in the liquid phase when ice crystals form, which will result in even higher concentrations in the remaining water compared to what is expected from sea-ice formation, making river-ice formation the most likely explanation for the pronounced excess of REE concentrations observed in the Laptev Sea. Because the Laptev Sea is an area of net ice export (e.g. Rosén et al., 2015), the deficiency at the surface is not as high as the excess in the bottom layer.

Analogously and in support of the above argument about REE transfer during formation of sea ice and river ice, exceptionally high concentrations of dissolved Fe and Ba have previously been observed near the shelf bottom of the Laptev Sea, and have been attributed to either sediment resuspension, sinking of brines, or regeneration of these elements in the bottom layer (Abrahamsen et al., 2009; Klunder et al., 2012; Roeske et al., 2012). It is thus likely that formation and melting of sea ice and river ice is at least partially responsible for the depletion and excess of elements such as Fe and Ba.

6. Summary and conclusions

Dissolved Nd isotope compositions, rare earth element concentrations and stable oxygen isotopes are presented for waters collected across the Laptev Sea during the Arctic summer of 2013 and 2014 and complemented by samples collected close to the Lena Delta in late winter 2012.

- No evidence is found for significant REE release from suspended or deposited riverine sediments or benthic fluxes. Together with the salinity corrected for sea-ice processes, the Nd isotopes can thus be used directly to assess water mass mixing, riverine inputs and the behavior of river-derived REEs.
- The discharge of the Lena River controlled the freshwater budget of the eastern Laptev Sea during the summers of 2013 and 2014, while the western Laptev Sea was dominated by Kara Sea freshwater and riverine discharge from the Khatanga River. The bottom layer was dominated by contributions of Arctic Atlantic Water that exceeds 90 % in samples below 40 m depth.
- Two main processes are responsible for the distribution of dissolved REEs on the Laptev Shelf. The coagulation of riverine nanoparticles and colloids results in REE removal from the water column in the mid to high salinity range with an initial removal of all REEs by ~30 % occurring at salinities below 10. After this initial drop, the LREEs are preferentially removed over the HREEs, consistent with experiments simulating estuarine mixing with organic-rich river water. The removal of LREEs is at least 75 % for Nd in relatively old near-bottom waters in the NW Laptev Sea, and significantly higher than HREE removal, which for Yb is above 30 %. The formation and melting of sea ice and river ice redistribute the REEs within the water column, resulting in a REE deficiency at the surface (-40 %) and a REE excess in the bottom layer (100 %) compared to what can be expected from water mass advection and mixing. While river-ice formation is not

directly traceable with classical hydrographic parameters our data suggest that this process is important for the REE distribution. The ice-related processes also contribute to the redistribution of other elements and may affect macronutrient distribution and have implications for primary productivity in high latitude estuaries.

Acknowledgements

We like to thank the Captain and Crew of the RV Viktor Buynitskiy and all members of the project "Laptev Sea System" for help in collecting the samples. We acknowledge Heidemarie Kassens as the project coordinator in particular for designing the project and facilitate sample recovery and transport. Many thanks also to Jutta Heinze (GEOMAR) for laboratory assistance. Furthermore, we thank the German Federal Ministry of Education and Research (BMBF) and the Ministry of Education and Science of the Russian Federation for support of the "Laptev Sea System" project (BMBF grant 03G0833). Dorothea Bauch acknowledges financial support from DFG project BA1689.

Supplementary material

A. Sample collection, preparation and analysis

Samples for Nd isotope and REE analyses from the summer expeditions were collected in 10 L acid-cleaned LDPE-cubitainers and filtered through AcroPak™500 Capsules containing Supor Membrane (pore size: 0.8/0.2 µm) filter cartridges immediately after sampling and were acidified to pH ~2.2 with ultra-pure concentrated HCl at the Otto-Schmidt Laboratory in St. Petersburg, Russia. An aliquot of 1 L of each sample was separated into acid-cleaned LDPE-bottle for REE analyses. About 100 mg of Fe were added to the remaining samples as a purified $FeCl_3$ solution and after sufficient time for equilibration the pH was adjusted to ~8 leading to co-precipitation of the dissolved REEs together with FeOOH. After discarding most of the supernatant, the Fe-precipitates were transferred into 1 L acid-cleaned LDPE-bottles and returned to the home laboratory at GEOMAR. Samples from the winter expedition were treated in the same manner, except that they were filtered through 0.45 µm Millipore® cellulose acetate filters using a peristaltic pump after transport to the home laboratory.

For the extraction and isolation of dissolved Nd, the procedure outlined in Stichel et al. (2012) was applied. The Nd isotopic compositions were measured on a Nu Plasma (Nu Instruments Limited) and a Neptune Plus (Thermo Scientific) MC-ICP-MS at GEOMAR, Kiel. Based on repeated measurements of JNdi-1 and in-house standards with concentrations similar to those of the samples, the 2σ external reproducibility ranged between 0.1 and 0.4 ε_{Nd} units for the individual measurement runs. Duplicate analyses (n = 6) resulted in identical Nd isotope compositions within these uncertainties. The REE concentrations ([REE]) were measured using an online pre-concentration (OP) ICP-MS

technique at GEOMAR, Kiel by directly coupling a "seaFAST" system (Elemental Scientific Inc., Nebraska, USA) to an ICP-MS (Agilent 7500ce) (Hathorne et al., 2012) and calibration standards with a mixed REE solution of a seawater-like composition in a natural seawater matrix (Osborne et al., 2015). Repeated measurements of GEOTRACES inter-calibration sample BATS 15m (van de Flierdt et al., 2012) were used to monitor the external reproducibility.

B. Representative REE patterns

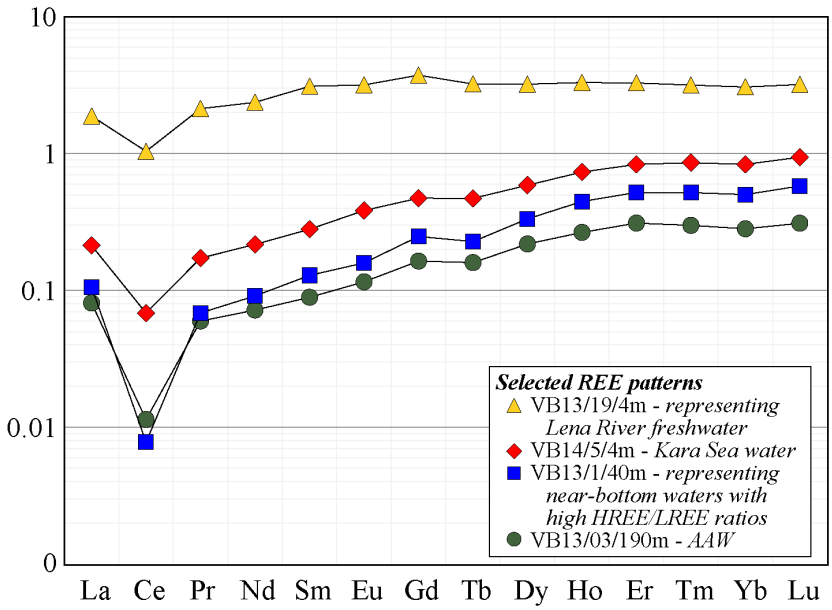

Figure B: Representative REE patterns. Note, "Kara Sea water" is the water observed in the Vilkistky Strait Current and is not identical with the calculated end-member "Kara Sea freshwater". The sample VB13/1/40m represents near-bottom shelf waters with strongest REE removal.

C. Calculation of water mass fractions and other parameters

C.1 Determination of the initial salinity S_0

We use the measured salinity (S_m) and $\delta^{18}O$ to determine the fractions (f) of sea-ice meltwater (SIM), river water (RW) and marine water (SW) by applying a mass balance calculation (Östlund and Hut, 1984). The calculations were conducted following Bauch et al. (2011).

To determine the initial salinity (S_0, i.e. this salinity corresponds to the salinity expected without sea-ice formation or melting), the S_m of each sample is iteratively adjusted to the condition $f_{SIM} = 0$. Note, the initial salinity determined with this method is identical to that calculated from equations of Rosén et al. (2015).

C.2 Determination of initial water mass fractions based on S_0 and ε_{Nd}

Three end-members are expected to contribute to mixing in the Laptev Sea: Arctic Atlantic Water (AAW), Lena River freshwater (L) and Kara Sea freshwater (KS). For each sample, the initial fraction of AAW (f_{AAW}) can be calculated as

$$f_{AAW} = \frac{S_0}{S_{AAW}} \quad (1)$$

where S_0 is the initial salinity of the sample and S_{AAW} the salinity of the AAW end-member. The initial fractions of Lena River freshwater (f_L) and Kara Sea freshwater (f_{KS}) are then calculated by iteratively solving the following equations:

$$f_L = 1 - f_{KS} - f_{AAW} \quad (2)$$

$$f_{KS} = \frac{[Nd]_0 - [Nd]_{AAW} - f_L * ([Nd]_L - [Nd]_{AAW})}{[Nd]_{KS} - [Nd]_{AAW}} \quad (3)$$

$$f_{AAW} = \frac{\varepsilon Nd_m * [Nd]_0 - \varepsilon Nd_{KS} * [Nd]_{KS} - f_L * (\varepsilon Nd_L * [Nd]_L - \varepsilon Nd_{KS} * [Nd]_{KS})}{\varepsilon Nd_{AAW} * [Nd]_{AAW} - \varepsilon Nd_{KS} * [Nd]_{KS}} \quad (4)$$

where $\varepsilon_{Nd\text{-}AAW}$, $\varepsilon_{Nd\text{-}KS}$ and $\varepsilon_{Nd\text{-}L}$ are the end-member Nd isotopic compositions and $[Nd]_{AAW}$, $[Nd]_{KS}$ and $[Nd]_L$ the end-member Nd concentrations of AAW, KS and L, respectively. The iteration was performed on a spreadsheet program through a goal-seek subroutine. Note, for the Lena River end-member we use two different end-member compositions, one for the winter samples and another for the summer samples. The $\varepsilon_{Nd\text{-}m}$ is the measured Nd isotopic composition of the sample and $[Nd]_0$ the initial Nd concentration of the sample (i.e. the concentration that is expected from water mass advection and mixing). The $[Nd]_0$ is calculated during the iteration and requires to meet the additional condition

$$[Nd]_0 \; of \; equation \; (3) = [Nd]_0 \; of \; equation \; (4) \quad (5)$$

The initial concentration of any other rare earth element ($[REE]_0$) can be calculated in the same way. Note, the sum of f_L and f_{KS} differs only slightly from f_{MW} calculated with S_m and $\delta^{18}O$, which means that f_L and f_{KS} can be used together with f_{SW} to assess the actual water mass distribution.

C.3 Estimation of $[REE]_{SIM}$

The REE concentration expected from water mass mixing and sea-ice formation and melting ($[REE]_{SIM}$) can be estimated from the change in salinity through sea-ice formation and melting (i.e. from S_m to S_0), following

$$[REE]_{SIM} = [REE]_0 - \frac{[REE]_0 * 100 - \frac{S_m * 100}{S_0}}{100} \quad (6)$$

Note, while $[Nd]_0$ corresponds to S_0, the calculated $[Nd]_{SIM}$ corresponds to S_m (Fig. C).

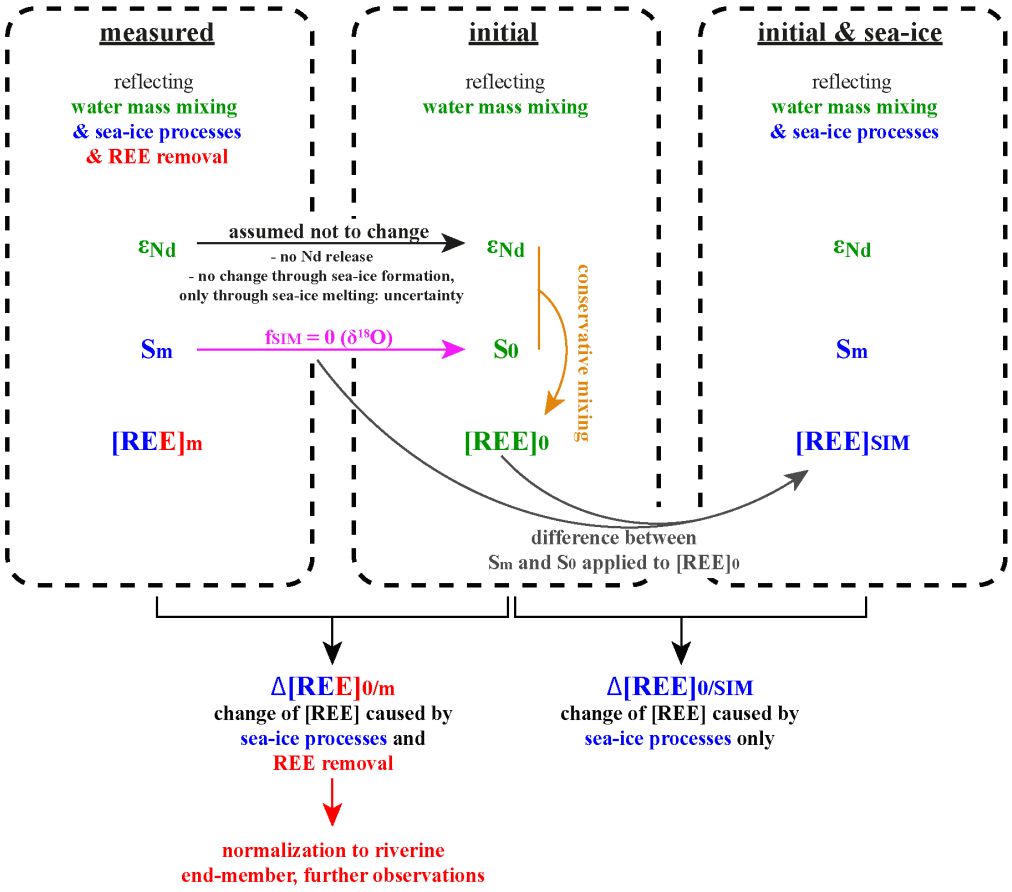

Figure C: Schematic drawing of the calculation performed in chapter II.

D. Impact of formation and melting of sea ice and river ice on the salinity-ε_{Nd} based water mass assessment

Here we address the question whether the dissolved Nd isotopes can be applied together with the salinity to assess water mass advection and mixing in areas influenced by formation or melting of sea ice and river ice. We assume that Nd isotopes are not fractionated during the formation of ice and use the terms 'sea ice' and 'river ice' to distinguish between ice that has formed from saline water and from riverine freshwater, respectively. While sea-ice formation and melting can be quantified based on the salinity and the $\delta^{18}O$ of the water (Östlund and Hut, 1984), the formation of river ice can only be quantified through determination of $\delta^{18}O$ in both the ice and the water from which it has formed (Macdonald et al., 1995). For the quantification of river-ice melt a third conservative parameter is required.

The formation of sea ice will not affect the seawater ε_{Nd} signature but increase the salinity of the remaining water. This causes changes of the initial relation between the Nd isotopes and the salinity, but can be corrected with the use of $\delta^{18}O$ through adjustment of the measured salinity (S_m) to the initial salinity (S_0) when the fraction of sea-ice melt (f_{SIM}) is set to zero. The S_0 represents the salinity of the seawater prior to sea-ice formation or melting. Sea-ice melting affects salinity and in contrast to sea-ice formation also most likely the Nd isotopic composition. Again, the change in salinity due to sea-ice melt can be corrected with the use of $\delta^{18}O$ by setting f_{SIM} to zero. However, the change in the Nd isotopic composition cannot be determined unless the Nd isotope composition of the sea ice is known. Most of our samples have negative f_{SIM}, which suggests that their seawater ε_{Nd} signatures are not affected by sea-ice melt and which is in agreement with the common observation that the Laptev Sea is an area of net sea-ice export (Bareis and Görgen, 2005). Positive f_{SIM} are observed only in surface samples recovered in the NW Laptev Sea in 2013 and 2014 and in a small area of the SW Laptev Sea in 2013. For these samples, we use the change in salinity from S_0 to S_m to estimate the extent of potential changes of their ε_{Nd} signatures. The change from S_0 to S_m is on average 4.6 % (1 SD = 6, n = 16), which is relatively small and it does not argue for significant changes of the Nd isotopic composition through admixture of sea-ice melt, if the following assumptions are made: (i) the redistribution of REEs is proportional to salinity and (ii) the Nd/S ratio is similar in sea ice and seawater in the region of melting. The latter assumption may not always be justified, but for the NW Laptev Sea it is corroborated by the fact that the Nd concentrations in surface waters of the whole western Laptev Sea region including the SW Laptev Sea (i.e. the potential formation region of the sea ice encountered in the NW Laptev Sea) are similar with values ranging between 30 and 55 pmol/kg. In the SE Laptev Sea, significant differences in the Nd/S ratio between the sea ice and the seawater are unlikely as well, since landfast ice governs most parts of this area precluding import of sea ice with a differing Nd/S ratio. Moreover, surface waters most likely are involved in wind driven transport of pack ice, which in addition argues against large shifts in the Nd isotopic composition of the seawater through addition of sea-ice melt. It is noted that the calculation of S_0 is based on f_{SIM} and therefore only accounts for net excess or deficiency of sea-ice melt, not providing direct information on total ice production and melting.

River ice can be formed in significant quantities in areas with high freshwater contributions, e.g. in high-latitude estuaries (Macdonald et al. 1995). Similar to sea ice, significant amounts of Nd are not expected in river ice as Nd will be removed from the ice during the freezing process and released to the water column. The removal might be even stronger compared to that during sea-ice formation, since river ice has no trapped interstitial brines that could host Nd. The enrichment during river-ice formation does also not result in changes of the Nd isotopic composition in the remaining water. In contrast to the change of the salinity from S_0 to S_m during sea ice formation, no changes in salinity occur during river-ice formation. Furthermore, the admixture of river-ice melt does not significantly affect the dissolved seawater Nd isotopic composition because Nd is not expected in river-ice or river-ice melt (see above). These considerations indicate

that the assessment within the water column and its composition through S_0 and Nd isotopes will not account for river-ice formation or melting. The change in salinity through admixture of river-ice melt in the Laptev Sea is expected to be relatively small as it is unlikely that more river ice than sea ice forms as the areas with a river water fraction above 50 % are small (i.e. Bauch et al., 2013). This is supported by observations from the Beaufort Sea, where the amount of river ice was shown not to exceed that of sea ice even in areas that are characterized by high contributions of freshwater (Macdonald et al., 1995).

Overall, our observations and considerations suggest that the changes through formation and melting of sea ice and river ice either can be corrected or are relatively small for the assessment of the water composition through S_0 and Nd isotopes. To account for changes that cannot be corrected, we estimate an absolute uncertainty of 5 % for the calculated water mass fractions.

E. Distribution of Lena river plume and Kara Sea freshwater

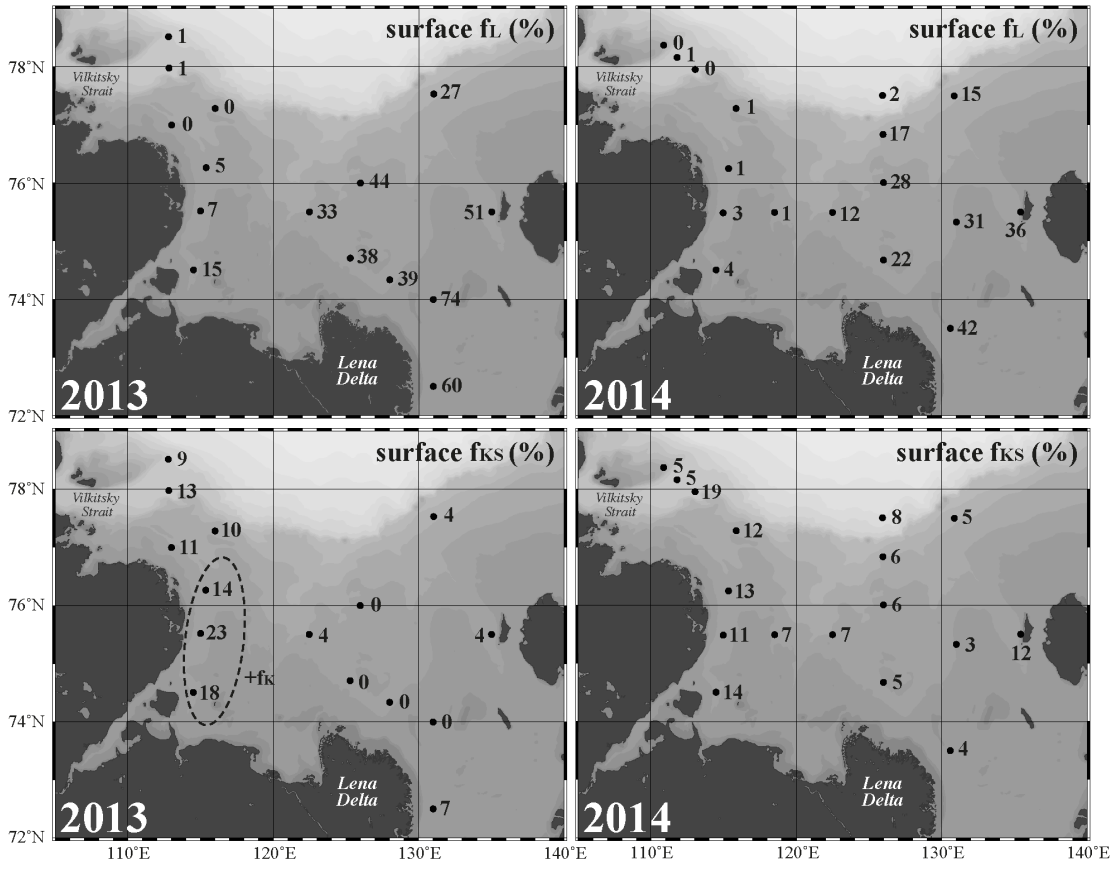

Figure E: Distribution in % of Lena River freshwater (f_L) and Kara Sea freshwater (f_{KS}) in the Laptev Sea for the summers of 2013 and 2014. Elevated f_{KS} in the SW Laptev Sea in 2013 (circled values) can partly be attributed to Khatanga River freshwater.

F. REE change in % corrected for REE removal

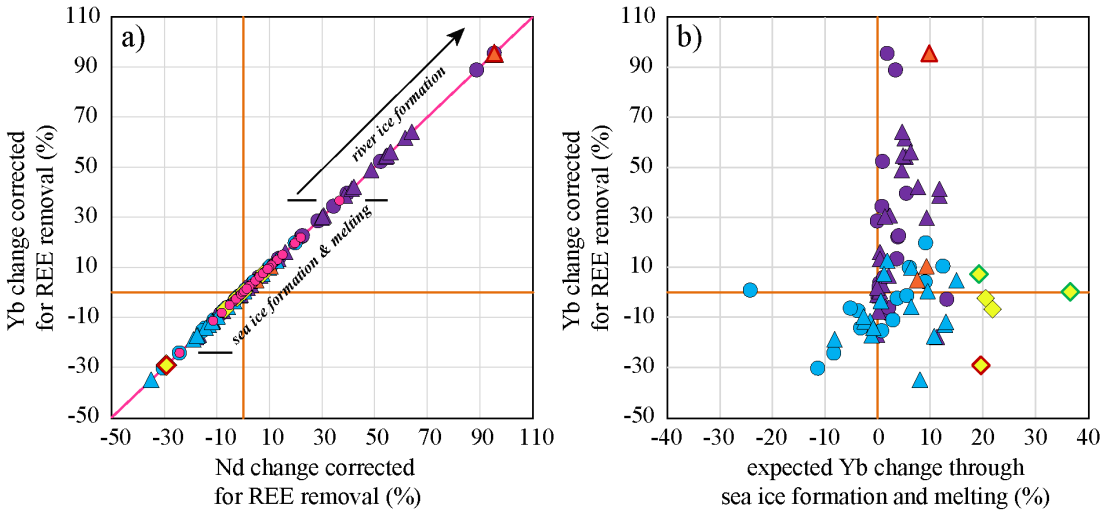

Figure F: a) Changes in % of Nd and Yb that have been corrected for REE removal. Strong HREE excess in the bottom layer cannot be explained by sea-ice formation and indicates that river-ice formation additionally leads to REE enrichment in the bottom layer. b) Change in Yb concentration that has been corrected for REE removal vs. change in Yb concentrations expected from water mass mixing and sea-ice formation and melting.

CHAPTER III

Propagation of Greenland freshwater in the western Fram Strait – Evidence from dissolved Nd isotopes and REEs

***To be submitted to GRL as**: Laukert, G., Frank, M., Hathorne, E. C., Rabe, B., von Appen, W.-J., Bauch, D., Wildau, A., Werner, K., Kassens, H.: Propagation of Greenland freshwater in the western Fram Strait – Evidence from dissolved Nd isotopes and REEs.*

Abstract

The flux of Greenland freshwater (GFW) to the ocean has accelerated since the 1990s, but observational studies investigating its fate are scarce. Here, we report new dissolved radiogenic neodymium (Nd) isotope (ε_{Nd}) and REE data from the North-East Greenland Shelf and the Fram Strait documenting GFW contributions to Arctic-derived Polar Water (PW) in the years 2012 to 2015. Based on essentially constant compositions of PW (ε_{Nd} ~ -9) and other water masses over the observed time period similar fractions of GFW (~6 %) are found for shallow waters in the Norske Trough for 2014 and east of Ob Bank for 2015 reflecting southward and northward propagation of GFW along the Greenland coast. Future increased GFW supply will likely lead to additional freshening of the PW, which, once these waters have traversed the Nordic Seas, may ultimately affect overturning strength in the North Atlantic.

1. Introduction

Melting of the Greenland Ice Sheet has dramatically increased in the recent past (e.g. Bamber et al., 2012; Box and Colgan, 2013; Gardner et al., 2011; Pritchard et al., 2009; Velicogna, 2009) and the associated accelerating flux of Greenland freshwater (GFW) to the adjacent seas reached ~1200 km^3/yr in 2010 (Yang et al., 2016). Further increased GFW discharge may significantly decrease surface ocean salinity around Greenland and may ultimately contribute to a weakening of the Atlantic Meridional Overturning Circulation (e.g. Böning et al., 2016; Brunnabend et al., 2015; Fichefet et al., 2003; Swingedouw et al., 2012; Yang et al., 2016). To determine the exact hydrographic feedbacks, detailed knowledge on the propagation and distribution of GFW around Greenland is required.

Despite the growing number of modeling studies investigating GFW distribution and its impacts (e.g. Böning et al., 2016; Dukhovskoy et al., 2016; Gillard et al., 2016; Yang et al., 2016) there are to date only two observational studies documenting GFW distribution on the North-East (NE) Greenland Shelf (Laukert et al., 2017; Stedmon et al., 2015). One of the reasons for this is the difficulty of finding tracers that allow differentiation between GFW and freshwater supplied from other sources, such as the Arctic rivers. Standard hydrographic tracers (T, S, NO_3, PO_4, Si) and stable oxygen isotopes ($\delta^{18}O$) have been successfully applied to distinguish between meteoric water, sea-ice meltwater as well as Atlantic Water (AW) and Pacific-derived waters (PAC) within the Arctic halocline (e.g. Ekwurzel et al., 2001; Jones et al., 2008a; 1998; Newton et al., 2013; Yamamoto-Kawai et al., 2008) but they do not provide information on the different origins of meteoric waters (i.e. river, glacial and precipitation) and their sources, which requires additional tracers. The Fram Strait is a key area in this respect, not only because it is the main gateway through which heat and freshwater are exchanged between the Nordic Seas and the Arctic Ocean, but also because it allows the investigation of GFW discharge from the marine outlets of the NE Greenland Ice Stream (NEGIS). The drainage basin area of NEGIS covers ~16 % of the entire Greenland ice sheet and has undergone substantial ice loss in the recent past (Khan et al., 2015).

Laukert et al. (2017) combined dissolved radiogenic neodymium (Nd) isotopes (expressed as $\varepsilon_{Nd} = [(^{143}Nd/^{144}Nd)_{sample}/(^{143}Nd/^{144}Nd)_{CHUR} -1] \times 10^4$ with CHUR = 0.512638 referring to the 'CHondritic Uniform Reservoir', Jacobsen and Wasserburg, 1980) and rare earth elements (REEs) with the above-mentioned parameters to assess the advection and mixing of water masses in the Fram Strait region in 2012. The distribution of dissolved Nd isotopes reflects the lateral advection of water masses and their mixing in the Arctic Ocean and the Fram Strait and provides information on their sources (Andersson et al., 2008; Laukert et al., 2017; Porcelli et al., 2009; see also Chapter II). The dissolved REE concentrations and their distribution patterns provide complementary information on the composition of the source rocks and input pathways, the amount of time that passed since the last exposure of waters to weathering inputs, and particle adsorption and desorption processes (e.g. Garcia-Solsona et al., 2014; Haley et al., 2014; Hathorne et al., 2015; Molina-Kescher et al., 2014). The Nd isotope, REE and

$\delta^{18}O$ data reported by Laukert et al. (2017) for 2012 documented the advection of Atlantic- and Arctic-derived waters in the upper water column of Fram Strait and showed that relatively radiogenic (ε_{Nd} ~ -9) Arctic-derived Polar Water (PW) formed the core of the East Greenland Current (EGC) above the Greenland continental slope (Fig. 1). Less radiogenic ε_{Nd} signatures (~ -12), as well as elevated meteoric water fractions and REE concentrations observed in shallow waters further west on the Greenland shelf were attributed to GFW addition to PW that resulted in the formation of NE Greenland Shelf Shallow Water (NEGSSW), for which the fraction of entrained GFW (up to ~6 %) was calculated based on the difference in $\delta^{18}O$ and salinity (S) between PW and the NEGSSW. It was inferred that the origin of the GFW contained in NEGSSW was the marine outlets Nioghalvfjerdsbræ (79° N Glacier) and Zachariæ Isstrøm of the NEGIS and the presence of GFW in the inter-trough area east of the Northwind Shoal was consistent with the near-surface anticyclonic circulation scheme on the shelf (cf. Budéus et al., 1997; Rabe et al., 2009).

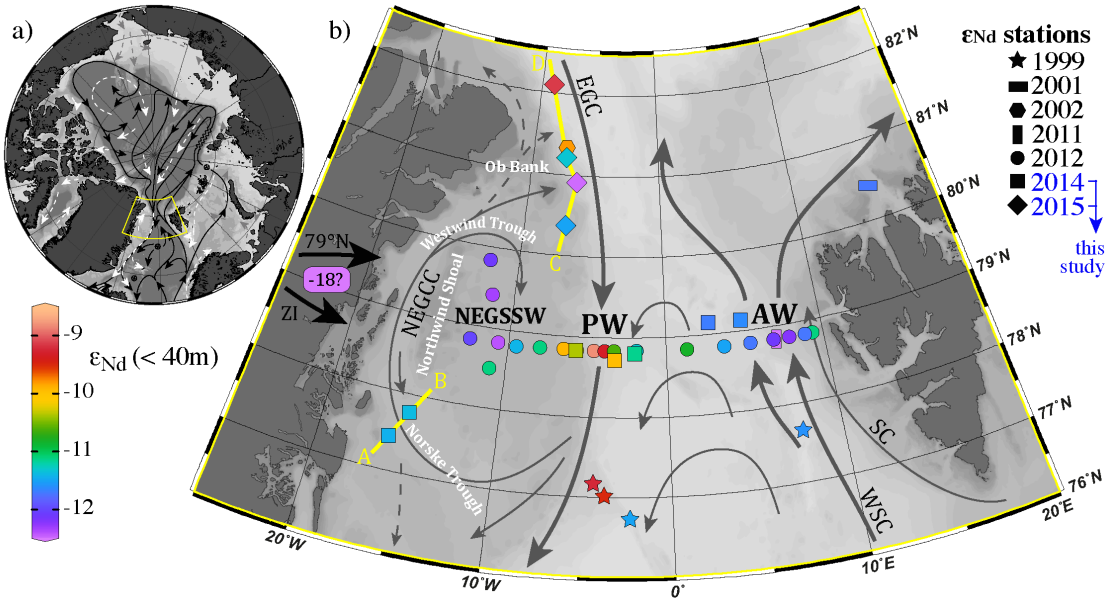

Figure 1: Bathymetric map of the Arctic region with the inset representing the Fram Strait area (IBCAO, Jakobsson et al., 2012). a) Map of the Arctic region with ocean circulation scheme of the upper layers (dashed white and grey lines) and subsurface Atlantic and intermediate layers (solid black lines) (modified after Rudels et al., 2012). b) Fram Strait region with schematic representation of the four major near surface currents (WSC, West Spitsbergen Current; EGC: East Greenland Current; NEGCC: North-East Greenland Coastal Current; SC, Sørkapp Current) and seawater ε_{Nd} data of this study (2014 and 2015) and from the literature (Andersson et al., 2008; Lacan and Jeandel, 2004a, b; Laukert et al., 2017; Werner et al., 2014). The surface ε_{Nd} signatures reflect the advection of Atlantic Water (AW) in the western Fram Strait (ε_{Nd} ~ -12) and Polar Water (PW) above the Greenland margin (ε_{Nd} ~ -9), while the NE Greenland Shelf Shallow Water (NEGSSW; ε_{Nd} ~ -12) covers the entire NE Greenland Shelf. Black arrows indicate the terminations Nioghalvfjerdsbræ and Zachariæ Isstrøm (ZI) of the NEGIS, which are the major sources of GFW in this region. Figures were produced using Ocean Data View (Schlitzer, 2016) and modified manually.

The quantification of GFW is possible without $\delta^{18}O$ data but requires conservative behavior of Nd isotopes and constant end-member compositions (ε_{Nd} and S or [Nd]) of GFW and PW over time. Apart from water mass advection and mixing the dissolved Nd isotope compositions of waters can be altered through release of Nd from particulate phases or through seawater-particle interactions (cf. reviews by Jeandel, 2016 and Jeandel and Oelkers, 2015). Laukert et al. (2017) observed particulate Nd release in NE Greenland Shelf Bottom Water (NEGSBW) and suggested that this process is linked to the relatively long residence time (10-20 years) of NEGSBW on the shallow shelf and strong decomposition of organic matter below ~150 m depth. In contrast, no evidence for particulate Nd release was observed in the upper water column, indicating that the ε_{Nd} signature of NEGSSW is mainly controlled by water mass mixing. While the GFW end-member composition can be assumed to have remained essentially constant over time (i.e. the onshore flow paths of GFW likely did not change on annual time scales), the PW composition has been shown to vary largely, both seasonally and interannually (e.g. de Steur et al., 2015; Dodd et al., 2012; Falck et al., 2005; Rabe et al., 2009; Sutherland et al., 2009; Taylor et al., 2003). Additional water masses are admixed to PW directly in the Fram Strait and potential variability of their compositions will also affect the mixing calculations based on Nd isotopes. Clearly, significant compositional changes would result in strong variations in the Nd isotopic composition of PW and complicate assessments of the fraction and propagation of GFW.

Here, we provide new Nd isotope and REE data from the full water column of the central Fram Strait and the Norske Trough for 2014 and from the upper water column east of Ob Bank for 2015. Based on these and literature data, we reconstruct the compositional variability of PW and other water masses in the Fram Strait and assess the distribution and propagation of GFW in the Fram Strait region.

2. Methods

The new seawater samples of this study were obtained during two expeditions of the German research vessel FS Polarstern between 6 June and 3 July 2014 (PS85, ARKXXVIII/2) and between 29 June and 17 July 2015 (PS93.1, ARKXXIX/2.1). The data are complemented by a comprehensive seawater data set reported previously for 2012 for the central Fram Strait and the inter-trough area east of Northwind Shoal (Laukert et al., 2017).

All sampling locations are shown in Fig. 1. At each location, CTD (conductivity, temperature, depth) profiles were obtained. Seawater samples for the analysis of Nd isotopes and REEs were collected in 2014 from the full water column of the central Fram Strait (at ~79 °N) and at two stations in the Norske Trough. Sampling in 2015 was performed along a zonal section (~80 to ~82 °N) east of Ob Bank down to a depth of 300 m. All samples were taken with a SBE32 rosette water sampler equipped with 24 Niskin-type sample bottles (12 L) and collected in 10 or 20 L acid-cleaned LDPE-cubitainers and filtered through AcroPak^{TM}500 Capsules with Supor Membrane (pore size: 0.8/0.2 µm)

filter cartridges immediately after sampling. Sample treatment including pre-concentration was performed following Laukert et al. (2017) after the samples had been transported to the home laboratory at GEOMAR, Kiel. For the extraction and isolation of dissolved Nd, the procedure outlined in Stichel et al. (2012) was applied.

The Nd isotopic compositions were measured on a Nu Plasma (Nu Instruments Limited) MC-ICP-MS at GEOMAR, Kiel. For correction of instrumental mass bias an exponential mass fractionation was applied using a $^{146}Nd/^{144}Nd$ ratio of 0.7219. The measured $^{143}Nd/^{144}Nd$ ratios of all samples were normalized to the value of 0.512115 for the JNdi-1 standard (Tanaka et al., 2000). Based on repeated measurements of JNdi-1 and in-house standards with concentrations similar to those of the samples, the 2σ external reproducibility ranged between 0.1 and 0.4 ε_{Nd} units for the individual measurement runs.

The REE concentrations were determined in all samples recovered in 2014 using an online pre-concentration (OP) ICP-MS technique at GEOMAR, Kiel by directly coupling a "seaFAST" system (Elemental Scientific Inc., Nebraska, USA) to an ICP-MS (Agilent 7500ce) (Hathorne et al., 2012). The method of Hathorne et al. (2012) was further improved by using 8 mL sample loop and by preparation of calibration standards with a mixed REE solution of a seawater-like composition in a natural seawater matrix (Osborne et al., 2015). Repeated measurements of GEOTRACES inter-calibration sample BATS 15m (van de Flierdt et al., 2012) were used to monitor the external reproducibility (see data table A1). The entire pre-concentration, purification and measurement techniques for REE concentrations and Nd isotope compositions reported here followed approved GEOTRACES protocols and were confirmed through participation of our laboratory in the international GEOTRACES inter-calibration study (van de Flierdt et al., 2012).

3. Results

All data are reported in the data table A1 and are available at the PANGAEA database. Figure 2 shows the θ-S distributions (black dots) of 2014 (Rabe et al., 2014) and of 2015 (von Appen et al., 2016b) combined with the Nd isotope data of this study, which are complemented by the previously published data for the year 2012 (Beszczynska-Möller and Wisotzki, 2012; Laukert et al., 2017). The θ-S distribution of 2014 closely resembles that of 2012 and is within the typical range observed at Fram Strait and on the NE Greenland Shelf (cf. Budéus et al., 1997; Schlichtholtz and Houssais, 2002), while the distribution of 2015 only represents shallow waters east of Ob Bank. Common to all years is the sharp inflection at S ~34, an increase in temperatures below S ~32 and data close to the freezing temperature of seawater at a given salinity in between.

The water mass classification applied here is adopted from Laukert et al. (2017). The flow path of PW above the Greenland continental margin is reflected by the most radiogenic ε_{Nd} signatures (reaching -9.3±0.2 and -9.2±0.4 in 2014 and 2015, respectively) and elevated [Nd] (~29 pmol/kg in 2014) in both years (Figs. 1 and 3). Less radiogenic ε_{Nd}

signatures (e.g. -10.7±0.3, sample 28/417/75) characterized modified PW in the Norske Trough in 2014 at intermediate depths between 80 and 300 m (Fig. 3). Below the PW layer, a less radiogenic ε_{Nd} signature of -11.4±0.1 (sample 28/413/320) and lower [Nd] (~19 pmol/kg) are observed in the Norske Trough in 2014 but do not represent a distinct water mass, while east of Ob Bank in 2015 significantly lower ε_{Nd} values (e.g. -12.4±0.4, sample 29/11/150) in combination with the hydrographic data can clearly be attributed to NEGSBW (Fig. 3). The presence of NEGSSW in the upper water column of the Norske Trough and east of Ob Bank is documented by similarly unradiogenic Nd isotopic compositions (reaching -11.9±0.1 and -12.5±0.4 in 2014 and 2015, respectively), which in the Norske Trough are accompanied by the highest [Nd] values (reaching ~43 pmol/kg) and the lowest heavy (H)REE to light (L)REE ratios (reaching ~3.6, here reflecting $([Tm]_N+[Yb]_N+[Lu]_N)/([La]_N+[Pr]_N+[Nd]_N)$, whereby "N" refers to concentrations normalized to Post-Archean Australian Sedimentary rocks, PAAS, McLennan, 2001).

The AW in 2014 was characterized by an ε_{Nd} signature of -11.6±0.2, a [Nd] of ~16 pmol/kg, and a HREE/LREE ratio of ~4. Recirculating AW (RAW) further west has slightly more radiogenic ε_{Nd} signatures (e.g. -11.3±0.1). Intermediate and deep waters in 2014 were characterized by the same [Nd] as AW and RAW but more radiogenic ε_{Nd} signatures (Fig. 2) averaging -10.3 (1 SD = 0.3, n = 15).

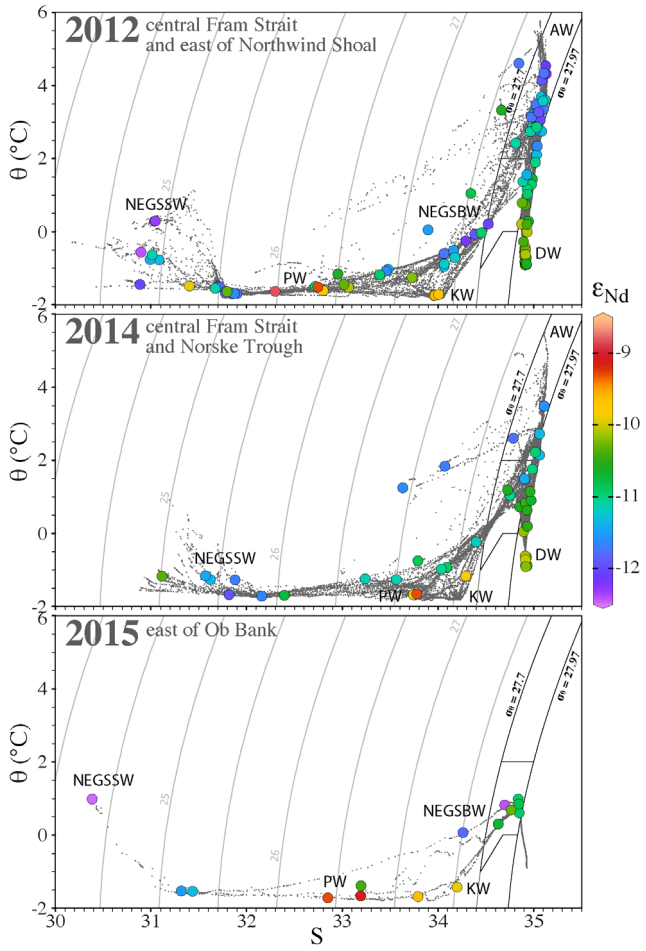

Figure 2: Potential temperature (°C) versus salinity plots with potential density isopycnals (solid back lines; σ_θ = potential density for reference pressure at 0 m), and ε_{Nd} values shown as color-coded circles for 2012 (Laukert et al., 2017), 2014 and 2015 (this study). In addition, all hydrographic data (black dots) are shown for every year. Water masses are labeled as follows: Polar Water – PW, Knee Water - KW, NE Greenland Shelf Shallow Water – NEGSSW, NE Greenland Shelf Bottom Water – NEGSBW, Atlantic Water – AW, deep waters – DW. Figures were produced using Ocean Data View (Schlitzer, 2016) and modified manually.

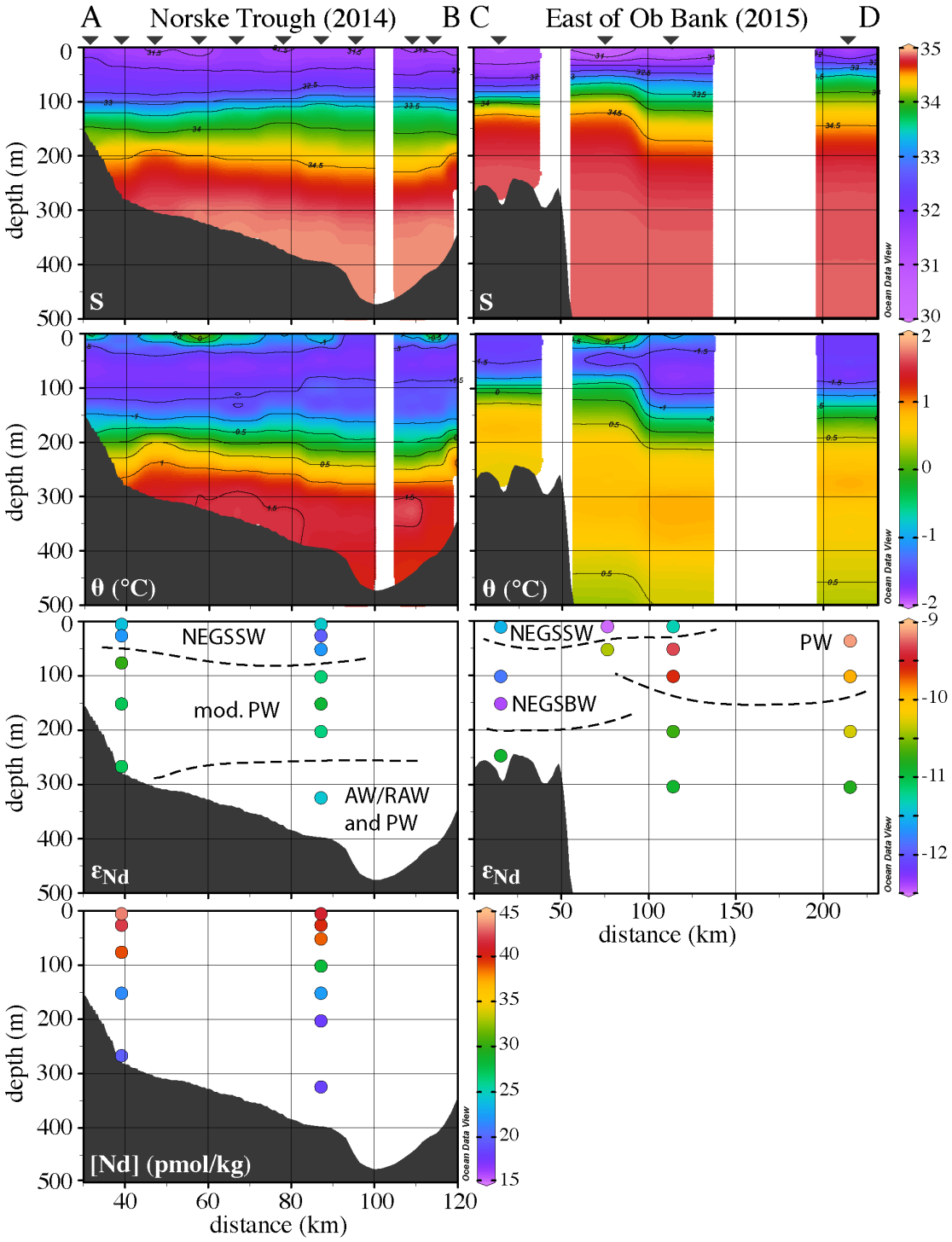

Figure 3: Distribution of salinity and potential temperature (all CTD data; inverted triangles are locations of CTD stations), as well as the Nd isotope compositions (ε_{Nd}) along the sections A-B and C-D as indicated in figure 1. For section A-B, the Nd concentration ([Nd] in pmol/kg) is also shown. Sections were produced using Ocean Data View (Schlitzer, 2016) and modified manually.

4. Variability of water masses in the Fram Strait

We use PW as the marine end-member to quantify GFW addition to shallow waters on the NE Greenland Shelf. Multiple assessments based on mass balance calculations involving different empirical nitrate-phosphate relationships and $\delta^{18}O$ data (here referred to as N/P methods) suggested that the PAC fraction contained in PW passing the Fram Strait has varied from nearly undiluted to almost completely absent in the past 20 years (de Steur et al., 2015; Dodd et al., 2012; Falck et al., 2005; Rabe et al., 2009; Sutherland et al., 2009; Taylor et al., 2003). Even though significant uncertainties were observed for the absolute PAC fractions calculated applying these methods (Alkire et al., 2015; Laukert et al., 2017), the observed variations in $\delta^{18}O$ and nutrient ratios clearly reflect significant compositional changes, implying that large interannual variations in the Nd isotopic composition of PW are also expected.

For years with available Nd isotope and [Nd] data in the western Fram Strait region (i.e. 1999, 2002, 2012, 2014 and 2015, see Fig. 1), the samples with the most radiogenic ε_{Nd} values only exhibit minor compositional variations (Fig. 4). These samples likely reflect pure PW advected from the Arctic Ocean without significant contributions of less radiogenic AW/RAW, GFW or NEGSBW (Laukert et al., 2017). Based on these samples and a mixing calculation between AW and the Nd-based Pacific-derived Water (PACW) end-member, the fraction of PACW contained in PW for these years was relatively constant at ~20 and ~30 % (Fig. 4a and b). We assume that the offset from the mixing lines is caused by admixture of small amounts of meteoric waters that resulted in lowered salinities and higher [Nd] but did not significantly affect the ε_{Nd} signatures of PW (Laukert et al., 2017). This is a reasonable assumption given that the Nd isotopic composition of the meteoric waters likely is similar to that of a PACW-AW mixture with a ratio between PACW and AW close to ~2:3, as indicated by the average ε_{Nd} signature of the Arctic rivers (~ -8.5; calculated by taking into account volume transport and [Nd], data from Persson et al. 2011; Porcelli et al., 2009; Zimmermann et al., 2009) that are assumed to contribute most to the meteoric water fraction. Our observation of constant PACW fractions is in line with the assessments based on the N/P methods, which suggest significantly higher but overall constant PAC fractions for the periods before 2004 and after 2010 (e.g. Dodd et al., 2012). Note that the N/P methods do not account for admixture of GFW, which imposes significant uncertainties also on the meteoric water fractions determined with these methods.

For the calculation of the amount of GFW contained in NEGSSW, we apply the same PW composition as in Laukert et al. (2017). This composition is different from that of purely advected PW (see Fig. 4c and d), as it accounts for the admixture of other water masses at Fram Strait, such as NEGSBW, AW/RAW or intermediate waters. Their compositions can also vary with time and require a careful evaluation. Of particular interest are changes in the composition of the bottom waters of the NE Greenland Shelf that constitute a mixture between AW/RAW and PW. Their composition can be altered by the release of particulate Nd which will result in the formation of NEGSBW that has less radiogenic ε_{Nd} signatures and higher [Nd] compared to values expected from water

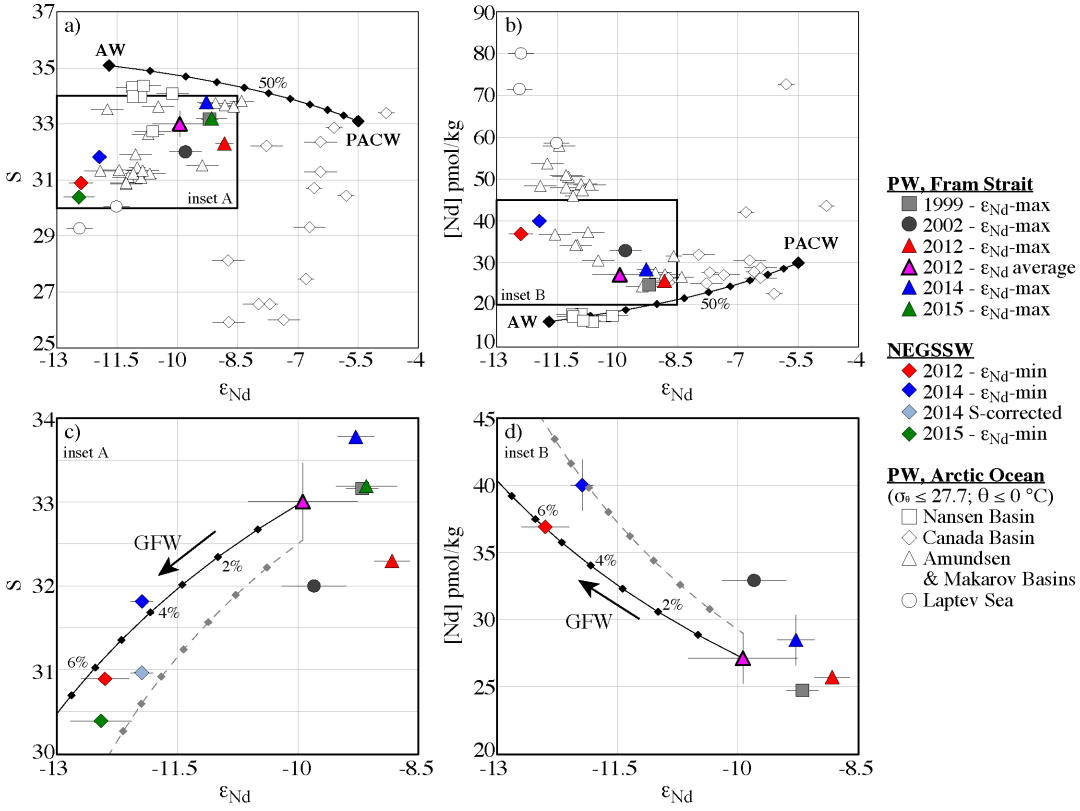

Figure 4: a) and b) Comparison of the PW samples with the most radiogenic ε_{Nd} values. Mixing lines between AW (at Fram Strait) and Pacific-derived Water (PACW) and literature Nd data from the Arctic Ocean (Zimmermann et al., 2009; Andersson et al., 2008; Porcelli et al., 2009; Laukert et al., submitted) are shown in addition. c) and d) insets A and B as defined in a) and b), respectively, documenting the admixture of GFW to PW resulting in the formation of NEGSSW.

mass advection and mixing alone (Laukert et al., 2017). The Nd characteristics east of Ob Bank in 2015 at ~150 m depth clearly indicate the presence of NEGSBW (Fig. 3), in agreement with similar Nd characteristics observed east of the Northwind Shoal in 2012 (Laukert et al., 2017). In contrast, the compositions of the bottom waters in the Norske Trough in 2014 can be entirely attributed to mixing between PW (~10 to 20 %) and AW/RAW, which suggests that the transformation of AW/RAW into NEGSBW occurs further north. This is in agreement with elevated bottom temperatures (~1.5 °C) observed at the Norske Trough in 2014, which also indicate the presence of AW/RAW (Heiderich, 2015). Furthermore, this observation is consistent with the shelf circulation that is characterized by northward transport of relatively young AW/RAW along the Norske Trough (e.g. Budéus et al., 1997; Heiderich, 2015; Rabe et al., 2009). Even though the transformation of AW/RAW into NEGSBW is clearly seen in the bottom layer, it did not affect the PW composition above the NEGSBW, given that similar PW compositions are observed in the Norske Trough in 2014 and east of the Northwind Shoal in 2012 (Laukert et al., 2017).

While the AW temperatures and volume transport were shown to vary on interannual timescales (e.g. Beszczynska-Möller et al., 2012), the Nd isotope signatures

are likely not sensitive enough to reflect the small changes observed at Fram Strait, which is supported by identical ε_{Nd} signatures of AW for all years with Nd data available (i.e. for 1999, 2001, 2011, 2012 and 2014, Fig. 1). Similarly, the ε_{Nd} signatures of intermediate and deep water masses found for 2014 are on average identical to those reported for 2012 (Laukert et al., 2017), which is unsurprising given that the mean ages of these water masses range between ~100 and ~300 years (Stöven et al., 2016) and water masses with different Nd isotope compositions are not expected to be admixed in different proportions during such short time intervals. Intermediate and deep water samples obtained for the period prior to 2012 showed more variable Nd isotope compositions and higher [Nd] (Lacan and Jeandel, 2004b; Piepgras and Wasserburg, 1987; Werner et al., 2014). However, these do likely not represent the pure dissolved compositions of the water masses since these samples were either not filtered or filtered only several weeks after sampling.

In summary, we suggest that the compositions of PW, AW/RAW, NEGSBW and intermediate and deep waters were relatively constant for the time period investigated here. The PW composition reported by Laukert et al. (2017) thus can be used as the marine end-member to quantify the addition of GFW to shallow waters on the NE Greenland Shelf.

5. Estimation of the fraction of Greenland freshwater

We quantified the contribution of GFW to shallow waters in 2014 and 2015 and compare the results to those obtained by Laukert et al. (2017) for 2012 in order to evaluate its temporal variability. Similar to the PW end-member, we apply the Nd isotope and [Nd] values of the GFW end-member determined by Laukert et al. (2017).

As can be seen in Figs. 4c and d, the NEGSSW samples with the least radiogenic ε_{Nd} signatures plot close to the PW-GFW mixing line in the ε_{Nd}-salinity and the ε_{Nd}-[Nd] space. The NEGSSW sample recovered in 2014 (28/413/25, Norske Trough) contains ~4 % GFW based on the ε_{Nd}-salinity relationship but higher GFW (~6 %) based on the ε_{Nd}-[Nd] relationship. The GFW contained in the NEGSSW sample recovered in 2015 (29/24/10, east of Ob Bank) can only be assessed based on the ε_{Nd}-salinity relation, which for this sample indicates GFW addition of up to ~7 %. A change in the salinity through brine addition likely accounts for the difference between the ε_{Nd}-salinity and ε_{Nd}-[Nd] relationships observed for the sample recovered in 2014. The salinity can be corrected by adjusting the fraction of sea-ice meltwater ($\delta^{18}O$ for this sample is ~ -2.8 ‰, Ben Rabe, personal communication; $\delta^{18}O$ and S end-member compositions were adopted from Laukert et al., 2017) to zero (see chapter II for more information). The salinity-corrected sample plots closer to ~6 % GFW in the ε_{Nd}-S field (Fig. 4c), resulting in a better match with the ε_{Nd}-[Nd] based estimate and the estimate based on $\delta^{18}O$ and S which is ~6 %. Laukert et al. (2017) pointed out that the actual [Nd] of the GFW end-member might be higher, since the calculated [Nd] (210 pmol/kg) does not account for any REEs likely present in the low-salinity range when GFW mixes with seawater (see

also Tepe and Bau, 2016). Thus, considerable uncertainties will persist unless the actual GFW end-member composition is determined and the removal of REEs is quantified. Furthermore, deviations away from the mixing line were observed by Laukert et al. (2017) and attributed to sea-ice formation and melting, or uncertainties in the Nd isotopic composition of the GFW end-member (the ε_{Nd} signature of the GFW end-member was set to -18 based on rock data). Deviations from the mixing line are observed for 2014 and 2015, too, and may also be attributed to sea-ice related changes or uncertainties of the end-members. However, despite these offsets our mixing calculations indicate that the Nd isotope and [Nd] data are suitable to estimate the amount of GFW in the western Fram Strait, which is mainly supported by the agreement with the $\delta^{18}O$ and S estimates.

6. Distribution and propagation of Greenland freshwater and implications

The marine outlets of the NEGIS (i.e. the Nioghalvfjerdsbræ or 79° N Glacier and the Zachariæ Isstrøm) are the likely the major contributors of GFW in this region (Fig. 1), which suggests that GFW is distributed in similar proportions both to the north and south along the Greenland coast. This is consistent with the presence of the northward flowing North-East Greenland Coastal Current (NEGCC; e.g. Budéus et al., 1997; Rabe et al., 2009) and a bi-directional (i.e. southward and northward) flow in the Norske Trough (Heiderich, 2015). Northward and southward flow of NEGIS-sourced GFW also agrees with recent modeling studies investigating the distribution of GFW around Greenland (Dukhovskoy et al., 2016; Gillard et al., 2016). Even though our data document that GFW in 2015 propagated only as far as ~81 °N (Fig. 1), the surface θ-S distribution (Stein and Rohardt, 2016) indicates that waters with similar θ-S properties were present as far as ~82 °N (i.e. north of Ob Bank), arguing for transport of NEGIS-sourced GFW towards the Arctic Ocean (cf. Gillard et al., 2016). The GFW-rich waters at ~81 °N in 2015 had temperatures ~1 °C at ~10 m depth, suggesting that they were advected from the Greenland coast after they had warmed up during the opening of the Northeast Water Polynya (NEWP) in June 2015 (the daily ice distribution is archived online at https://seaice.uni-bremen.de/sea-ice-concentration/). The formation of the NEWP was suggested to result from the combined effect of a fast ice barrier further south and the northward flowing NEGCC (Budéus and Schneider, 1995), which supports our observations of northward-directed flow of GFW.

We suggest that increased advection of warm GFW-rich waters to the area north of Greenland will result in significant changes of the hydrology and the sea-ice distribution of this sensitive Arctic region. The northward advection will also result in freshening of the PW before it enters the Nordic Seas and the North Atlantic. After the PW has entered the Nordic Seas, most of it is directly transported south via the EGC and leaves the Nordic Seas through the Denmark Strait (e.g. Hansen and Østerhus, 2000), the freshening of the PW will thus unlikely significantly affect sites of deep convection in

the Nordic Seas (i.e. the Greenland Sea and the Iceland Sea). However, once the GFW-rich PW has passed the Denmark Strait, it will be advected to the northern Labrador Sea (cf. Luo et al., 2016), which is one of the key areas of deep convection in the North Atlantic. Therefore, freshening of the PW through increased GFW supply may ultimately contribute to a weakening of the Atlantic Meridional Overturning Circulation.

Acknowledgements

We like to thank the Captain and Crew of Polarstern for help in collecting the samples and the expedition leaders Rüdiger Stein and Ingo Schewe for the opportunity to recover the big-volume samples. Jutta Heinze (GEOMAR) is greatly acknowledged for laboratory assistance. Furthermore, we thank the German Federal Ministry of Education and Research (BMBF) and the Ministry of Education and Science of the Russian Federation for support of the "Laptev Sea System" project (BMBF grant 03G0833).

4. SUMMARY, CONCLUSIONS AND OUTLOOK

4.1 Summary and Conclusions

Motivated by the recently observed strong warming of the Arctic region and related substantial changes in the Arctic Mediterranean (AM), this thesis (i) presents the compositions and fractional contributions of water masses passing the Fram Strait and the Laptev Sea and discusses them in terms of water mass origin, distribution and mixing, (ii) refines the knowledge of the ocean circulation in the AM based on the new data and provides a compilation and reassessment of literature Nd isotope and concentration data, (iii) assesses the interannual variability of freshwater inputs and distributions and water mass advection and mixing in the Fram Strait and in the Laptev Sea, (iv) provides new insights into the processes occurring on the Arctic shelves, and (v) deepens the current understanding of the behavior of rare earth elements (REEs) and neodymium (Nd) isotopes in the modern AM and in freshwater and ice-dominated regions. A multi-proxy geochemical inventory is presented and dissolved Nd isotopes, dissolved REEs, seawater stable oxygen isotopes ($\delta^{18}O$) together with standard hydrographic tracers (e.g. T, S, NO_3, PO_4, Si) are the tools applied.

In **chapter I** it is demonstrated that dissolved Nd isotope and REE distributions primarily reflect lateral advection of water masses and their mixing in the open AM, whereas seawater-particle interactions exert important control only above the shelf regions, as evidenced from the North-East Greenland Shelf. The seawater Nd isotope and REE data from the central Fram Strait reveal a relatively unradiogenic Nd isotope composition for the northward flowing Atlantic-derived waters, which can be traced from the Greenland-Scotland Ridge to the Canada Basin and is modified towards more radiogenic compositions through mixing with intermediate waters and admixture of

shallow Arctic waters. It is suggested that the more radiogenic signatures of the intermediate and deep waters are acquired mainly in the southwestern Nordic Seas through Nd inputs originating from relatively radiogenic basaltic formations of Iceland and Central-East Greenland. Less radiogenic compositions in the northern Nordic Seas and the Arctic Ocean are ascribed to deep convection of Atlantic-derived waters. The compositions of shallow waters exiting the Arctic Ocean through the western Fram Strait provide clear evidence for the advection of Pacific-derived waters and Arctic riverine freshwater to the Fram Strait and further south and indicate that these waters have been transported across the Amundsen and Makarov Basins. Comparison with widely applied $\delta^{18}O$ and nutrient based assessments of the contributions from sea-ice formation and melting, Arctic river waters and Pacific- and Atlantic-derived seawater contained in the shallow Arctic waters reveals that estimation of the Pacific-derived component is in particular challenging. However, in this regard, the application of Nd isotopes is shown to represent a new approach to estimate the amount of Pacific-derived seawater contained, and thus provides new information on the correctness and accuracy of estimates derived from other assessments. On the North-East Greenland Shelf, the Nd isotope and REE distributions indicate admixture of locally discharged Greenland freshwater in the upper 100 m, for which the contribution to the water column is quantified and the Nd end-member composition is estimated based on a mixing calculation involving $\delta^{18}O$ and salinity. This study concludes that the pronounced gradients in Nd isotope and REE signatures provide a reliable basis to determine shallow hydrological changes within the AM.

The seawater Nd isotope, REE and $\delta^{18}O$ data from the Laptev Sea reported in **chapter II** mainly show that different processes contribute to the distribution of dissolved REE concentrations in high latitude estuaries. No evidence for significant release of REEs from particulate phases is found, which is contrary to observations from most other estuaries but is in agreement with observations from the Severnaya Dvina River estuary, which, similarly to the Lena River estuary in the Laptev Sea, receives Siberian freshwaters rich in organic compounds that likely suppress release of particulate riverine REEs. The lack of REE release is also in agreement with recent estuarine mixing experiments, even though the latter do not provide information on REE release by dissolution of the lithogenic suspended riverine load. Based on these considerations and observations from mixing calculations and samples recovered by a multicorer device above the sediment-water interface, it is concluded that a pronounced alteration of the Nd isotope distribution through release of particulate Nd does not occur in the study area and that Nd isotopes thus can directly be used to trace water mass distribution and mixing. The REE distribution indicates that REEs originating from the rivers are removed from the water column through coagulation of REE-bearing riverine nanoparticles and colloids. This process is shown to start at mid salinities and to continue until high salinities are reached, with the overall fraction of Nd removal being similar to that reported for other estuaries worldwide. The onset and continuation of the removal agree remarkably well with results from recent experiments simulating estuarine mixing with organic-rich river waters indicating that river chemistry plays a major role for estuarine

REE behavior. Furthermore it is concluded that sea-ice formation and melting affect the Nd isotope and salinity distribution, but the associated changes can either be corrected for or are relatively small. In contrast, the REE redistribution within the water column caused by these processes is significant and causes a REE deficiency at the surface and REE excess in the bottom layer compared to what can be expected from water mass advection and mixing. It is suggested that river-ice formation and melting also contribute to the REE redistribution, at least close to the coast where riverine freshwater contributions are high. The ice-related processes likely have implications for the distribution of other metals and nutrients, perhaps even affecting primary productivity through removal or enrichment of nutrients. The assessment of water mass mixing based on pronounced variations in dissolved Nd isotope compositions, salinity and $\delta^{18}O$ documents variable riverine contributions from the Lena, Yenisei and Ob rivers to shallow waters of the Laptev Sea, while the bottom layer is dominated by advection of Arctic Atlantic Water. A strong interannual variability in the freshwater distribution was observed for the studied time period in the central and eastern Laptev Sea, in agreement with changing atmospheric pressure patterns.

Evidence for modern southward and northward propagation of North-East Greenland Ice Sheet sourced freshwater in the western Fram Strait and on the North-East Greenland Shelf based on multi-year seawater Nd isotope and REE data is provided in **chapter III**. The fractions of Greenland freshwater are estimated based on these parameters, as well as salinity and $\delta^{18}O$, and for the shallow waters on the North-East Greenland Shelf reach about six percent. The study includes the evaluation of interannual variability of the water masses passing the Fram Strait, which for the investigated time period for all water masses reveals relatively constant Nd isotope compositions and REE contents. The evaluation also suggests that alteration of the composition of Atlantic-derived waters through remineralization-induced release of particulate Nd only occurs in the bottom layer of the central and northern North-East Greenland Shelf, while the southern North-East Greenland Shelf is characterized by advection of a mixture of unaffected Atlantic- and Arctic-derived waters. The distribution and propagation of Greenland freshwater is shown to be consistent with the circulation on the North-East Greenland Shelf and with recent modeling studies. This suggests that increased advection of Greenland freshwater to the area north of Greenland will in the future significantly affect the hydrology and the sea-ice distribution of the region and will result in freshening of shallow Arctic waters that enter the North Atlantic through the Denmark Strait. Once there, Arctic-derived waters with high fractions of Greenland freshwater may influence deep convection, particularly in the northern Labrador Sea.

Overall, this study can be regarded the continuation of the pioneering Nd isotope studies performed in the AM in the 2000s. It clearly demonstrates that seawater Nd isotope compositions and REE contents are powerful geochemical tracers of ocean circulation in the AM but also that they can be widely applied to track numerous physiochemical and biogeochemical processes occurring in the oceans. The challenging observation that Nd isotopes and REE concentrations do not always behave

conservatively in the water column is not a drawback because it provides the opportunity to obtain information in excess of what can be learned if they behaved strictly conservatively. The additional application of stable oxygen isotopes is clearly an advantage given that additional information on the distribution of freshwater, brines and sea-ice melt is provided.

4.2 Outlook

A major focus in future Nd isotope and REE based ocean chemistry studies should be the assessment of seasonal and interannual changes in the upper circulation of the AM. The application of Nd isotopes to trace water mass origin, advection and mixing at surface and subsurface depths is clearly complementary to the assessments based on $\delta^{18}O$ and nutrients and improves the reliability of the results, and in the future may become the new standard to track climatically driven changes within the shallow Arctic water column. However, for this purpose, it is necessary to better determine and quantify all fluxes from all Nd sources that contribute to the AM. To date unstudied sources and input mechanisms include freshwater discharge from small rivers, supply of glacial meltwater and runoff, direct inputs of aeolian dust or melting of dust-bearing snow, melting of sea ice and river ice, and release from particulate phases, such as suspended and deposited riverine loads and sediments deposited on the shelves, the shelf slopes or continental margins, and in the deep basins. Once all sources and input mechanisms are included, the Nd isotopes and REEs could be widely applied to investigate water mass circulation and different physiochemical and biogeochemical processes. Clearly, standard hydrographic tracers and stable oxygen isotopes should be measured alongside these parameters to provide further information on sea-ice related processes and the origin and modification of distinct source-defined Arctic water mass components. Future studies should also report the complete set of REEs, given that the REE distribution patterns store important information on various seawater-particle interactions. Furthermore, paleoceanographic studies should consider the new data for paleoreconstructions on a variety of time scales. Deciphering of past water mass variability for example might significantly benefit from the refined knowledge of the modern circulation in the AM and the Nd isotope characteristics of water masses presented in this study.

Processes related to estuarine mixing need further attention and should be investigated in the field and in the lab. Given that rivers are the main direct source of REEs to the oceans, the behavior of the riverine REEs in estuaries is of significant importance for the formation of Nd isotope and REE signatures released into the open water column. The laboratory experiments can be performed for different size pools, including the truly dissolved, the dissolved and the colloidal size fractions. Measurable parameters such as pH, salinity, temperature, major and minor elements, trace elements and dissolved organic carbon should be determined in addition to the complete set of REEs. If possible, filtrates should be investigated under a scanning electron microscope

to document changes in physical properties of the particulate phases involved. Nevertheless, it should also always be kept in mind that laboratory experiments will never replace observational field studies. A combination of field and lab investigations is likely the best way to determine estuarine mixing processes, and requires large volume sampling of the marine and the riverine end-members during the field campaigns. Modeling including mixing calculations can then be applied to understand reactions and fluxes between the different components.

In a similar way, the REE fluxes related to sea-ice and river-ice processes should be investigated. To date, no information is available on the behavior of REEs during freezing of Arctic sea ice and river ice, but considerations and observations suggest that REE redistribution occurs. During freezing experiments in the laboratory, this redistribution could be quantified and the question whether the REEs fractionate during freezing of seawater and freshwater could be addressed. In the same manner as the estuarine mixing experiments, freezing tests should include the determination of all other relevant parameters to understand the observed changes. Aeolian inputs caused through melting of snow need to be investigated additionally. Missing information with regard to the behavior of REEs during melting of dust-bearing snow into seawater inhibits an assessment of the impact of absent aeolian input into the central Arctic Ocean caused by the permanent sea-ice cover. It is not clear if and how the absence of aeolian fluxes coincides with the absence of vertical gradients observed in the intermediate and deep water column of the AM. Here, laboratory experiments simulating snow melting on sea ice and subsequent transfer of snow melt into the underlying seawater may also provide valuable information.

Finally, there is a clear need to compare the behavior of seawater REEs to that of other particle-reactive elements such as barium and iron. A major interest in this regard is to understand the availability of nutrients that ultimately limits or amplifies primary productivity. The exact nutrient supply paths and changes of biogeochemical cycling as a consequence of sea-ice loss, increasing riverine freshwater runoff and other environmental parameters in the AM still need to be investigated and should be part of the international GEOTRACES program.

DANKSAGUNG

Martin, Du bist ein exzellenter Betreuer! Du hast mir so viel beigebracht, dass ich davon noch lange zehren kann. Du hast mir nie Deine Meinung aufgedrängt, hast mich aber auch nie zu weit abschweifen lassen mit meinen Ideen. Du hast mich in meinen Zielen immer unterstützt und mir gezeigt dass gute Wissenschaft viel Wert ist. Du warst mir gegenüber stets freundlich, gerecht und ehrlich. Das sind Eigenschaften, die ich am meisten schätze. Ein exzellenter Betreuer. Danke, danke, und nochmals danke! Und mach bitte weiter so!

Dear Don, thank you very much for being the second evaluator of my thesis and my defense, I really appreciate that!

Liebe Mitglieder des Projektes „Laptev Sea System“ (Heidi, Jens, Dorothea, Karen, Markus, Carolyn und viele mehr), und alle Kollegen die im legendären Gebäude 4 sitzen (vor allem Robert, Henning, Nadya und Evgenia): Danke für die produktive Zusammenarbeit bzw. für die Unterhaltung. Übrigens: Imperial-Stout ist „on the way“.

Dear Russian members of the project „Laptev Sea System“: Thank you for your support!

Ben und Wilken, danke Euch beiden für Eure Geduld und die vielen wertvollen Emails!

Ed, can we measure REEs next week? This is the question I probably asked most during the last four years. Thanks for never saying “no”, but rather telling me that next month “might work”. We made some good contributions together and I hope to continue working with you in the future. Oh, I almost forgot: I need to measure REEs next week…

Liebe Jutta, was hätte ich ohne Deine Hilfe geschafft? So gut wie nichts. Diese Arbeit ist auch Deine Arbeit! Ich danke Dir von ganzem Herzen für Deinen Einsatz!

Liebe Dorothea, Du bist eine tolle Kollegin! Es macht sehr viel Spaß mit Dir zu arbeiten. Das funkeln in Deinen Augen sobald Du neue Daten oder Berechnungen siehst ist wirklich sehr ansteckend und macht mich immer froh. Danke für viele schöne Momente!

Dear friends from Kiel (ok, I try: Sasha, Sasha, Fernando, Annuschka, Kristin, Janett, Moritz, Peer, Veit, Benoit, Christelle, Antje, Andrey, Vasya, Misha, Zhimian, Chris, Anne, Jaime, Carolina, Mario, Idoia, Daniel, Zeynep, Theo, Bennet, Sonya, Stefan, Martin, Jörn, Katya): You girls and guys are great! Keep pushing! And thanks to those of you who introduced me to Kiel, the lab, the coffee machine and Käptn Flint.

Liebe Familie: Ihr alle habt mich immer unterstützt und werdet es in Zukunft auch immer tun, da bin ich mir sicher. Dafür danke ich Euch zutiefst. Ihr steht hier unten, aber im wahren Leben seid ihr für mich extrem wichtig! Tamara & Sven, Vera & Dietmar, Viktor & Lena: Danke für alles!

Nastya, Du bist der hellblaue Himmel über meinem Kiel, die wärmende Sonne an meinem Kieler Strand und mein mediterraner Kieler Sommerabend. Und Du bist natürlich noch viel mehr: Du bist ein wundervoller Mensch! Danke dafür, dass es Dich gibt! Etwas Romantik ist hier doch erlaubt ;)

Adiós, Euer Georgi. Kiel, den 26. Januar 2017

REFERENCES

Aagaard, K. (1989) A synthesis of the Arctic Ocean circulation. Rapp. P. V. Reun. Cons. Int. Explor. Mer, 1188,11–22.

Aagaard, K. and Carmack, E.C. (1989) The Role of Sea Ice and Other Fresh-Water in the Arctic Circulation. *J Geophys Res-Oceans* **94**, 14485-14498. http://dx.doi.org/10.1029/JC094iC10p14485

Aagaard, K., Coachman, L.K. and Carmack, E. (1981) On the Halocline of the Arctic Ocean. *Deep-Sea Research Part a-Oceanographic Research Papers* **28**, 529-&. http://dx.doi.org/10.1016/0198-0149(81)90115-1

Aagaard, K., Foldvik, A. and Hillman, S.R. (1987) The West Spitsbergen Current - Disposition and Water Mass Transformation. *J Geophys Res-Oceans* **92**, 3778-3784. http://dx.doi.org/10.1029/JC092iC04p03778

Aagaard, K., Swift, J.H. and Carmack, E.C. (1985) Thermohaline Circulation in the Arctic Mediterranean Seas. J Geophys Res-Oceans 90, 4833-4846. http://dx.doi.org/10.1029/JC090iC03p04833

Abbott, A.N., Haley, B.A. and McManus, J. (2015) Bottoms up: Sedimentary control of the deep North Pacific Ocean's εNd signature. Geology 43, 1035-1035. http://dx.doi.org/10.1130/g37114.1

Abrahamsen, E.P., Meredith, M.P., Falkner, K.K., Torres-Valdes, S., Leng, M.J., Alkire, M.B., Bacon, S., Laxon, S.W., Polyakov, I. and Ivanov, V. (2009) Tracer-derived freshwater composition of the Siberian continental shelf and slope following the extreme Arctic summer of 2007. Geophysical Research Letters 36, n/a-n/a. http://dx.doi.org/10.1029/2009gl037341

Aksenov, Y., Ivanov, V.V., Nurser, A.J.G., Bacon, S., Polyakov, I.V., Coward, A.C., Naveira-Garabato, A.C. and Beszczynska-Moeller, A. (2011) The Arctic Circumpolar Boundary Current. Journal of Geophysical Research 116. http://dx.doi.org/10.1029/2010jc006637

Aksenov, Y., Karcher, M., Proshutinsky, A., Gerdes, R., de Cuevas, B., Golubeva, E., Kauker, F., Nguyen, A.T., Platov, G.A., Wadley, M., Watanabe, E., Coward, A.C. and Nurser, A.J.G. (2016) Arctic pathways of Pacific Water: Arctic Ocean Model Intercomparison experiments. J Geophys Res-Oceans 121, 27-59. http://dx.doi.org/10.1002/2015jc011299

Alkire, M.B., Morison, J. and Andersen, R. (2015) Variability in the meteoric water, sea-ice melt, and Pacific water contributions to the central Arctic Ocean, 2000-2014. J Geophys Res-Oceans 120, 1573-1598. http://dx.doi.org/10.1002/2014jc010023

Ambaum, M.H.P., Hoskins, B.J. and Stephenson, D.B. (2001) Arctic Oscillation or North Atlantic Oscillation? Journal of Climate 14, 3495-3507. http://dx.doi.org/10.1175/1520-0442(2001)014%3C3495:aoonao%3E2.0.co;2

Anderson, L.G., Andersson, P.S., Bjork, G., Jones, E.P., Jutterstrom, S. and Wahlstrom, I. (2013) Source and formation of the upper halocline of the Arctic Ocean. J Geophys Res-Oceans 118, 410-421. http://dx.doi.org/10.1029/2012jc008291

Andersson, P.S., Porcelli, D., Frank, M., Bjork, G., Dahlqvist, R. and Gustafsson, O. (2008) Neodymium isotopes in seawater from the Barents Sea and Fram Strait Arctic-Atlantic gateways. Geochimica Et Cosmochimica Acta 72, 2854-2867. http://dx.doi.org/10.1016/j.gca.2008.04.008

Anisimov, O.A., Vaughan, D.G., Callaghan, T.V., Furgal, C., Marchant, H., Prowse, T.D., Vilhjálmsson, H. and Wals, J.E. (2007) Polar regions (Arctic and Antarctic). Climate Change 2007: Impacts, Adaptation and Vulnerability. Contribution of Working Group II to the Fourth Assessment Report of the Intergovernmental Panel on Climate Change, M.L. Parry, O.F. Canziani, J.P. Palutikof, P.J. van der Linden and C.E. Hanson, Eds., Cambridge University Press, Cambridge, 653-685. 15, 653-685.

Arsouze, T., Dutay, J.C., Lacan, F. and Jeandel, C. (2009) Reconstructing the Nd oceanic cycle using a coupled dynamical – biogeochemical model. Biogeosciences 6, 2829-2846. http://dx.doi.org/10.5194/bg-6-2829-2009

Åström, M.E., Österholm, P., Gustafsson, J.P., Nystrand, M., Peltola, P., Nordmyr, L. and Boman, A. (2012) Attenuation of rare earth elements in a boreal estuary. Geochimica et Cosmochimica Acta 96, 105-119. http://dx.doi.org/10.1016/j.gca.2012.08.004

Bamber, J., van den Broeke, M., Ettema, J., Lenaerts, J. and Rignot, E. (2012) Recent large increases in freshwater fluxes from Greenland into the North Atlantic. Geophysical Research Letters 39. http://dx.doi.org/10.1029/2012gl052552

Bareiss, J. and Görgen, K. (2005) Spatial and temporal variability of sea ice in the Laptev Sea: Analyses and review of satellite passive-microwave data and model results, 1979 to 2002. Global and Planetary Change 48, 28-54. http://dx.doi.org/10.1016/j.gloplacha.2004.12.004

Barrat, J.A., Keller, F., AmossÉ, J., Taylor, R.N., Nesbitt, R.W. and Hirata, T. (1996) Determination of Rare Earth Elements in Sixteen Silicate Reference Samples by Icp-Ms after Tm Addition and Ion Exchange Separation. Geostandards and Geoanalytical Research 20, 133-139. http://dx.doi.org/10.1111/j.1751-908X.1996.tb00177.x

Baskaran, M. (2011) Handbook of environmental isotope geochemistry. Springer Science & Business Media. http://dx.doi.org/10.1007/978-3-642-10637-8

Bau, M., Dulski, P. and Moller, P. (1995) Yttrium and holmium in South Pacific seawater: vertical distribution and possible fractionation mechanisms. Oceanographic Literature Review 11, 955.

Bauch, D., Hölemann, J., Willmes, S., Gröger, M., Novikhin, A., Nikulina, A., Kassens, H. and Timokhov, L. (2010) Changes in distribution of brine waters on the Laptev Sea shelf in 2007. Journal of Geophysical Research 115. http://dx.doi.org/10.1029/2010jc006249

Bauch, D., Hölemann, J.A., Nikulina, A., Wegner, C., Janout, M.A., Timokhov, L.A. and Kassens, H. (2013) Correlation of river water and local sea-ice melting on the Laptev Sea shelf (Siberian Arctic). Journal of Geophysical Research: Oceans 118, 550-561. http://dx.doi.org/10.1002/jgrc.20076

Bauch, D., Rudgers van der Loeff, M., Andersen, N., Torres-Valdes, S., Bakker, K. and Abrahamsen, E.P. (2011) Origin of freshwater and polynya water in the Arctic Ocean halocline in summer 2007. Progress in Oceanography 91, 482-495. http://dx.doi.org/10.1016/j.pocean.2011.07.017

Bauch, D., Schlosser, P. and Fairbanks, R.G. (1995) Freshwater balance and the sources of deep and bottom waters in the Arctic Ocean inferred from the distribution of H218O. Progress in Oceanography 35, 53-80. http://dx.doi.org/10.1016/0079-6611(95)00005-2

Beszczynska-Möller, A. (2013) The expedition of the research vessel "Polarstern" to the Arctic in 2012 (ARK-XXVII/1). Berichte zur Polar-und Meeresforschung = Reports on polar and marine research 660. http://dx.doi.org/10013/epic.41150.d007

Beszczynska-Möller, A., Fahrbach, E., Schauer, U. and Hansen, E. (2012) Variability in Atlantic water temperature and transport at the entrance to the Arctic Ocean, 1997-2010. ICES Journal of Marine Science 69, 852-863. http://dx.doi.org/10.1093/icesjms/fss056

Beszczynska-Möller, A., Weslawski, J.M., Walczowski, W. and Zajaczkowski, M. (1997) Estimation of glacial meltwater discharge into Svalbard coastal waters. Oceanologia 39.

Beszczynska-Möller, A. and Wisotzki, A. (2012) Physical oceanography during POLARSTERN cruise ARK-XXVII/1. PANGAEA. http://dx.doi.org/10.1594/PANGAEA.801791

Bignami, F. and Hopkins, T.S. (1997) The water mass characteristics of the Northeast Water Polynya: Polar Sea data 1992-1993. Journal of Marine Systems 10, 139-156. http://dx.doi.org/10.1016/S0924-7963(96)00079-6

Böhm, E., Lippold, J., Gutjahr, M., Frank, M., Blaser, P., Antz, B., Fohlmeister, J., Frank, N., Andersen, M.B. and Deininger, M. (2015) Strong and deep Atlantic meridional overturning circulation during the last glacial cycle. *Nature* **517**, 73-76. http://dx.doi.org/10.1038/nature14059

Böning, C.W., Behrens, E., Biastoch, A., Getzlaff, K. and Bamber, J.L. (2016) Emerging impact of Greenland meltwater on deepwater formation in the North Atlantic Ocean. Nature Geoscience 9, 523-527. http://dx.doi.org/10.1038/ngeo2740

Bourke, R.H., Newton, J.L., Paquette, R.G. and Tunnicliffe, M.D. (1987) Circulation and Water Masses of the East-Greenland Shelf. J Geophys Res-Oceans 92, 6729-6740. http://dx.doi.org/10.1029/JC092iC07p06729

Box, J.E. and Colgan, W. (2013) Greenland Ice Sheet Mass Balance Reconstruction. Part III: Marine Ice Loss and Total Mass Balance (1840–2010). Journal of Climate 26, 6990-7002. http://dx.doi.org/10.1175/jcli-d-12-00546.1

Boyle, E.A., Edmond, J.M. and Sholkovitz, E.R. (1977) The mechanism of iron removal in estuaries. Geochimica et Cosmochimica Acta 41, 1313-1324. http://dx.doi.org/10.1016/0016-7037(77)90075-8

Broecker, W.S. and Peng, T.-H. (1982) Tracers in the Sea. Eldigo Press, New York.

Broecker, W.S., Takahashi, T. and Takahashi, T. (1985) Sources and flow patterns of deep-ocean waters as deduced from potential temperature, salinity, and initial phosphate concentration. J Geophys Res-Oceans 90, 6925-6939. http://dx.doi.org/10.1029/JC090iC04p06925

Brookins, D.G. (1989) Aqueous Geochemistry of Rare-Earth Elements. Reviews in Mineralogy 21, 201-225.

Brunnabend, S.E., Schröter, J., Rietbroek, R. and Kusche, J. (2015) Regional sea level change in response to ice mass loss in Greenland, the West Antarctic and Alaska. Journal of Geophysical Research: Oceans 120, 7316-7328. http://dx.doi.org/10.1002/2015jc011244

Budéus, G. and Schneider, W. (1995) On the hydrography of the Northeast Water Polynya. J Geophys Res-Oceans 100, 4287-4299. http://dx.doi.org/10.1029/94JC02024

Budéus, G., Schneider, W. and Kattner, G. (1997) Distribution and exchange of water masses in the Northeast Water polynya (Greenland Sea). Journal of Marine Systems 10, 123-138. http://dx.doi.org/10.1016/s0924-7963(96)00074-7

Byrne, R.H. and Sholkovitz, E.R. (1996) Chapter 158 Marine chemistry and geochemistry of the lanthanides. 23, 497-593. http://dx.doi.org/10.1016/s0168-1273(96)23009-0

Carmack, E.C. (1990) Large-Scale Physical Oceanography of Polar Oceans. 171-222. http://dx.doi.org/10.1016/b978-0-12-653031-5.50009-6

Chen, T. (2013) The geochemical cycling and paleoceanographic application of combined oceanic Nd-Hf isotopes. Doctoral Thesis, Christian-Albrechts-Universität Kiel (CAU), 201pp.

Chen, T., Frank, M., Haley, B.A., Gutjahr, M. and Spielhagen, R.F. (2012) Variations of North Atlantic inflow to the central Arctic Ocean over the last 14 million years inferred from hafnium and neodymium isotopes. Earth and Planetary Science Letters 353-354, 82-92. http://dx.doi.org/10.1016/j.epsl.2012.08.012

Chen, T.Y., Stumpf, R., Frank, M., Beldowski, J. and Staubwasser, M. (2013) Contrasting geochemical cycling of hafnium and neodymium in the central Baltic Sea. Geochimica Et Cosmochimica Acta 123, 166-180. http://dx.doi.org/10.1016/j.gca.2013.09.011

Cohen, J., Screen, J.A., Furtado, J.C., Barlow, M., Whittleston, D., Coumou, D., Francis, J., Dethloff, K., Entekhabi, D., Overland, J. and Jones, J. (2014) Recent Arctic amplification and extreme mid-latitude weather. Nature Geoscience 7, 627-637. http://dx.doi.org/10.1038/nge02234

Craig, H. (1961) Isotopic Variations in Meteoric Waters. Science 133, 1702-1703. http://dx.doi.org/10.1126/science.133.3465.1702

Craig, H. and Gordon, L.I. (1965) Deuterium and oxygen 18 variations in the ocean and the marine atmosphere. In: Stable Isotopes in Oceanographic Studies and Paleotemperatures, Spoleto, Italy. pp 9-130.

Dahlqvist, R., Andersson, P.S. and Porcelli, D. (2007) Nd isotopes in Bering Strait and Chukchi Sea Water. Geochim. Cosmochim. Acta 71, A196.

Dausmann, V., Frank, M., Siebert, C., Christl, M. and Hein, J.R. (2015) The evolution of climatically driven weathering inputs into the western Arctic Ocean since the late Miocene: Radiogenic isotope evidence. Earth and Planetary Science Letters 419, 111-124. http://dx.doi.org/10.1016/j.epsl.2015.03.007

de Baar, H.J.W. (1983) The marine geochemistry of the rare earth elements. Doctoral Thesis, Woodshole Oceanographic Institution.

de Steur, L., Hansen, E., Mauritzen, C., Beszczynska-Möller, A. and Fahrbach, E. (2014) Impact of recirculation on the East Greenland Current in Fram Strait: Results from moored current meter measurements between 1997 and 2009. Deep Sea Research Part I: Oceanographic Research Papers 92, 26-40. http://dx.doi.org/10.1016/j.dsr.2014.05.018

de Steur, L., Pickart, R.S., Torres, D.J. and Valdimarsson, H. (2015) Recent changes in the freshwater composition east of Greenland. Geophysical Research Letters 42, 2326-2332. http://dx.doi.org/10.1002/2014gl062759

Dittmar, T. and Kattner, G. (2003) The biogeochemistry of the river and shelf ecosystem of the Arctic Ocean: a review. Marine Chemistry 83, 103-120. http://dx.doi.org/10.1016/s0304-4203(03)00105-1

Dmitrenko, I.A., Kirillov, S.A., Bloshkina, E. and Lenn, Y.-D. (2012) Tide-induced vertical mixing in the Laptev Sea coastal polynya. J Geophys Res-Oceans 117, n/a-n/a. http://dx.doi.org/10.1029/2011jc006966

Dmitrenko, I.A., Kirillov, S.A., Serra, N., Koldunov, N.V., Ivanov, V.V., Schauer, U., Polyakov, I.V., Barber, D., Janout, M., Lien, V.S., Makhotin, M. and Aksenov, Y. (2014) Heat loss from the Atlantic water layer in the northern Kara Sea: causes and consequences. Ocean Science 10, 719-730. http://dx.doi.org/10.5194/os-10-719-2014

Dmitrenko, I.A., Kirillov, S.A. and Tremblay, L.B. (2008) The long-term and interannual variability of summer fresh water storage over the eastern Siberian shelf: Implication for climatic change. J Geophys Res-Oceans 113. http://dx.doi.org/10.1029/2007jc004304

Dodd, P.A., Heywood, K.J., Meredith, M.P., Naveira-Garabato, A.C., Marca, A.D. and Falkner, K.K. (2009) Sources and fate of freshwater exported in the East Greenland Current. Geophysical Research Letters 36. http://dx.doi.org/10.1029/2009gl039663

Dodd, P.A., Rabe, B., Hansen, E., Falck, E., Mackensen, A., Rohling, E., Stedmon, C. and Kristiansen, S. (2012) The freshwater composition of the Fram Strait outflow derived from a decade of tracer measurements. J Geophys Res-Oceans 117. http://dx.doi.org/10.1029/2012jc008011

Dukhovskoy, D.S., Myers, P.G., Platov, G., Timmermans, M.-L., Curry, B., Proshutinsky, A., Bamber, J.L., Chassignet, E., Hu, X., Lee, C.M. and Somavilla, R. (2016) Greenland freshwater pathways in the sub-Arctic Seas from model experiments with passive tracers. Journal of Geophysical Research: Oceans 121, 877-907. http://dx.doi.org/10.1002/2015jc011290

Ekwurzel, B., Schlosser, P., Mortlock, R.A., Fairbanks, R.G. and Swift, J.H. (2001) River runoff, sea ice meltwater, and Pacific water distribution and mean residence times in the Arctic Ocean. J Geophys Res-Oceans 106, 9075-9092. http://dx.doi.org/10.1029/1999jc000024

Elderfield, H. and Greaves, M.J. (1982) The rare earth elements in seawater. Nature 296, 214-219. http://dx.doi.org/10.1038/296214a0

Elderfield, H., Upstill-Goddard, R. and Sholkovitz, E.R. (1990) The rare earth elements in rivers, estuaries, and coastal seas and their significance to the composition of ocean waters. Geochimica et Cosmochimica Acta 54, 971-991. http://dx.doi.org/10.1016/0016-7037(90)90432-k

Epstein, S. and Mayeda, T. (1953) Variation of O-18 Content of Waters from Natural Sources. Geochimica Et Cosmochimica Acta 4, 213-224. http://dx.doi.org/10.1016/0016-7037(53)90051-9

Fagel, N. and Mattielli, N. (2011) Holocene evolution of deep circulation in the northern North Atlantic traced by Sm, Nd and Pb isotopes and bulk sediment mineralogy. Paleoceanography 26. http://dx.doi.org/10.1029/2011pa002168

Fagel, N., Not, C., Gueibe, J., Mattielli, N. and Bazhenova, E. (2014) Late Quaternary evolution of sediment provenances in the Central Arctic Ocean: mineral assemblage, trace element composition and Nd and Pb isotope fingerprints of detrital fraction from the Northern Mendeleev Ridge. Quaternary Science Reviews 92, 140-154. http://dx.doi.org/10.1016/j.quascirev.2013.12.011

Falck, E. (2001) Contribution of waters of Atlantic and Pacific origin in the Northeast Water Polynya. Polar Research 20, 193-200. http://dx.doi.org/10.1111/j.1751-8369.2001.tb00056.x

Falck, E., Kattner, G. and Budéus, G. (2005) Disappearance of Pacific Water in the northwestern Fram Strait. Geophysical Research Letters 32. http://dx.doi.org/10.1029/2005gl023400

Fernández-Méndez, M., Katlein, C., Rabe, B., Nicolaus, M., Peeken, I., Bakker, K., Flores, H. and Boetius, A. (2015) Photosynthetic production in the central Arctic Ocean during the record sea-ice minimum in 2012. Biogeosciences 12, 3525-3549. http://dx.doi.org/10.5194/bg-12-3525-2015

Fichefet, T., Poncin, C., Goosse, H., Huybrechts, P., Janssens, I. and Le Treut, H. (2003) Implications of changes in freshwater flux from the Greenland ice sheet for the climate of the 21st century. Geophysical Research Letters 30, n/a-n/a. http://dx.doi.org/10.1029/2003gl017826

Fournier, J., Grange, J.L. and Vergara, S. (1974) Water desalination by natural freezing. Desalination 15, 167-175. http://dx.doi.org/10.1016/s0011-9164(00)82080-9

Frank, M. (2002) Radiogenic isotopes: Tracers of past ocean circulation and erosional input. Reviews of Geophysics 40, 1001. http://dx.doi.org/10.1029/2000rg000094

Garcia-Solsona, E., Jeandel, C., Labatut, M., Lacan, F., Vance, D., Chavagnac, V. and Pradoux, C. (2014) Rare earth elements and Nd isotopes tracing water mass mixing and particle-seawater interactions in the SE Atlantic. Geochimica Et Cosmochimica Acta 125, 351-372. http://dx.doi.org/10.1016/j.gca.2013.10.009

Gardner, A.S., Moholdt, G., Wouters, B., Wolken, G.J., Burgess, D.O., Sharp, M.J., Cogley, J.G., Braun, C. and Labine, C. (2011) Sharply increased mass loss from glaciers and ice caps in the Canadian Arctic Archipelago. Nature 473, 357-360. http://dx.doi.org/10.1038/nature10089

Gascard, J.C., Raisbeck, G., Sequeira, S., Yiou, F. and Mork, K.A. (2004) The Norwegian Atlantic Current in the Lofoten basin inferred from hydrological and tracer data (129I) and its interaction with the Norwegian Coastal Current. Geophysical Research Letters 31. http://dx.doi.org/10.1029/2003gl018303

German, C.R., Klinkhammer, G.P., Edmond, J.M., Mura, A. and Elderfield, H. (1990) Hydrothermal scavenging of rare-earth elements in the ocean. Nature 345, 516-518. http://dx.doi.org/10.1038/345516a0

Giles, K.A., Laxon, S.W., Ridout, A.L., Wingham, D.J. and Bacon, S. (2012) Western Arctic Ocean freshwater storage increased by wind-driven spin-up of the Beaufort Gyre. Nature Geoscience 5, 194-197. http://dx.doi.org/10.1038/ngeo1379

Gillard, L.C., Hu, X., Myers, P.G. and Bamber, J.L. (2016) Meltwater pathways from marine terminating glaciers of the Greenland ice sheet. Geophysical Research Letters 43, 10,873-810,882. http://dx.doi.org/10.1002/2016gl070969

Goldstein, S.J. and Jacobsen, S.B. (1987) The Nd and Sr isotopic systematics of river-water dissolved material: Implications for the sources of Nd and Sr in seawater. Chemical Geology: Isotope Geoscience section 66, 245-272. http://dx.doi.org/10.1016/0168-9622(87)90045-5

Goldstein, S.J. and Jacobsen, S.B. (1988a) Rare earth elements in river waters. Earth and Planetary Science Letters 89, 35-47. http://dx.doi.org/10.1016/0012-821x(88)90031-3

Goldstein, S.J. and Jacobsen, S.B. (1988b) REE in the Great Whale River estuary, northwest Quebec. Earth and Planetary Science Letters 88, 241-252. http://dx.doi.org/10.1016/0012-821x(88)90081-7

Goldstein, S.L. and Hemming, S.R. (2003) Long-lived Isotopic Tracers in Oceanography, Paleoceanography, and Ice-sheet Dynamics. Treatise on geochemistry 6, 453-489. http://dx.doi.org/10.1016/B0-08-043751-6/06179-X

Goldstein, S.L., O'Nions, R.K. and Hamilton, P.J. (1984) A Sm-Nd isotopic study of atmospheric dusts and particulates from major river systems. Earth and Planetary Science Letters 70, 221-236. http://dx.doi.org/10.1016/0012-821x(84)90007-4

Goswami, V., Singh, S.K. and Bhushan, R. (2014) Impact of water mass mixing and dust deposition on Nd concentration and εNd of the Arabian Sea water column. Geochimica et Cosmochimica Acta 145, 30-49. http://dx.doi.org/10.1016/j.gca.2014.09.006

Grasshoff, K., Kremling, K. and Ehrhardt, M. (2009) Methods of seawater analysis. John Wiley & Sons. http://dx.doi.org/10.1002/9783527613984

Greaves, M.J., Elderfield, H. and Sholkovitz, E.R. (1999) Aeolian sources of rare earth elements to the Western Pacific Ocean. Marine Chemistry 68, 31-38. http://dx.doi.org/10.1016/S0304-4203(99)00063-8

Haley, B.A., Frank, M., Hathorne, E.C. and Pisias, N. (2014) Biogeochemical implications from dissolved rare earth element and Nd isotope distributions in the Gulf of Alaska. Geochimica Et Cosmochimica Acta 126, 455-474. http://dx.doi.org/10.1016/j.gca.2013.11.012

Haley, B.A., Klinkhammer, G.P. and McManus, J. (2004) Rare earth elements in pore waters of marine sediments. Geochimica et Cosmochimica Acta 68, 1265-1279. http://dx.doi.org/10.1016/j.gca.2003.09.012

Haley, B.A. and Polyak, L. (2013) Pre-modern Arctic Ocean circulation from surface sediment neodymium isotopes. Geophysical Research Letters 40, 893-897. http://dx.doi.org/10.1002/grl.50188

Halliday, A.N., Davidson, J.P., Holden, P., Owen, R.M. and Olivarez, A.M. (1992) Metalliferous sediments and the scavenging residence time of Nd near hydrothermal vents. Geophysical Research Letters 19, 761-764. http://dx.doi.org/10.1029/92gl00393

Hansen, B. and Østerhus, S. (2000) North Atlantic–Nordic Seas exchanges. Progress in Oceanography 45, 109-208. http://dx.doi.org/10.1016/s0079-6611(99)00052-x

Hathorne, E.C., Haley, B.A., Stichel, T., Grasse, P., Zieringer, M. and Frank, M. (2012) Online preconcentration ICP-MS analysis of rare earth elements in seawater. Geochemistry, Geophysics, Geosystems 13, n/a-n/a. http://dx.doi.org/10.1029/2011gc003907

Hathorne, E.C., Stichel, T., Bruck, B. and Frank, M. (2015) Rare earth element distribution in the Atlantic sector of the Southern Ocean: The balance between particle scavenging and vertical supply. Marine Chemistry 177, 157-171. http://dx.doi.org/10.1016/j.marchem.2015.03.011

Hattermann, T., Isachsen, P.E., von Appen, W.-J., Albretsen, J. and Sundfjord, A. (2016) Eddy-driven recirculation of Atlantic Water in Fram Strait. Geophysical Research Letters 43, 3406-3414. http://dx.doi.org/10.1002/2016gl068323

Havik, L., Pickard, R.S., Vage, K., Beszczynska-Möller, A., Walczowski, W. and von Appen, W.-J. (2016) Evolution of the East Greenland Current from Fram Strait to Denmark Strait: Synoptic measurements from summer 2012. Journal of Geophysical Research in press.

Heiderich, J. (2015) Flow of warm Atlantic Water in the Norske trough on the East Greenland shelf. Bachelor Thesis. Jacobs University Bremen, 100pp.

Hofmann, A.W. (1988) Chemical differentiation of the Earth: the relationship between mantle, continental crust, and oceanic crust. Earth and Planetary Science Letters 90, 297-314. http://dx.doi.org/10.1016/0012-821x(88)90132-x

Hölemann, J.A., Kirillov, S.A., Klagge, T., Novikhin, A., Kassens, H. and Timokhov, L. (2011) Near-bottom water warming in the Laptev Sea in response to atmospheric and sea-ice conditions in 2007. Polar Research 30. http://dx.doi.org/10.3402/polar.v30i0.6425

Holland, M.M., Bitz, C.M. and Tremblay, B. (2006) Future abrupt reductions in the summer Arctic sea ice. Geophysical Research Letters 33. http://dx.doi.org/10.1029/2006gl028024

Hopwood, M.J., Bacon, S., Arendt, K., Connelly, D.P. and Statham, P.J. (2015) Glacial meltwater from Greenland is not likely to be an important source of Fe to the North Atlantic. Biogeochemistry 124, 1-11. http://dx.doi.org/10.1007/s10533-015-0091-6

Hoyle, J., Elderfield, H., Gledhill, A. and Greaves, M. (1984) The behaviour of the rare earth elements during mixing of river and sea waters. Geochimica et Cosmochimica Acta 48, 143-149. http://dx.doi.org/10.1016/0016-7037(84)90356-9

Jacobsen, S.B. and Wasserburg, G.J. (1980) Sm-Nd Isotopic Evolution of Chondrites. Earth and Planetary Science Letters 50, 139-155. http://dx.doi.org/10.1016/0012-821x(80)90125-9

Jakobsson, M., Mayer, L., Coakley, B., Dowdeswell, J.A., Forbes, S., Fridman, B., Hodnesdal, H., Noormets, R., Pedersen, R., Rebesco, M., Schenke, H.W., Zarayskaya, Y., Accettella, D., Armstrong, A., Anderson, R.M., Bienhoff, P., Camerlenghi, A.,

Church, I., Edwards, M., Gardner, J.V., Hall, J.K., Hell, B., Hestvik, O., Kristoffersen, Y., Marcussen, C., Mohammad, R., Mosher, D., Nghiem, S.V., Pedrosa, M.T., Travaglini, P.G. and Weatherall, P. (2012) The International Bathymetric Chart of the Arctic Ocean (IBCAO) Version 3.0. Geophysical Research Letters 39. http://dx.doi.org/10.1029/2012gl052219

Janout, M.A., Aksenov, Y., Hölemann, J.A., Rabe, B., Schauer, U., Polyakov, I.V., Bacon, S., Coward, A.C., Karcher, M., Lenn, Y.D., Kassens, H. and Timokhov, L. (2015) Kara Sea freshwater transport through Vilkitsky Strait: Variability, forcing, and further pathways toward the western Arctic Ocean from a model and observations. J Geophys Res-Oceans 120, 4925-4944. http://dx.doi.org/10.1002/2014jc010635

Janout, M.A., Hölemann, J.A., Juhls, B., Krumpen, T., Rabe, B., Bauch, D., Wegner, C., Kassens, H. and Timokhov, L. (2016) Episodic warming of near-bottom waters under the Arctic sea ice on the central Laptev Sea shelf. Geophysical Research Letters 43, 264-272. http://dx.doi.org/10.1002/2015gl066565

Janout, M.A. and Lenn, Y.D. (2014) Semidiurnal Tides on the Laptev Sea Shelf with Implications for Shear and Vertical Mixing. Journal of Physical Oceanography 44, 202-219. http://dx.doi.org/10.1175/Jpo-D-12-0240.1

Jeandel, C. (2016) Overview of the mechanisms that could explain the 'Boundary Exchange' at the land–ocean contact. Philosophical Transactions of the Royal Society A: Mathematical, Physical and Engineering Sciences 374, 20150287. http://dx.doi.org/10.1098/rsta.2015.0287

Jeandel, C. and Oelkers, E.H. (2015) The influence of terrigenous particulate material dissolution on ocean chemistry and global element cycles. Chemical Geology 395, 50-66. http://dx.doi.org/10.1016/j.chemgeo.2014.12.001

Jones, E.P. (2001) Circulation in the Arctic Ocean. Polar Research 20, 139-146. http://dx.doi.org/10.1111/j.1751-8369.2001.tb00049.x

Jones, E.P. and Anderson, L.G. (1986) On the Origin of the Chemical-Properties of the Arctic-Ocean Halocline. J Geophys Res-Oceans 91, 759-767. http://dx.doi.org/10.1029/JC091iC09p10759

Jones, E.P., Anderson, L.G., Jutterstrom, S., Mintrop, L. and Swift, J.H. (2008a) Pacific freshwater, river water and sea ice meltwater across Arctic Ocean basins: Results from the 2005 Beringia Expedition. J Geophys Res-Oceans 113. http://dx.doi.org/10.1029/2007jc004124

Jones, E.P., Anderson, L.G., Jutterstrom, S. and Swift, J.H. (2008b) Sources and distribution of fresh water in the East Greenland Current. Progress in Oceanography 78, 37-44. http://dx.doi.org/10.1016/j.pocean.2007.06.003

Jones, E.P., Anderson, L.G. and Swift, J.H. (1998) Distribution of Atlantic and Pacific waters in the upper Arctic Ocean: Implications for circulation. Geophysical Research Letters 25, 765-768. http://dx.doi.org/10.1029/98gl00464

Jones, E.P., Swift, J.H., Anderson, L.G., Lipizer, M., Civitarese, G., Falkner, K.K., Kattner, G. and McLaughlin, F. (2003) Tracing Pacific water in the North Atlantic Ocean. J Geophys Res-Oceans 108. http://dx.doi.org/10.1029/2001jc001141

Kattsov, V.M., Walsh, J.E., Chapman, W.L., Govorkova, V.A., Pavlova, T.V. and Zhang, X. (2007) Simulation and Projection of Arctic Freshwater Budget Components by the IPCC AR4 Global Climate Models. Journal of Hydrometeorology 8, 571-589. http://dx.doi.org/10.1175/jhm575.1

Khan, S.A., Aschwanden, A., Bjork, A.A., Wahr, J., Kjeldsen, K.K. and Kjaer, K.H. (2015) Greenland ice sheet mass balance: a review. Rep Prog Phys 78, 046801. http://dx.doi.org/10.1088/0034-4885/78/4/046801

Kim, I. and Kim, G. (2014) Submarine groundwater discharge as a main source of rare earth elements in coastal waters. Marine Chemistry 160, 11-17. http://dx.doi.org/10.1016/j.marchem.2014.01.003

Klunder, M.B., Bauch, D., Laan, P., de Baar, H.J.W., van Heuven, S. and Ober, S. (2012) Dissolved iron in the Arctic shelf seas and surface waters of the central Arctic Ocean: Impact of Arctic river water and ice-melt. Journal of Geophysical Research: Oceans 117, n/a-n/a. http://dx.doi.org/10.1029/2011jc007133

Lacan, F. (2002) Masses d'eau des Mers Nordiques et de l'Atlantique Subarctique tracées par les isotopes du néodyme. Doctoral Thesis, Université Paul Sabatier-Toulouse III.

Lacan, F. and Jeandel, C. (2004a) Denmark Strait water circulation traced by heterogeneity in neodymium isotopic compositions. Deep-Sea Research Part I-Oceanographic Research Papers 51, 71-82. http://dx.doi.org/10.1016/j.dsr.2003.09.006

Lacan, F. and Jeandel, C. (2004b) Neodymium isotopic composition and rare earth element concentrations in the deep and intermediate Nordic Seas: Constraints on the Iceland Scotland Overflow Water signature. Geochemistry Geophysics Geosystems 5. http://dx.doi.org/10.1029/2004gc000742

Lacan, F. and Jeandel, C. (2005) Neodymium isotopes as a new tool for quantifying exchange fluxes at the continent–ocean interface. Earth and Planetary Science Letters 232, 245-257. http://dx.doi.org/10.1016/j.epsl.2005.01.004

Lambelet, M., van de Flierdt, T., Crocket, K., Rehkamper, M., Kreissig, K., Coles, B., Rijkenberg, M.J.A., Gerringa, L.J.A., de Baar, H.J.W. and Steinfeldt, R. (2016) Neodymium isotopic composition and concentration in the western North Atlantic Ocean: Results from the GEOTRACES GA02 section. Geochimica Et Cosmochimica Acta 177, 1-29. http://dx.doi.org/10.1016/j.gca.2015.12.019

Laukert, G., Frank, M., Bauch, D.-., Hathorne, E.C., Rabe, B., von Appen, W.-J., Wegner, C., Zieringer, M. and Kassens, H. (2017) Ocean circulation and freshwater pathways in the Arctic Mediterranean based on a combined Nd isotope, REE and oxygen isotope section across Fram Strait. Geochimica et Cosmochimica Acta 202, 285-309. http://dx.doi.org/10.1016/j.gca.2016.12.028

Lawrence, M.G. and Kamber, B.S. (2006) The behaviour of the rare earth elements during estuarine mixing-revisited. Marine Chemistry 100, 147-161. http://dx.doi.org/10.1016/j.marchem.2005.11.007

Le Fèvre, B. and Pin, C. (2005) A straightforward separation scheme for concomitant Lu–Hf and Sm–Nd isotope ratio and isotope dilution analysis. Analytica Chimica Acta 543, 209-221. http://dx.doi.org/10.1016/j.aca.2005.04.044

Lee, J.H. and Byrne, R.H. (1993) Complexation of trivalent rare earth elements (Ce, Eu, Gd, Tb, Yb) by carbonate ions. Geochimica et Cosmochimica Acta 57, 295-302. http://dx.doi.org/10.1016/0016-7037(93)90432-v

Loeng, H. (1991) Features of the Physical Oceanographic Conditions of the Barents Sea. Polar Research 10, 5-18. http://dx.doi.org/10.1111/j.1751-8369.1991.tb00630.x

Luo, H., Castelao, R.M., Rennermalm, A.K., Tedesco, M., Bracco, A., Yager, P.L. and Mote, T.L. (2016) Oceanic transport of surface meltwater from the southern Greenland ice sheet. Nature Geoscience 9, 528-532. http://dx.doi.org/10.1038/ngeo2708

Macdonald, R.W., Paton, D.W., Carmack, E.C. and Omstedt, A. (1995) The freshwater budget and under-ice spreading of Mackenzie River water in the Canadian Beaufort Sea based on salinity and18O/16O measurements in water and ice. Journal of Geophysical Research 100, 895. http://dx.doi.org/10.1029/94jc02700

Marnela, M., Rudels, B., Houssais, M.N., Beszczynska-Möller, A. and Eriksson, P.B. (2013) Recirculation in the Fram Strait and transports of water in and north of the Fram Strait derived from CTD data. Ocean Science 9, 499-519. http://dx.doi.org/10.5194/os-9-499-2013

Mauritzen, C., Rudels, B. and Toole, J. (2013) The Arctic and Subarctic Oceans/Seas. 103, 443-470. http://dx.doi.org/10.1016/b978-0-12-391851-2.00017-9

McLennan, S.M. (2001) Relationships between the trace element composition of sedimentary rocks and upper continental crust. Geochemistry Geophysics Geosystems 2. http://dx.doi.org/10.1029/2000GC000109

Melling, H. and Lewis, E.L. (1982) Shelf drainage flows in the Beaufort Sea and their effect on the Arctic Ocean pycnocline. Deep Sea Research Part A. Oceanographic Research Papers 29, 967-985. http://dx.doi.org/10.1016/0198-0149(82)90021-8

Merschel, G., Bau, M. and Dantas, E.L. (2017) Contrasting impact of organic and inorganic nanoparticles and colloids on the behavior of particle-reactive elements in tropical estuaries: An experimental study. Geochimica et Cosmochimica Acta 197, 1-13. http://dx.doi.org/10.1016/j.gca.2016.09.041

Molina-Kescher, M., Frank, M. and Hathorne, E.C. (2014) South Pacific dissolved Nd isotope compositions and rare earth element distributions: Water mass mixing versus biogeochemical cycling. Geochimica Et Cosmochimica Acta 127, 171-189. http://dx.doi.org/10.1016/j.gca.2013.11.038

Moore, G.W.K., Våge, K., Pickart, R.S. and Renfrew, I.A. (2015) Decreasing intensity of open-ocean convection in the Greenland and Iceland seas. Nature Climate Change 5, 877-882. http://dx.doi.org/10.1038/nclimate2688

Morison, J., Kwok, R., Peralta-Ferriz, C., Alkire, M., Rigor, I., Andersen, R. and Steele, M. (2012) Changing Arctic Ocean freshwater pathways. Nature 481, 66-70. http://dx.doi.org/10.1038/nature10705

Nebbia, G. and Menozzi, G.N. (1968) Early experiments on water desalination by freezing. Desalination 5, 49-54. http://dx.doi.org/10.1016/s0011-9164(00)80191-5

Newton, R., Schlosser, P., Mortlock, R., Swift, J. and MacDonald, R. (2013) Canadian Basin freshwater sources and changes: Results from the 2005 Arctic Ocean Section. J Geophys Res-Oceans 118, 2133-2154. http://dx.doi.org/10.1002/jgrc.20101

Nicolsky, D.J., Romanovsky, V.E., Romanovskii, N.N., Kholodov, A.L., Shakhova, N.E. and Semiletov, I.P. (2012) Modeling sub-sea permafrost in the East Siberian Arctic Shelf: The Laptev Sea region. Journal of Geophysical Research: Earth Surface 117, n/a-n/a. http://dx.doi.org/10.1029/2012jf002358

Nitishinsky, M., Anderson, L.G. and Hölemann, J.A. (2007) Inorganic carbon and nutrient fluxes on the Arctic Shelf. Continental Shelf Research 27, 1584-1599. http://dx.doi.org/10.1016/j.csr.2007.01.019

Notz, D. and Worster, M.G. (2009) Desalination processes of sea ice revisited. J Geophys Res-Oceans 114. http://dx.doi.org/10.1029/2008jc004885

Nozaki, Y. and Alibo, D.S. (2003) Dissolved rare earth elements in the Southern Ocean, southwest of Australia: Unique patterns compared to the South Atlantic data. Geochemical Journal 37, 47-62. http://dx.doi.org/10.2343/geochemj.37.47

Nozaki, Y., Lerche, D., Alibo, D.S. and Snidvongs, A. (2000) The estuarine geochemistry of rare earth elements and indium in the Chao Phraya River, Thailand. Geochimica et Cosmochimica Acta 64, 3983-3994. http://dx.doi.org/10.1016/s0016-7037(00)00473-7

Osborne, A.H., Haley, B.A., Hathorne, E.C., Plancherel, Y. and Frank, M. (2015) Rare earth element distribution in Caribbean seawater: Continental inputs versus lateral transport of distinct REE compositions in subsurface water masses. Marine Chemistry 177, 172-183. http://dx.doi.org/10.1016/j.marchem.2015.03.013

Östlund, H.G. and Hut, G. (1984) Arctic Ocean water mass balance from isotope data. Journal of Geophysical Research 89, 6373. http://dx.doi.org/10.1029/JC089iC04p06373

Persson, P.O., Andersson, P.S., Porcelli, D. and Semiletov, I. (2011) The influence of Lena River water inflow and shelf sediment-sea water exchange for the Nd isotopic composition in the Laptev Sea and Arctic Ocean. Geophysical Research Abstracts 13.

Peterson, B.J., Holmes, R.M., McClelland, J.W., Vorosmarty, C.J., Lammers, R.B., Shiklomanov, A.I., Shiklomanov, I.A. and Rahmstorf, S. (2002) Increasing river discharge to the Arctic Ocean. Science 298, 2171-2173. http://dx.doi.org/10.1126/science.1077445

Petrova, M. (2015) Neodymium isotopes and rare earth element distribution in the Barents Sea, Arctic Ocean. Master thesis, Saint Petersburg State University / University of Hamburg, Saint Petersburg / Hamburg, 60pp.

Piepgras, D.J. and Wasserburg, G.J. (1987) Rare-Earth Element Transport in the Western North-Atlantic Inferred from Nd Isotopic Observations. Geochimica Et Cosmochimica Acta 51, 1257-1271. http://dx.doi.org/10.1016/0016-7037(87)90217-1

Pin, C. and Zalduegui, J.F.S. (1997) Sequential separation of light rare-earth elements, thorium and uranium by miniaturized extraction chromatography: Application to isotopic analyses of silicate rocks. Analytica Chimica Acta 339, 79-89. http://dx.doi.org/10.1016/s0003-2670(96)00499-0

Pokrovsky, O.S., Manasypov, R.M., Loiko, S.V., Krickov, I.A., Kopysov, S.G., Kolesnichenko, L.G., Vorobyev, S.N. and Kirpotin, S.N. (2016) Trace element transport in western Siberian rivers across a permafrost gradient. Biogeosciences 13, 1877-1900. http://dx.doi.org/10.5194/bg-13-1877-2016

Pokrovsky, O.S., Shirokova, L.S., Viers, J., Gordeev, V.V., Shevchenko, V.P., Chupakov, A.V., Vorobieva, T.Y., Candaudap, F., Causserand, C., Lanzanova, A. and Zouiten, C. (2014) Fate of colloids during estuarine mixing in the Arctic. Ocean Science 10, 107-125. http://dx.doi.org/10.5194/os-10-107-2014

Polyakov, I.V., Timokhov, L.A., Alexeev, V.A., Bacon, S., Dmitrenko, I.A., Fortier, L., Frolov, I.E., Gascard, J.-C., Hansen, E., Ivanov, V.V., Laxon, S., Mauritzen, C., Perovich, D., Shimada, K., Simmons, H.L., Sokolov, V.T., Steele, M. and Toole, J. (2010) Arctic Ocean Warming Contributes to Reduced Polar Ice Cap. Journal of Physical Oceanography 40, 2743-2756. http://dx.doi.org/10.1175/2010jp04339.1

Porcelli, D., Andersson, P.S., Baskaran, M., Frank, M., Bjork, G. and Semiletov, I. (2009) The distribution of neodymium isotopes in Arctic Ocean basins. Geochimica Et Cosmochimica Acta 73, 2645-2659. http://dx.doi.org/10.1016/j.gca.2008.11.046

Pritchard, H.D., Arthern, R.J., Vaughan, D.G. and Edwards, L.A. (2009) Extensive dynamic thinning on the margins of the Greenland and Antarctic ice sheets. Nature 461, 971-975. http://dx.doi.org/10.1038/nature08471

Rabe, B., Dodd, P.A., Hansen, E., Falck, E., Schauer, U., Mackensen, A., Beszczynska-Möller, A., Kattner, G., Rohling, E.J. and Cox, K. (2013) Liquid export of Arctic freshwater components through the Fram Strait 1998-2011. Ocean Science 9, 91-109. http://dx.doi.org/10.5194/os-9-91-2013

Rabe, B., Schauer, U., Mackensen, A., Karcher, M., Hansen, E. and Beszczynska-Möller, A. (2009) Freshwater components and transports in the Fram Strait - recent observations and changes since the late 1990s. Ocean Science 5, 219-233. http://dx.doi.org/10.5194/os-5-219-2009

Rabe, B., von Appen, W.-J., Latarius, K. and Wisotzki, A. (2014) Physical oceanography during POLARSTERN cruise PS85 (ARK-XXVIII/2). PANGAEA. http://dx.doi.org/10.1594/PANGAEA.837425

Rahmstorf, S., Box, J.E., Feulner, G., Mann, M.E., Robinson, A., Rutherford, S. and Schaffernicht, E.J. (2015) Exceptional twentieth-century slowdown in Atlantic Ocean overturning circulation. Nature Climate Change 5, 475-480. http://dx.doi.org/10.1038/nclimate2554

Rempfer, J., Stocker, T.F., Joos, F., Dutay, J.C. and Siddall, M. (2011) Modelling Nd-isotopes with a coarse resolution ocean circulation model: Sensitivities to model parameters and source/sink distributions. Geochimica Et Cosmochimica Acta 75, 5927-5950. http://dx.doi.org/10.1016/j.gca.2011.07.044

Rickli, J., Frank, M., Baker, A.R., Aciego, S., de Souza, G., Georg, R.B. and Halliday, A.N. (2010) Hafnium and neodymium isotopes in surface waters of the eastern Atlantic Ocean: Implications for sources and inputs of trace metals to the ocean. Geochimica Et Cosmochimica Acta 74, 540-557. http://dx.doi.org/10.1016/j.gca.2009.10.006

Rickli, J., Frank, M. and Halliday, A.N. (2009) The hafnium-neodymium isotopic composition of Atlantic seawater. Earth and Planetary Science Letters 280, 118-127. http://dx.doi.org/10.1016/j.epsl.2009.01.026

Rippeth, T.P., Lincoln, B.J., Lenn, Y.-D., Green, J.A.M., Sundfjord, A. and Bacon, S. (2015) Tide-mediated warming of Arctic halocline by Atlantic heat fluxes over rough topography. Nature Geoscience 8, 191-194. http://dx.doi.org/10.1038/ngeo2350

Roeske, T., Bauch, D., Rudgers Van der Loeff, M. and Rabe, B. (2012) Utility of dissolved barium in distinguishing North American from Eurasian runoff in the Arctic Ocean. Marine Chemistry 132, 1-14. http://dx.doi.org/10.1016/j.marchem.2012.01.007

Rosén, P.-O., Andersson, P.S., Alling, V., Mörth, C.-M., Björk, G., Semiletov, I. and Porcelli, D. (2015) Ice export from the Laptev and East Siberian Sea derived from δ18O values. Journal of Geophysical Research: Oceans 120, 5997-6007. http://dx.doi.org/10.1002/2015jc010866

Rousseau, T.C., Sonke, J.E., Chmeleff, J., van Beek, P., Souhaut, M., Boaventura, G., Seyler, P. and Jeandel, C. (2015) Rapid neodymium release to marine waters from lithogenic sediments in the Amazon estuary. Nat Commun 6, 7592. http://dx.doi.org/10.1038/ncomms8592

Rudels, B. (2009) Arctic Ocean Circulation. Encyclopedia of Ocean Sciences. Elsevier, 211-225. http://dx.doi.org/10.1016/B978-012374473-9.00601-9

Rudels, B., Anderson, L., Eriksson, P., Fahrbach, E., Jakobsson, M., Jones, E.P., Melling, H., Prinsenberg, S., Schauer, U. and Yao, T. (2012) Observations in the ocean, Arctic Climate Change. Springer, pp. 117-198. http://dx.doi.org/10.1007/978-94-007-2027-5_4

Rudels, B., Bjork, G., Nilsson, J., Winsor, P., Lake, I. and Nohr, C. (2005) The interaction between waters from the Arctic Ocean and the Nordic Seas north of Fram Strait and along the East Greenland Current: results from the Arctic Ocean-02 Oden expedition. Journal of Marine Systems 55, 1-30. http://dx.doi.org/10.1016/j.jmarsys.2004.06.008

Rudels, B., Friedrich, H.J., Hainbucher, D. and Lohmann, G. (1999a) On the parameterisation of oceanic sensible heat loss to the atmosphere and to ice in an ice-covered mixed layer in winter. Deep-Sea Research Part Ii-Topical Studies in Oceanography 46, 1385-1425. http://dx.doi.org/10.1016/S0967-0645(99)00028-4

Rudels, B., Friedrich, H.J. and Quadfasel, D. (1999b) The arctic circumpolar boundary current. Deep-Sea Research Part Ii-Topical Studies in Oceanography 46, 1023-1062. http://dx.doi.org/10.1016/S0967-0645(99)00015-6

Rudels, B., Jones, E.P., Schauer, U. and Eriksson, P. (2004) Atlantic sources of the Arctic Ocean surface and halocline waters. Polar Research 23, 181-208. http://dx.doi.org/10.1111/j.1751-8369.2004.tb00007.x

Rudels, B., Korhonen, M., Schauer, U., Pisarev, S., Rabe, B. and Wisotzki, A. (2015) Circulation and transformation of Atlantic water in the Eurasian Basin and the contribution of the Fram Strait inflow branch to the Arctic Ocean heat budget. Progress in Oceanography 132, 128-152. http://dx.doi.org/10.1016/j.pocean.2014.04.003

Rudels, B., Meyer, R., Fahrbach, E., Ivanov, V.V., Østerhus, S., Quadfasel, D., Schauer, U., Tverberg, V. and Woodgate, R.A. (2000) Water mass distribution in Fram Strait and over the Yermak Plateau in summer 1997, Annales Geophysicae. Springer, pp. 687-705. http://dx.doi.org/10.1007/s00585-000-0687-5

Schauer, U., Beszczynska-Möller, A., Walczowski, W., Fahrbach, E., Piechura, J. and Hansen, E. (2008) Variation of measured heat flow through the Fram Strait between 1997 and 2008, In: Arctic-Subarctic Ocean Fluxes. R.R. Dickson, J. Meincke, P. Rhines (eds.), Dordrecht, 2008. pp. 65-85.

Schlichtholz, P. and Houssais, M.-N. (2002) An overview of the teta-S correlations in Fram Strait based on the MIZEX 84 data. Oceanologia 44.

Schlitzer, R. (2016) Ocean Data View. http://odv.awi.de.

Schmitt, W. (2007) Application of the Sm-Nd isotope system to the late quaternary paleoceanography of the Yermak Plateau (Arctic Ocean), Doctoral Thesis, Fakultät für Geowissenschaften. Ludwig-Maximilians-Universität München, 121pp.

Semiletov, I., Pipko, I., Gustafsson, Ö., Anderson, L.G., Sergienko, V., Pugach, S., Dudarev, O., Charkin, A., Gukov, A., Bröder, L., Andersson, A., Spivak, E. and Shakhova, N. (2016) Acidification of East Siberian Arctic Shelf waters through addition of freshwater and terrestrial carbon. Nature Geoscience 9, 361-365. http://dx.doi.org/10.1038/ngeo2695

Serreze, M.C., Barrett, A.P., Stroeve, J.C., Kindig, D.N. and Holland, M.M. (2009) The emergence of surface-based Arctic amplification. The Cryosphere 3, 11-19. http://dx.doi.org/10.5194/tc-3-11-2009

Serreze, M.C. and Barry, R.G. (2011) Processes and impacts of Arctic amplification: A research synthesis. Global and Planetary Change 77, 85-96. http://dx.doi.org/10.1016/j.gloplacha.2011.03.004

Shakhova, N., Semiletov, I., Salyuk, A., Yusupov, V., Kosmach, D. and Gustafsson, O. (2010) Extensive methane venting to the atmosphere from sediments of the East Siberian Arctic Shelf. Science 327, 1246-1250. http://dx.doi.org/10.1126/science.1182221

Sharma, M., Basu, A.R. and Nesterenko, G.V. (1992) Temporal Sr-, Nd- and Pb-isotopic variations in the Siberian flood basalts: Implications for the plume-source characteristics. Earth and Planetary Science Letters 113, 365-381. http://dx.doi.org/10.1016/0012-821x(92)90139-m

Sholkovitz, E. and Szymczak, R. (2000) The estuarine chemistry of rare earth elements: comparison of the Amazon, Fly, Sepik and the Gulf of Papua systems. Earth and Planetary Science Letters 179, 299-309. http://dx.doi.org/10.1016/s0012-821x(00)00112-6

Sholkovitz, E.R. (1992) Chemical evolution of rare earth elements: fractionation between colloidal and solution phases of filtered river water. Earth and Planetary Science Letters 114, 77-84. http://dx.doi.org/10.1016/0012-821x(92)90152-l

Sholkovitz, E.R. (1993) The geochemistry of rare earth elements in the Amazon River estuary. Geochimica et Cosmochimica Acta 57, 2181-2190. http://dx.doi.org/10.1016/0016-7037(93)90559-f

Sholkovitz, E.R. (1995) The aquatic chemistry of rare earth elements in rivers and estuaries. Aquatic Geochemistry 1, 1-34. http://dx.doi.org/10.1007/bf01025229

Siddall, M., Khatiwala, S., van de Flierdt, T., Jones, K., Goldstein, S.L., Hemming, S. and Anderson, R.F. (2008) Towards explaining the Nd paradox using reversible scavenging in an ocean general circulation model. Earth and Planetary Science Letters 274, 448-461. http://dx.doi.org/10.1016/j.epsl.2008.07.044

Spielhagen, R.F., Werner, K., Sorensen, S.A., Zamelczyk, K., Kandiano, E., Budéus, G., Husum, K., Marchitto, T.M. and Hald, M. (2011) Enhanced modern heat transfer to the Arctic by warm Atlantic Water. Science 331, 450-453. http://dx.doi.org/10.1126/science.1197397

Stedmon, C.A., Granskog, M.A. and Dodd, P.A. (2015) An approach to estimate the freshwater contribution from glacial melt and precipitation in East Greenland shelf waters using colored dissolved organic matter (CDOM). J Geophys Res-Oceans 120, 1107-1117. http://dx.doi.org/10.1002/2014jc010501

Steele, M., Morison, J., Ermold, W., Rigor, I., Ortmeyer, M. and Shimada, K. (2004) Circulation of summer Pacific halocline water in the Arctic Ocean. J Geophys Res-Oceans 109. http://dx.doi.org/ArtnC0202710.1029/2003jc002009

Stichel, T. (2010) Tracing water masses and continental weathering by neodymium and hafnium isotopes in the Atlantic sector of the Southern Ocean. Doctoral Thesis, Christian-Albrechts-Universität (CAU), 129pp.

Stichel, T., Frank, M., Rickli, J. and Haley, B.A. (2012) The hafnium and neodymium isotope composition of seawater in the Atlantic sector of the Southern Ocean. Earth and Planetary Science Letters 317, 282-294. http://dx.doi.org/10.1016/j.epsl.2011.11.025

Stichel, T., Hartman, A.E., Duggan, B., Goldstein, S.L., Scher, H. and Pahnke, K. (2015) Separating biogeochemical cycling of neodymium from water mass mixing in the Eastern North Atlantic. Earth and Planetary Science Letters 412, 245-260. http://dx.doi.org/10.1016/j.epsl.2014.12.008

Stöven, T., Tanhua, T., Hoppema, M. and von Appen, W.-J. (2016) Transient tracer distributions in the Fram Strait in 2012 and inferred anthropogenic carbon content and transport. Ocean Science 12, 319-333. http://dx.doi.org/10.5194/os-12-319-2016

Sutherland, D.A., Pickart, R.S., Jones, E.P., Azetsu-Scott, K., Eert, A.J. and Olafsson, J. (2009) Freshwater composition of the waters off southeast Greenland and their link to the Arctic Ocean. J Geophys Res-Oceans 114. http://dx.doi.org/10.1029/2008jc004808

Swingedouw, D., Rodehacke, C.B., Behrens, E., Menary, M., Olsen, S.M., Gao, Y., Mikolajewicz, U., Mignot, J. and Biastoch, A. (2012) Decadal fingerprints of freshwater discharge around Greenland in a multi-model ensemble. Climate Dynamics 41, 695-720. http://dx.doi.org/10.1007/s00382-012-1479-9

Tachikawa, K., Athias, V. and Jeandel, C. (2003) Neodymium budget in the modern ocean and paleo-oceanographic implications. J Geophys Res-Oceans 108. http://dx.doi.org/10.1029/1999jc000285

Tachikawa, K., Jeandel, C. and Roy-Barman, M. (1999) A new approach to the Nd residence time in the ocean: the role of atmospheric inputs. Earth and Planetary Science Letters 170, 433-446. http://dx.doi.org/10.1016/s0012-821x(99)00127-2

Tanaka, T., Togashi, S., Kamioka, H., Amakawa, H., Kagami, H., Hamamoto, T., Yuhara, M., Orihashi, Y., Yoneda, S., Shimizu, H., Kunimaru, T., Takahashi, K., Yanagi, T., Nakano, T., Fujimaki, H., Shinjo, R., Asahara, Y., Tanimizu, M. and Dragusanu, C. (2000) JNdi-1: a neodymium isotopic reference in consistency with LaJolla neodymium. Chemical Geology 168, 279-281. http://dx.doi.org/10.1016/S0009-2541(00)00198-4

Tanhua, T., Jones, E.P., Jeansson, E., Jutterström, S., Smethie, W.M., Wallace, D.W.R. and Anderson, L.G. (2009) Ventilation of the Arctic Ocean: Mean ages and inventories of anthropogenic CO2and CFC-11. Journal of Geophysical Research 114. http://dx.doi.org/10.1029/2008jc004868

Taylor, J.R., Falkner, K.K., Schauer, U. and Meredith, M. (2003) Quantitative considerations of dissolved barium as a tracer in the Arctic Ocean. J Geophys Res-Oceans 108. http://dx.doi.org/10.1029/2002jc001635

Tepe, N. and Bau, M. (2014) Importance of nanoparticles and colloids from volcanic ash for riverine transport of trace elements to the ocean: evidence from glacial-fed rivers after the 2010 eruption of Eyjafjallajokull Volcano, Iceland. Sci Total Environ 488-489, 243-251. http://dx.doi.org/10.1016/j.scitotenv.2014.04.083

Tepe, N. and Bau, M. (2015) Distribution of rare earth elements and other high field strength elements in glacial meltwaters and sediments from the western Greenland Ice Sheet: Evidence for different sources of particles and nanoparticles. Chemical Geology 412, 59-68. http://dx.doi.org/10.1016/j.chemgeo.2015.07.026

Tepe, N. and Bau, M. (2016) Behavior of rare earth elements and yttrium during simulation of arctic estuarine mixing between glacial-fed river waters and seawater and the impact of inorganic (nano-)particles. Chemical Geology 438, 134-145. http://dx.doi.org/10.1016/j.chemgeo.2016.06.001

Teschner, C., Frank, M., Haley, B.A. and Knies, J. (2016) Plio-Pleistocene evolution of water mass exchange and erosional input at the Atlantic-Arctic gateway. Paleoceanography 31, 582-599. http://dx.doi.org/10.1002/2015pa002843

Thibodeau, B., Bauch, D., Kassens, H. and Timokhov, L.A. (2014) Interannual variations in river water content and distribution over the Laptev Sea between 2007 and 2011: The Arctic Dipole connection. Geophysical Research Letters 41, 7237-7244. http://dx.doi.org/10.1002/2014gl061814

Top, Z., Bignami, F. and Hopkins, T. (1997) Tritium-3He ages of deep waters in the NEW Polynya. Journal of Marine Systems 10, 175-184. http://dx.doi.org/10.1016/s0924-7963(96)00064-4

van de Flierdt, T. and Frank, M. (2010) Neodymium isotopes in paleoceanography. Quaternary Science Reviews 29, 2439-2441. http://dx.doi.org/10.1016/j.quascirev.2010.07.001

van de Flierdt, T., Griffiths, A.M., Lambelet, M., Little, S.H., Stichel, T. and Wilson, D.J. (2016) Neodymium in the oceans: a global database, a regional comparison and implications for palaeoceanographic research. Philosophical Transactions of the Royal Society A: Mathematical, Physical and Engineering Sciences 374, 20150293. http://dx.doi.org/10.1098/rsta.2015.0293

van de Flierdt, T., Pahnke, K., Amakawa, H., Andersson, P.S., Basak, C., Coles, B., Colin, C., Crocket, K., Frank, M., Frank, N., Goldstein, S.L., Goswami, V., Haley, B.A., Hathorne, E.C., Hemming, S.R., Henderson, G.M., Jeandel, C., Jones, K., Kreissig, K.,

Lacan, F., Lambelet, M., Martin, E.E., Newkirk, D.R., Obata, H., Pena, L., Piotrowski, A.M., Pradoux, C., Scher, H.D., Schöberg, H., Singh, S.K., Stichel, T., Tazoe, H., Vance, D. and Yang, J. (2012) GEOTRACES intercalibration of neodymium isotopes and rare earth element concentrations in seawater and suspended particles. Part 1: reproducibility of results for the international intercomparison. Limnology and Oceanography: Methods 10, 234-251. http://dx.doi.org/10.4319/lom.2012.10.234

Vancoppenolle, M., Fichefet, T. and Goosse, H. (2009) Simulating the mass balance and salinity of Arctic and Antarctic sea ice. 2. Importance of sea ice salinity variations. Ocean Modelling 27, 54-69. http://dx.doi.org/10.1016/j.ocemod.2008.11.003

Velicogna, I. (2009) Increasing rates of ice mass loss from the Greenland and Antarctic ice sheets revealed by GRACE. Geophysical Research Letters 36. http://dx.doi.org/10.1029/2009gl040222

von Appen, W.-J., Schauer, U., Hattermann, T. and Beszczynska-Möller, A. (2016a) Seasonal Cycle of Mesoscale Instability of the West Spitsbergen Current. Journal of Physical Oceanography 46, 1231-1254. http://dx.doi.org/10.1175/jpo-d-15-0184.1

von Appen, W.-J., Schauer, U., Somavilla, R., Bauerfeind, E. and Beszczynska-Möller, A. (2015) Exchange of warming deep waters across Fram Strait. Deep Sea Research Part I: Oceanographic Research Papers 103, 86-100. http://dx.doi.org/10.1016/j.dsr.2015.06.003

von Appen, W.-J., Stein, R. and Wisotzki, A. (2016b) Physical oceanography measured on water bottle samples during POLARSTERN cruise PS93.1 (ARK-XXIX/2.1). PANGAEA. http://dx.doi.org/10.1594/PANGAEA.863064

Walczowski, W. (2013) Frontal structures in the West Spitsbergen Current margins. Ocean Science 9, 957-975. http://dx.doi.org/10.5194/os-9-957-2013

Walczowski, W., Piechura, J., Osinski, R. and Wieczorek, P. (2005) The West Spitsbergen Current volume and heat transport from synoptic observations in summer. Deep-Sea Research Part I-Oceanographic Research Papers 52, 1374-1391. http://dx.doi.org/10.1016/j.dsr.2005.03.009

Wang, M. and Overland, J.E. (2009) A sea ice free summer Arctic within 30 years? Geophysical Research Letters 36. http://dx.doi.org/10.1029/2009gl037820

Wassmann, P., Duarte, C.M., AgustÍ, S. and Sejr, M.K. (2011) Footprints of climate change in the Arctic marine ecosystem. Global Change Biology 17, 1235-1249. http://dx.doi.org/10.1111/j.1365-2486.2010.02311.x

Werner, K., Frank, M., Teschner, C., Muller, J. and Spielhagen, R.F. (2014) Neoglacial change in deep water exchange and increase of sea-ice transport through eastern Fram Strait: evidence from radiogenic isotopes. Quaternary Science Reviews 92, 190-207. http://dx.doi.org/10.1016/j.quascirev.2013.06.015

Westerlund, S. and Öhman, P. (1992) Rare earth elements in the Arctic Ocean. Deep-Sea Research Part a-Oceanographic Research Papers 39, 1613-1626. http://dx.doi.org/10.1016/0198-0149(92)90051-T

Wilson, D.J., Piotrowski, A.M., Galy, A. and Clegg, J.A. (2013) Reactivity of neodymium carriers in deep sea sediments: Implications for boundary exchange and paleoceanography. Geochimica Et Cosmochimica Acta 109, 197-221. http://dx.doi.org/10.1016/j.gca.2013.01.042

Woodgate, R.A., Fahrbach, E. and Rohardt, G. (1999) Structure and transports of the East Greenland Current at 75 degrees N from moored current meters. J Geophys Res-Oceans 104, 18059-18072. http://dx.doi.org/10.1029/1999jc900146

Yamamoto-Kawai, M., McLaughlin, F.A., Carmack, E.C., Nishino, S. and Shimada, K. (2008) Freshwater budget of the Canada Basin, Arctic Ocean, from salinity, δ18O, and nutrients. Journal of Geophysical Research 113. http://dx.doi.org/10.1029/2006jc003858

Yang, J. and Haley, B. (2016) The profile of the rare earth elements in the Canada Basin, Arctic Ocean. Geochemistry, Geophysics, Geosystems 17, 3241-3253. http://dx.doi.org/10.1002/2016gc006412

Yang, Q., Dixon, T.H., Myers, P.G., Bonin, J., Chambers, D. and van den Broeke, M.R. (2016) Recent increases in Arctic freshwater flux affects Labrador Sea convection and Atlantic overturning circulation. Nat Commun 7, 10525. http://dx.doi.org/10.1038/ncomms10525

Zheng, X.-Y., Plancherel, Y., Saito, M.A., Scott, P.M. and Henderson, G.M. (2016) Rare earth elements (REEs) in the tropical South Atlantic and quantitative deconvolution of their non-conservative behavior. Geochimica et Cosmochimica Acta 177, 217-237. http://dx.doi.org/10.1016/j.gca.2016.01.018

Zimmermann, B., Porcelli, D., Frank, M., Andersson, P.S., Baskaran, M., Lee, D.C. and Halliday, A.N. (2009) Hafnium isotopes in Arctic Ocean water. Geochimica Et Cosmochimica Acta 73, 3218-3233. http://dx.doi.org/10.1016/j.gca.2009.02.028

Table A1, Chapter I: Composition of Nd sources - Arctic Mediterranean (averages)

n	*Name / Abbreviation*	*Full Name*	*ε_{Nd}*	*ε_{Nd} 1SD**	*ε_{Nd} 2SD***	*[Nd] (pmol/kg)*	*[Nd] 1SD**	*pot. T (°C)*	*pot. T 1SD**	*Salinity*	*Salinity 1SD**	*σ_θ*	*σ_θ 1SD**
7	AW-ISR	Atlantic Water @ Iceland-Scotland Ridge	-13.0	0.6		16.2	2.1	8.97	1.29	35.27	0.05	27.33	0.20
2	AW-DS	Atlantic Water @ Denmark Strait	-12.6	0.8		19.1	0.5	6.55	0.36	35.10	0.05	27.56	0.01
2	NCW	Norwegian Coastal Water @ western Barents Sea	-14.5	0.0		22.5	0.3	5.05	1.07	34.52	0.09	27.28	0.19
1	PACW	Pacific Water emerging from Chuckchi Sea	-5.5			30.0				32.70			
2	Lena	Lena River water	-15 to -16			~600				0.00			
1	Ob	Ob River water	-6.1			2152				0.00			
1	Kolyma	Kolyma River water	-6.0			129				0.00			
1	Yenisei	Yenisei River water	-5.2			154				0.00			
1	Mackenzie	Mackenzie River water	-12.9			111				0.00			
1	GFW	Greenland freshwater at Fram Strait	-18.0			~200				0.00			
1	small Rivers	small Rivers Arctic Ocean (sum)	various?			various?				0.00			

n	*Name / Abbreviation*	*Full Name*	*$\sigma_{0.5}$*	*$\sigma_{0.5}$ 1SD**	*depth (m)*	*Inflow (Sv) ****	*Inflow km^3/yr****	*Nd input*	*depth (m)*	*Classification / sample selection based on*
7	AW-ISR	Atlantic Water @ Iceland-Scotland Ridge	29.580	0.211	159	6.2		45.5	159	Rudels et al. (2012)
2	AW-DS	Atlantic Water @ Denmark Strait	29.824	0.008	140	0.8		6.9	140	Rudels et al. (2012)
2	NCW	Norwegian Coastal Water @ western Barents Sea	29.583	0.207	53	1.8		18.4	53	Loeng (1991)
1	PACW	Pacific Water emerging from Chuckchi Sea				0.8		10.9	<60	Porcelli et al. (2009)
2	Lena	Lena River water					485.0	4.2		
1	Ob	Ob River water					394.0	12.2		
1	Kolyma	Kolyma River water					103.0	0.2		
1	Yenisei	Yenisei River water					580.0	1.3		
1	Mackenzie	Mackenzie River water					282.0	0.4		
1	GFW	Greenland freshwater at Fram Strait					200.0			
1	small Rivers	small Rivers Arctic Ocean (sum)					383.7			

* standard deviation of sample mean

** measurement uncertainty, shown if only one sample is used

*** data taken from Siedler, G., Griffies, S. M., Gould, J., & Church, J. A. (2013). Ocean circulation and climate: a 21st century perspective (Vol. 103). Academic Press.

**** data taken from R-Arctic-NET (http://www.r-arcticnet.sr.unh.edu/)

Table A1, Chapter I: Composition of Nd sources - Arctic Mediterranean (all samples)

#	*Name / Abbreviation*	*Full Name*	*Filtration*	*εNd*	*εNd 2SD*	*[Nd] pmol/kg*	*pot. T (°C)*	*Salinity*	σ_θ	$\sigma_{0.5}$	*depth (m)*	*Latitude*	*Longitude*	*Date*	*Station*	*Reference*
1	AW-ISR	Atlantic Water @ Iceland-Scotland Ridge	not filtered	-13.2	0.2	12.7	10.96	35.24	26.97	29.199	20	62.750	-9.010	04.08.99	Signature 22	Lacan & Jeandel (2004b)
2	AW-ISR	Atlantic Water @ Iceland-Scotland Ridge	not filtered	-13.2	0.2	17.5	9.19	35.29	27.31	29.562	50	62.750	-9.010	04.08.99	Signature 22	Lacan & Jeandel (2004b)
3	AW-ISR	Atlantic Water @ Iceland-Scotland Ridge	not filtered	-13.8	0.2	17.7	8.18	35.26	27.45	29.710	200	62.750	-9.010	04.08.99	Signature 22	Lacan & Jeandel (2004b)
4	AW-ISR	Atlantic Water @ Iceland-Scotland Ridge	not filtered	-11.9	0.2	13.9	7.41	35.21	27.53	29.794	411	62.750	-9.010	04.08.99	Signature 22	Lacan & Jeandel (2004b)
5	AW-ISR	Atlantic Water @ Iceland-Scotland Ridge	not filtered	-13.0	0.2	16.9	10.13	35.34	27.20	29.432	51	60.500	-5.000	06.08.99	Signature 23	Lacan & Jeandel (2004b)
6	AW-ISR	Atlantic Water @ Iceland-Scotland Ridge	not filtered	-12.8	0.2	18.3	9.20	35.33	27.34	29.592	99	60.500	-5.000	06.08.99	Signature 23	Lacan & Jeandel (2004b)
7	AW-ISR	Atlantic Water @ Iceland-Scotland Ridge	not filtered	-12.8	0.2	16.5	7.72	35.24	27.50	29.769	280	60.500	-5.000	06.08.99	Signature 23	Lacan & Jeandel (2004b)
	AW-ISR	**Average AW-ISR**		**-13.0**		**16.2**	**8.97**	**35.27**	**27.33**	**29.580**	**159**					
	AW-ISR	**1 SD AW-ISR**		**0.6**		**2.1**	**1.29**	**0.05**	**0.20**	**0.211**						
1	AW-DS	Atlantic Water @ Denmark Strait	not filtered	-13.2	0.2	18.7	6.80	35.13	27.55	29.818	97	66.080	-27.250	29.08.99	SGN 55	Lacan & Jeandel (2004a)
2	AW-DS	Atlantic Water @ Denmark Strait	not filtered	-12.1	0.2	19.4	6.29	35.06	27.56	29.829	182	66.010	-26.980	29.08.99	SGN 56	Lacan & Jeandel (2004a)
	AW-DS	**Average AW-DS**		**-12.6**		**19.1**	**6.55**	**35.10**	**27.56**	**29.824**	**140**					
	AW-DS	**1 SD AW-DS**		**0.8**		**0.5**	**0.36**	**0.05**	**0.01**	**0.008**						
1	NCW	Norwegian Coastal Water @ western Barents Sea	0.8-0.2 µm	-14.5	0.4	22.7	5.80	34.45	27.15	29.44	5					Petrova (2015)
2	NCW	Norwegian Coastal Water @ western Barents Sea	0.8-0.2 µm	-14.5	0.4	22.4	4.29	34.58	27.42	29.73	100					Petrova (2015)
	NCW	**Average NCW-BS**		**-14.5**		**22.5**	**5.05**	**34.52**	**27.28**	**29.583**	**53**					
	NCW	**1 SD NCW-BS**		**0.0**		**0.3**	**1.07**	**0.09**	**0.19**	**0.207**						
1	**PACW**	**Pacific Water emerging from Chuckchi Sea**		**-5.5**	**-**	**30.0**		**32.7***						?	Chuckchi Sea	Porcelli et al. (2009)/Dahlqvist et al. (2007)
1	**Lena**	**Lena River water**	0.22 µm	**-15**	**-**	**600**		**0.00**						summer 2008	Lena River mouth?	Persson et al. (2011)
2	**Lena**	**Lena River water**	0.8-0.2 µm	**-15.7**	**0.2**	**550**		**0.00**						summer 2013-2014	SE Laptev Sea	This study, not pure freshwater
1	**Ob**	**Ob River water**	0.22 µm, 5-15 d after splg	**-6.1**	**0.3**	**2152**		**0.00**				66.516	66.600	summer 2003	Salekhard	Zimmermann et al. (2009)
1	**Kolyma**	**Kolyma River water**	? (filtered, 0.22 µm)	**-6.0**	**0.4**	**129**		**0.00**						06.09.04	Kolyma River mouth?	Porcelli et al. (2009)
1	**Yenisei**	**Yenisei River water**	0.22 µm, 5-15 d after splg	**-5.2**	**0.3**	**154**		**0.00**				69.383	86.150	summer 2003	Dudinka	Zimmermann et al. (2009)
1	**Mackenzie**	**Mackenzie River water**	0.22 µm, 5-15 d after splg	**-12.9**	**0.3**	**111**		**0.00**				67.433	-133.750	summer 2003	Tsiigehtchic	Zimmermann et al. (2009)

* taken from Bauch, D., Hölemann, J. A., Dmitrenko, I. A., Janout, M. A., Nikulina, A., Kirillov, S. A., ... & Timokhov, L. (2012). Impact of Siberian coastal polynyas on shelf-derived Arctic Ocean halocline waters. Journal of Geophysical Research: Oceans, 117(C9).

Table A2, Chapter I: Composition of NE Greenland Shelf waters (averages)

n	*Name / Abbreviation*	*Full Name*	*εNd*	*εNd 1SD**	*εNd 2SD***	*[Nd] pmol/kg*	*[Nd] 1SD**	*pot. T (°C)*	*pot. T 1SD**	*Salinity*	*S 1SD**	*σ_θ*	*σ_θ 1SD**	*depth (m)*	*Classification / sample selection based on*
13	NEGSSW	Surface and intermediate waters @ NE Greenland Shelf	-11.7	0.5		36.6	1.0	-1.1	0.7	31.41	0.41	25.24	0.35	34	Bignami & Hopkins (1997) / This study
4	NEGSBW	Bottom Water @ NE Greenland Shelf	-11.8	0.2		24.0	1.4	-0.2	0.4	34.28	0.21	27.54	0.15	250	Bignami & Hopkins (1997) / This study

Table A2, Chapter I (continued): Composition of upper waters ($\sigma_0 \leq 27.70$; Arctic Ocean: $\theta \leq 0$ °C) - Arctic Mediterranean (averages)

n	*Name / Abbreviation*	*Full Name*	*εNd*	*εNd 1SD**	*εNd 2SD***	*[Nd] pmol/kg*	*[Nd] 1SD**	*pot. T (°C)*	*pot. T 1SD**	*Salinity*	*S 1SD**	*σ_θ*	*σ_θ 1SD**	*depth (m)*	*Classification / sample selection based on*
7	PW	Polar Water @ Fram Strait (including modified PW)	-9.9	0.7		27.1	1.9	-1.45	0.17	33.01	0.46	26.55	0.37	91	Bignami & Hopkins (1997) / Budéus et al. (1997) / This study
1	PW-εNd-max	most radiogenic Polar Water sample @ Fram Strait	-8.8		0.2	25.7		-1.63		32.30		25.98		14	This study
3	KW	Knee Water @ Fram Strait	-9.6	0.0		22.3	1.2	-1.73	0.01	33.98	0.02	27.35	0.02	93	Bignami & Hopkins (1997) / Budéus et al. (1997) / This study
7	EGC-77	East Greenland Current Upper Water @ 77 °N	-10.8	1.1		19.8	3.5	1.07	2.67	34.12	0.88	27.10	0.52	49	Rudels et al. (2012)
1	EGC-73	East Greenland Current Upper Water @ 73 °N	-10.9		0.2	22.3		-0.94		34.33		27.61		50	Rudels et al. (2012)
8	UW-SWNS	Upper Water @ southern and western Nodic Seas	-12.9	0.5		16.8	4.5	9.42	1.63	35.24	0.10	27.23	0.32	57	Rudels et al. (2012)
8	UW-DS	Upper Water @ Denmark Strait	-10.9	0.7		42.1	27.4	2.20	2.90	33.41	1.03	26.64	0.92	54	Rudels et al. (2012)
1	SW-IS	Iceland Sea Surface Water	-8.0		0.2	14.8		7.94		34.65		27.01		20	Rudels et al. (2012)
4	PW-NB	Nansen Basin Polar Water	-10.8	0.5		17.5	0.3	-1.64	0.07	34.09	0.16	27.43	0.13	16	Rudels et al. (2012)
15	PW-AB	Amundsen Basin Polar Water	-10.7	1.1		38.7	11.9	-1.65	0.12	32.26	1.26	25.95	1.03	30	Rudels et al. (2012)
5	PW-MB	Makarov Basin Polar Water	-11.1	0.5		44.2	7.7	-1.64	0.04	31.75	1.05	25.53	0.85	26	Rudels et al. (2012)
13	PW-CB	Canada Basin Polar Water	-6.9	1.1		29.6	6.3	-0.91	0.48	29.44	2.81	23.65	2.28	44	Rudels et al. (2012)

Table A2, Chapter I (continued): Composition of Atlantic layer waters (θ > 0 °C; Arctic Ocean AW and AAW: 27.70 < σ_0 ≤ 27.97) - Arctic Mediterranean (averages)

n	*Name / Abbreviation*	*Full Name*	*εNd*	*εNd 1SD**	*εNd 2SD***	*[Nd] pmol/kg*	*[Nd] 1SD**	*pot. T (°C)*	*pot. T 1SD**	*Salinity*	*S 1SD**	σ_θ	σ_θ *1SD**	$\sigma_{0.5}$	$\sigma_{0.5}$ *1SD**	*depth (m)*	*Classification / sample selection based on*
7	AW-ISR	Atlantic Water @ Iceland-Scotland Ridge	-13.0	0.6		16.2	2.1	8.97	1.29	35.27	0.05	27.33	0.20	29.580	0.211	159	Rudels et al. (2012)
2	AW-DS	Atlantic Water @ Denmark Strait	-12.6	0.8		19.1	0.5	6.55	0.36	35.10	0.05	27.56	0.01	29.824	0.008	140	Rudels et al. (2012)
2	AW-eNWSLB	Atlantic Water @ eastern Norwegian Seas & Lofoten Basin	-12.6	0.7		22.1	2.5	7.69	0.59	35.25	0.04	27.51	0.06	29.777	0.067	88	Rudels et al. (2012)
5	AW-wBS	Atlantic Water @ western Barents Sea	-12.4	0.4		16.7	1.3	2.60	1.59	35.02	0.01	27.93	0.15	30.258	0.168	141	Rudels et al. (2012)
1	AW-FS11	Atlantic Water @ Fram Strait	-11.9		0.3	16.8		3.19		35.10		27.95		30.269		150	Rudels et al. (2012)
11	AW	Atlantic Water @ Fram Strait	-11.7	0.4		15.9	0.5	3.80	0.47	35.09	0.03	27.88	0.04	30.190	0.050	106	Rudels et al. (2005) / This study
2	AW-northS	Atlantic Water @ north of Svalbard	-11.8	0.5		16.6	0.2	2.40	0.22	34.92	0.06	27.87	0.06	30.200	0.065	177	Rudels et al. (2012)
3	RAW	Recirculating Atlantic Water @ Fram Strait	-11.6	0.1		16.3	0.1	2.76	0.40	35.01	0.03	27.92	0.06	30.244	0.065	229	Rudels et al. (2005) / This study
1	AAW-LS	Arctic Atlantic Water @ Laptev Sea margin	-10.0		0.1	16.4		1.15		34.85		27.92		30.269		200	Rudels et al. (2012)
3	AAW-NB	Arctic Atlantic Water @ Nansen Basin	-11.2	0.4		16.1	0.0	1.69	0.47	34.93	0.01	27.94	0.03	30.279	0.037	367	Rudels et al. (2012)
3	AAW-AB	Arctic Atlantic Water @ Amundsen Basin	-11.0	0.6		16.9	0.8	1.10	0.50	34.87	0.00	27.93	0.03	30.285	0.040	367	Rudels et al. (2012)
2	AAW-MB	Arctic Atlantic Water @ Makarov Basin	-10.6	0.4		16.6	0.4	0.71	0.30	34.86	0.02	27.95	0.04	30.306	0.041	400	Rudels et al. (2012)
3	AAW-CB	Arctic Atlantic Water @ Canada Basin	-9.3	0.3		18.6	2.3	0.58	0.15	34.81	0.02	27.92	0.02	30.282	0.018	433	Rudels et al. (2012)
5	dAAW	Dense Arctic Atlantic Water @ Fram Strait	-10.4	0.2		16.3	1.1	0.45	0.29	34.91	0.03	28.01	0.04	30.367	0.039	669	Rudels et al. (2012) / This study

Table A2, Chapter I (continued): Composition of intermediate waters (27.97 < σ_0, $\sigma_{0.5}$ ≤ 30.444; Arctic Ocean: θ ≤ 0 °C) - Arctic Mediterranean (avergaes)

n	*Name / Abbreviation*	*Full Name*	*εNd*	*εNd 1SD**	*εNd 2SD***	*[Nd] pmol/kg*	*[Nd] 1SD**	*pot. T (°C)*	*pot. T 1SD**	*Salinity*	*S 1SD**	σ_θ	σ_θ *1SD**	$\sigma_{0.5}$	$\sigma_{0.5}$ *1SD**	$\sigma_{1.5}$	$\sigma_{1.5}$ *1SD**	*depth (m)*	*Classification / sample selection based on*
8	AIW-GS	Greenland Sea Arctic Intermediate Water - DSOW precursor	-10.8	0.2		16.8	0.3	-0.24	0.41	34.89	0.01	28.03	0.03	30.398	0.032	35.061	0.044	679	Rudels et al. (2012)
1	AIW-IS	Iceland Sea Arctic Intermediate Water	-8.4		0.2	19.9		0.22		34.86		27.98		30.346		34.996		331	Rudels et al. (2012)
1	AIW-NWS	Norwegian Sea Arctic Intermediate Water	-8.1		0.2	20.0		0.33		34.88		27.99		30.354		35.001		599	Rudels et al. (2012)
2	AIW-eNWSLB	eastern Norwegian Sea & Lofoten Basin Arctic Intermediate Water	-10.0	0.1		16.8	1.0	-0.23	0.02	34.89	0.01	28.03	0.01	30.397	0.007	35.059	0.008	1000	Rudels et al. (2012)
4	AIW	Arctic Intermediate Water @ Fram Strait	-10.1	0.2		15.5	0.1	-0.51	0.09	34.91	0.00	28.06	0.00	30.433	0.005	35.103	0.007	988	Rudels et al. (2005)
2	UPDW-NB	Nansen Basin Upper Polar Deep Water	-10.8	0.1		16.2	2.9	-0.25	0.00	34.91	0.00	28.05	0.00	30.418	0.000	35.082	0.000	1000	Rudels et al. (2012)
1	UPDW-AB	Amundsen Basin Upper Polar Deep Water	-10.8		0.2	16.3		-0.23		34.89		28.03		30.401		35.064		1000	Rudels et al. (2012)
1	UPDW-MB	Makarov Basin Upper Polar Deep Water	-10.5		0.4	15.3		-0.18		34.89		28.03		30.398		35.059		1000	Rudels et al. (2012)
1	UPDW-CB	Canada Basin Upper Polar Deep Water	-10.7		0.4	15.5		-0.03		34.88		28.01		30.379		35.036		1000	Rudels et al. (2012)
5	UPDW	Upper Polar Deep Water @ Fram Strait	-10.2	0.4		15.7	0.3	-0.46	0.19	34.90	0.01	28.05	0.02	30.427	0.019	35.097	0.025	1318	Rudels et al. (2005)
3	pISOW	pure Iceland-Scotland Overflow Water	-8.1	0.9		21.5	2.7	-0.35	0.59	34.89	0.01	28.03	0.04	30.407	0.047	35.073	0.064	796	Rudels et al. (2012) / Lacan & Jeandel (2004a)
4	pDSOW	pure Denmark Strait Overflow Water	-8.0	0.9		22.1	5.0	-0.18	0.23	34.88	0.01	28.02	0.02	30.389	0.026	35.050	0.033	514	Rudels et al. (2012) / Lacan & Jeandel (2004a)

Table A2, Chapter I (continued): Composition of deep waters (30.444 < $\sigma_{0.5}$; *Nordic Seas: S ≤ 34.915; Arctic Ocean: 34.915 < S) - Arctic Mediterranean (averages)*

n	*Name / Abbreviation*	*Full Name*	*εNd*	*εNd 1SD**	*εNd 2SD***	*[Nd] pmol/kg*	*[Nd] 1SD**	*pot. T (°C)*	*pot. T 1SD**	*Salinity*	*S 1SD**	$\sigma_{0.5}$	$\sigma_{0.5}$ *1SD**	$\sigma_{1.5}$	$\sigma_{1.5}$ *1SD**	$\sigma_{2.5}$	$\sigma_{2.5}$ *1SD**	*depth (m)*	*Classification based on*
6	DW-GS	Greenland Sea Deep Water	-10.4	0.3		19.4	2.3	-0.97	0.12	34.90	0.01	30.457	0.007	35.142	0.010	39.721	0.013	2308	Rudels et al. (2012)
3	DW-NWS	Norwegian Sea Deep Water	-8.2	1.3		21.3	3.0	-0.89	0.13	34.90	0.00	30.450	0.007	35.132	0.011	39.708	0.015	1637	Rudels et al. (2012)
3	DW-eNWSLB	eastern Norwegian Sea & Lofoten Basin Deep Water	-9.7	0.6		22.4	5.1	-0.93	0.10	34.90	0.00	30.452	0.006	35.135	0.009	39.713	0.011	2019	Rudels et al. (2012)
3	NDW	Nordic Seas Deep Water @ Fram Strait	-10.0	0.2		16.1	0.7	-0.83	0.12	34.91	0.00	30.454	0.008	35.134	0.012	39.709	0.016	1085	Rudels et al. (2012)
2	DW-NB	Nansen Basin Deep Water	-10.9	0.1		17.1	0.1	-0.75	0.06	34.94	0.01	30.469	0.002	35.147	0.000	39.719	0.002	3100	Rudels et al. (2012)
2	DW-AB	Amundsen Basin Deep Water	-11.5	1.2		18.2	0.0	-0.95	0.00	34.94	0.01	30.481	0.006	35.165	0.006	39.743	0.006	3450	Rudels et al. (2012)
2	DW-MB	Makarov Basin Deep Water	-10.6	0.1		16.5	0.8	-0.53	0.01	34.96	0.01	30.472	0.007	35.144	0.007	39.709	0.007	3000	Rudels et al. (2012)
2	DW-CB	Canada Basin Deep Water	-9.9	1.4		19.4	3.2	-0.52	0.01	34.96	0.01	30.471	0.005	35.142	0.005	39.707	0.005	2750	Rudels et al. (2012)
6	EBDW/GSDW	Eurasian Basin / Greenland Sea Deep Water @ Fram Strait	-10.5	0.2		15.8	0.3	-0.89	0.01	34.92	0.00	30.467	0.003	35.149	0.003	39.726	0.004	2386	Rudels et al. (2005)
3	CBDW	Canadian Basin Deep Water @ Fram Strait	-10.1	0.5		15.4	0.1	-0.79	0.08	34.92	0.00	30.459	0.002	35.138	0.005	39.712	0.007	2057	Rudels et al. (2005)

* standard deviation of sample mean

** measurement uncertainty, shown if only one sample is used

*** data taken from Siedler, G., Griffies, S. M., Gould, J., & Church, J. A. (2013). Ocean circulation and climate: a 21st century perspective (Vol. 103). Academic Press.

**** data taken from R-Arctic-NET (http://www.r-arcticnet.sr.unh.edu/)

References

Bignami, F., & Hopkins, T. S. (1997). The water mass characteristics of the Northeast Water Polynya: Polar Sea data 1992–1993. Journal of marine systems, 10(1), 139-156.

Budéus, G., Schneider, W., & Kattner, G. (1997). Distribution and exchange of water masses in the Northeast Water Polynya (Greenland Sea). Journal of marine systems, 10(1), 123-138.

Lacan, F., & Jeandel, C. (2004a). Denmark Strait water circulation traced by heterogeneity in neodymium isotopic compositions. Deep Sea Research Part I: Oceanographic Research Papers, 51(1), 71-82.

Loeng, H. (1991). Features of the physical oceanographic conditions of the Barents Sea. Polar research, 10(1), 5-18.

Porcelli, D., Andersson, P. S., Baskaran, M., Frank, M., Björk, G., & Semiletov, I. (2009). The distribution of neodymium isotopes in Arctic Ocean basins. Geochimica et Cosmochimica Acta, 73(9), 2645-2659.

Rudels, B., Anderson, L., Eriksson, P., Fahrbach, E., Jakobsson, M., Jones, E. P., ... & Yao, T. (2012). Observations in the ocean. In Arctic Climate Change (pp. 117-198). Springer Netherlands.

Rudels, B., Björk, G., Nilsson, J., Winsor, P., Lake, I., & Nohr, C. (2005). The interaction between waters from the Arctic Ocean and the Nordic Seas north of Fram Strait and along the East Greenland Current: results from the Arctic Ocean-02 Oden expedition. Journal of Marine Systems, 55(1), 1-30.

Table A2, Chapter I (continued): Composition of NE Greenland Shelf waters (all samples)

#	*Name / Abbreviation*	*Full Name*	*Filtration*	*εNd*	*εNd 2SD*	*[Nd] pmol/kg*	*pot. T (°C)*	*Salinity*	*σ_θ*	*depth (m)*	*Latitude*	*Longitude*	*Date*	*Station*	*Reference*
1	NEGSSW	Surface and intermediate waters @ NE Greenland	0.45 µm	-12.4	0.2	36.8	0.29	31.04	24.90	1	79.833	-12.004	03.07.12	27/92/S	This study
2	NEGSSW	Surface and intermediate waters @ NE Greenland	0.45 µm	-12.1	0.2	36.9	-1.49	31.70	25.50	31	79.833	-12.004	03.07.12	27/92/30	This study
3	NEGSSW	Surface and intermediate waters @ NE Greenland	0.45 µm	-12.3	0.3	37.5	0.30	31.05	24.90	10	79.415	-11.484	04.07.12	27/97/10	This study
4	NEGSSW	Surface and intermediate waters @ NE Greenland	0.45 µm	-11.8	0.3	37.3	-1.51	31.72	25.51	50	79.415	-11.484	04.07.12	27/97/50	This study
5	NEGSSW	Surface and intermediate waters @ NE Greenland	0.45 µm	-12.4	0.3	36.9	-0.56	30.89	24.81	10	78.832	-10.671	05.07.12	27/106/10	This study
6	NEGSSW	Surface and intermediate waters @ NE Greenland	0.45 µm	-11.4	0.3	36.0	-1.63	31.79	25.57	77	78.832	-10.671	05.07.12	27/106/75	This study
7	NEGSSW	Surface and intermediate waters @ NE Greenland	0.45 µm	-11.3	0.3	35.9	-0.76	31.08	24.97	11	78.499	-10.995	05.07.12	27/110/10	This study
8	NEGSSW	Surface and intermediate waters @ NE Greenland	0.45 µm	-11.1	0.3	35.1	-1.55	31.67	25.47	35	78.499	-10.995	05.07.12	27/110/35	This study
9	NEGSSW	Surface and intermediate waters @ NE Greenland	0.45 µm	-12.0	0.3	37.1	-1.44	30.89	24.83	15	78.827	-12.456	06.07.12	27/113/15	This study
10	NEGSSW	Surface and intermediate waters @ NE Greenland	0.45 µm	-11.1	0.3	35.0	-1.67	31.83	25.60	71	78.827	-12.456	06.07.12	27/113/70	This study
11	NEGSSW	Surface and intermediate waters @ NE Greenland	0.45 µm	-11.4	0.2	35.5	-0.75	30.99	24.90	10	78.816	-9.499	06.07.12	27/118/10	This study
12	NEGSSW	Surface and intermediate waters @ NE Greenland	0.45 µm	-11.6	0.2	38.1	-1.69	31.87	25.64	75	78.816	-9.499	06.07.12	27/118/75	This study
13	NEGSSW	Surface and intermediate waters @ NE Greenland	0.45 µm	-11.9	0.2	37.5	-1.68	31.78	25.56	51	78.833	-7.996	07.07.12	27/121/50	This study
	NEGSSW	**Average NEGSSW**		**-11.7**		**36.6**	**-1.09**	**31.41**	**25.24**	**34**					
	NEGSSW	**1 SD NEGSSW**		**0.5**		**1.0**	**0.73**	**0.41**	**0.35**						
1	NEGSBW	Bottom waters @ NE Greenland Shelf	0.45 µm	-11.9	0.3	23.3	-0.07	34.38	27.61	253	78.832	-10.671	05.07.12	27/106/250	This study
2	NEGSBW	Bottom waters @ NE Greenland Shelf	0.45 µm	-12.0	0.3	22.5	0.21	34.53	27.71	354	78.832	-10.671	05.07.12	27/106/350	This study
3	NEGSBW	Bottom waters @ NE Greenland Shelf	0.45 µm	-11.5	0.3	24.5	-0.51	34.16	27.45	172	78.499	-10.995	05.07.12	27/110/170	This study
4	NEGSBW	Bottom waters @ NE Greenland Shelf	0.45 µm	-11.7	0.3	25.7	-0.59	34.06	27.38	223	78.827	-12.456	06.07.12	27/113/220	This study
	NEGSBW	**Average NEGSBW**		**-11.8**		**24.0**	**-0.24**	**34.28**	**27.54**	**250**					
	NEGSBW	**1 SD NEGSBW**		**0.2**		**1.4**	**0.38**	**0.21**	**0.15**						

Table A2, Chapter I (continued): Composition of upper waters (mostly $\sigma_0 \leq 27.70$; Arctic Ocean: $\theta \leq 0$ °C) - Arctic Mediterranean (all samples)

#	*Name / Abbreviation*	*Full Name*	*Filtration*	*εNd*	*εNd 2SD*	*[Nd] pmol/kg*	*pot. T (°C)*	*Salinity*	σ_0	*depth (m)*	*Latitude*	*Longitude*	*Date*	*Station*	*Reference*
1	PW-mod	modified Polar Water @ Fram Strait	0.45 µm	-10.9	0.3	28.5	-1.17	33.39	26.86	150.5	78.832	-10.671	05.07.12	27/106/150	This study
2	PW-mod	modified Polar Water @ Fram Strait	0.45 µm	-9.8	0.3	29.0	-1.61	32.80	26.39	100.9	78.499	-10.995	05.07.12	27/110/100	This study
3	PW-mod	modified Polar Water @ Fram Strait	0.45 µm	-10.1	0.3	28.2	-1.52	33.06	26.60	141.8	78.827	-12.456	06.07.12	27/113/140	This study
4	PW-mod	modified Polar Water @ Fram Strait	0.45 µm	-10.3	0.2	28.5	-1.44	33.01	26.56	126.2	78.816	-9.499	06.07.12	27/118/125	This study
5	PW-mod	modified Polar Water @ Fram Strait	0.45 µm	-10.2	0.2	25.7	-1.25	33.73	27.13	91.6	78.838	-6.497	08.07.12	27/124/90	This study
7	PW-mod	modified Polar Water @ Fram Strait	0.45 µm	-9.3	0.2	24.3	-1.51	32.74	26.34	10.3	78.833	-3.920	09.07.12	27/132/10	This study
6	PW-εNd-max	most radiogenic Polar Water @ Fram Strait	0.45 µm	-8.8	0.2	25.7	-1.63	32.30	25.98	14.1	78.833	-4.577	08.07.12	27/130/14	This study
	PW	**Average PW**		**-9.9**		**27.1**	**-1.4**	**33.01**	**26.55**	**91**					
	PW	**1 SD PW**		**0.7**		**1.9**	**0.2**	**0.46**	**0.37**						
1	**PW-εNd-max**	**most radiogenic Polar Water sample @ Fram Strait**	0.45 µm	**-8.8**	**0.2**	**25.7**	**-1.63**	**32.30**	**25.98**	**14**	78.833	-4.577	08.07.12	27/130/14	This study
1	KW	Knee Water @ Fram Strait	0.45 µm	-9.6	0.2	23.6	-1.74	33.96	27.33	152	78.833	-5.684	08.07.12	27/126/150	This study
2	KW	Knee Water @ Fram Strait	0.45 µm	-9.6	0.2	22.0	-1.73	33.97	27.34	76	78.833	-4.577	08.07.12	27/130/75	This study
3	KW	Knee Water @ Fram Strait	0.45 µm	-9.7	0.2	21.2	-1.71	34.01	27.37	51	78.833	-3.920	09.07.12	27/132/50	This study
	KW	**Average KW**		**-9.6**		**22.3**	**-1.73**	**33.98**	**27.35**	**93**					
	KW	**1 SD KW**		**0.0**		**1.2**	**0.01**	**0.02**	**0.02**						
1	EGC-77	East Greenland Current Upper Water @ 77 °N	not filtered	-11.5	0.3	17.4	4.60	34.68	27.47	5	76.74	-2.330	22.08.99	SGN 30	Lacan & Jeandel (2004a)
2	EGC-77	East Greenland Current Upper Water @ 77 °N	0.45 µm	-12.2	0.2	15.8	4.56	34.72	27.50	21	76.74	-2.330	22.08.99	SGN 30	Lacan & Jeandel (2004a)
3	EGC-77	East Greenland Current Upper Water @ 77 °N	not filtered	-11.3	0.2	17.7	2.21	34.97	27.93	103	76.74	-2.330	22.08.99	SGN 30	Lacan & Jeandel (2004a)
4	EGC-77	East Greenland Current Upper Water @ 77 °N	0.45 µm	-9.5	0.2		-1.25	33.24	26.74	21	77.03	-3.750	23.08.99	SGN 32	Lacan & Jeandel (2004a)
5	EGC-77	East Greenland Current Upper Water @ 77 °N	not filtered	-11.5	0.2	19.6	-1.25	34.89	26.74	123	77.03	-3.750	23.08.99	SGN 32	Lacan & Jeandel (2004a)
6	EGC-77	East Greenland Current Upper Water @ 77 °N	not filtered	-9.2	0.2	24.7	-0.69	33.16	26.65	20	77.18	-4.390	23.08.99	SGN 33	Lacan & Jeandel (2004a)
7	EGC-77	East Greenland Current Upper Water @ 77 °N	not filtered	-10.3	0.2	23.3	-0.69	33.16	26.65	50	77.18	-4.390	23.08.99	SGN 33	Lacan & Jeandel (2004a)
	EGC-77	**Average EGC-77**		**-10.8**		**19.8**	**1.07**	**34.12**	**27.10**	**49**					
	EGC-77	**1 SD EGC-77**		**1.1**		**3.5**	**2.67**	**0.88**	**0.52**						
1	**EGC-73**	**East Greenland Current Upper Water @ 73 °N**	not filtered	**-10.9**	**0.2**	**22.3**	**-0.94**	**34.33**	**27.61**	**50**	**72.870**	**-16.180**	26.08.99	SGN 46	Lacan & Jeandel (2004a)
1	UW-SWNS	Upper Water @ southern and western Nodic Seas	not filtered	-13.2	0.2	12.7	10.96	35.24	26.97	20	62.750	-9.010	04.08.99	Signature 22	Lacan & Jeandel (2004b)
2	UW-SWNS	Upper Water @ southern and western Nodic Seas	not filtered	-13.2	0.2	17.5	9.19	35.29	27.32	50	62.750	-9.010	04.08.99	Signature 22	Lacan & Jeandel (2004b)
3	UW-SWNS	Upper Water @ southern and western Nodic Seas	not filtered	-13.0	0.2	16.9	10.13	35.34	27.20	51	60.500	-5.000	06.08.99	Signature 23	Lacan & Jeandel (2004b)
4	UW-SWNS	Upper Water @ southern and western Nodic Seas	not filtered	-12.8	0.2	18.3	9.20	35.33	27.35	99	60.500	-5.000	06.08.99	Signature 23	Lacan & Jeandel (2004b)
5	UW-SWNS	Upper Water @ southern and western Nodic Seas	not filtered	-13.2	0.2	15.5	12.23	35.04	26.57	21	64.650	4.180	11.08.99	Signature 25	Lacan & Jeandel (2004b)
6	UW-SWNS	Upper Water @ southern and western Nodic Seas	not filtered	-13.1	0.2	23.8	8.11	35.27	27.47	101	64.650	4.180	11.08.99	Signature 25	Lacan & Jeandel (2004b)
7	UW-SWNS	Upper Water @ southern and western Nodic Seas	not filtered	-12.2	0.2	9.0	8.29	35.19	27.38	43	69.030	7.950	14.08.99	Signature 26	Lacan & Jeandel (2004b)
8	UW-SWNS	Upper Water @ southern and western Nodic Seas	not filtered	-12.1	0.2	20.4	7.27	35.22	27.55	74	69.030	7.950	14.08.99	Signature 26	Lacan & Jeandel (2004b)
	UW-SWNS	**Average UW-SWNS**		**-12.9**		**16.8**	**9.42**	**35.24**	**27.23**	**57**					
	UW-SWNS	**1 SD UW-SWNS**		**0.5**		**4.5**	**1.63**	**0.10**	**0.32**						

Table A2, Chapter I (continued): Composition of upper waters (mostly $\sigma_0 \leq 27.70$; Arctic Ocean: $\theta \leq 0$ °C) - Arctic Mediterranean (all samples)

#	Name / Abbreviation	Full Name	Filtration	εNd	εNd 2SD	[Nd] pmol/kg	pot. T (°C)	Salinity	σ_θ	depth (m)	Latitude	Longitude	Date	Station	Reference
1	UW-DS	Upper Water @ Denmark Strait	not filtered	-10.5	0.2	41.6	3.81	31.40	24.94	5	66.160	-27.520	29.08.99	SGN54	Lacan & Jeandel (2004a)
2	UW-DS	Upper Water @ Denmark Strait	not filtered	-11.2	0.2	101.9	-1.41	33.65	27.07	59	66.160	-27.520	29.08.99	SGN54	Lacan & Jeandel (2004a)
3	UW-DS	Upper Water @ Denmark Strait	not filtered	-11.3	0.2		-1.39	34.19	27.51	120	66.160	-27.520	29.08.99	SGN54	Lacan & Jeandel (2004a)
4	UW-DS	Upper Water @ Denmark Strait	not filtered	-11	0.2	27.7	5.71	33.45	26.36	11	66.080	-27.250	29.08.99	SGN55	Lacan & Jeandel (2004a)
5	UW-DS	Upper Water @ Denmark Strait	not filtered	-11.5	0.4	40.9	2.62	34.39	27.43	51	66.080	-27.250	29.08.99	SGN55	Lacan & Jeandel (2004a)
6	UW-DS	Upper Water @ Denmark Strait	not filtered	-10.4	0.2	29.8	5.16	32.52	25.70	10	66.010	-26.980	29.08.99	SGN56	Lacan & Jeandel (2004a)
7	UW-DS	Upper Water @ Denmark Strait	not filtered	-9.3	0.2	31.9	-0.46	33.30	26.75	54	66.010	-26.980	29.08.99	SGN56	Lacan & Jeandel (2004a)
8	UW-DS	Upper Water @ Denmark Strait	not filtered	-11.5	0.2	20.8	3.58	34.40	27.35	120	66.010	-26.980	29.08.99	SGN56	Lacan & Jeandel (2004a)
	UW-DS	**Average UW-DS**		**-10.9**		**42.1**	**2.20**	**33.41**	**26.64**	**54**					
	UW-DS	**1 SD UW-DS**		**0.7**		**27.4**	**2.90**	**1.03**	**0.92**						
1	**SW-IS**	**Iceland Sea Surface Water**	not filtered	**-8.0**	**0.2**	**14.8**	**7.94**	**34.65**	**27.01**	**20**	66.550	-10.110	03.08.99	Signature 21	Lacan & Jeandel (2004b)
1	PW-NB	Nansen Basin Polar Water II	0.22 µm	-10.9	0.2	17.8	-1.59	33.98	27.35	8	84.281	33.664	18.07.01	Leg II, Station 11	Zimmermann et al. (2009)
2	PW-NB	Nansen Basin Polar Water II	0.22 µm	-11.1	0.4	17.1	-1.58	33.98	27.35	8	84.280	33.660	18.07.01	Leg II Station 11	Andersson et al. (2008)
3	PW-NB	Nansen Basin Polar Water II	0.22 µm	-11.1	0.4	17.6	-1.73	34.31	27.62	40	83.770	31.950	18.07.01	Leg II Station 10	Andersson et al. (2008)
4	PW-NB	Nansen Basin Polar Water II	0.22 µm	-10.1	0.4	17.3	-1.65	34.08	27.43	8	84.730	35.250	19.07.01	Leg II Station 12	Andersson et al. (2008)
	PW-NB	**Average PW-NB**		**-10.8**		**17.5**	**-1.64**	**34.09**	**27.43**	**16**					
	PW-NB	**1 SD PW-NB**		**0.5**		**0.3**	**0.07**	**0.16**	**0.13**						
1	PW-AB	Amundsen Basin Polar Water I	0.22 µm	-11.0	0.2	34.2	-1.58	31.45	25.29	8	88.905	-2.226	02.08.01	Leg V, St Drift 2	Zimmermann et al. (2009)
2	PW-AB	Amundsen Basin Polar Water I	0.22 µm	-10.7	0.4	37.3	-1.66	32.63	26.25	8	88.280	82.910	22.07.01	Leg II Station 20	Porcelli et al. (2009)
3	PW-AB	Amundsen Basin Polar Water I	0.22 µm	-11.0	0.4	34.2	-1.59	31.91	25.66	8	88.410	95.380	22.07.01	Leg II Station 21	Porcelli et al. (2009)
4	PW-AB	Amundsen Basin Polar Water I	0.22 µm	-11.5	0.4	36.7	-	-	-	8	88.430	109.840	23.07.01	Leg II Station 22	Porcelli et al. (2009)
5	PW-AB	Amundsen Basin Polar Water I	0.22 µm	-11.5	0.4	58.0	-1.55	31.35	25.21	10	88.430	109.840	23.07.01	Leg II Station 22	Porcelli et al. (2009)
6	PW-AB	Amundsen Basin Polar Water I	0.22 µm	-9.4	0.4	24.3	-1.57	31.51	25.34	20	88.430	109.840	23.07.01	Leg II Station 22	Porcelli et al. (2009)
7	PW-AB	Amundsen Basin Polar Water I	0.22 µm	-11.2	0.4	50.5	-1.53	31.10	25.01	8	88.370	126.500	23.07.01	Leg II Station 24	Porcelli et al. (2009)
8	PW-AB	Amundsen Basin Polar Water I	0.22 µm	-11.3	0.4	51.0	-1.53	30.85	24.80	8	88.140	132.550	23.07.01	Leg II Station 26	Porcelli et al. (2009)
9	PW-AB	Amundsen Basin Polar Water II	0.22 µm	-8.4	0.3	26.6	-1.81	33.81	27.21	75	88.905	-2.226	02.08.01	Leg V, St Drift 2	Zimmermann et al. (2009)
10	PW-AB	Amundsen Basin Polar Water I	0.22 µm	-9.1	0.4	27.7	-1.81	33.74	27.16	75	88.410	95.380	22.07.01	Leg II Station 21	Porcelli et al. (2009)
11	PW-AB	Amundsen Basin Polar Water I	0.22 µm	-11.7	0.4	53.7	-1.82	33.52	26.98	40	88.430	109.840	23.07.01	Leg II Station 22	Porcelli et al. (2009)
12	PW-AB	Amundsen Basin Polar Water I	0.22 µm	-8.8	0.4	27.3	-1.83	33.66	27.09	60	88.430	109.840	23.07.01	Leg II Station 22	Porcelli et al. (2009)
13	PW-AB	Amundsen Basin Polar Water II	0.22 µm	-10.4	0.4	22.5	-1.58	34.18	27.51	100	88.430	109.840	23.07.01	Leg II Station 22	Porcelli et al. (2009)
14	PW-AB	Amundsen Basin Polar Water I	0.22 µm	-11.3	0.4	48.0	-1.57	30.90	24.84	8	87.700	148.460	28.07.01	Leg II Station 28	Porcelli et al. (2009)
15	PW-AB	Amundsen Basin Polar Water I	0.22 µm	-10.9	0.4	48.8	-1.60	31.07	24.98	8	90.000	0.000	28.07.01	Leg II North Pole	Porcelli et al. (2009)
	PW-AB	**Average PW-AB**		**-10.7**		**38.7**	**-1.65**	**32.26**	**25.95**	**30**					
	PW-AB	**1 SD PW-AB**		**1.1**		**11.9**	**0.12**	**1.26**	**1.03**						
1	PW-MB	Makarov Basin Polar Water I	0.22 µm	-11.1	0.2	46.0	-1.60	31.23	25.11	8	87.916	154.375	26.07.01	Leg II Station Mak	Zimmermann et al. (2009)
2	PW-MB	Makarov Basin Polar Water I	0.22 µm	-10.7	0.4	48.7	-1.60	31.23	25.11	8	87.920	154.380	26.07.01	Leg II Station Makarov	Porcelli et al. (2009)
3	PW-MB	Makarov Basin Polar Water I	0.22 µm	-10.5	0.4	30.6	-1.71	33.62	27.06	75	87.920	154.380	26.07.01	Leg II Station Makarov	Porcelli et al. (2009)
4	PW-MB	Makarov Basin Polar Water I	0.22 µm	-11.9	0.4	48.4	-1.64	31.32	25.19	10	87.920	154.380	26.07.01	Leg II Station Makarov	Porcelli et al. (2009)
5	PW-MB	Makarov Basin Polar Water I	0.22 µm	-10.9	0.4	47.4	-1.64	31.33	25.19	30	87.920	154.380	26.07.01	Leg II Station Makarov	Porcelli et al. (2009)
	PW-MB	**Average PW-MB**		**-11.1**		**44.2**	**-1.64**	**31.75**	**25.53**	**26**					
	PW-MB	**1 SD PW-MB**		**0.5**		**7.7**	**0.04**	**1.05**	**0.85**						

Table A2, Chapter I (continued): Composition of upper waters (mostly $\sigma_0 \leq 27.70$; Arctic Ocean: $\theta \leq 0$ °C) - Arctic Mediterranean (all samples)

#	*Name / Abbreviation*	*Full Name*	*Filtration*	*εNd*	*εNd 2SD*	*[Nd] pmol/kg*	*pot. T (°C)*	*Salinity*	*σ_0*	*depth (m)*	*Latitude*	*Longitude*	*Date*	*Station*	*Reference*
1	PW-CB	Canada Basin Polar Water I	0.22 µm	-8.7	0.4	25.3	-1.22	25.92	20.80	5	72.210	-149.950	24.08.00	Stn 3	Porcelli et al. (2009)
2	PW-CB	Canada Basin Polar Water I	0.22 µm	-8.7	0.4	26.3	-0.98	28.12	22.58	25	72.210	-149.950	24.08.00	Stn 3	Porcelli et al. (2009)
3	PW-CB	Canada Basin Polar Water I	0.22 µm	-7.4	0.4	27.1	-1.19	26.00	20.87	5	73.830	-152.010	26.08.00	Stn 4	Porcelli et al. (2009)
4	PW-CB	Canada Basin Polar Water I	0.22 µm	-6.7	0.4	30.6	-0.69	29.31	23.54	25	73.830	-152.010	26.08.00	Stn 4	Porcelli et al. (2009)
5	PW-CB	Canada Basin Polar Water I	0.22 µm	-8.0	0.4	32.0	-0.44	26.56	21.31	5	72.240	-155.070	28.08.00	Stn 5	Porcelli et al. (2009)
6	PW-CB	Canada Basin Polar Water I	0.22 µm	-6.4	0.4	26.4	-0.07	31.29	25.11	50	-149.950	50.545	24.08.00	Stn 3	Porcelli et al. (2009)
7	PW-CB	Canada Basin Polar Water I	0.22 µm	-7.8	0.4	25.1	-1.14	32.22	25.90	80	-149.950	80.878	24.08.00	Stn 3	Porcelli et al. (2009)
8	PW-CB	Canada Basin Polar Water I	0.22 µm	-6.4	0.4	28.8	-1.27	32.36	26.02	85	-152.010	85.941	26.08.00	Stn 4	Porcelli et al. (2009)
9	PW-CB	Canada Basin Polar Water I	0.45 µm	-4.8	0.2	43.6	-1.64	33.39	26.87	125	206.007	126.383	22.08.00	Station 2	Zimmermann et al. (2009)
10	PW-CB	Canada Basin Polar Water I	0.45 µm	-6.6	0.2	27.8	-0.37	30.71	24.66	35	207.083	35.384	24.08.00	Station 4	Zimmermann et al. (2009)
11	PW-CB	Canada Basin Polar Water I	0.45 µm	-6.1	0.2	22.6	-1.54	32.86	26.43	125	204.900	126.392	26.08.00	Station 5	Zimmermann et al. (2009)
12	PW-CB	Canada Basin Polar Water I	0.45 µm	-6.8	0.2	42.1	-0.89	27.46	22.04	5	71.835	206.007	22.08.00	Station 2	Zimmermann et al. (2009)
13	PW-CB	Canada Basin Polar Water I	0.45 µm	-7.7	0.2	27.7	-0.44	26.56	21.31	5	73.250	204.900	26.08.00	Station 5	Zimmermann et al. (2009)
	PW-CB	**Average PW-CB**		**-6.9**		**29.6**	**-0.91**	**29.44**	**23.65**	**44**					
	PW-CB	**1 SD PW-CB**		**1.1**		**6.3**	**0.48**	**2.81**	**2.28**						

Table A2, Chapter I (continued): Composition of Atlantic layer waters (θ > 0 °C; Arctic Ocean AW and AAW: 27.70 < σθ ≤ 27.97) - Arctic Mediterranean (all samples)

#	Name / Abbreviation	Full Name	Filtration	εNd	εNd 2SD	[Nd] pmol/kg	pot. T (°C)	Salinity	σ_θ	$\sigma_{0.5}$	depth (m)	Latitude	Longitude	Date	Station	Reference
1	AW-ISR	Atlantic Water @ Iceland-Scotland Ridge	not filtered	-13.2	0.2	12.7	10.96	35.24	26.97	29.199	20	62.750	-9.010	04.08.99	Signature 22	Lacan & Jeandel (2004b)
2	AW-ISR	Atlantic Water @ Iceland-Scotland Ridge	not filtered	-13.2	0.2	17.5	9.19	35.29	27.31	29.562	50	62.750	-9.010	04.08.99	Signature 22	Lacan & Jeandel (2004b)
3	AW-ISR	Atlantic Water @ Iceland-Scotland Ridge	not filtered	-13.8	0.2	17.7	8.18	35.26	27.45	29.710	200	62.750	-9.010	04.08.99	Signature 22	Lacan & Jeandel (2004b)
4	AW-ISR	Atlantic Water @ Iceland-Scotland Ridge	not filtered	-11.9	0.2	13.9	7.41	35.21	27.53	29.794	411	62.750	-9.010	04.08.99	Signature 22	Lacan & Jeandel (2004b)
5	AW-ISR	Atlantic Water @ Iceland-Scotland Ridge	not filtered	-13.0	0.2	16.9	10.13	35.34	27.20	29.432	51	60.500	-5.000	06.08.99	Signature 23	Lacan & Jeandel (2004b)
6	AW-ISR	Atlantic Water @ Iceland-Scotland Ridge	not filtered	-12.8	0.2	18.3	9.20	35.33	27.34	29.592	99	60.500	-5.000	06.08.99	Signature 23	Lacan & Jeandel (2004b)
7	AW-ISR	Atlantic Water @ Iceland-Scotland Ridge	not filtered	-12.8	0.2	16.5	7.72	35.24	27.50	29.769	280	60.500	-5.000	06.08.99	Signature 23	Lacan & Jeandel (2004b)
	AW-ISR	**Average AW-ISR**		**-13.0**		**16.2**	**8.97**	**35.27**	**27.33**	**29.580**	**159**					
	AW-ISR	**1 SD AW-ISR**		**0.6**		**2.1**	**1.29**	**0.05**	**0.20**	**0.211**						
1	AW-DS	Atlantic Water @ Denmark Strait	not filtered	-13.2	0.2	18.7	6.80	35.13	27.55	29.818	97	66.080	-27.250	29.08.99	SGN 55	Lacan & Jeandel (2004a)
2	AW-DS	Atlantic Water @ Denmark Strait	not filtered	-12.1	0.2	19.4	6.29	35.06	27.56	29.829	182	66.010	-26.980	29.08.99	SGN 56	Lacan & Jeandel (2004a)
	AW-DS	**Average AW-DS**		**-12.6**		**19.1**	**6.55**	**35.10**	**27.56**	**29.824**	**140**					
	AW-DS	**1 SD AW-DS**		**0.8**		**0.5**	**0.36**	**0.05**	**0.01**	**0.008**						
1	AW-eNWSLB	Atlantic Water @ eastern Norwegian Seas & Lofoten Basin	not filtered	-13.1	0.2	23.8	8.11	35.27	27.47	29.729	101	64.650	4.180	11.08.99	Signature 25	Lacan & Jeandel (2004b)
2	AW-eNWSLB	Atlantic Water @ eastern Norwegian Seas & Lofoten Basin	not filtered	-12.1	0.2	20.4	7.27	35.22	27.55	29.824	74	69.030	7.950	14.08.99	Signature 26	Lacan & Jeandel (2004b)
	AW-eNWSLB	**Average AW-eNWSLB**		**-12.6**		**22.1**	**7.69**	**35.25**	**27.51**	**29.777**	**88**					
	AW-eNWSLB	**1 SD AW-eNWSLB**		**0.7**		**2.5**	**0.59**	**0.04**	**0.06**	**0.067**						
1	AW-wBS	Atlantic Water @ western Barents Sea	0.8-0.2 µm	-12.9	0.2	18.2	4.47	35.02	27.75	30.056	50					Petrova (2015)
2	AW-wBS	Atlantic Water @ western Barents Sea	0.8-0.2 µm	-12.7	0.3	18.0	4.08	35.03	27.80	30.109	150					Petrova (2015)
3	AW-wBS	Atlantic Water @ western Barents Sea	0.8-0.2 µm	-12.1	0.2	16.3	1.90	35.01	27.99	30.327	80					Petrova (2015)
4	AW-wBS	Atlantic Water @ western Barents Sea	0.8-0.2 µm	-12.0	0.2	16.0	1.76	35.03	28.01	30.353	150					Petrova (2015)
5	AW-wBS	Atlantic Water @ western Barents Sea	0.8-0.2 µm	-12.2	0.2	15.1	0.80	35.04	28.09	30.447	275					Petrova (2015)
	AW-wBS	**Average AW-wBS**		**-12.4**		**16.7**	**2.60**	**35.02**	**27.93**	**30.258**	**141**					
	AW-wBS	**1 SD AW-wBS**		**0.4**		**1.3**	**1.59**	**0.01**	**0.15**	**0.168**						
1	**AW-FS11**	**Atlantic Water @ Fram Strait**	0.45 µm, after transp. to lab	**-11.9**	**0.3**	**16.8**	**3.19**	**35.10**	**27.95**	**30.269**	**150**	78.834	7.003	26.06.11	PS78-025	Werner et al. (2014)
1	AW	Atlantic Water @ Fram Strait	0.45 µm	-11.9	0.2	15.8	4.15	35.09	27.84	30.147	50.9	78.834	8.830	Juli 12	27/16/50	This study
2	AW	Atlantic Water @ Fram Strait	0.45 µm	-11.7	0.2	15.2	3.48	35.02	27.86	30.176	101.6	78.834	8.830	Juli 12	27/16/100	This study
3	AW	Atlantic Water @ Fram Strait	0.45 µm	-11.3	0.2	15.1	3.70	35.08	27.88	30.195	152.5	78.834	8.830	Juli 12	27/16/150	This study
4	AW	Atlantic Water @ Fram Strait	0.45 µm	-11.6	0.3	15.3	3.68	35.09	27.89	30.208	196.6	78.834	8.830	Juli 12	27/16/194	This study
5	AW	Atlantic Water @ Fram Strait	0.45 µm	-12.2	0.2	16.3	4.33	35.13	27.86	30.163	20.7	78.833	7.831	Juli 12	27/19/20	This study
6	AW	Atlantic Water @ Fram Strait	0.45 µm	-11.1	0.2	16.1	3.61	35.12	27.92	30.240	101.1	78.833	7.831	Juli 12	27/19/100	This study
7	AW	Atlantic Water @ Fram Strait	0.45 µm	-12.1	0.2	16.6	4.54	35.12	27.83	30.130	15.8	78.833	6.835	Juli 12	27/26/18	This study
8	AW	Atlantic Water @ Fram Strait	0.45 µm	-11.7	0.3	16.1	3.37	35.10	27.93	30.253	202.5	78.833	6.835	Juli 12	27/26/200	This study
9	AW	Atlantic Water @ Fram Strait	0.45 µm	-11.7	0.2	15.9	4.34	35.11	27.83	30.141	20.4	78.833	5.353	Juli 12	27/50/20	This study
10	AW	Atlantic Water @ Fram Strait	0.45 µm	-12.0	0.3	16.0	3.07	35.07	27.93	30.258	202.7	78.832	3.664	Juli 12	27/55/200	This study
11	AW	Atlantic Water @ Fram Strait	0.45 µm	-11.2	0.3	15.9	3.57	35.10	27.91	30.223	101.7	78.835	1.295	Juli 12	27/68/100	This study
	AW	**Average AW**		**-11.7**		**15.9**	**3.80**	**35.09**	**27.88**	**30.194**	**106**					
	AW	**1 SD AW**		**0.4**		**0.5**	**0.47**	**0.03**	**0.04**	**0.046**						

Table A2, Chapter I (continued): Composition of Atlantic layer waters (θ > 0 °C; Arctic Ocean AW and AAW: 27.70 < σθ ≤ 27.97) - Arctic Mediterranean (all samples)

#	*Name / Abbreviation*	*Full Name*	*Filtration*	*εNd*	*εNd 2SD*	*[Nd] pmol/kg*	*pot. T (°C)*	*Salinity*	σ_0	$\sigma_{0,5}$	*depth (m)*	*Latitude*	*Longitude*	*Date*	*Station*	*Reference*
1	AW-northS	Atlantic Water @ north of Svalbard	0.22 µm	-11.9	0.4	16.7	2.37	34.86	27.81	30.131	80	81.280	26.380	17.07.01	Leg II Station 1	Andersson et al. (2008)
2	AW-northS	Atlantic Water @ north of Svalbard	0.22 µm	-12.2	0.4	16.7	2.63	34.95	27.88	30.209	150	81.280	26.380	17.07.01	Leg II Station 1	Andersson et al. (2008)
3	AW-northS	Atlantic Water @ north of Svalbard	0.22 µm	-11.2	0.4	16.4	2.20	34.96	27.92	30.259	300	81.280	26.380	17.07.01	Leg II Station 1	Andersson et al. (2008)
	AW-northS	**Average AW-northS**		**-11.8**		**16.6**	**2.40**	**34.92**	**27.87**	**30.200**	**177**					
	AW-northS	**1 SD AW-northS**		**0.5**		**0.2**	**0.22**	**0.06**	**0.06**	**0.065**						
1	RAW	Recirculating Atlantic Water @ Fram Strait	0.45 µm	-11.7	0.3	16.2	3.14	34.98	27.85	30.177	81	78.838	-1.894	01.07.12	27/86/80	This study
2	RAW	Recirculating Atlantic Water @ Fram Strait	0.45 µm	-11.6	0.3	16.4	2.79	35.02	27.92	30.249	202	78.838	-1.894	01.07.12	27/86/200	This study
3	RAW	Recirculating Atlantic Water @ Fram Strait	0.45 µm	-11.6	0.3	16.2	2.35	35.04	27.97	30.306	405	78.838	-1.894	01.07.12	27/86/400	This study
	RAW	**Average RAW**		**-11.6**		**16.3**	**2.76**	**35.01**	**27.92**	**30.244**	**229**					
	RAW	**1 SD RAW**		**0.1**		**0.1**	**0.40**	**0.03**	**0.06**	**0.065**						
1	**AAW-LS**	**Arctic Atlantic Water @ Laptev Sea margin**	0.8-0.2 µm	**-10.0**	**0.1**	**16.4**	**1.15**	**34.85**	**27.92**	**30.269**	**200**	125.909	77.501	20.09.14	VB14-17-1-5	This study
1	AAW-NB	Arctic Atlantic Water @ Nansen Basin	0.22 µm	-11	0.4	16.1	1.98	34.93	27.92	30.256	300	83.770	31.950	18.07.01	Leg II Station 10	Andersson et al. (2008)
2	AAW-NB	Arctic Atlantic Water @ Nansen Basin	0.22 µm	-10.9	0.4	16.1	1.15	34.92	27.97	30.322	500	83.770	31.950	18.07.01	Leg II Station 10	Andersson et al. (2008)
3	AAW-NB	Arctic Atlantic Water @ Nansen Basin	0.22 µm	-11.6	0.2	16.1	1.94	34.93	27.92	30.260	300	83.782	31.952	18.07.01	Leg II, Station 10	Zimmermann et al. (2009)
	AAW-NB	**Average AAW-NB**		**-11.2**		**16.1**	**1.69**	**34.93**	**27.94**	**30.279**	**367**					
	AAW-NB	**1 SD AAW-NB**		**0.4**		**0.0**	**0.47**	**0.01**	**0.03**	**0.037**						
1	AAW-AB	Arctic Atlantic Water @ Amundsen Basin	0.22 µm	-11	0.4	17.3	1.31	34.87	27.92	30.269	300	88.410	95.380	22.07.01	Leg II Station 21	Porcelli et al. (2009)
2	AAW-AB	Arctic Atlantic Water @ Amundsen Basin	0.22 µm	-11.6	0.4	16	0.53	34.87	27.97	30.331	500	88.410	95.380	22.07.01	Leg II Station 21	Porcelli et al. (2009)
3	AAW-AB	Arctic Atlantic Water @ Amundsen Basin	0.22 µm	-10.5	0.3	17.3	1.45	34.87	27.91	30.256	300	88.905	-2.226	02.08.01	Leg V, St Drift 2	Zimmermann et al. (2009)
	AAW-AB	**Average AAW-AB**		**-11.0**		**16.9**	**1.10**	**34.87**	**27.93**	**30.285**	**367**					
	AAW-AB	**1 SD AAW-AB**		**0.6**		**0.8**	**0.50**	**0.00**	**0.03**	**0.040**						
1	AAW-MB	Arctic Atlantic Water @ Makarov Basin	0.22 µm	-10.3	0.2	16.9	0.92	34.84	27.92	30.277	300	87.916	154.375	26.07.01	Leg II Station Mak	Porcelli et al. (2009)
2	AAW-MB	Arctic Atlantic Water @ Makarov Basin	0.22 µm	-10.9	0.4	16.3	0.49	34.87	27.97	30.334	500	87.920	154.380	26.07.01	Leg II Station Makarov	Zimmermann et al. (2009)
	AAW-MB	**Average AAW-MB**		**-10.6**		**16.6**	**0.71**	**34.86**	**27.95**	**30.306**	**400**					
	AAW-MB	**1 SD AAW-NB**		**0.4**		**0.4**	**0.30**	**0.02**	**0.04**	**0.041**						
1	AAW-CB	Arctic Atlantic Water @ Canada Basin	0.22 µm	-9.6	0.4	19.3	0.50	34.79	27.91	30.269	400	72.210	-149.950	24.08.00	Stn 3	Porcelli et al. (2009)
2	AAW-CB	Arctic Atlantic Water @ Canada Basin	0.22 µm	-9.1	0.4	16.1	0.48	34.83	27.94	30.303	500	73.830	-152.010	26.08.00	Stn 4	Porcelli et al. (2009)
3	AAW-CB	Arctic Atlantic Water @ Canada Basin	0.22 µm	-9.1	0.4	20.5	0.75	34.82	27.92	30.274	400	72.240	-155.070	28.08.00	Stn 5	Porcelli et al. (2009)
	AAW-CB	**Average AAW-CB**		**-9.3**		**18.6**	**0.58**	**34.81**	**27.92**	**30.282**	**433**					
	AAW-CB	**1 SD AAW-CB**		**0.3**		**2.3**	**0.15**	**0.02**	**0.02**	**0.018**						
1	dAAW	Dense Arctic Atlantic Water @ Fram Strait	0.45 µm	-10.7	0.3	15.9	0.29	34.95	28.05	30.41	811	78.838	-1.894	01.07.12	27/86/800	This study
2	dAAW	Dense Arctic Atlantic Water @ Fram Strait	0.45 µm	-10.4	0.2	16.1	0.74	34.91	27.99	30.35	608	78.833	-4.577	08.07.12	27/130/600	This study
3	dAAW	Dense Arctic Atlantic Water @ Fram Strait	0.45 µm	-10.3	0.2	18.2	0.80	34.88	27.96	30.32	405	78.833	-3.920	09.07.12	27/132/400	This study
4	dAAW	Dense Arctic Atlantic Water @ Fram Strait	0.45 µm	-10.1	0.2	15.5	0.22	34.87	27.99	30.36	608	78.833	-3.920	09.07.12	27/132/600	This study
5	dAAW	Dense Arctic Atlantic Water @ Fram Strait	0.45 µm	-10.4	0.2	15.9	0.20	34.93	28.04	30.41	913	78.837	-3.309	09.07.12	27/134/900	This study
	dAAW	**Average dAAW**		**-10.4**		**16.3**	**0.45**	**34.91**	**28.01**	**30.368**	**669**					
	dAAW	**1 SD dAAW**		**0.2**		**1.1**	**0.29**	**0.03**	**0.04**	**0.039**						

Table A2, Chapter I (continued): Composition of intermediate waters (27.97 < σθ, σ0.5 ≤ 30.444; Arctic Ocean: θ ≤ 0 °C) - Arctic Mediterranean (all samples)

#	Name / Abbreviation	Full Name	Filtration	εNd	εNd 2SD	[Nd] pmol/kg	pot. T (°C)	Salinity	σ_0	$\sigma_{0.5}$	$\sigma_{1.5}$	depth (m)	Latitude	Longitude	Date	Station	Reference
1	AIW-GS	Greenland Sea Arctic Intermediate Water - DSOW precursor	not filtered	-11.2	0.2	16.9	0.00	34.89	28.02	30.385	35.042	505	76.740	-2.330	22.08.99	SGN 30	Lacan & Jeandel (2004a)
2	AIW-GS	Greenland Sea Arctic Intermediate Water - DSOW precursor	not filtered	-10.7	0.2	17.1	0.61	34.88	27.97	30.333	34.972	608	77.030	-3.750	23.08.99	SGN 32	Lacan & Jeandel (2004a)
3	AIW-GS	Greenland Sea Arctic Intermediate Water - DSOW precursor	not filtered	-10.9	0.2	16.3	-0.54	34.88	28.04	30.413	35.085	707	72.910	-12.970	25.08.99	SGN 42	Lacan & Jeandel (2004a)
4	AIW-GS	Greenland Sea Arctic Intermediate Water - DSOW precursor	not filtered	-10.6	0.2	16.7	-0.46	34.89	28.04	30.416	35.085	900	72.870	-16.180	26.08.99	SGN 46	Lacan & Jeandel (2004a)
5	AIW-GS	Greenland Sea Arctic Intermediate Water - DSOW precursor	not filtered	-11.1	0.2	16.5	-0.05	34.88	28.01	30.381	35.038	431	70.000	-17.010	26.08.99	SGN 48	Lacan & Jeandel (2004a)
6	AIW-GS	Greenland Sea Arctic Intermediate Water - DSOW precursor	not filtered	-10.8	0.2	16.6	-0.42	34.89	28.04	30.413	35.082	698	70.000	-17.010	26.08.99	SGN 48	Lacan & Jeandel (2004a)
7	AIW-GS	Greenland Sea Arctic Intermediate Water - DSOW precursor	not filtered	-10.6	0.2	16.7	-0.35	34.89	28.04	30.409	35.075	573	70.000	-18.000	27.08.99	SGN 50	Lacan & Jeandel (2004a)
8	AIW-GS	Greenland Sea Arctic Intermediate Water - DSOW precursor	not filtered	-10.7	0.2	17.3	-0.67	34.90	28.06	30.437	35.112	1007	70.000	-18.000	27.08.99	SGN 50	Lacan & Jeandel (2004a)
	AIW-GS	**Average AIW-GS**		**-10.8**		**16.8**	**-0.24**	**34.89**	**28.03**	**30.398**	**35.061**	**679**					
	AIW-GS	**1 SD AIW-GS**		**0.2**		**0.3**	**0.41**	**0.01**	**0.03**	**0.032**	**0.044**						
1	**AIW-IS**	**Iceland Sea Arctic Intermediate Water**	not filtered	**-8.4**	**0.2**	**19.9**	**0.22**	**34.86**	**27.98**	**30.346**	**34.996**	**331**	69.210	-6.850	02.08.99	Signature 20	Lacan & Jeandel (2004b)
1	**AIW-NWS**	**Norwegian Sea Arctic Intermediate Water**	not filtered	**-8.1**	**0.2**	**20.0**	**0.33**	**34.88**	**27.99**	**30.354**	**35.001**	**599**	60.500	-5.000	06.08.99	Signature 23	Lacan & Jeandel (2004b)
1	AIW-eNWSLB	eastern Norwegian Sea & Lofoten Basin Arctic Intermediate '	not filtered	-10.1	0.2	17.5	-0.24	34.89	28.03	30.402	35.065	600	64.650	4.180	11.08.99	Signature 25	Lacan & Jeandel (2004b)
2	AIW-eNWSLB	eastern Norwegian Sea & Lofoten Basin Arctic Intermediate '	not filtered	-9.9	0.2	16.1	-0.21	34.88	28.02	30.392	35.054	1001	69.030	7.950	14.08.99	Signature 26	Lacan & Jeandel (2004b)
	AIW-eNWSLB	**Average AIW-eNWSLB**		**-10.0**		**16.8**	**-0.23**	**34.89**	**28.03**	**30.397**	**35.059**	**801**					
	AIW-eNWSLB	**1 SD AIW-eNWSLB**		**0.1**		**1.0**	**0.02**	**0.01**	**0.01**	**0.007**	**0.008**						
1	AIW	Arctic Intermediate Water @ Fram Strait	0.45 µm	-10.4	0.2	15.5	-0.55	34.90	28.06	30.433	35.105	709	78.833	6.835	21.06.12	27/26/700	This study
2	AIW	Arctic Intermediate Water @ Fram Strait	0.45 µm	-10.2	0.2	15.5	-0.46	34.91	28.06	30.430	35.100	810	78.833	5.353	24.06.12	27/50/800	This study
3	AIW	Arctic Intermediate Water @ Fram Strait	0.45 µm	-9.9	0.3	15.4	-0.41	34.91	28.05	30.428	35.096	1014	78.832	3.664	25.06.12	27/55/1000	This study
4	AIW	Arctic Intermediate Water @ Fram Strait	0.45 µm	-10.1	0.3	15.6	-0.61	34.91	28.06	30.439	35.113	1420	78.838	-1.894	01.07.12	27/86/1400	This study
	AIW	**Average AIW**		**-10.1**		**15.5**	**-0.51**	**34.91**	**28.06**	**30.433**	**35.103**	**988**					
	AIW	**1 SD AIW**		**0.2**		**0.1**	**0.09**	**0.00**	**0.00**	**0.005**	**0.007**						
1	UPDW-NB	Nansen Basin Upper Polar Deep Water	0.22 µm	-10.8	0.4	18.2	-0.25	34.91	28.05	30.418	35.082	1000	84.280	33.660	18.07.01	Leg II Station 11	Andersson et al. (2008)
2	UPDW-NB	Nansen Basin Upper Polar Deep Water	0.22 µm	-10.7	0.4	14.1	-0.25	34.91	28.05	30.418	35.082	1000	83.782	31.952	18.07.01	Leg II, Station 10	Zimmermann et al. (2009)
	UPDW-NB	**Average UPDW-NB**		**-10.8**		**16.2**	**-0.25**	**34.91**	**28.05**	**30.418**	**35.082**	**1000**					
	UPDW-NB	**1 SD UPDW-NB**		**0.1**		**2.9**	**0.00**	**0.00**	**0.00**	**0.000**	**0.000**						
1	**UPDW-AB**	**Amundsen Basin Upper Polar Deep Water**	0.22 µm	**-10.8**	**0.2**	**16.3**	**-0.23**	**34.89**	**28.03**	**30.401**	**35.064**	**1000**	88.905	-2.226	02.08.01	Leg V, Stn Drift 2	Zimmermann et al. (2009)
1	**UPDW-MB**	**Makarov Basin Upper Polar Deep Water**	0.22 µm	**-10.5**	**0.4**	**15.3**	**-0.18**	**34.89**	**28.03**	**30.398**	**35.059**	**1000**	87.920	154.380	26.07.01	Leg II Station Makarov	Porcelli et al. (2009)
1	**UPDW-CB**	**Canada Basin Upper Polar Deep Water**	0.22 µm	**-10.7**	**0.4**	**15.5**	**-0.03**	**34.88**	**28.01**	**30.379**	**35.036**	**1000**	72.210	-149.950	24.08.00	Stn 3	Porcelli et al. (2009)

Table A2, Chapter I (continued): Composition of intermediate waters (27.97 < σθ, σ0.5 ≤ 30.444; Arctic Ocean: θ ≤ 0 °C) - Arctic Mediterranean (all samples)

#	*Name / Abbreviation*	*Full Name*	*Filtration*	*εNd*	*εNd 2SD*	*[Nd] pmol/kg*	*pot. T (°C)*	*Salinity*	σ_0	$\sigma_{0.5}$	$\sigma_{1.5}$	*depth (m)*	*Latitude*	*Longitude*	*Date*	*Station*	*Reference*
1	pISOW	pure Iceland-Scotland Overflow Water	not filtered	-8.1	0.2	20.0	0.33	34.88	27.99	30.354	35.001	599	60.500	-5.000	06.08.99	Signature 23	Lacan & Jeandel (2004b)
2	pISOW	pure Iceland-Scotland Overflow Water	not filtered	-9.1	0.2	19.9	-0.60	34.89	28.05	30.424	35.098	800	60.500	-5.000	06.08.99	Signature 23	Lacan & Jeandel (2004b)
3	pISOW	pure Iceland-Scotland Overflow Water	not filtered	-7.3	0.2	24.6	-0.77	34.90	28.06	30.442	35.121	988	60.500	-5.000	06.08.99	Signature 23	Lacan & Jeandel (2004b)
	pISOW	**Average pISOW**		**-8.1**		**21.5**	**-0.35**	**34.89**	**28.03**	**30.407**	**35.073**	**796**					
	pISOW	**1 SD pISOW**		**0.9**		**2.7**	**0.59**	**0.01**	**0.04**	**0.047**	**0.064**						
1	pDSOW	pure Denmark Strait Overflow Water	not filtered	-9.2	0.3	23.1	-0.04	34.87	28.00	30.372	35.030	479	66.160	-27.520	29.08.99	SGN 54	Lacan & Jeandel (2004a)
2	pDSOW	pure Denmark Strait Overflow Water	not filtered	-7.2	0.2	19.6	-0.03	34.87	28.00	30.371	35.029	442	66.160	-27.520	29.08.99	SGN 54	Lacan & Jeandel (2004a)
3	pDSOW	pure Denmark Strait Overflow Water	ım ([Nd] = unfi	-8.3	0.2	17.1	-0.12	34.88	28.02	30.386	35.045	610	66.080	-27.250	29.08.99	SGN 55	Lacan & Jeandel (2004a)
4	pDSOW	pure Denmark Strait Overflow Water	not filtered	-7.3	0.2	28.6	-0.51	34.90	28.05	30.427	35.098	523	66.010	-26.980	29.08.99	SGN 56	Lacan & Jeandel (2004a)
	pDSOW	**Average pDSOW**		**-8.0**		**22.1**	**-0.18**	**34.88**	**28.02**	**30.389**	**35.050**	**514**					
	pDSOW	**1 SD pDSOW**		**0.9**		**5.0**	**0.23**	**0.01**	**0.02**	**0.026**	**0.033**						

Table A2, Chapter I (continued): Composition of deep waters (30.444 < σ0.5; Nordic Seas: S ≤ 34.915; Arctic Ocean: 34.915 < S) - Arctic Mediterranean (all samples)

#	Name / Abbreviation	Full Name	Filtration	εNd	εNd 2SD	[Nd] pmol/kg	pot. T (°C)	Salinity	$\sigma_{0.5}$	$\sigma_{1.5}$	$\sigma_{2.5}$	depth (m)	Latitude	Longitude	Date	Station	Reference
1	DW-GS	Greenland Sea Deep Water	not filtered	-10.1	0.3	16.7	-0.9	34.90	30.447	35.128	39.704	1513	77.670	7.690	22.08.99	Signature 29	Lacan & Jeandel (2004b)
2	DW-GS	Greenland Sea Deep Water	not filtered	-10.5	0.2	18.9	-1.0	34.91	30.463	35.149	39.728	3360	77.670	7.690	22.08.99	Signature 29	Lacan & Jeandel (2004b)
4	DW-GS	Greenland Sea Deep Water	not filtered	-10.8	0.2	17.9	-1.1	34.90	30.459	35.147	39.728	2512	76.740	-2.330	22.08.99	Signature 30	Lacan & Jeandel (2004b)
5	DW-GS	Greenland Sea Deep Water	not filtered	-10.2	0.3	21.8	-1.1	34.90	30.462	35.152	39.735	2635	72.910	-12.970	25.08.99	Signature 42	Lacan & Jeandel (2004b)
6	DW-GS	Greenland Sea Deep Water	not filtered	-10.5	0.2	21.6	-0.8	34.91	30.455	35.136	39.711	1521	72.910	-15.850	25.08.99	Signature 45	Lacan & Jeandel (2004b)
	DW-GS	**Average DW-GS**		**-10.4**		**19.4**	**-0.97**	**34.90**	**30.457**	**35.142**	**39.721**	**2308**					
	DW-GS	**1 SD DW-GS**		**0.3**		**2.3**	**0.12**	**0.01**	**0.007**	**0.010**	**0.013**						
1	DW-NWS	Norwegian Sea Deep Water	not filtered	-9.8	0.2	18.7	-1.02	34.90	30.457	35.143	39.724	2491	69.210	-6.850	02.08.99	Signature 20	Lacan & Jeandel (2004b)
2	DW-NWS	Norwegian Sea Deep Water	not filtered	-7.9	0.2	20.5	-0.87	34.90	30.448	35.130	39.706	1431	66.550	-10.110	03.08.99	Signature 21	Lacan & Jeandel (2004b)
3	DW-NWS	Norwegian Sea Deep Water	not filtered	-7.3	0.2	24.6	-0.77	34.90	30.444	35.122	39.695	988	60.500	-5.000	06.08.99	Signature 23	Lacan & Jeandel (2004b)
	DW-NWS	**Average DW-NWS**		**-8.2**		**21.3**	**-0.89**	**34.90**	**30.450**	**35.132**	**39.708**	**1637**					
	DW-NWS	**1 SD DW-NWS**		**1.3**		**3.0**	**0.13**	**0.00**	**0.007**	**0.011**	**0.014**						
1	DW-eNWSLB	eastern Norwegian Sea & Lofoten Basin Deep Water	not filtered	-9.1	0.2	22.8	-0.96	34.90	30.453	35.138	39.717	1385	64.650	4.180	11.08.99	Signature 25	Lacan & Jeandel (2004b)
2	DW-eNWSLB	eastern Norwegian Sea & Lofoten Basin Deep Water	not filtered	-10.3	0.2	17.2	-0.82	34.90	30.445	35.126	39.700	1700	69.030	7.950	14.08.99	Signature 26	Lacan & Jeandel (2004b)
3	DW-eNWSLB	eastern Norwegian Sea & Lofoten Basin Deep Water	not filtered	-9.8	0.2	27.3	-1.01	34.90	30.456	35.142	39.722	2972	69.030	7.950	14.08.99	Signature 26	Lacan & Jeandel (2004b)
	DW-eNWSLB	**Average DW-eNWSLB**		**-9.7**		**22.4**	**-0.93**	**34.90**	**30.452**	**35.135**	**39.713**	**2019**					
	DW-eNWSLB	**1 SD DW-eNWSLB**		**0.6**		**5.1**	**0.10**	**0.00**	**0.006**	**0.009**	**0.011**						
1	NDW	Nordic Seas Deep Water @ Fram Strait	0.45 µm	-9.9	0.3	16.71	-0.69	34.91	30.444	35.121	39.691	709	78.833	7.831	20.06.12	27/19/700	This study
2	NDW	Nordic Seas Deep Water @ Fram Strait	0.45 µm	-9.8	0.2	15.35	-0.90	34.91	30.458	35.141	39.717	1014	78.833	7.831	20.06.12	27/19/1000	This study
3	NDW	Nordic Seas Deep Water @ Fram Strait	0.45 µm	-10.2	0.2	16.18	-0.90	34.91	30.459	35.142	39.719	1531	78.833	6.835	21.06.12	27/26/1509	This study
	NDW	**Average NDW**		**-10.0**		**16.1**	**-0.83**	**34.91**	**30.454**	**35.134**	**39.709**	**1085**					
	NDW	**1 SD NDW**		**0.2**		**0.7**	**0.12**	**0.00**	**0.008**	**0.012**	**0.016**						
1	DW-NB	Nansen Basin Deep Water	0.22 µm	-10.9	0.4	17.1	-0.79	34.93	30.468	35.147	39.720	2500	84.280	33.660	18.07.01	Leg II Station 11	Andersson et al. (2008)
2	DW-NB	Nansen Basin Deep Water	0.22 µm	-11.0	0.4	17.0	-0.70	34.94	30.471	35.147	39.718	3700	84.280	33.660	18.07.01	Leg II Station 11	Andersson et al. (2008)
	DW-NB	**Average NBDW**		**-10.9**		**17.1**	**-0.75**	**34.94**	**30.469**	**35.147**	**39.719**	**3100**					
	DW-NB	**1 SD NBDW**		**0.1**		**0.1**	**0.06**	**0.01**	**0.002**	**0.000**	**0.002**						
1	DW-AB	Amundsen Basin Deep Water	0.22 µm	-12.3	0.4	18.2	-0.95	34.93	30.477	35.161	39.739	3900	88.410	95.380	22.07.01	Leg II Station 21	Porcelli et al. (2009)
2	DW-AB	Amundsen Basin Deep Water	0.22 µm	-10.6	0.2	18.2	-0.95	34.94	30.485	35.169	39.747	3000	88.279	-4.839	16.08.01	Leg V, St Drift 8	Zimmermann et al. (2009)
	DW-AB	**Average ABDW**		**-11.5**		**18.2**	**-0.95**	**34.94**	**30.481**	**35.165**	**39.743**	**3450**					
	DW-AB	**1 SD ABDW**		**1.2**		**0.0**	**0.00**	**0.01**	**0.006**	**0.006**	**0.006**						

Table A2, Chapter I (continued): Composition of deep waters (30.444 < σ0.5; Nordic Seas: S ≤ 34.915; Arctic Ocean: 34.915 < S) - Arctic Mediterranean (all samples)

#	Name / Abbreviation	Full Name	Filtration	εNd	εNd 2SD	[Nd] pmol/kg	pot. T (°C)	Salinity	$\sigma_{0.5}$	$\sigma_{1.5}$	$\sigma_{2.5}$	depth (m)	Latitude	Longitude	Date	Station	Reference
1	DW-MB	Makarov Basin Deep Water	0.22 µm	-10.5	0.4	15.9	-0.52	34.95	30.468	35.139	39.704	2500	87.920	154.380	26.07.01	Leg II Station Makarov	Porcelli et al. (2009)
2	DW-MB	Makarov Basin Deep Water	0.22 µm	-10.7	0.4	17.0	-0.54	34.96	30.477	35.148	39.714	3500	87.920	154.380	26.07.01	Leg II Station Makarov	Porcelli et al. (2009)
	DW-MB	**Average MBDW**		**-10.6**		**16.5**	**-0.53**	**34.96**	**30.472**	**35.144**	**39.709**	**3000**					
	DW-MB	**1 SD MBDW**		**0.1**		**0.8**	**0.01**	**0.01**	**0.007**	**0.007**	**0.007**						
1	DW-CB	Canada Basin Deep Water	0.22 µm	-11.0	0.4	17.1	-0.51	34.96	30.475	35.146	39.711	3000	72.210	-149.950	24.08.00	Stn 3	Porcelli et al. (2009)
2	DW-CB	Canada Basin Deep Water	0.22 µm	-9.0	0.4	21.6	-0.52	34.95	30.468	35.139	39.704	2500	73.830	-152.010	26.08.00	Stn 4	Porcelli et al. (2009)
	DW-CB	**Average CBDW**		**-9.9**		**19.4**	**-0.52**	**34.96**	**30.471**	**35.142**	**39.707**	**2750**					
	DW-CB	**1 SD CBDW**		**1.4**		**3.2**	**0.01**	**0.01**	**0.005**	**0.005**	**0.005**						
1	EBDW/GSDW	Eurasian Basin / Greenland Sea Deep Water @ Fram S	0.45 µm	-10.6	0.29	15.7	-0.87	34.92	30.461	35.143	39.719	2031	78.833	5.353	24.06.12	27/50/2000	This study
2	EBDW/GSDW	Eurasian Basin / Greenland Sea Deep Water @ Fram S	0.45 µm	-10.2	0.15	15.9	-0.89	34.93	30.470	35.152	39.728	2568	78.833	5.353	24.06.12	27/50/2525	This study
3	EBDW/GSDW	Eurasian Basin / Greenland Sea Deep Water @ Fram S	0.45 µm	-10.5	0.29	15.6	-0.89	34.92	30.468	35.151	39.727	2241	78.832	3.664	25.06.12	27/55/2205	This study
4	EBDW/GSDW	Eurasian Basin / Greenland Sea Deep Water @ Fram S	0.45 µm	-10.2	0.23	15.7	-0.89	34.92	30.468	35.150	39.726	2450	78.835	1.295	27.06.12	27/68/2410	This study
5	EBDW/GSDW	Eurasian Basin / Greenland Sea Deep Water @ Fram S	0.45 µm	-10.6	0.29	16.4	-0.90	34.92	30.469	35.151	39.728	2668	78.838	-1.894	01.07.12	27/86/2625	This study
6	EBDW/GSDW	Eurasian Basin / Greenland Sea Deep Water @ Fram S	0.45 µm	-10.6	0.22	15.7	-0.88	34.92	30.467	35.150	39.726	2358	78.837	-3.309	09.07.12	27/134/2325	This study
	EBDW/GSDW	**Average EBDW/GSDW**		**-10.5**		**15.8**	**-0.89**	**34.92**	**30.467**	**35.149**	**39.726**	**2386**					
	EBDW/GSDW	**1 SD EBDW/GSDW**		**0.2**		**0.3**	**0.01**	**0.00**	**0.003**	**0.003**	**0.004**						
1	CBDW	Canadian Basin Deep Water @ Fram Strait	0.45 µm	-9.6	0.3	15.3	-0.85	34.92	30.460	35.141	39.716	2028	78.835	1.295	27.06.12	27/68/2000	This study
2	CBDW	Canadian Basin Deep Water @ Fram Strait	0.45 µm	-10.1	0.3	15.5	-0.83	34.92	30.461	35.141	39.716	2235	78.838	-1.894	01.07.12	27/86/2200	This study
3	CBDW	Canadian Basin Deep Water @ Fram Strait	0.45 µm	-10.6	0.2	15.4	-0.71	34.92	30.456	35.133	39.704	1908	78.833	-3.920	09.07.12	27/132/1880	This study
	CBDW	**Average CBDW**		**-10.1**		**15.4**	**-0.79**	**34.92**	**30.459**	**35.138**	**39.712**	**2057**					
	CBDW	**1 SD CBDW**		**0.5**		**0.1**	**0.08**	**0.00**	**0.002**	**0.005**	**0.007**						

(a) normalized to McLennan, S. M. (2001). Relationships between the trace element composition of sedimentary rocks and upper continental crust. Geochemistry, Geophysics, Geosystems, 2(4).
(b) based on repeated measurements of GEOTRACES inter-calibration samples BATS15m from the Bermuda Atlantic Time-Series Study (see electronic supplement D)

References

Andersson, P. S., Porcelli, D., Frank, M., Björk, G., Dahlqvist, R., & Gustafsson, Ö. (2008). Neodymium isotopes in seawater from the Barents Sea and Fram Strait Arctic–Atlantic gateways. Geochimica et Cosmochimica Acta, 72(12), 2854-2867.

Bauch, D., van der Loeff, M. R., Andersen, N., Torres-Valdes, S., Bakker, K., & Abrahamsen, E. P. (2011). Origin of freshwater and polynya water in the Arctic Ocean halocline in summer 2007. Progress in Oceanography, 91(4), 482-495.

Dahlqvist, R., Andersson, P. S., & Porcelli, D. (2007). Nd isotopes in Bering Strait and Chukchi Sea water. Geochim. Cosmochim. Acta, 71, A196.

Lacan, F. (2002). Masses d'eau des Mers Nordiques et de l'Atlantique Subarctique tracées par les isotopes du néodyme (Doctoral dissertation, Université Paul Sabatier-Toulouse III).

Lacan, F., & Jeandel, C. (2004a). Denmark Strait water circulation traced by heterogeneity in neodymium isotopic compositions. Deep Sea Research Part I: Oceanographic Research Papers, 51(1), 71-82.

Lacan, F., & Jeandel, C. (2004b). Neodymium isotopic composition and rare earth element concentrations in the deep and intermediate Nordic Seas: Constraints on the Iceland Scotland Overflow Water signature. Geochemistry, Geophysics, Geosystems, 5(11).

Persson, P.-O., Andersson, P. S., Porcelli, D., & Semiletov, I. (2011). The influence of Lena River water inflow and shelf sediment-sea water exchange for the Nd isotopic composition in the Laptev Sea and Arctic Ocean. Geophysical Research Abstracts Vol. 13, EGU2011-672

Petrova, M. (2015) Neodymium isotopes and rare earth element distribution in the Barents Sea, Arctic Ocean (Master thesis), Saint Petersburg State University / University of Hamburg, Saint Petersburg / Hamburg, 60 pp.

Porcelli, D., Andersson, P. S., Baskaran, M., Frank, M., Björk, G., & Semiletov, I. (2009). The distribution of neodymium isotopes in Arctic Ocean basins. Geochimica et Cosmochimica Acta, 73(9), 2645-2659.

Werner, K., Frank, M., Teschner, C., Müller, J., & Spielhagen, R. F. (2014). Neoglacial change in deep water exchange and increase of sea-ice transport through eastern Fram Strait: evidence from radiogenic isotopes. Quaternary Science Reviews, 92, 190-207.

Zimmermann, B., Porcelli, D., Frank, M., Andersson, P. S., Baskaran, M., Lee, D. C., & Halliday, A. N. (2009). Hafnium isotopes in Arctic Ocean water. Geochimica et Cosmochimica Acta, 73(11), 3218-3233.

Table A3, Chapter I: CTD, Nd isotope and REE data

Nr.	Sample ID	Cruise	Station	Year	Month	Day	Longitude [°E]	Latitude [°N]	Bot. Depth [m]	Depth [m]	Pressure [dB]	Temperature [°C]	Conductivity [mS/cm]
1	27/13/S	ARKXXVII/1	13	2012	6	20	9.330	78.834	199	2.38	2.41	3.33	31.903
2	27/13/30	ARKXXVII/1	13	2012	6	20	9.330	78.834	199	30.91	31.25	2.43	31.017
3	27/13/100	ARKXXVII/1	13	2012	6	20	9.330	78.834	199	101.98	103.13	3.18	31.727
4	27/13/140	ARKXXVII/1	13	2012	6	20	9.330	78.834	199	141.80	143.42	3.23	31.925
5	27/13/180	ARKXXVII/1	13	2012	6	20	9.330	78.834	199	182.45	184.55	3.16	31.897
6	27/16/20	ARKXXVII/1	16	2012	6	20	8.830	78.834	227	20.75	20.98	4.61	33.084
7	27/16/50	ARKXXVII/1	16	2012	6	20	8.830	78.834	227	50.86	51.43	4.16	32.830
8	27/16/100	ARKXXVII/1	16	2012	6	20	8.830	78.834	227	101.59	102.74	3.49	32.258
9	27/16/150	ARKXXVII/1	16	2012	6	20	8.830	78.834	227	152.45	154.20	3.71	32.435
10	27/16/194	ARKXXVII/1	16	2012	6	20	8.830	78.834	227	196.62	198.89	3.69	32.446
11	27/19/20	ARKXXVII/1	19	2012	6	20	7.831	78.833	1055	20.66	20.89	4.33	33.083
12	27/19/100	ARKXXVII/1	19	2012	6	20	7.831	78.833	1055	101.08	102.23	3.61	32.303
13	27/19/300	ARKXXVII/1	19	2012	6	20	7.831	78.833	1055	303.91	307.50	2.13	31.074
14	27/19/700	ARKXXVII/1	19	2012	6	20	7.831	78.833	1055	709.16	718.18	-0.66	28.726
15	27/19/1000	ARKXXVII/1	19	2012	6	20	7.831	78.833	1055	1013.57	1027.17	-0.86	28.695
16	27/26/18	ARKXXVII/1	26	2012	6	21	6.835	78.833	1563	15.82	15.99	4.54	33.912
17	27/26/200	ARKXXVII/1	26	2012	6	21	6.835	78.833	1563	202.54	204.88	3.38	32.160
18	27/26/400	ARKXXVII/1	26	2012	6	21	6.835	78.833	1563	404.77	409.64	1.46	30.399
19	27/26/700	ARKXXVII/1	26	2012	6	21	6.835	78.833	1563	709.23	718.25	-0.52	28.853
20	27/26/1200	ARKXXVII/1	26	2012	6	21	6.835	78.833	1563	1216.27	1233.16	-0.77	28.863
21	27/26/1509	ARKXXVII/1	26	2012	6	21	6.835	78.833	1563	1531.36	1553.75	-0.84	28.941
22	27/50/20	ARKXXVII/1	50	2012	6	24	5.353	78.833	2574	20.35	20.58	4.34	33.008
23	27/50/100	ARKXXVII/1	50	2012	6	24	5.353	78.833	2574	101.44	102.58	2.76	31.674
24	27/50/800	ARKXXVII/1	50	2012	6	24	5.353	78.833	2574	809.83	820.32	-0.42	28.961
25	27/50/2000	ARKXXVII/1	50	2012	6	24	5.353	78.833	2574	2030.92	2062.97	-0.77	29.208
26	27/50/2525	ARKXXVII/1	50	2012	6	24	5.353	78.833	2574	2567.95	2611.68	-0.75	29.458
27	27/55/5	ARKXXVII/1	55	2012	6	25	3.664	78.832	2254	10.07	10.18	0.06	28.223
28	27/55/200	ARKXXVII/1	55	2012	6	25	3.664	78.832	2254	202.74	205.09	3.08	31.817
29	27/55/400	ARKXXVII/1	55	2012	6	25	3.664	78.832	2254	404.85	409.71	1.19	29.884
30	27/55/500	ARKXXVII/1	55	2012	6	25	3.664	78.832	2254	506.76	512.97	1.32	30.377
31	27/55/1000	ARKXXVII/1	55	2012	6	25	3.664	78.832	2254	1014.01	1027.62	-0.37	29.095
32	27/55/2205	ARKXXVII/1	55	2012	6	25	3.664	78.832	2254	2240.67	2277.12	-0.77	29.304
33	27/68/15	ARKXXVII/1	68	2012	6	27	1.295	78.835	2465	15.30	15.47	1.06	32.478
34	27/68/100	ARKXXVII/1	68	2012	6	27	1.295	78.835	2465	101.75	102.90	3.58	32.296
35	27/68/400	ARKXXVII/1	68	2012	6	27	1.295	78.835	2465	404.99	409.86	1.92	30.765
36	27/68/800	ARKXXVII/1	68	2012	6	27	1.295	78.835	2465	809.70	820.19	0.04	29.331
37	27/68/2000	ARKXXVII/1	68	2012	6	27	1.295	78.835	2465	2027.62	2059.59	-0.75	29.231
38	27/68/2410	ARKXXVII/1	68	2012	6	27	1.295	78.835	2465	2450.07	2491.12	-0.76	29.401
39	27/86/20	ARKXXVII/1	86	2012	7	1	-1.894	78.838	2700	20.57	20.79	-1.02	26.486
40	27/86/80	ARKXXVII/1	86	2012	7	1	-1.894	78.838	2700	81.05	81.97	3.15	31.781
41	27/86/200	ARKXXVII/1	86	2012	7	1	-1.894	78.838	2700	202.30	204.63	2.81	31.625
42	27/86/400	ARKXXVII/1	86	2012	7	1	-1.894	78.838	2700	405.02	409.89	2.37	31.348
43	27/86/800	ARKXXVII/1	86	2012	7	1	-1.894	78.838	2700	810.63	821.13	0.33	29.661
44	27/86/1400	ARKXXVII/1	86	2012	7	1	-1.894	78.838	2700	1420.13	1440.53	-0.55	29.137
45	27/86/2200	ARKXXVII/1	86	2012	7	1	-1.894	78.838	2700	2235.40	2271.74	-0.72	29.325
46	27/86/2625	ARKXXVII/1	86	2012	7	1	-1.894	78.838	2700	2668.23	2714.30	-0.75	29.489
47	27/92/S	ARKXXVII/1	92	2012	7	3	-12.004	79.833	154	1.46	1.47	0.28	26.344
48	27/92/30	ARKXXVII/1	92	2012	7	3	-12.004	79.833	154	30.66	31.00	-1.49	25.389
49	27/92/100	ARKXXVII/1	92	2012	7	3	-12.004	79.833	154	101.34	102.49	-1.70	25.340
50	27/92/130	ARKXXVII/1	92	2012	7	3	-12.004	79.833	154	131.50	133.00	-1.49	26.131
51	27/97/10	ARKXXVII/1	97	2012	7	4	-11.484	79.415	244	9.89	10.00	0.30	26.288
52	27/97/50	ARKXXVII/1	97	2012	7	4	-11.484	79.415	244	50.23	50.79	-1.51	25.376
53	27/97/100	ARKXXVII/1	97	2012	7	4	-11.484	79.415	244	101.10	102.25	-1.69	25.423
54	27/97/150	ARKXXVII/1	97	2012	7	4	-11.484	79.415	244	151.49	153.23	-1.06	26.851
55	27/97/220	ARKXXVII/1	97	2012	7	4	-11.484	79.415	244	222.33	224.92	-0.23	28.370
56	27/106/10	ARKXXVII/1	106	2012	7	5	-10.671	78.832	374	10.12	10.23	-0.56	25.372
57	27/106/75	ARKXXVII/1	106	2012	7	5	-10.671	78.832	374	76.52	77.38	-1.63	25.374
58	27/106/150	ARKXXVII/1	106	2012	7	5	-10.671	78.832	374	150.53	152.25	-1.17	26.901
59	27/106/250	ARKXXVII/1	106	2012	7	5	-10.671	78.832	374	252.56	255.50	-0.06	28.635
60	27/106/350	ARKXXVII/1	106	2012	7	5	-10.671	78.832	374	354.07	358.28	0.23	29.035
61	27/110/10	ARKXXVII/1	110	2012	7	5	-10.995	78.499	196	10.52	10.64	-0.76	25.462
62	27/110/35	ARKXXVII/1	110	2012	7	5	-10.995	78.499	196	35.16	35.56	-1.55	25.306
63	27/110/100	ARKXXVII/1	110	2012	7	5	-10.995	78.499	196	100.89	102.03	-1.61	26.081
64	27/110/170	ARKXXVII/1	110	2012	7	5	-10.995	78.499	196	171.73	173.70	-0.51	28.035
65	27/113/15	ARKXXVII/1	113	2012	7	6	-12.456	78.827	249	15.13	15.29	-1.44	24.834
66	27/113/70	ARKXXVII/1	113	2012	7	6	-12.456	78.827	249	71.28	72.08	-1.67	25.344
67	27/113/140	ARKXXVII/1	113	2012	7	6	-12.456	78.827	249	141.79	143.41	-1.52	26.410
68	27/113/220	ARKXXVII/1	113	2012	7	6	-12.456	78.827	249	222.87	225.46	-0.59	27.948
69	27/118/10	ARKXXVII/1	118	2012	7	6	-9.499	78.816	217	10.01	10.12	-0.75	25.297
70	27/118/75	ARKXXVII/1	118	2012	7	6	-9.499	78.816	217	75.25	76.10	-1.69	25.360
71	27/118/125	ARKXXVII/1	118	2012	7	6	-9.499	78.816	217	126.16	127.59	-1.44	26.404
72	27/118/180	ARKXXVII/1	118	2012	7	6	-9.499	78.816	217	181.78	183.87	-0.71	27.905
73	27/121/10	ARKXXVII/1	121	2012	7	7	-7.996	78.833	187	10.54	10.66	-0.63	26.056
74	27/121/50	ARKXXVII/1	121	2012	7	7	-7.996	78.833	187	50.55	51.12	-1.68	25.340
75	27/121/145	ARKXXVII/1	121	2012	7	7	-7.996	78.833	187	146.90	148.58	-0.94	26.775
76	27/124/15	ARKXXVII/1	124	2012	7	8	-6.497	78.838	280	15.35	15.52	-1.48	25.169
77	27/124/90	ARKXXVII/1	124	2012	7	8	-6.497	78.838	280	91.57	92.60	-1.25	27.162
78	27/124/180	ARKXXVII/1	124	2012	7	8	-6.497	78.838	280	182.87	184.98	-0.02	28.875
79	27/124/245	ARKXXVII/1	124	2012	7	8	-6.497	78.838	280	248.26	251.15	1.39	30.361
80	27/126/10	ARKXXVII/1	126	2012	7	8	-5.684	78.833	417	10.29	10.41	-1.64	25.304
81	27/126/150	ARKXXVII/1	126	2012	7	8	-5.684	78.833	417	152.24	153.98	-1.74	27.001
82	27/126/300	ARKXXVII/1	126	2012	7	8	-5.684	78.833	417	303.13	306.70	2.86	31.714
83	27/126/390	ARKXXVII/1	126	2012	7	8	-5.684	78.833	417	394.66	399.40	1.59	30.541
84	27/130/14	ARKXXVII/1	130	2012	7	8	-4.577	78.833	1388	14.09	14.25	-1.63	25.772

Table A3, Chapter I: CTD, Nd isotope and REE data (continued)

Nr.	Salinity [PSU]	Pot. Temp. [°C]	Sigma-theta [kg/m3]	Sigma0.5 [kg/m3]	Sigma1.5 [kg/m3]	Sigma2.5 [kg/m3]	Classification this study	Nd ID [pmol/kg]	Nd ID repeat [pmol/kg]	143/144	Epsilon Nd	143/144 [2sig]	Epsilon Nd [2sig]
1	34.665	3.327	27.587	29.908	34.474	38.936		15.46		0.512094	-10.61	0.000010	0.19
2	34.812	2.427	27.786	30.120	34.708	39.193		14.76		0.512071	-11.06	0.000010	0.19
3	34.973	3.170	27.847	30.170	34.737	39.201		14.87	15.11	0.512043	-11.60	0.000010	0.19
4	34.992	3.219	27.858	30.180	34.746	39.208		14.89		0.512057	-11.34	0.000010	0.19
5	34.999	3.148	27.871	30.193	34.761	39.225		16.01		0.512076	-10.96	0.000010	0.19
6	34.844	4.613	27.596	29.900	34.430	38.859		15.56		0.512037	-11.72	0.000010	0.19
7	35.086	4.153	27.838	30.147	34.688	39.126	AW	15.79	15.84	0.512030	-11.85	0.000010	0.19
8	35.024	3.483	27.858	30.176	34.734	39.190	AW	15.24		0.512036	-11.74	0.000010	0.19
9	35.078	3.698	27.880	30.195	34.747	39.197	AW	15.10	15.14	0.512057	-11.34	0.000010	0.19
10	35.093	3.680	27.893	30.208	34.761	39.211	AW	15.30		0.512045	-11.57	0.000015	0.28
11	35.132	4.326	27.856	30.163	34.699	39.133	AW	16.31		0.512011	-12.24	0.000010	0.19
12	35.121	3.605	27.923	30.240	34.794	39.246	AW	16.13		0.512071	-11.05	0.000010	0.19
13	35.031	2.116	27.987	30.324	34.919	39.410		15.76		0.512058	-11.31	0.000015	0.28
14	34.908	-0.686	28.066	30.444	35.121	39.691	NDW	16.71	16.33	0.512131	-9.90	0.000015	0.29
15	34.910	-0.898	28.076	30.458	35.141	39.717	NDW	15.35		0.512135	-9.81	0.000008	0.15
16	35.124	4.537	27.826	30.130	34.661	39.089	AW	16.55		0.512016	-12.13	0.000010	0.19
17	35.104	3.366	27.933	30.253	34.813	39.272	AW	16.12		0.512041	-11.65	0.000015	0.28
18	34.987	1.436	28.005	30.352	34.966	39.476		16.07	15.74	0.512090	-10.68	0.000015	0.28
19	34.904	-0.547	28.057	30.433	35.105	39.671	AIW	15.50		0.512106	-10.37	0.000008	0.15
20	34.909	-0.818	28.072	30.452	35.133	39.707		15.44		0.512099	-10.51	0.000008	0.15
21	34.911	-0.904	28.077	30.459	35.142	39.719	NDW	16.18		0.512115	-10.21	0.000008	0.15
22	35.106	4.339	27.834	30.141	34.676	39.110	AW	15.85		0.512038	-11.70	0.000008	0.15
23	35.081	2.752	27.972	30.300	34.877	39.352		16.00		0.512057	-11.34	0.000008	0.15
24	34.908	-0.457	28.056	30.430	35.100	39.664	AIW	15.49		0.512116	-10.19	0.000008	0.15
25	34.915	-0.873	28.080	30.461	35.143	39.719	EBDW / GSDW	15.69		0.512093	-10.62	0.000015	0.29
26	34.926	-0.886	28.089	30.470	35.152	39.728	EBDW / GSDW	15.88		0.512114	-10.22	0.000008	0.15
27	33.897	0.058	27.213	29.585	34.247	38.805		15.93		0.512048	-11.51	0.000015	0.29
28	35.069	3.066	27.934	30.258	34.827	39.293	AW	16.03		0.512024	-11.98	0.000015	0.29
29	34.933	1.172	27.980	30.330	34.952	39.470		15.82		0.512076	-10.97	0.000015	0.29
30	34.976	1.295	28.006	30.355	34.973	39.487		15.91		0.512082	-10.85	0.000015	0.29
31	34.909	-0.413	28.054	30.428	35.096	39.659	AIW	15.37		0.512133	-9.86	0.000015	0.29
32	34.924	-0.886	28.087	30.468	35.151	39.727	EBDW / GSDW	15.57		0.512098	-10.54	0.000015	0.29
33	34.345	1.055	27.515	29.870	34.500	39.025		38.11	38.11	0.512082	-10.84	0.000015	0.29
34	35.096	3.574	27.906	30.223	34.778	39.231	AW	15.94	16.09	0.512065	-11.19	0.000015	0.29
35	35.018	1.894	27.995	30.335	34.936	39.433		16.08	15.82	0.512072	-11.04	0.000015	0.29
36	34.931	0.002	28.050	30.418	35.074	39.624		15.64		0.512120	-10.11	0.000016	0.31
37	34.916	-0.847	28.079	30.460	35.141	39.716	CBDW	15.25		0.512147	-9.58	0.000015	0.29
38	34.923	-0.889	28.086	30.468	35.150	39.726	EBDW / GSDW	15.74		0.512114	-10.23	0.000012	0.23
39	33.477	-1.023	26.919	29.309	34.008	38.601		16.87		0.512061	-11.26	0.000015	0.29
40	34.977	3.141	27.854	30.177	34.744	39.209	RAW	16.23		0.512037	-11.72	0.000015	0.29
41	35.022	2.794	27.921	30.249	34.825	39.299	RAW	16.39		0.512042	-11.62	0.000015	0.29
42	35.036	2.346	27.972	30.306	34.894	39.380	RAW	16.15		0.512045	-11.56	0.000015	0.29
43	34.946	0.289	28.046	30.410	35.057	39.599	DAAW	15.85		0.512092	-10.66	0.000015	0.29
44	34.907	-0.613	28.062	30.439	35.113	39.681	AIW	15.57		0.512120	-10.10	0.000015	0.29
45	34.918	-0.831	28.080	30.461	35.141	39.716	CBDW	15.48		0.512120	-10.10	0.000015	0.29
46	34.923	-0.898	28.087	30.469	35.151	39.728	EBDW / GSDW	16.39		0.512093	-10.64	0.000015	0.29
47	31.036	0.285	24.895	27.275	31.956	36.531	NEGSSW	36.82	37.02	0.512003	-12.38	0.000012	0.23
48	31.704	-1.486	25.495	27.900	32.629	37.252	NEGSSW	36.90		0.512016	-12.13	0.000012	0.23
49	31.847	-1.702	25.616	28.023	32.758	37.386		36.06		0.512028	-11.89	0.000012	0.23
50	32.719	-1.496	26.319	28.720	33.440	38.054		30.39	30.55	0.512072	-11.04	0.000012	0.23
51	31.047	0.298	24.903	27.283	31.963	36.538	NEGSSW	37.52		0.512009	-12.28	0.000016	0.31
52	31.719	-1.514	25.508	27.913	32.643	37.266	NEGSSW	37.27		0.512032	-11.83	0.000015	0.29
53	31.901	-1.691	25.659	28.066	32.800	37.427		35.30		0.512035	-11.76	0.000017	0.34
54	33.459	-1.065	26.907	29.297	33.998	38.592		27.99		0.512044	-11.58	0.000016	0.31
55	34.293	-0.238	27.547	29.921	34.590	39.152		24.30		0.512011	-12.22	0.000015	0.29
56	30.894	-0.555	24.813	27.207	31.915	36.516	NEGSSW	36.93		0.512002	-12.40	0.000017	0.34
57	31.787	-1.629	25.566	27.973	32.706	37.331	NEGSSW	36.03		0.512055	-11.38	0.000017	0.34
58	33.391	-1.174	26.855	29.248	33.952	38.550	PW-mod	28.51		0.512081	-10.87	0.000016	0.31
59	34.384	-0.067	27.613	29.984	34.646	39.203	NEGSBW	23.26		0.512028	-11.91	0.000015	0.29
60	34.526	0.213	27.712	30.078	34.731	39.279	NEGSBW	22.46		0.512022	-12.02	0.000015	0.29
61	31.084	-0.761	24.973	27.369	32.082	36.687	NEGSSW	35.87		0.512060	-11.27	0.000015	0.29
62	31.673	-1.550	25.472	27.878	32.609	37.234	NEGSSW	35.12		0.512070	-11.07	0.000017	0.34
63	32.801	-1.613	26.388	28.791	33.514	38.130	PW-mod	29.05		0.512134	-9.84	0.000016	0.31
64	34.160	-0.514	27.453	29.832	34.510	39.081	NEGSBW	24.54		0.512050	-11.46	0.000015	0.29
65	30.885	-1.436	24.830	27.238	31.972	36.600	NEGSSW	37.10		0.512025	-11.96	0.000017	0.33
66	31.833	-1.668	25.603	28.011	32.744	37.371	NEGSSW	34.97		0.512070	-11.07	0.000017	0.34
67	33.063	-1.520	26.599	28.999	33.717	38.328	PW-mod	28.20		0.512119	-10.12	0.000017	0.33
68	34.060	-0.594	27.375	29.756	34.437	39.012	NEGSBW	25.65		0.512039	-11.68	0.000015	0.29
69	30.993	-0.754	24.900	27.296	32.009	36.615	NEGSSW	35.51		0.512055	-11.37	0.000012	0.23
70	31.871	-1.693	25.635	28.043	32.777	37.404	NEGSSW	38.13		0.512046	-11.56	0.000012	0.23
71	33.015	-1.442	26.558	28.957	33.673	38.282	PW-mod	28.47		0.512111	-10.29	0.000012	0.23
72	34.174	-0.711	27.472	29.854	34.538	39.115		24.05		0.512064	-11.21	0.000012	0.23
73	31.013	-0.629	24.912	27.306	32.015	36.617		33.43		0.512070	-11.08	0.000012	0.23
74	31.779	-1.680	25.560	27.967	32.702	37.330	NEGSSW	37.53		0.512026	-11.93	0.000012	0.23
75	34.066	-0.948	27.395	29.781	34.472	39.058		23.82		0.512060	-11.28	0.000012	0.23
76	31.399	-1.482	25.248	27.654	32.386	37.010		31.42		0.512129	-9.93	0.000017	0.34
77	33.729	-1.251	27.132	29.524	34.228	38.825	PW-mod	25.72		0.512113	-10.24	0.000012	0.23
78	34.452	-0.029	27.666	30.036	34.697	39.252		20.14	20.17	0.512079	-10.91	0.000012	0.23
79	34.887	1.377	27.929	30.277	34.893	39.406		17.51		0.512071	-11.06	0.000012	0.23
80	31.796	-1.640	25.573	27.980	32.713	37.339		35.38		0.512109	-10.32	0.000012	0.23
81	33.959	-1.744	27.333	29.732	34.449	39.060	KW	23.64		0.512146	-9.60	0.000012	0.23
82	34.983	2.844	27.886	30.213	34.788	39.261		18.00		0.512067	-11.14	0.000012	0.23
83	34.926	1.568	27.946	30.291	34.902	39.408		17.63		0.512054	-11.40	0.000012	0.23
84	32.297	-1.628	25.980	28.384	33.113	37.734	PW-εNd-max	25.68		0.512185	-8.83	0.000011	0.22

Table A3, Chapter I: CTD, Nd isotope and REE data (continued)

Nr.	Epsilon Nd repeat	143/144 repeat [2sig]	Epsilon Nd repeat [2sig]	Y [pmol/kg]	La [pmol/kg]	Ce [pmol/kg]	Pr [pmol/kg]	Nd [pmol/kg]	Sm [pmol/kg]
1				130.42	18.10	9.55	3.46	15.24	2.99
2				128.72	17.12	7.55	3.05	14.46	3.12
3				135.01	24.01	13.59	3.42	14.72	3.06
4				141.41	20.71	7.65	3.53	15.15	2.95
5				134.17	21.84	11.66	3.89	15.69	3.06
6				138.80	19.67	8.41	3.73	16.70	2.92
7				134.06	19.96	7.61	3.63	15.30	2.57
8				132.76	18.67	6.67	3.39	16.29	2.84
9				123.76	19.16	6.49	3.42	15.11	3.00
10				118.12	19.13	6.97	3.51	16.37	3.06
11				137.66	20.51	9.10	3.90	17.46	3.43
12				138.50	21.64	8.30	4.08	17.31	3.19
13				131.05	19.79	5.89	3.63	15.78	3.28
14				120.43	22.36	7.22	3.87	17.14	2.58
15				126.12	20.47	3.50	3.43	14.82	3.03
16				120.31	18.98	8.88	3.37	14.69	3.24
17				122.62	19.07	6.49	3.20	14.95	3.59
18				120.89	18.99	6.13	3.13	15.24	3.51
19				124.28	19.38	5.36	3.38	14.97	3.13
20				127.79	20.70	5.46	3.28	15.28	3.06
21				116.28	19.41	4.89	3.24	14.55	3.56
22				124.03	18.94	6.91	3.59	15.18	3.26
23				121.53	19.52	7.41	3.29	14.36	3.54
24				131.99	21.14	6.32	3.47	16.56	3.45
25				123.93	20.35	5.40	3.71	16.30	2.97
26				119.00	19.52	3.86	3.50	14.82	3.13
27				122.06	18.02	6.63	3.29	14.53	3.84
28				123.42	19.52	6.50	3.31	14.59	3.39
29				126.78	20.80	9.41	3.34	14.84	3.29
30				121.66	19.40	5.67	3.23	14.17	3.07
31				121.12	18.47	4.82	3.22	13.51	3.23
32				114.15	18.75	3.58	3.11	14.29	3.20
33				142.26	79.77	83.44	11.13	39.64	3.34
34				138.51	21.48	7.90	3.80	16.68	3.29
35				125.02	19.39	6.09	3.75	15.87	3.33
36				131.47	19.67	5.46	3.40	15.68	2.91
37				128.22	19.84	3.56	3.44	15.01	2.70
38				123.38	19.87	3.91	3.64	15.50	3.39
39				121.74	19.70	5.21	3.83	18.47	3.24
40				135.69	19.21	8.37	3.57	16.62	3.44
41				122.71	20.27	6.76	3.79	16.10	3.20
42				138.33	21.43	6.96	3.78	16.71	3.56
43				126.18	20.33	7.48	3.45	14.87	2.88
44				133.12	19.40	5.00	3.56	15.17	3.02
45				116.45	19.74	4.87	3.54	17.60	2.75
46				127.07	20.39	4.52	3.67	16.95	2.67
47				270.05	53.95	22.44	9.03	40.08	7.40
48				265.14	51.44	18.55	9.10	38.67	7.73
49				269.41	51.04	16.76	8.93	35.67	6.69
50				234.78	40.52	12.44	6.78	28.99	5.54
51	-12.10	0.000017	0.34	257.40	51.28	19.14	8.86	36.94	7.36
52				257.60	49.80	17.18	8.70	37.07	7.53
53	-11.98	0.000016	0.31	226.44	45.19	14.34	8.01	36.61	6.64
54				210.75	37.97	11.62	6.03	27.22	4.98
55				179.77	31.13	8.11	5.17	24.48	4.58
56	-12.14	0.000016	0.31	257.39	51.18	19.65	8.77	36.33	7.44
57	-11.92	0.000016	0.31	262.88	50.26	17.04	8.51	39.50	7.34
58				206.74	36.72	14.00	6.23	26.49	4.92
59				168.56	29.74	9.62	5.15	23.78	4.54
60				169.31	29.08	9.48	5.38	23.24	4.94
61				229.96	46.77	15.49	8.06	37.52	6.34
62	-11.26	0.000016	0.31	269.80	48.40	15.89	8.51	33.62	6.43
63				240.65	39.19	9.73	6.66	31.28	5.49
64				182.44	32.30	10.21	5.50	25.80	5.27
65	-11.89	0.000017	0.33	250.16	50.12	19.31	8.62	35.73	6.51
66	-11.38	0.000016	0.31	263.14	48.35	15.01	8.00	36.33	7.85
67				217.83	36.85	13.31	6.35	29.78	6.10
68				161.49	31.25	10.28	5.82	28.26	4.94
69				270.94	52.45	20.17	8.94	38.15	7.49
70				259.90	51.13	18.95	8.52	38.22	6.70
71				216.14	37.93	12.71	6.26	28.23	5.55
72				179.09	31.75	11.40	5.80	24.41	4.85
73	-10.63	0.000017	0.34	262.49	45.05	13.16	7.12	33.67	6.35
74	-11.93	0.000017	0.34	254.99	54.36	35.92	8.39	36.21	6.48
75				186.08	32.00	10.92	5.83	26.37	4.95
76	-9.49	0.000012	0.23	259.01	41.58	9.60	6.92	30.06	6.05
77				205.35	33.89	11.11	5.64	27.09	4.87
78				166.16	27.14	9.19	4.85	21.35	3.97
79				142.50	23.04	6.55	4.21	18.24	3.52
80				224.48	47.61	19.22	8.20	36.26	6.77
81				187.17	31.92	13.21	5.61	25.37	4.78
82				136.83	24.48	11.65	4.09	17.47	3.16
83				144.43	24.63	7.77	4.01	18.23	3.65
84				191.90	31.79	5.89	5.67	26.29	5.06

Table A3, Chapter I: CTD, Nd isotope and REE data (continued)

Nr.	Gd [pmol/kg]	Tb [pmol/kg]	Dy [pmol/kg]	Ho [pmol/kg]	Er [pmol/kg]	Tm [pmol/kg]	Yb [pmol/kg]	Lu [pmol/kg]
1	4.43	0.77	5.56	1.46	4.52	0.70	4.27	0.73
2	4.77	0.75	5.25	1.28	4.61	0.62	4.39	0.69
3	4.38	0.77	5.31	1.54	4.69	0.72	4.49	0.75
4	4.54	0.72	5.68	1.50	4.65	0.64	4.55	0.71
5	4.38	0.81	5.76	1.41	4.62	0.69	4.71	0.77
6	4.60	0.79	5.58	1.37	4.66	0.67	4.69	0.69
7	4.70	0.72	5.82	1.51	4.79	0.71	4.22	0.72
8	4.23	0.76	5.23	1.53	4.59	0.71	4.25	0.70
9	4.74	0.78	5.78	1.44	5.17	0.92	4.82	0.59
10	4.54	0.74	5.67	1.53	5.13	0.82	4.91	0.59
11	4.32	0.78	5.46	1.39	4.66	0.73	4.28	0.73
12	4.82	0.76	5.74	1.47	4.51	0.66	4.42	0.74
13	4.25	0.67	5.18	1.34	4.37	0.72	4.49	0.71
14	4.90	0.82	5.57	1.53	5.21	0.77	5.32	0.68
15	4.34	0.73	5.22	1.23	4.58	0.69	4.37	0.74
16	4.34	0.65	5.31	1.23	4.43	0.65	4.09	0.70
17	4.47	0.67	5.16	1.34	4.53	0.60	3.80	0.66
18	4.52	0.68	5.14	1.27	4.35	0.66	4.30	0.68
19	4.01	0.74	5.07	1.24	4.44	0.62	4.38	0.74
20	4.49	0.76	5.37	1.35	4.74	0.61	4.57	0.72
21	4.79	0.64	5.31	1.23	4.29	0.63	4.18	0.72
22	5.21	0.72	5.03	1.36	4.49	0.66	4.53	0.66
23	4.63	0.71	5.11	1.32	4.52	0.67	4.27	0.71
24	4.09	0.69	5.23	1.29	4.21	0.67	4.65	0.76
25	4.58	0.77	5.37	1.46	4.87	0.71	4.71	0.79
26	3.93	0.70	5.04	1.34	3.92	0.63	4.23	0.65
27	4.81	0.72	5.37	1.37	4.16	0.57	4.00	0.68
28	4.39	0.71	5.48	1.33	4.37	0.58	4.58	0.74
29	4.03	0.75	5.61	1.36	4.28	0.69	4.77	0.67
30	4.78	0.63	5.18	1.28	4.27	0.70	4.34	0.72
31	4.60	0.73	5.63	1.36	4.19	0.63	4.15	0.72
32	4.73	0.75	5.20	1.34	4.62	0.66	4.60	0.80
33	6.16	0.94	5.96	1.71	5.26	0.75	4.86	0.74
34	4.18	0.76	5.45	1.52	5.12	0.68	4.33	0.72
35	4.51	0.75	5.50	1.51	4.99	0.77	5.01	0.85
36	4.30	0.77	4.69	1.46	4.41	0.71	3.97	0.70
37	4.65	0.83	5.39	1.32	4.60	0.72	4.81	0.76
38	4.27	0.71	5.21	1.49	4.82	0.73	4.47	0.75
39	5.08	0.86	6.07	1.54	5.18	0.88	5.04	0.61
40	4.12	0.72	5.66	1.53	4.75	0.69	4.64	0.67
41	4.69	0.83	5.92	1.62	5.05	0.83	4.52	0.69
42	4.23	0.78	5.39	1.50	4.72	0.68	4.56	0.76
43	4.18	0.68	4.87	1.37	4.55	0.69	4.40	0.66
44	4.06	0.81	5.27	1.44	4.78	0.74	4.50	0.75
45	3.77	0.81	5.84	1.47	4.92	0.78	4.63	0.69
46	4.59	0.86	5.33	1.47	4.82	0.75	4.77	0.63
47	10.73	1.70	11.38	3.09	9.47	1.37	9.07	1.49
48	10.22	1.57	12.17	3.04	9.15	1.41	8.82	1.45
49	9.88	1.60	11.70	3.00	9.93	1.33	8.87	1.51
50	8.90	1.25	9.55	2.37	7.87	1.07	7.29	1.14
51	10.11	1.68	11.30	2.95	9.45	1.28	8.54	1.43
52	10.72	1.60	10.96	2.94	9.04	1.36	8.75	1.43
53	10.35	1.59	11.88	3.13	9.82	1.47	8.98	1.12
54	7.27	1.13	8.95	2.32	7.79	1.06	6.59	1.27
55	6.91	1.08	7.89	2.09	6.52	0.92	6.15	1.06
56	9.61	1.34	10.01	2.90	9.01	1.32	8.51	1.33
57	9.83	1.58	11.29	2.97	9.21	1.34	8.51	1.47
58	8.20	1.25	9.35	2.39	7.81	1.08	6.84	1.16
59	6.99	1.04	7.35	2.02	6.25	0.92	5.66	0.96
60	6.07	1.03	7.40	1.88	5.69	0.95	5.84	0.90
61	10.56	1.69	12.21	3.13	10.59	1.62	9.58	1.23
62	9.26	1.59	11.15	2.79	9.73	1.27	8.16	1.41
63	8.40	1.48	9.82	2.57	8.39	1.13	7.83	1.34
64	6.19	1.12	7.75	2.01	6.49	0.85	6.86	1.09
65	9.02	1.59	10.72	2.92	8.33	1.31	8.82	1.42
66	9.13	1.46	10.86	2.74	9.50	1.21	8.18	1.44
67	7.77	1.12	9.80	2.32	7.66	1.13	7.20	1.17
68	7.10	1.24	8.90	2.40	7.76	1.20	7.49	0.92
69	9.95	1.77	11.87	3.07	9.67	1.41	9.26	1.42
70	10.10	1.59	11.70	2.80	9.33	1.34	8.58	1.51
71	8.20	1.23	9.17	2.32	7.64	1.16	6.97	1.16
72	7.17	1.04	8.03	2.03	6.68	0.97	6.34	1.06
73	9.22	1.27	10.72	2.49	8.79	1.30	8.61	1.32
74	9.39	1.42	10.70	2.71	8.91	1.13	8.05	1.39
75	8.28	1.20	8.31	2.19	6.66	1.00	6.72	1.03
76	9.65	1.41	10.79	2.59	8.80	1.21	8.54	1.28
77	6.97	1.23	8.52	2.34	7.30	0.95	7.15	1.21
78	5.79	1.03	7.12	1.79	5.69	0.89	5.63	0.90
79	5.01	0.73	5.96	1.56	5.20	0.69	4.68	0.78
80	9.66	1.63	11.59	3.11	10.06	1.58	9.86	1.21
81	7.43	1.09	8.08	2.11	6.92	0.97	6.79	1.04
82	4.96	0.78	5.43	1.45	4.67	0.70	4.51	0.74
83	4.94	0.89	6.00	1.51	5.08	0.79	4.45	0.79
84	8.06	1.35	9.50	2.65	8.21	1.24	7.87	1.11

Table A3, Chapter I: CTD, Nd isotope and REE data (continued)

Nr.	Sample ID	Cruise	Station	Year	Month	Day	Longitude [−E]	Latitude [−N]	Bot. Depth [m]	Depth [m]	Pressure [dB]	Temperature [°C]	Conductivity [mS/cm]
85	27/130/75	ARKXXVII/1	130	2012	7	8	-4.577	78.833	1388	75.80	76.65	-1.73	26.821
86	27/130/200	ARKXXVII/1	130	2012	7	8	-4.577	78.833	1388	202.55	204.89	2.75	31.529
87	27/130/600	ARKXXVII/1	130	2012	7	8	-4.577	78.833	1388	608.20	615.79	0.77	29.888
88	27/130/1000	ARKXXVII/1	130	2012	7	8	-4.577	78.833	1388	1013.48	1027.09	-0.23	29.223
89	27/130/1350	ARKXXVII/1	130	2012	7	8	-4.577	78.833	1388	1368.44	1387.92	-0.43	29.222
90	27/132/10	ARKXXVII/1	132	2012	7	9	-3.920	78.833	1923	10.25	10.36	-1.51	25.910
91	27/132/50	ARKXXVII/1	132	2012	7	9	-3.920	78.833	1923	50.66	51.22	-1.71	26.835
92	27/132/200	ARKXXVII/1	132	2012	7	9	-3.920	78.833	1923	202.49	204.83	2.88	32.011
93	27/132/400	ARKXXVII/1	132	2012	7	9	-3.920	78.833	1923	405.19	410.07	0.81	31.056
94	27/132/600	ARKXXVII/1	132	2012	7	9	-3.920	78.833	1923	607.92	615.52	0.24	29.462
95	27/132/1000	ARKXXVII/1	132	2012	7	9	-3.920	78.833	1923	1013.55	1027.16	-0.22	29.214
96	27/132/1550	ARKXXVII/1	132	2012	7	9	-3.920	78.833	1923	1572.64	1595.78	-0.55	29.221
97	27/132/1880	ARKXXVII/1	132	2012	7	9	-3.920	78.833	1923	1908.40	1937.96	-0.61	29.275
98	27/134/11	ARKXXVII/1	134	2012	7	9	-3.309	78.837	2380	11.13	11.25	-1.15	26.471
99	27/134/50	ARKXXVII/1	134	2012	7	9	-3.309	78.837	2380	50.83	51.40	-0.88	27.596
100	27/134/200	ARKXXVII/1	134	2012	7	9	-3.309	78.837	2380	202.89	205.23	3.28	32.118
101	27/134/600	ARKXXVII/1	134	2012	7	9	-3.309	78.837	2380	608.12	615.72	1.06	30.214
102	27/134/900	ARKXXVII/1	134	2012	7	9	-3.309	78.837	2380	912.92	924.96	0.25	29.669
103	27/134/1600	ARKXXVII/1	134	2012	7	9	-3.309	78.837	2380	1624.21	1648.30	-0.58	29.193
104	27/134/2325	ARKXXVII/1	134	2012	7	9	-3.309	78.837	2380	2358.38	2397.39	-0.76	29.351

Table A3, Chapter I: CTD, Nd isotope and REE data (continued)

Nr.	Salinity [PSU]	Pot. Temp. [°C]	Sigma-theta [kg/m3]	Sigma0.5 [kg/m3]	Sigma1.5 [kg/m3]	Sigma2.5 [kg/m3]	Classification this study	Nd ID [pmol/kg]	Nd ID repeat [pmol/kg]	143/144	Epsilon Nd	143/144 [2sig]	Epsilon Nd [2sig]
85	33.969	-1.734	27.341	29.740	34.457	39.066	KW	22.05		0.512144	-9.64	0.000011	0.22
86	34.966	2.738	27.882	30.210	34.789	39.264		16.81		0.512069	-11.10	0.000011	0.22
87	34.913	0.738	27.993	30.350	34.984	39.514	DAAW	16.13		0.512107	-10.36	0.000012	0.23
88	34.892	-0.271	28.033	30.405	35.069	39.628	UPDW	15.97		0.512089	-10.72	0.000012	0.23
89	34.914	-0.491	28.062	30.437	35.107	39.672	UPDW	16.02		0.512110	-10.31	0.000012	0.23
90	32.744	-1.514	26.340	28.741	33.462	38.075	PW-mod	24.27		0.512164	-9.26	0.000011	0.22
91	34.006	-1.714	27.370	29.769	34.485	39.094	KW	21.25		0.512142	-9.68	0.000011	0.22
92	35.029	2.868	27.921	30.247	34.822	39.293		27.03		0.512073	-11.02	0.000011	0.22
93	34.878	0.795	27.961	30.317	34.950	39.479	DAAW	18.21		0.512111	-10.27	0.000011	0.22
94	34.872	0.217	27.991	30.356	35.006	39.551	DAAW	15.51		0.512121	-10.09	0.000011	0.22
95	34.895	-0.267	28.035	30.407	35.071	39.629	UPDW	15.63	15.67	0.512105	-10.40	0.000011	0.22
96	34.913	-0.624	28.067	30.444	35.118	39.687	UPDW	15.39		0.512122	-10.06	0.000011	0.22
97	34.922	-0.706	28.078	30.456	35.133	39.704	CBDW	15.40		0.512096	-10.58	0.000011	0.22
98	32.954	-1.152	26.500	28.894	33.602	38.203		22.86		0.512096	-10.58	0.000011	0.22
99	34.066	-0.880	27.391	29.776	34.466	39.049		30.53		0.512066	-11.17	0.000011	0.22
100	35.051	3.271	27.900	30.221	34.785	39.246		16.65		0.512027	-11.92	0.000011	0.22
101	34.936	1.031	27.992	30.344	34.970	39.492		16.24	15.67	0.512081	-10.87	0.000011	0.22
102	34.932	0.202	28.040	30.405	35.055	39.599	DAAW	15.91		0.512104	-10.43	0.000011	0.22
103	34.908	-0.656	28.064	30.442	35.118	39.687	UPDW	15.61		0.512149	-9.54	0.000011	0.22
104	34.923	-0.883	28.086	30.467	35.150	39.726	3DW / GSD	15.72		0.512096	-10.58	0.000011	0.22

Table A3, Chapter I: CTD, Nd isotope and REE data (continued)

Nr.	Epsilon Nd repeat	143/144 repeat [2sig]	Epsilon Nd repeat [2sig]	Y [pmol/kg]	La [pmol/kg]	Ce [pmol/kg]	Pr [pmol/kg]	Nd [pmol/kg]	Sm [pmol/kg]
85				179.43	26.71	8.49	4.85	23.46	4.52
86				148.99	24.39	10.88	4.57	19.41	3.60
87				134.38	21.52	6.98	3.65	15.89	3.49
88				141.89	21.76	6.09	3.69	16.73	3.43
89				136.14	21.33	4.72	3.73	17.27	3.36
90				202.13	33.56	8.38	5.56	25.00	4.82
91				169.27	27.54	11.46	4.74	22.24	4.67
92				138.42	50.95	49.93	7.18	26.65	2.94
93				135.68	27.85	17.68	4.21	18.20	2.95
94				133.43	18.87	4.32	3.45	16.28	3.09
95				124.85	20.54	7.55	3.73	16.88	2.84
96				132.96	20.93	5.85	3.56	16.02	2.89
97				120.96	19.59	3.93	3.63	16.10	3.09
98				187.57	31.20	10.60	5.00	23.21	4.76
99				171.66	30.30	12.38	4.87	22.93	4.45
100				134.87	21.64	9.36	3.90	16.84	2.89
101				134.07	21.81	7.41	3.81	16.84	3.20
102				138.98	22.76	7.19	3.61	16.47	3.63
103				124.74	20.66	6.46	3.65	15.36	3.21
104				119.69	19.85	3.58	3.79	15.92	2.70

Table A3, Chapter I: CTD, Nd isotope and REE data (continued)

Nr.	Gd [pmol/kg]	Tb [pmol/kg]	Dy [pmol/kg]	Ho [pmol/kg]	Er [pmol/kg]	Tm [pmol/kg]	Yb [pmol/kg]	Lu [pmol/kg]
85	5.93	0.99	7.67	1.88	6.02	0.82	6.37	0.93
86	5.48	0.85	6.22	1.65	5.10	0.73	4.90	0.82
87	4.47	0.75	5.98	1.53	4.72	0.73	4.51	0.71
88	5.12	0.76	5.56	1.48	5.04	0.72	4.60	0.75
89	5.00	0.69	5.35	1.40	4.89	0.73	4.47	0.74
90	7.47	1.18	8.25	2.25	7.33	1.05	6.82	1.02
91	6.03	1.04	6.93	1.83	6.00	0.88	5.69	1.02
92	5.39	0.65	5.47	1.50	4.39	0.61	4.35	0.71
93	5.08	0.88	5.80	1.60	4.60	0.75	4.79	0.74
94	4.64	0.63	5.54	1.32	4.69	0.63	4.30	0.74
95	4.29	0.74	5.50	1.39	5.02	0.76	4.41	0.87
96	4.06	0.73	5.11	1.40	4.77	0.71	4.38	0.73
97	4.65	0.71	5.45	1.60	4.88	0.76	4.81	0.85
98	6.09	0.99	7.61	1.93	6.53	0.96	6.27	1.08
99	5.97	1.06	7.42	1.95	6.46	0.93	5.86	1.00
100	4.79	0.74	5.63	1.52	4.86	0.67	4.58	0.75
101	4.71	0.79	5.18	1.44	4.85	0.73	4.30	0.75
102	4.56	0.77	5.49	1.54	4.61	0.67	4.86	0.69
103	4.37	0.68	5.14	1.36	4.27	0.71	4.24	0.73
104	4.39	0.82	5.56	1.41	4.86	0.73	4.72	0.67

Table A3, Chapter I: REE standard data

Nr.	Sample ID	Y [pmol/kg]	La [pmol/kg]	Ce [pmol/kg]	Pr [pmol/kg]	Nd [pmol/kg]	Sm [pmol/kg]	Eu [pmol/kg]	Gd [pmol/kg]	Tb [pmol/kg]
1	BATS15m	137.12	13.47	9.92	3.03	13.86	3.20	0.75	4.71	0.77
2	BATS15m	136.65	13.48	9.91	2.83	13.09	3.09	0.84	4.58	0.74
3	BATS15m	134.31	13.41	10.48	2.80	13.62	3.51	0.71	4.83	0.77
4	BATS15m	130.77	13.58	10.24	2.81	13.56	3.28	0.85	5.00	0.82
5	BATS15m	134.96	14.00	10.40	3.08	14.23	3.35	0.89	4.84	0.74
6	BATS15m	131.97	13.35	10.24	2.91	13.22	3.72	0.76	4.57	0.70
7	BATS15m	130.45	14.28	10.02	3.18	14.18	3.03	0.77	4.78	0.76
8	BATS15m	132.65	13.74	10.09	3.24	15.21	3.36	0.76	4.26	0.83
9	BATS15m	124.76	13.99	10.21	3.10	14.08	3.27	0.81	5.04	0.90
10	BATS15m	134.67	14.09	10.80	2.94	14.40	2.89	0.80	4.67	0.82
11	BATS15m	137.78	15.01	10.94	3.17	15.05	3.00	0.78	4.83	0.81
12	BATS15m	135.17	14.81	11.18	3.26	14.82	3.25	0.76	4.87	0.82
13	BATS15m	140.35	14.68	10.76	3.17	15.29	3.45	0.75	4.67	0.88
14	BATS15m	138.80	14.52	10.92	3.24	14.53	3.25	0.83	5.14	0.86
15	BATS15m	132.27	15.10	10.26	3.35	15.30	3.54	0.80	4.83	0.80
1	BATS2000m	130.02	21.29	3.79	3.51	15.94	4.02	0.79	4.69	0.69
2	BATS2000m	128.98	22.58	3.93	3.60	16.66	3.58	0.77	4.52	0.74
3	BATS2000m	139.26	22.45	3.96	3.95	16.31	3.29	0.80	4.74	0.79
4	BATS2000m	138.68	21.93	4.01	4.07	16.86	3.64	0.79	4.34	0.76
5	BATS2000m	135.93	21.68	3.77	3.75	16.26	3.54	0.79	4.26	0.75
6	BATS2000m	142.88	22.78	3.91	3.85	17.27	3.00	0.74	4.82	0.80
7	BATS2000m	134.16	22.48	3.82	4.04	17.82	3.39	0.78	4.47	0.87
8	BATS2000m	136.84	22.81	3.63	4.28	18.07	3.30	0.84	4.91	0.84
9	BATS2000m	146.26	23.83	4.00	4.34	18.66	3.67	0.86	5.09	0.72
10	BATS2000m	138.95	23.02	3.49	3.97	16.37	3.21	0.74	4.46	0.69
11	BATS2000m	142.15	22.68	3.89	3.90	17.31	3.10	0.79	5.03	0.68
12	BATS2000m	140.42	22.53	3.98	3.71	16.71	2.73	0.81	4.90	0.75
13	BATS2000m	143.52	23.74	4.09	3.88	18.41	3.18	0.79	4.70	0.81

Nr.	Sample ID	Dy [pmol/kg]	Ho [pmol/kg]	Er [pmol/kg]	Tm [pmol/kg]	Yb [pmol/kg]	Lu [pmol/kg]
1	BATS15m	6.20	1.60	4.75	0.65	4.23	0.64
2	BATS15m	6.05	1.36	4.63	0.66	4.22	0.68
3	BATS15m	5.60	1.46	4.83	0.64	4.50	0.72
4	BATS15m	5.65	1.46	4.86	0.70	4.53	0.63
5	BATS15m	5.65	1.43	4.64	0.61	4.30	0.67
6	BATS15m	5.82	1.39	4.58	0.68	4.22	0.68
7	BATS15m	5.82	1.51	4.74	0.74	4.41	0.66
8	BATS15m	6.12	1.51	4.61	0.71	4.29	0.75
9	BATS15m	6.53	1.67	5.30	0.79	4.48	0.62
10	BATS15m	5.82	1.53	4.57	0.70	3.94	0.59
11	BATS15m	6.07	1.62	4.83	0.71	4.54	0.69
12	BATS15m	6.20	1.62	5.04	0.76	4.47	0.65
13	BATS15m	6.01	1.53	5.07	0.69	4.26	0.63
14	BATS15m	6.18	1.69	4.92	0.70	4.28	0.68
15	BATS15m	5.95	1.62	4.85	0.72	4.40	0.75
1	BATS2000m	5.47	1.42	4.92	0.62	4.98	0.90
2	BATS2000m	5.72	1.39	4.50	0.76	4.62	0.80
3	BATS2000m	5.29	1.45	4.58	0.80	5.03	0.79
4	BATS2000m	5.28	1.50	4.85	0.71	4.86	0.78
5	BATS2000m	5.57	1.36	4.76	0.74	4.22	0.77
6	BATS2000m	5.51	1.42	4.94	0.74	5.04	0.88
7	BATS2000m	5.93	1.52	5.18	0.83	5.45	0.88
8	BATS2000m	5.54	1.68	5.35	0.83	5.74	0.74
9	BATS2000m	6.20	1.62	5.65	0.73	5.38	0.89
10	BATS2000m	5.88	1.40	4.78	0.72	5.25	0.74
11	BATS2000m	5.05	1.44	4.54	0.69	4.54	0.77
12	BATS2000m	5.21	1.51	4.90	0.66	4.36	0.74
13	BATS2000m	5.27	1.37	4.83	0.66	4.94	0.77

Table A3, Chapter I: CTD and stable oxygen isotope data

Nr.	Cruise	Station	Year	Month	Day	Longitude [¬E]	Latitude [¬N]	Depth [m]	Pressure [dB]	Temperature [°C]	Salinity [PSU]	Pot. Temp. [°C]	O2 [µmol/kg]	δ18O (‰ VSMOW)	o18-stdev	o18-n
1	ARKXXVII/1	15	2012	6	20	9.001	78.835	210.82	210.82	3.65	35.087	3.632	301.27	0.28	0.06	6
2	ARKXXVII/1	15	2012	6	20	9.001	78.835	202.72	202.72	3.65	35.087	3.635	301.87	0.34	0.04	3
3	ARKXXVII/1	15	2012	6	20	9.001	78.835	101.34	101.34	4.15	35.108	4.144	304.08	0.31	0.10	7
4	ARKXXVII/1	15	2012	6	20	9.001	78.835	51.02	51.02	2.57	34.852	2.566	322.46	0.34	0.02	3
5	ARKXXVII/1	15	2012	6	20	9.001	78.835	10.54	10.54	2.83	34.733	2.825	0.00	0.21	0.09	5
6	ARKXXVII/1	27	2012	6	21	7.012	78.831	607.26	607.26	-0.28	34.912	-0.300	300.99	0.21	0.04	5
7	ARKXXVII/1	27	2012	6	21	7.012	78.831	404.35	404.35	1.02	34.963	1.004	302.09	0.22	0.04	5
8	ARKXXVII/1	27	2012	6	21	7.012	78.831	303.50	303.50	2.13	35.029	2.116	307.95	0.23	0.08	6
9	ARKXXVII/1	27	2012	6	21	7.012	78.831	202.37	202.37	3.15	35.095	3.136	306.06	0.32	0.04	5
10	ARKXXVII/1	27	2012	6	21	7.012	78.831	101.27	101.27	3.66	35.113	3.656	308.11	0.32	0.05	5
11	ARKXXVII/1	27	2012	6	21	7.012	78.831	50.36	50.36	3.97	35.128	3.965	308.17	0.30	0.04	5
12	ARKXXVII/1	27	2012	6	21	7.012	78.831	10.95	10.95	4.68	35.096	4.682	323.57	0.24	0.10	5
13	ARKXXVII/1	37	2012	6	22	5.992	78.833	404.71	404.71	1.39	34.990	1.373	310.41	0.24	0.01	5
14	ARKXXVII/1	37	2012	6	22	5.992	78.833	303.25	303.25	2.63	35.066	2.616	309.94	0.23	0.10	8
15	ARKXXVII/1	37	2012	6	22	5.992	78.833	202.35	202.35	3.40	35.111	3.386	306.29	0.29	0.03	5
16	ARKXXVII/1	37	2012	6	22	5.992	78.833	100.99	100.99	3.73	35.124	3.723	307.60	0.21	0.10	7
17	ARKXXVII/1	37	2012	6	22	5.992	78.833	50.18	50.18	3.95	35.128	3.943	306.53	0.33	0.02	5
18	ARKXXVII/1	37	2012	6	22	5.992	78.833	10.60	10.60	4.75	35.112	4.745	340.46	0.35	0.05	5
19	ARKXXVII/1	53	2012	6	25	4.004	78.835	607.72	607.72	0.35	34.934	0.323	313.92	0.20	0.04	5
20	ARKXXVII/1	53	2012	6	25	4.004	78.835	404.46	404.46	1.29	34.958	1.271	305.62	0.21	0.10	9
21	ARKXXVII/1	53	2012	6	25	4.004	78.835	304.94	304.94	2.68	35.067	2.660	309.83	0.29	0.03	6
22	ARKXXVII/1	53	2012	6	25	4.004	78.835	202.28	202.28	3.39	35.112	3.373	307.79	0.34	0.06	5
23	ARKXXVII/1	53	2012	6	25	4.004	78.835	101.17	101.17	3.73	35.120	3.726	308.38	0.27	0.11	10
24	ARKXXVII/1	53	2012	6	25	4.004	78.835	9.91	9.91	4.92	34.944	4.917	326.84	0.27	0.08	5
25	ARKXXVII/1	61	2012	6	26	0.395	78.835	506.16	506.16	-0.18	34.915	-0.200		0.20	0.06	5
26	ARKXXVII/1	61	2012	6	26	0.395	78.835	405.01	405.01	-0.06	34.917	-0.075		0.22	0.06	5
27	ARKXXVII/1	61	2012	6	26	0.395	78.835	354.06	354.06	0.16	34.930	0.149		0.22	0.03	5
28	ARKXXVII/1	61	2012	6	26	0.395	78.835	303.88	303.88	0.36	34.942	0.342		0.20	0.05	5
29	ARKXXVII/1	61	2012	6	26	0.395	78.835	253.16	253.16	0.62	34.957	0.613		0.24	0.05	5
30	ARKXXVII/1	61	2012	6	26	0.395	78.835	200.64	200.64	0.97	34.979	0.958		0.25	0.04	6
31	ARKXXVII/1	61	2012	6	26	0.395	78.835	151.74	151.74	1.20	34.988	1.192		0.28	0.03	5
32	ARKXXVII/1	61	2012	6	26	0.395	78.835	101.52	101.52	1.85	35.008	1.843		0.22	0.03	5
33	ARKXXVII/1	61	2012	6	26	0.395	78.835	71.11	71.11	2.37	34.992	2.364		0.22	0.07	5
34	ARKXXVII/1	61	2012	6	26	0.395	78.835	50.65	50.65	2.59	34.939	2.590		0.26	0.08	5
35	ARKXXVII/1	61	2012	6	26	0.395	78.835	35.75	35.75	3.02	34.772	3.020		0.25	0.05	5
36	ARKXXVII/1	61	2012	6	26	0.395	78.835	24.55	24.55	2.09	34.268	2.088		0.19	0.02	3
37	ARKXXVII/1	61	2012	6	26	0.395	78.835	20.22	20.22	2.01	34.218	2.009		0.17	0.06	5
38	ARKXXVII/1	61	2012	6	26	0.395	78.835	11.54	11.54	1.21	33.614	1.207		0.11	0.11	7
39	ARKXXVII/1	61	2012	6	26	0.395	78.835	9.88	9.88	0.61	33.076	0.607		0.08	0.04	4
40	ARKXXVII/1	67	2012	6	27	1.918	78.831	607.33	607.33	0.72	34.957	0.695	314.36	0.21	0.04	3
41	ARKXXVII/1	67	2012	6	27	1.918	78.831	404.70	404.70	2.28	35.039	2.258	307.22	0.23	0.02	4
42	ARKXXVII/1	67	2012	6	27	1.918	78.831	303.28	303.28	3.03	35.083	3.014	311.85	0.29	0.05	3
43	ARKXXVII/1	67	2012	6	27	1.918	78.831	202.55	202.55	3.39	35.096	3.375	302.24	0.29	0.04	4
44	ARKXXVII/1	67	2012	6	27	1.918	78.831	100.98	100.98	3.88	35.124	3.872	301.18	0.27	0.01	3
45	ARKXXVII/1	67	2012	6	27	1.918	78.831	50.60	50.60	4.00	35.082	3.995	319.19	0.25	0.01	3
46	ARKXXVII/1	67	2012	6	27	1.918	78.831	10.42	10.42	1.45	33.724	1.450	397.79	0.20	0.07	5
47	ARKXXVII/1	79	2012	6	30	-2.362	78.826	607.20	607.20	0.61	34.882	0.578	293.22	0.15	0.08	5
48	ARKXXVII/1	79	2012	6	30	-2.362	78.826	404.09	404.09	2.46	35.015	2.433	300.09	0.21	0.03	3
49	ARKXXVII/1	79	2012	6	30	-2.362	78.826	303.61	303.61	3.43	35.092	3.411	300.17	0.29	0.01	3
50	ARKXXVII/1	79	2012	6	30	-2.362	78.826	202.68	202.68	3.64	35.086	3.626	299.53	0.32	0.06	4
51	ARKXXVII/1	79	2012	6	30	-2.362	78.826	101.38	101.38	2.97	34.930	2.967	296.64	0.23	0.07	3
52	ARKXXVII/1	79	2012	6	30	-2.362	78.826	76.18	76.18	0.33	34.531	0.331	294.18	-0.01	0.07	4
53	ARKXXVII/1	79	2012	6	30	-2.362	78.826	50.78	50.78	-1.00	34.168	-1.000	306.35	-0.40	0.06	4
54	ARKXXVII/1	79	2012	6	30	-2.362	78.826	25.16	25.16	-1.77	33.992	-1.769	339.98	-0.72	0.05	5
55	ARKXXVII/1	79	2012	6	30	-2.362	78.826	10.24	10.24	-1.74	33.904	-1.743	339.46	-0.21	0.03	3
56	ARKXXVII/1	92	2012	7	3	-12.004	79.833	150.53	150.53	-1.08	33.400	-1.088	323.26	-1.20	0.06	5
57	ARKXXVII/1	92	2012	7	3	-12.004	79.833	121.71	121.71	-1.63	32.258	-1.635	354.58	-2.15	0.05	5
58	ARKXXVII/1	92	2012	7	3	-12.004	79.833	80.93	80.93	-1.71	31.789	-1.706	376.90	-2.68	0.08	5
59	ARKXXVII/1	92	2012	7	3	-12.004	79.833	61.02	61.02	-1.68	31.755	-1.677	380.18	-2.67	0.09	4
60	ARKXXVII/1	92	2012	7	3	-12.004	79.833	51.10	51.10	-1.61	31.731	-1.611	382.12	-2.76	0.09	5
61	ARKXXVII/1	92	2012	7	3	-12.004	79.833	40.97	40.97	-1.52	31.718	-1.525	385.13	-2.66	0.07	4
62	ARKXXVII/1	92	2012	7	3	-12.004	79.833	30.68	30.68	-1.48	31.704	-1.482	387.70	-2.64	0.02	3
63	ARKXXVII/1	92	2012	7	3	-12.004	79.833	20.86	20.86	-1.41	31.690	-1.405	403.41	-2.74	0.09	7
64	ARKXXVII/1	92	2012	7	3	-12.004	79.833	10.48	10.48	0.24	31.188	0.237	386.73	-2.68	0.01	3
65	ARKXXVII/1	92	2012	7	3	-12.004	79.833	1.43	1.43	0.28	31.050	0.274	383.42	-2.71	0.05	3
66	ARKXXVII/1	94	2012	7	3	-12.006	79.669	252.82	252.82	-0.26	34.279	-0.268	294.43	-0.46	0.06	3
67	ARKXXVII/1	94	2012	7	3	-12.006	79.669	242.92	242.92	-0.26	34.275	-0.271	294.18	-0.39	0.01	4
68	ARKXXVII/1	94	2012	7	3	-12.006	79.669	202.32	202.32	-0.42	34.179	-0.423	299.28	-0.58	0.09	9
69	ARKXXVII/1	94	2012	7	3	-12.006	79.669	161.79	161.79	-0.82	33.785	-0.828	312.86	-0.88	0.09	6
70	ARKXXVII/1	94	2012	7	3	-12.006	79.669	121.21	121.21	-1.54	32.513	-1.542	352.58	-2.12	0.01	3
71	ARKXXVII/1	94	2012	7	3	-12.006	79.669	80.80	80.80	-1.70	31.807	-1.697	374.91	-2.68	0.05	4
72	ARKXXVII/1	94	2012	7	3	-12.006	79.669	60.55	60.55	-1.67	31.766	-1.669	381.57	-2.72	0.01	3
73	ARKXXVII/1	94	2012	7	3	-12.006	79.669	50.31	50.31	-1.65	31.736	-1.647	382.41	-2.66	0.09	7
74	ARKXXVII/1	94	2012	7	3	-12.006	79.669	40.57	40.57	-1.60	31.721	-1.601	383.80	-2.74	0.08	7
75	ARKXXVII/1	94	2012	7	3	-12.006	79.669	29.70	29.70	-1.48	31.469	-1.479	408.33	-2.78	0.07	3
76	ARKXXVII/1	94	2012	7	3	-12.006	79.669	20.30	20.30	-1.39	31.402	-1.389	414.88	-2.73	0.05	3
77	ARKXXVII/1	94	2012	7	3	-12.006	79.669	10.13	10.13	-0.04	31.105	-0.044	396.10	-2.67	0.04	3
78	ARKXXVII/1	94	2012	7	3	-12.006	79.669	2.54	2.54	-0.03	31.091	-0.027	399.33	-2.76	0.04	3
79	ARKXXVII/1	96	2012	7	3	-11.920	79.503	237.69	237.69	-0.27	34.270	-0.275	285.95	-0.39	0.04	3
80	ARKXXVII/1	96	2012	7	3	-11.920	79.503	202.24	202.24	-0.42	34.170	-0.424	300.90	-0.66	0.13	3
81	ARKXXVII/1	96	2012	7	3	-11.920	79.503	161.58	161.58	-0.91	33.684	-0.916	316.41	-0.91	0.08	4
82	ARKXXVII/1	96	2012	7	3	-11.920	79.503	121.52	121.52	-1.63	32.411	-1.628	347.23	-2.02	0.15	7
83	ARKXXVII/1	96	2012	7	3	-11.920	79.503	80.60	80.60	-1.69	31.800	-1.690	375.02	-2.65	0.05	3
84	ARKXXVII/1	96	2012	7	3	-11.920	79.503	61.06	61.06	-1.64	31.745	-1.644	381.69	-1.61	2.35	5
85	ARKXXVII/1	96	2012	7	3	-11.920	79.503	50.67	50.67	-1.57	31.717	-1.566	383.16	-2.71	0.06	5
86	ARKXXVII/1	96	2012	7	3	-11.920	79.503	40.31	40.31	-1.44	31.680	-1.444	390.00	-2.72	0.06	3

Table A3, Chapter I: CTD and stable oxygen isotope data (continued)

Nr.	Cruise	Station	Year	Month	Day	Longitude [−E]	Latitude [−N]	Depth [m]	Pressure [dB]	Temperature [°C]	Salinity [PSU]	Pot. Temp. [°C]	O2 [µmol/kg]	δ18O (‰ VSMOW)	o18-stdev	o18-n
87	ARKXXVII/1	96	2012	7	3	-11.920	79.503	30.49	30.49	-1.15	31.476	-1.152	411.37	-2.67	0.06	6
88	ARKXXVII/1	96	2012	7	3	-11.920	79.503	20.04	20.04	0.65	31.272	0.645	399.56	-2.71	0.10	6
89	ARKXXVII/1	96	2012	7	3	-11.920	79.503	10.20	10.20	0.35	31.046	0.350	378.13	-2.68	0.06	3
90	ARKXXVII/1	96	2012	7	3	-11.920	79.503	1.54	1.54	0.01	30.782	0.013	378.12	-2.72	0.11	5
91	ARKXXVII/1	100	2012	7	4	-11.118	79.334	236.42	236.42	-0.14	34.349	-0.143	291.17	-0.31	0.09	3
92	ARKXXVII/1	100	2012	7	4	-11.118	79.334	236.48	236.48	-0.13	34.349	-0.142	0.00	-0.31	0.06	5
93	ARKXXVII/1	100	2012	7	4	-11.118	79.334	202.96	202.96	-0.39	34.194	-0.391	298.46	-0.54	0.04	5
94	ARKXXVII/1	100	2012	7	4	-11.118	79.334	162.07	162.07	-0.94	33.662	-0.942	316.39	-0.97	0.09	7
95	ARKXXVII/1	100	2012	7	4	-11.118	79.334	142.06	142.06	-1.24	33.126	-1.245	329.10	-1.46	0.08	3
96	ARKXXVII/1	100	2012	7	4	-11.118	79.334	121.62	121.62	-1.61	32.358	-1.615	347.78	-2.08	0.06	3
97	ARKXXVII/1	100	2012	7	4	-11.118	79.334	81.14	81.14	-1.70	31.791	-1.697	372.77	-2.65	0.08	3
98	ARKXXVII/1	100	2012	7	4	-11.118	79.334	60.75	60.75	-1.66	31.748	-1.660	379.88	-2.69	0.13	8
99	ARKXXVII/1	100	2012	7	4	-11.118	79.334	51.00	51.00	-1.65	31.742	-1.647	383.33	-2.66	0.02	3
100	ARKXXVII/1	100	2012	7	4	-11.118	79.334	40.65	40.65	-1.59	31.728	-1.587	388.19	-2.71	0.07	3
101	ARKXXVII/1	100	2012	7	4	-11.118	79.334	30.69	30.69	-1.52	31.713	-1.524	398.41	-2.61	0.06	3
102	ARKXXVII/1	100	2012	7	4	-11.118	79.334	20.74	20.74	-0.97	31.645	-0.966	404.37	-2.72	0.00	1
103	ARKXXVII/1	100	2012	7	4	-11.118	79.334	10.54	10.54	0.05	31.111	0.051	391.23	-2.70	0.03	3
104	ARKXXVII/1	100	2012	7	4	-11.118	79.334	1.13	1.13	-0.08	30.988	-0.078	382.05	-2.70	0.11	4
105	ARKXXVII/1	102	2012	7	4	-10.725	79.166	295.29	295.29	0.01	34.421	-0.005	288.55	-0.27	0.08	3
106	ARKXXVII/1	102	2012	7	4	-10.725	79.166	283.15	283.15	-0.01	34.413	-0.020	290.38	-0.21	0.09	4
107	ARKXXVII/1	102	2012	7	4	-10.725	79.166	242.47	242.47	-0.09	34.373	-0.098	292.13	-0.31	0.11	2
108	ARKXXVII/1	102	2012	7	4	-10.725	79.166	201.96	201.96	-0.38	34.224	-0.385	299.01	-0.41	0.11	5
109	ARKXXVII/1	102	2012	7	4	-10.725	79.166	161.62	161.62	-1.03	33.617	-1.029	314.76	-0.87	0.07	4
110	ARKXXVII/1	102	2012	7	4	-10.725	79.166	141.59	141.59	-1.38	33.028	-1.380	334.01	-1.57	0.03	3
111	ARKXXVII/1	102	2012	7	4	-10.725	79.166	121.28	121.28	-1.64	32.267	-1.644	350.28	-2.10	0.07	3
112	ARKXXVII/1	102	2012	7	4	-10.725	79.166	80.90	80.90	-1.69	31.820	-1.694	375.04	-2.65	0.11	6
113	ARKXXVII/1	102	2012	7	4	-10.725	79.166	60.42	60.42	-1.67	31.767	-1.669	377.53	-2.74	0.00	1
114	ARKXXVII/1	102	2012	7	4	-10.725	79.166	50.71	50.71	-1.66	31.744	-1.662	378.86	-2.68	0.05	5
115	ARKXXVII/1	102	2012	7	4	-10.725	79.166	40.98	40.98	-1.64	31.732	-1.645	380.72	-2.69	0.00	3
116	ARKXXVII/1	102	2012	7	4	-10.725	79.166	30.30	30.30	-1.62	31.723	-1.622	385.25	-2.70	0.00	1
117	ARKXXVII/1	102	2012	7	4	-10.725	79.166	10.40	10.40	-1.34	31.212	-1.336	405.94	-2.71	0.06	3
118	ARKXXVII/1	102	2012	7	4	-10.725	79.166	2.86	2.86	-1.11	30.362	-1.111	399.61	-2.67	0.00	1
119	ARKXXVII/1	106	2012	7	5	-10.671	78.832	372.49	372.49	0.25	34.535	0.231	288.42	-0.11	0.05	3
120	ARKXXVII/1	106	2012	7	5	-10.671	78.832	303.10	303.10	0.11	34.457	0.097	294.80	-0.20	0.06	3
121	ARKXXVII/1	106	2012	7	5	-10.671	78.832	202.28	202.28	-0.46	34.179	-0.465	301.16	-0.34	0.04	3
122	ARKXXVII/1	106	2012	7	5	-10.671	78.832	161.43	161.43	-1.37	33.601	-1.373	316.80	-0.87	0.10	5
123	ARKXXVII/1	106	2012	7	5	-10.671	78.832	141.13	141.13	-1.31	33.091	-1.311	332.16	-1.52	0.07	6
124	ARKXXVII/1	106	2012	7	5	-10.671	78.832	121.08	121.08	-1.60	32.454	-1.604	352.63	-2.21	0.02	2
125	ARKXXVII/1	106	2012	7	5	-10.671	78.832	81.05	81.05	-1.64	31.810	-1.642	373.41	-2.60	0.05	3
126	ARKXXVII/1	106	2012	7	5	-10.671	78.832	60.34	60.34	-1.62	31.750	-1.618	377.53	-2.77	0.03	3
127	ARKXXVII/1	106	2012	7	5	-10.671	78.832	50.13	50.13	-1.57	31.733	-1.573	380.40	-2.73	0.09	7
128	ARKXXVII/1	106	2012	7	5	-10.671	78.832	40.24	40.24	-1.51	31.716	-1.507	385.65	-2.75	0.10	3
129	ARKXXVII/1	106	2012	7	5	-10.671	78.832	30.18	30.18	-1.42	31.703	-1.415	395.09	-2.69	0.08	6
130	ARKXXVII/1	106	2012	7	5	-10.671	78.832	20.32	20.32	-1.35	31.675	-1.352	402.93	-2.77	0.14	3
131	ARKXXVII/1	106	2012	7	5	-10.671	78.832	10.08	10.08	-0.59	30.957	-0.592	395.27	-2.67	0.06	7
132	ARKXXVII/1	106	2012	7	5	-10.671	78.832	1.64	1.64	-0.44	30.649	-0.438	389.74	-2.69	0.06	3
133	ARKXXVII/1	112	2012	7	6	-11.998	78.833	197.88	197.88	-0.58	34.112	-0.586	308.15	-0.56	0.04	2
134	ARKXXVII/1	112	2012	7	6	-11.998	78.833	160.45	160.45	-1.35	33.526	-1.350	327.74	-1.22	0.03	3
135	ARKXXVII/1	112	2012	7	6	-11.998	78.833	141.52	141.52	-1.45	33.256	-1.454	332.58	-1.49	0.05	4
136	ARKXXVII/1	112	2012	7	6	-11.998	78.833	122.29	122.29	-1.60	32.618	-1.601	341.12	-1.81	0.03	5
137	ARKXXVII/1	112	2012	7	6	-11.998	78.833	81.30	81.30	-1.69	31.959	-1.695	371.86	-2.62	0.06	3
138	ARKXXVII/1	112	2012	7	6	-11.998	78.833	61.22	61.22	-1.64	31.801	-1.638	376.15	-2.63	0.03	5
139	ARKXXVII/1	112	2012	7	6	-11.998	78.833	50.93	50.93	-1.59	31.756	-1.586	379.93	-2.68	0.08	5
140	ARKXXVII/1	112	2012	7	6	-11.998	78.833	40.79	40.79	-1.58	31.730	-1.578	382.78	-2.73	0.03	5
141	ARKXXVII/1	112	2012	7	6	-11.998	78.833	30.54	30.54	-1.43	31.698	-1.427	395.09	-2.68	0.04	5
142	ARKXXVII/1	112	2012	7	6	-11.998	78.833	19.92	19.92	-1.38	31.337	-1.385	407.13	-2.73	0.04	3
143	ARKXXVII/1	112	2012	7	6	-11.998	78.833	10.50	10.50	-1.41	31.137	-1.410	410.03	-2.72	0.06	3
144	ARKXXVII/1	112	2012	7	6	-11.998	78.833	1.75	1.75	-1.44	30.804	-1.439	413.48	-2.70	0.08	5
145	ARKXXVII/1	114	2012	7	6	-12.784	78.754	203.82	203.82	-0.63	34.042	-0.636	306.51	-0.63	0.03	6
146	ARKXXVII/1	114	2012	7	6	-12.784	78.754	161.80	161.80	-1.14	33.761	-1.139	327.27	-0.92	0.08	5
147	ARKXXVII/1	114	2012	7	6	-12.784	78.754	140.95	140.95	-1.50	33.230	-1.503	331.75	-1.41	0.07	6
148	ARKXXVII/1	114	2012	7	6	-12.784	78.754	121.24	121.24	-1.60	32.760	-1.601	338.61	-1.80	0.05	4
149	ARKXXVII/1	114	2012	7	6	-12.784	78.754	101.24	101.24	-1.68	32.175	-1.677	350.36	-2.17	0.11	6
150	ARKXXVII/1	114	2012	7	6	-12.784	78.754	81.31	81.31	-1.70	31.914	-1.699	366.65	-2.49	0.06	5
151	ARKXXVII/1	114	2012	7	6	-12.784	78.754	40.49	40.49	-1.59	31.748	-1.590	381.99	-2.72	0.10	7
152	ARKXXVII/1	114	2012	7	6	-12.784	78.754	30.41	30.41	-1.50	31.587	-1.497	402.28	-2.67	0.07	4
153	ARKXXVII/1	114	2012	7	6	-12.784	78.754	20.45	20.45	-1.54	31.448	-1.544	409.43	-2.72	0.02	3
154	ARKXXVII/1	114	2012	7	6	-12.784	78.754	9.84	9.84	-1.53	30.720	-1.532	415.48	-2.72	0.08	7
155	ARKXXVII/1	114	2012	7	6	-12.784	78.754	1.50	1.50	-1.53	30.655	-1.530	409.77	-2.68	0.04	3
156	ARKXXVII/1	115	2012	7	6	-10.996	78.832	321.04	321.04	0.22	34.524	0.210	289.99	-0.16	0.12	7
157	ARKXXVII/1	115	2012	7	6	-10.996	78.832	283.96	283.96	0.12	34.467	0.110	296.31	-0.23	0.10	7
158	ARKXXVII/1	115	2012	7	6	-10.996	78.832	243.39	243.39	-0.05	34.389	-0.057	296.89	-0.39	0.02	3
159	ARKXXVII/1	115	2012	7	6	-10.996	78.832	202.76	202.76	-0.46	34.181	-0.469	301.50	-0.51	0.16	3
160	ARKXXVII/1	115	2012	7	6	-10.996	78.832	162.21	162.21	-1.23	33.640	-1.231	318.54	-0.98	0.13	6
161	ARKXXVII/1	115	2012	7	6	-10.996	78.832	141.94	141.94	-1.53	33.090	-1.532	328.67	-1.34	0.12	7
162	ARKXXVII/1	115	2012	7	6	-10.996	78.832	122.00	122.00	-1.61	32.480	-1.613	345.85	-2.10	0.08	3
163	ARKXXVII/1	115	2012	7	6	-10.996	78.832	101.38	101.38	-1.69	31.998	-1.691	366.64	-2.53	0.11	3
164	ARKXXVII/1	115	2012	7	6	-10.996	78.832	81.51	81.51	-1.66	31.819	-1.657	372.93	-2.69	0.05	3
165	ARKXXVII/1	115	2012	7	6	-10.996	78.832	40.20	40.20	-1.47	31.705	-1.474	385.98	-2.82	0.04	2
166	ARKXXVII/1	115	2012	7	6	-10.996	78.832	30.75	30.75	-1.37	31.680	-1.371	398.82	-2.87	0.00	1
167	ARKXXVII/1	115	2012	7	6	-10.996	78.832	20.90	20.90	-1.15	31.637	-1.149	405.81	-2.70	0.08	5
168	ARKXXVII/1	115	2012	7	6	-10.996	78.832	10.64	10.64	-1.04	31.241	-1.040	410.59	-2.72	0.03	3
169	ARKXXVII/1	115	2012	7	6	-10.996	78.832	1.41	1.41	-0.20	30.620	-0.203	385.78	-2.81	0.03	3
184	ARKXXVII/1	119	2012	7	7	-9.001	78.834	218.40	218.40	-0.44	34.199	-0.449	302.09	-0.48	0.11	7
185	ARKXXVII/1	119	2012	7	7	-9.001	78.834	202.00	202.00	-0.45	34.196	-0.455	302.21	-0.48	0.09	7
186	ARKXXVII/1	119	2012	7	7	-9.001	78.834	161.48	161.48	-1.07	33.826	-1.074	313.20	-0.62	0.06	3

Table A3, Chapter I: CTD and stable oxygen isotope data (continued)

Nr.	Cruise	Station	Year	Month	Day	Longitude [¬E]	Latitude [¬N]	Depth [m]	Pressure [dB]	Temperature [°C]	Salinity [PSU]	Pot. Temp. [°C]	O2 [µmol/kg]	δ18O (‰ VSMOW)	o18-stdev	o18-n
187	ARKXXVII/1	119	2012	7	7	-9.001	78.834	141.37	141.37	-1.35	33.483	-1.352	325.08	-1.08	0.08	5
188	ARKXXVII/1	119	2012	7	7	-9.001	78.834	121.25	121.25	-1.63	32.477	-1.634	344.37	-2.07	0.06	3
189	ARKXXVII/1	119	2012	7	7	-9.001	78.834	100.96	100.96	-1.72	32.056	-1.720	364.86	-2.51	0.07	3
189	ARKXXVII/1	119	2012	7	7	-9.001	78.834	100.96	100.96	-1.72	32.056	-1.720	364.86	-2.51	0.07	3
190	ARKXXVII/1	119	2012	7	7	-9.001	78.834	80.83	80.83	-1.72	31.884	-1.717	374.60	-2.66	0.03	3
191	ARKXXVII/1	119	2012	7	7	-9.001	78.834	40.31	40.31	-1.55	31.784	-1.550	402.60	-2.70	0.07	6
192	ARKXXVII/1	119	2012	7	7	-9.001	78.834	30.47	30.47	-1.07	31.691	-1.070	406.89	-2.72	0.02	3
193	ARKXXVII/1	119	2012	7	7	-9.001	78.834	20.24	20.24	-1.01	31.524	-1.008	409.34	-2.74	0.10	5
194	ARKXXVII/1	119	2012	7	7	-9.001	78.834	9.94	9.94	-0.64	31.070	-0.636	408.45	-2.79	0.11	7
195	ARKXXVII/1	119	2012	7	7	-9.001	78.834	1.59	1.59	-0.35	30.915	-0.352	375.58	-2.79	0.10	7
196	ARKXXVII/1	121	2012	7	7	-7.996	78.833	184.04	184.04	-0.50	34.268	-0.506	306.62	-0.40	0.06	5
197	ARKXXVII/1	121	2012	7	7	-7.996	78.833	162.41	162.41	-0.70	34.221	-0.707	308.08	-0.42	0.08	6
198	ARKXXVII/1	121	2012	7	7	-7.996	78.833	142.05	142.05	-0.97	34.048	-0.972	319.42	-0.65	0.08	5
199	ARKXXVII/1	121	2012	7	7	-7.996	78.833	121.28	121.28	-1.18	33.449	-1.186	323.96	-1.18	0.07	5
200	ARKXXVII/1	121	2012	7	7	-7.996	78.833	101.40	101.40	-1.57	32.519	-1.567	338.05	-1.78	0.09	4
201	ARKXXVII/1	121	2012	7	7	-7.996	78.833	81.25	81.25	-1.71	31.967	-1.707	359.68	-2.31	0.06	5
202	ARKXXVII/1	121	2012	7	7	-7.996	78.833	41.01	41.01	-1.67	31.754	-1.665	382.33	-2.72	0.06	7
203	ARKXXVII/1	121	2012	7	7	-7.996	78.833	30.79	30.79	-1.54	31.726	-1.540	386.59	-2.78	0.04	3
204	ARKXXVII/1	121	2012	7	7	-7.996	78.833	20.37	20.37	-1.17	31.461	-1.165	399.32	-2.77	0.08	5
205	ARKXXVII/1	121	2012	7	7	-7.996	78.833	10.55	10.55	-0.63	31.012	-0.625	405.94	-2.80	0.08	7
206	ARKXXVII/1	121	2012	7	7	-7.996	78.833	2.69	2.69	-0.61	31.010	-0.614	324.67	-2.74	0.07	4
207	ARKXXVII/1	123	2012	7	7	-7.009	78.709	225.76	225.76	1.07	34.821	1.061	305.52	0.10	0.13	9
208	ARKXXVII/1	123	2012	7	7	-7.009	78.709	202.64	202.64	0.98	34.785	0.969	292.85	0.03	0.09	5
209	ARKXXVII/1	123	2012	7	7	-7.009	78.709	161.84	161.84	-0.15	34.405	-0.154	297.99	-0.29	0.08	5
210	ARKXXVII/1	123	2012	7	7	-7.009	78.709	141.65	141.65	-0.62	34.263	-0.627	304.52	-0.38	0.10	5
211	ARKXXVII/1	123	2012	7	7	-7.009	78.709	121.38	121.38	-1.51	34.033	-1.516	328.86	-0.62	0.10	7
212	ARKXXVII/1	123	2012	7	7	-7.009	78.709	101.34	101.34	-1.74	33.936	-1.740	334.43	-0.61	0.11	6
213	ARKXXVII/1	123	2012	7	7	-7.009	78.709	80.91	80.91	-1.73	33.832	-1.729	336.53	-0.73	0.13	7
214	ARKXXVII/1	123	2012	7	7	-7.009	78.709	40.84	40.84	-1.65	33.189	-1.648	333.70	-1.19	0.07	5
215	ARKXXVII/1	123	2012	7	7	-7.009	78.709	30.11	30.11	-1.58	32.762	-1.582	339.20	-1.65	0.07	3
216	ARKXXVII/1	123	2012	7	7	-7.009	78.709	20.21	20.21	-1.52	31.988	-1.515	359.83	-2.30	0.10	5
217	ARKXXVII/1	123	2012	7	7	-7.009	78.709	10.29	10.29	-1.55	31.665	-1.554	363.44	-2.38	0.06	3
218	ARKXXVII/1	123	2012	7	7	-7.009	78.709	1.32	1.32	-1.55	31.674	-1.549	365.04	-2.34	0.10	7
219	ARKXXVII/1	125	2012	7	8	-6.017	78.843	331.83	331.83	1.48	34.918	1.460	294.56	0.14	0.10	5
220	ARKXXVII/1	125	2012	7	8	-6.017	78.843	303.68	303.68	1.81	34.913	1.797	294.73	0.13	0.10	8
221	ARKXXVII/1	125	2012	7	8	-6.017	78.843	253.18	253.18	1.44	34.794	1.429	295.69	0.02	0.08	5
222	ARKXXVII/1	125	2012	7	8	-6.017	78.843	202.80	202.80	-0.44	34.353	-0.444	299.80	-0.24	0.05	4
223	ARKXXVII/1	125	2012	7	8	-6.017	78.843	151.64	151.64	-1.79	33.943	-1.788	338.09	-0.65	0.00	2
224	ARKXXVII/1	125	2012	7	8	-6.017	78.843	101.25	101.25	-1.60	33.434	-1.603	331.03	-1.11	0.06	6
225	ARKXXVII/1	125	2012	7	8	-6.017	78.843	75.71	75.71	-1.63	33.083	-1.631	329.06	-1.60	0.11	7
226	ARKXXVII/1	125	2012	7	8	-6.017	78.843	50.71	50.71	-1.66	32.214	-1.664	348.97	-2.29	0.11	5
227	ARKXXVII/1	125	2012	7	8	-6.017	78.843	25.30	25.30	-1.53	31.528	-1.530	376.38	-2.68	0.07	5
228	ARKXXVII/1	125	2012	7	8	-6.017	78.843	10.17	10.17	-1.50	31.446	-1.502	372.16	-2.77	0.08	6
229	ARKXXVII/1	128	2012	7	8	-4.939	78.834	1049.70	1049.70	-0.18	34.893	-0.227	296.85	0.00	0.04	3
230	ARKXXVII/1	128	2012	7	8	-4.939	78.834	811.01	811.01	0.04	34.880	0.008	295.77	0.14	0.11	5
231	ARKXXVII/1	128	2012	7	8	-4.939	78.834	607.04	607.04	0.34	34.871	0.309	294.25	0.10	0.14	6
232	ARKXXVII/1	128	2012	7	8	-4.939	78.834	406.31	406.31	1.19	34.890	1.168	292.98	0.16	0.11	7
233	ARKXXVII/1	128	2012	7	8	-4.939	78.834	304.81	304.81	2.13	34.936	2.116	295.85	0.12	0.09	5
234	ARKXXVII/1	128	2012	7	8	-4.939	78.834	253.57	253.57	2.59	34.955	2.579	294.89	0.17	0.15	7
235	ARKXXVII/1	128	2012	7	8	-4.939	78.834	202.57	202.57	1.15	34.685	1.143	293.92	0.11	0.13	7
236	ARKXXVII/1	128	2012	7	8	-4.939	78.834	151.87	151.87	-1.08	34.216	-1.085	307.09	-0.35	0.08	5
237	ARKXXVII/1	128	2012	7	8	-4.939	78.834	101.36	101.36	-1.81	34.011	-1.808	344.03	-0.72	0.16	6
238	ARKXXVII/1	128	2012	7	8	-4.939	78.834	76.08	76.08	-1.78	33.954	-1.781	340.04	-0.86	0.11	5
239	ARKXXVII/1	128	2012	7	8	-4.939	78.834	50.82	50.82	-1.67	33.326	-1.672	336.05	-1.25	0.10	7
240	ARKXXVII/1	128	2012	7	8	-4.939	78.834	25.24	25.24	-1.69	32.332	-1.689	340.09	-2.23	0.10	7
241	ARKXXVII/1	128	2012	7	8	-4.939	78.834	10.37	10.37	-1.64	32.078	-1.637	351.20	-2.36	0.09	5
242	ARKXXVII/1	128	2012	7	8	-4.939	78.834	1.48	1.48	-1.63	32.072	-1.630	352.16	-2.37	0.12	5
243	ARKXXVII/1	132	2012	7	9	-3.920	78.833	608.16	608.16	0.24	34.872	0.216	296.69	0.18	0.13	7
244	ARKXXVII/1	132	2012	7	9	-3.920	78.833	405.02	405.02	0.82	34.878	0.796	297.64	0.15	0.10	7
245	ARKXXVII/1	132	2012	7	9	-3.920	78.833	405.37	405.37	0.81	34.878	0.795	303.76	0.23	0.10	4
246	ARKXXVII/1	132	2012	7	9	-3.920	78.833	202.37	202.37	2.88	35.029	2.863	306.35	0.24	0.13	7
247	ARKXXVII/1	132	2012	7	9	-3.920	78.833	100.56	100.56	2.82	34.930	2.812	304.41	0.24	0.09	5
248	ARKXXVII/1	132	2012	7	9	-3.920	78.833	76.11	76.11	0.89	34.491	0.883	312.31	0.21	0.06	5
249	ARKXXVII/1	132	2012	7	9	-3.920	78.833	50.64	50.64	-1.70	34.010	-1.701	317.21	0.12	0.11	5
250	ARKXXVII/1	132	2012	7	9	-3.920	78.833	50.68	50.68	-1.73	34.002	-1.728	325.95	-0.09	0.04	5
251	ARKXXVII/1	132	2012	7	9	-3.920	78.833	37.81	37.81	-1.69	33.933	-1.686	366.78	-0.34	0.09	5
252	ARKXXVII/1	132	2012	7	9	-3.920	78.833	12.40	12.40	-1.53	32.827	-1.525	376.96	-0.67	0.10	6
253	ARKXXVII/1	132	2012	7	9	-3.920	78.833	5.13	5.13	-1.51	32.701	-1.512	393.82	-0.90	0.08	8
254	ARKXXVII/1	135	2012	7	9	-3.019	78.835	607.76	607.76	0.33	34.866	0.304	293.67	0.22	0.07	7
255	ARKXXVII/1	135	2012	7	9	-3.019	78.835	404.78	404.78	1.34	34.913	1.322	295.96	0.20	0.06	6
256	ARKXXVII/1	135	2012	7	9	-3.019	78.835	303.19	303.19	2.86	35.044	2.836	301.07	0.19	0.11	7
257	ARKXXVII/1	135	2012	7	9	-3.019	78.835	253.19	253.19	2.92	35.030	2.903	300.43	0.20	0.05	5
258	ARKXXVII/1	135	2012	7	9	-3.019	78.835	202.18	202.18	3.21	35.042	3.194	301.18	0.23	0.11	5
259	ARKXXVII/1	135	2012	7	9	-3.019	78.835	151.30	151.30	3.08	34.990	3.069	304.43	0.19	0.10	6
260	ARKXXVII/1	135	2012	7	9	-3.019	78.835	101.42	101.42	-0.02	34.488	-0.024	296.89	-0.04	0.07	5
261	ARKXXVII/1	135	2012	7	9	-3.019	78.835	75.74	75.74	-0.84	34.285	-0.841	313.73	-0.33	0.08	5
262	ARKXXVII/1	135	2012	7	9	-3.019	78.835	50.79	50.79	-1.71	34.062	-1.712	342.50	-0.57	0.10	4
263	ARKXXVII/1	135	2012	7	9	-3.019	78.835	25.79	25.79	-1.48	33.704	-1.477	330.84	-0.95	0.06	5
264	ARKXXVII/1	135	2012	7	9	-3.019	78.835	10.42	10.42	-0.90	32.331	-0.895	379.16	-0.50	0.09	5

Table A3, Chapter I: CTD and nutrient data

Nr.	Cruise	Station	Year	Month	Day	Longitude [°E]	Latitude [°N]	Depth [m]	Pressure [dB]	Temperature [°C]	Salinity [PSU]	Pot. Temp. [°C]	O2 [µmol/kg]	nitrite [mumol/kg]	nitrate [mumol/kg]	phosphate [mumol/kg]	silicate [mumol/kg]
1	ARKXXVII/1	8	2012	6	19	11.107	75.001	2476.289	2476.289	-0.789	34.912	-0.916	293.895	0.022	15.036	1.113	12.238
2	ARKXXVII/1	8	2012	6	19	11.107	75.001	2029.731	2029.731	-0.789	34.911	-0.885	298.248	0.013	15.316	1.051	10.955
3	ARKXXVII/1	8	2012	6	19	11.107	75.001	1776.247	1776.247	-0.757	34.91	-0.838	312.214	0.127	12.74	0.919	9.609
4	ARKXXVII/1	8	2012	6	19	11.107	75.001	1521.208	1521.208	-0.689	34.907	-0.755	304.704	0.081	14.38	1.02	9.318
5	ARKXXVII/1	8	2012	6	19	11.107	75.001	1265.807	1265.807	-0.589	34.904	-0.642	312.506	0	20.07	1.395	11.368
6	ARKXXVII/1	8	2012	6	19	11.107	75.001	1012.26	1012.26	-0.452	34.904	-0.494	312.392	0.059	11.639	0.72	6.307
7	ARKXXVII/1	8	2012	6	19	11.107	75.001	810.163	810.163	-0.22	34.904	-0.253	314.359	0.053	12.536	0.967	6.365
8	ARKXXVII/1	8	2012	6	19	11.107	75.001	606.878	606.878	0.547	34.93	0.519	311.348	0.07	11.368	0.859	5.36
9	ARKXXVII/1	8	2012	6	19	11.107	75.001	405.039	405.039	2.544	35.052	2.519	312.635	0.052	11.232	0.876	4.461
10	ARKXXVII/1	8	2012	6	19	11.107	75.001	302.541	302.541	3.358	35.101	3.338	306.229	0.047	10.992	0.842	4.418
11	ARKXXVII/1	8	2012	6	19	11.107	75.001	201.719	201.719	3.804	35.132	3.79	308.372	0.07	10.787	0.744	4.237
12	ARKXXVII/1	8	2012	6	19	11.107	75.001	100.146	100.146	4.164	35.145	4.157	308.643	0.275	12.157	0.838	4.974
13	ARKXXVII/1	8	2012	6	19	11.107	75.001	50.642	50.642	4.575	35.15	4.571	308.808	0.319	10.944	0.878	4.791
14	ARKXXVII/1	8	2012	6	19	11.107	75.001	9.666	9.666	5.633	35.156	5.632	330.664	0.128	6.059	0.398	3.253
15	ARKXXVII/1	15	2012	6	20	9.001	78.835	210.824	210.824	3.647	35.087	3.632	301.267	0.208	11.488	0.678	4.834
16	ARKXXVII/1	15	2012	6	20	9.001	78.835	202.722	202.722	3.649	35.087	3.635	301.865	0.218	11.491	0.68	4.839
17	ARKXXVII/1	15	2012	6	20	9.001	78.835	101.34	101.34	4.152	35.108	4.144	304.082	0.315	10.834	0.635	3.986
18	ARKXXVII/1	15	2012	6	20	9.001	78.835	51.024	51.024	2.569	34.852	2.566	322.464	0.17	4.918	0.42	1.397
19	ARKXXVII/1	15	2012	6	20	9.001	78.835	10.536	10.536	2.825	34.733	2.825		0.096	1.197	0.172	0.595
20	ARKXXVII/1	20	2012	6	20	8.027	78.852	1020.495	1020.495	-0.855	34.91	-0.893	294.027	0.014	14.74	0.792	12.083
21	ARKXXVII/1	20	2012	6	20	8.027	78.852	810.182	810.182	-0.691	34.908	-0.721	296.303	0.012	14.464	0.711	10.097
22	ARKXXVII/1	20	2012	6	20	8.027	78.852	607.633	607.633	-0.061	34.919	-0.086	299.762	0.009	13.839	0.718	8.439
23	ARKXXVII/1	20	2012	6	20	8.027	78.852	404.946	404.946	1.312	34.984	1.292	311.77	0.026	12.647	0.638	5.532
24	ARKXXVII/1	20	2012	6	20	8.027	78.852	303.695	303.695	2.155	35.036	2.138	312.621	0.03	11.825	0.611	4.886
25	ARKXXVII/1	20	2012	6	20	8.027	78.852	203.065	203.065	2.877	35.079	2.864	307.47	0.045	11.991	0.666	4.858
26	ARKXXVII/1	20	2012	6	20	8.027	78.852	101.916	101.916	3.502	35.122	3.496	312.102	0.192	10.436	0.608	4.307
27	ARKXXVII/1	20	2012	6	20	8.027	78.852	51.193	51.193	3.78	35.126	3.777	314.796	0.157	9.749	0.611	4.241
28	ARKXXVII/1	20	2012	6	20	8.027	78.852	10.567	10.567	5.21	35.054	5.209	365.095	0.034	0.373	0.123	2.071
29	ARKXXVII/1	27	2012	6	21	7.012	78.831	1434.696	1434.696	-0.847	34.911	-0.906	292.439	0.022	14.73	0.788	11.398
30	ARKXXVII/1	27	2012	6	21	7.012	78.831	1267.313	1267.313	-0.833	34.91	-0.884	294.292	0.01	14.6	0.752	10.972
31	ARKXXVII/1	27	2012	6	21	7.012	78.831	1012.975	1012.975	-0.758	34.908	-0.797	296.481	0.005	14.248	0.713	10.662
32	ARKXXVII/1	27	2012	6	21	7.012	78.831	809.697	809.697	-0.653	34.905	-0.684	307.203	0.006	13.627	0.678	8.533
33	ARKXXVII/1	27	2012	6	21	7.012	78.831	607.257	607.257	-0.277	34.912	-0.3	300.994	0.011	13.768	0.722	8.593
34	ARKXXVII/1	27	2012	6	21	7.012	78.831	404.346	404.346	1.023	34.963	1.004	302.093	0.011	13.166	0.691	6.418
35	ARKXXVII/1	27	2012	6	21	7.012	78.831	303.496	303.496	2.134	35.029	2.116	307.948	0.021	12.116	0.606	5.35
36	ARKXXVII/1	27	2012	6	21	7.012	78.831	202.374	202.374	3.149	35.095	3.136	306.058	0.068	11.539	0.565	4.791
37	ARKXXVII/1	27	2012	6	21	7.012	78.831	101.266	101.266	3.663	35.113	3.656	308.107	0.197	10.571	0.535	4.375
38	ARKXXVII/1	27	2012	6	21	7.012	78.831	50.356	50.356	3.968	35.128	3.965	308.172	0.198	10.432	0.534	4.284
39	ARKXXVII/1	27	2012	6	21	7.012	78.831	10.95	10.95	4.683	35.096	4.682	323.574	0.181	6.42	0.399	3.119
40	ARKXXVII/1	37	2012	6	22	5.992	78.833	2452.866	2452.866	-0.793	34.916	-0.918	294.776	0.021	14.445	0.72	11.437
41	ARKXXVII/1	37	2012	6	22	5.992	78.833	2031.327	2031.327	-0.789	34.912	-0.886	293.708	0.019	14.405	0.715	11.175
42	ARKXXVII/1	37	2012	6	22	5.992	78.833	1776.407	1776.407	-0.766	34.911	-0.846	295.892	0	14.209	0.754	10.52
43	ARKXXVII/1	37	2012	6	22	5.992	78.833	1521.73	1521.73	-0.703	34.908	-0.769	299.98	0.014	13.677	0.725	9.494
44	ARKXXVII/1	37	2012	6	22	5.992	78.833	1267.044	1267.044	-0.626	34.906	-0.679	314.461	0.017	13.083	0.64	7.474
45	ARKXXVII/1	37	2012	6	22	5.992	78.833	1012.817	1012.817	-0.495	34.907	-0.536	318.001	0.009	12.92	0.657	7.247
46	ARKXXVII/1	37	2012	6	22	5.992	78.833	810.175	810.175	-0.298	34.912	-0.331	314.34	0.018	12.951	0.627	7.186
47	ARKXXVII/1	37	2012	6	22	5.992	78.833	404.712	404.712	1.393	34.99	1.373	310.405	0.025	12.214	0.61	6.004
48	ARKXXVII/1	37	2012	6	22	5.992	78.833	303.253	303.253	2.634	35.066	2.616	309.937	0.072	11.652	0.606	4.863
49	ARKXXVII/1	37	2012	6	22	5.992	78.833	202.352	202.352	3.4	35.111	3.386	306.288	0.051	11.514	0.589	4.927
50	ARKXXVII/1	37	2012	6	22	5.992	78.833	100.989	100.989	3.73	35.124	3.723	307.596	0.203	10.931	0.553	4.672
51	ARKXXVII/1	37	2012	6	22	5.992	78.833	50.18	50.18	3.947	35.128	3.943	306.532	0.242	10.612	0.585	4.662
52	ARKXXVII/1	37	2012	6	22	5.992	78.833	10.604	10.604	4.746	35.112	4.745	340.462	0.147	4.158	0.319	3.788
53	ARKXXVII/1	51	2012	6	24	5.110	78.834	2648.547	2648.547	-0.742	34.926	-0.883	295.439	0.033	14.384	0.838	10.808
54	ARKXXVII/1	51	2012	6	24	5.110	78.834	2542.006	2542.006	-0.75	34.925	-0.883	295.191	0.027	14.314	0.834	10.87
55	ARKXXVII/1	51	2012	6	24	5.110	78.834	2031.01	2031.01	-0.781	34.915	-0.877	294.06	0.033	14.575	0.911	11.073
56	ARKXXVII/1	51	2012	6	24	5.110	78.834	1818.141	1818.141	-0.754	34.914	-0.838	295.26	0.028	14.463	0.86	10.853
57	ARKXXVII/1	51	2012	6	24	5.110	78.834	1776.134	1776.134	-0.751	34.914	-0.832	297.73	0.03	14.397	0.842	10.193
58	ARKXXVII/1	51	2012	6	24	5.110	78.834	1521.42	1521.42	-0.741	34.909	-0.807	299.644	0.026	14.005	0.829	9.493
59	ARKXXVII/1	51	2012	6	24	5.110	78.834	1267.385	1267.385	-0.653	34.91	-0.706	309.59	0.028	13.523	0.79	8.034
60	ARKXXVII/1	51	2012	6	24	5.110	78.834	1013.478	1013.478	-0.589	34.907	-0.629	310.602	0.031	13.331	0.779	7.413
61	ARKXXVII/1	51	2012	6	24	5.110	78.834	810.29	810.29	-0.46	34.908	-0.492	312.162	0.031	13.15	0.768	6.892
62	ARKXXVII/1	51	2012	6	24	5.110	78.834	606.868	606.868	-0.242	34.913	-0.266	310.672	0.03	12.838	0.729	6.363
63	ARKXXVII/1	51	2012	6	24	5.110	78.834	404.421	404.421	0.154	34.929	0.138	309.424	0.034	12.781	0.733	6.185
64	ARKXXVII/1	51	2012	6	24	5.110	78.834	303.596	303.596	0.557	34.945	0.544	314.529	0.089	11.832	0.691	4.917
65	ARKXXVII/1	51	2012	6	24	5.110	78.834	202.052	202.052	1.301	34.989	1.292	315.708	0.155	10.98	0.667	4.597
66	ARKXXVII/1	51	2012	6	24	5.110	78.834	75.723	75.723	2.92	35.092	2.916	312.833	0.157	10.926	0.65	4.499
67	ARKXXVII/1	51	2012	6	24	5.110	78.834	9.922	9.922	4.428	35.099	4.427	355.027	0.117	2.573	0.294	3.473
68	ARKXXVII/1	53	2012	6	25	4.004	78.835	2324.771	2324.771	-0.768	34.923	-0.885	296.197	0.028	14.764	0.924	11.548
69	ARKXXVII/1	53	2012	6	25	4.004	78.835	2031.216	2031.216	-0.788	34.915	-0.884	296.367	0.05	14.919	0.92	11.423
70	ARKXXVII/1	53	2012	6	25	4.004	78.835	1776.223	1776.223	-0.746	34.915	-0.826	296.479	0.036	14.701	0.966	11.014
71	ARKXXVII/1	53	2012	6	25	4.004	78.835	1519.028	1519.028	-0.654	34.917	-0.721	296.849	0.044	14.316	0.971	10.644
72	ARKXXVII/1	53	2012	6	25	4.004	78.835	1268.014	1268.014	-0.568	34.912	-0.622	304.721	0.049	13.814	0.876	8.791
73	ARKXXVII/1	53	2012	6	25	4.004	78.835	1013.57	1013.57	-0.431	34.909	-0.473	296.702	0.043	13.46	0.877	8.318
74	ARKXXVII/1	53	2012	6	25	4.004	78.835	810.34	810.34	-0.059	34.923	-0.093	324.485	0.035	12.861	0.922	6.424
75	ARKXXVII/1	53	2012	6	25	4.004	78.835	607.722	607.722	0.35	34.934	0.323	313.922	0.03	12.744	0.865	6.131
76	ARKXXVII/1	53	2012	6	25	4.004	78.835	404.464	404.464	1.291	34.958	1.271	305.617	0.045	12.061	0.82	5.482
77	ARKXXVII/1	53	2012	6	25	4.004	78.835	304.942	304.942	2.678	35.067	2.66	309.83	0.022	12.109	0.838	4.705
78	ARKXXVII/1	53	2012	6	25	4.004	78.835	202.282	202.282	3.387	35.112	3.373	307.786	0.073	11.611	0.794	4.514
79	ARKXXVII/1	53	2012	6	25	4.004	78.835	101.168	101.168	3.733	35.12	3.726	308.376	0.166	11.146	0.715	4.152
80	ARKXXVII/1	53	2012	6	25	4.004	78.835	50.488	50.488	3.978	35.122	3.975	308.313	0.282	11.125	0.82	3.984
81	ARKXXVII/1	53	2012	6	25	4.004	78.835	9.908	9.908	4.918	34.944	4.917	326.835	0.234	6.241	0.598	2.987
82	ARKXXVII/1	57	2012	6	25	2.997	78.832	2452.28	2452.28	-0.756	34.925	-0.882	290.533	0.014	14.385	0.859	11.012
83	ARKXXVII/1	57	2012	6	25	2.997	78.832	2031.554	2031.554	-0.763	34.916	-0.859	289.932	0.046	14.531	0.825	11.011
84	ARKXXVII/1	57	2012	6	25	2.997	78.832	1776.418	1776.418	-0.709	34.916	-0.79	290.857	0.025	14.342	0.822	10.491
85	ARKXXVII/1	57	2012	6	25	2.997	78.832	1522.323	1522.323	-0.609	34.917	-0.676	292.983	0.016	13.988	0.822	9.791
86	ARKXXVII/1	57	2012	6	25	2.997	78.832	1267.998	1267.998	-0.542	34.908	-0.596	300.565	0.016	13.582	0.771	8.392
87	ARKXXVII/1	57	2012	6	25	2.997	78.832	1013.512	1013.512	-0.352	34.903	-0.395	294.525	0.012	12.941	0.804	7.749
88	ARKXXVII/1	57	2012	6	25	2.997	78.832	810.4	810.4	-0.211	34.89	-0.244	296.266	0.02	12.383	0.729	6.91
89	ARKXXVII/1	57	2012	6	25	2.997	78.832	608.001	608.001	0.497	34.916	0.469	300.198	0.02	12.266	0.689	5.98
90	ARKXXVII/1	57	2012	6	25	2.997	78.832	404.9	404.9	2.084	35.016	2.061	301.151	0.018	11.868	0.668	5.095
91	ARKXXVII/1	57	2012	6	25	2.997	78.832	303.769	303.769	2.746	35.045	2.727	299.216	0.023	11.751	0.714	4.729
92	ARKXXVII/1	57	2012	6	25	2.997	78.832	202.666	202.666	3.254	35.077	3.241	299.9	0.044	11.423	0.638	4.56
93	ARKXXVII/1	57	2012	6	25	2.997	78.832	101.7	101.7	3.508	35.074	3.502	300.951	0.338	10.999	0.618	4.39
94	ARKXXVII/1	57	2012	6	25	2.997	78.832	50.89	50.89	1.338	34.658	1.335	316.922	0.096	7.028	0.523	4.602
95	ARKXXVII/1	57	2012	6	25	2.997	78.832	10.285	10.285	-1.282	33.334	-1.282	363.336	0.077	5.81	0.37	2.858
96	ARKXXVII/1	67	2012	6	27	1.918	78.831	2541.127	2541.127	-0.75	34.925	-0.882	290.37	0.024	14.406	0.876	10.914
97	ARKXXVII/1	67	2012	6	27	1.918	78.831	2541.127	2541.127	-0.75	34.925	-0.882	290.782				
98	ARKXXVII/1	67	2012	6	27	1.918	78.831	2030.814	2030.814	-0.777	34.915	-0.873	289.347	0.018	14.562	0.866	11.282

Table A3, Chapter I: CTD and nutrient data (continued)

Nr.	Cruise	Station	Year	Month	Day	Longitude [°E]	Latitude [°N]	Depth [m]	Pressure [dB]	Temperature [°C]	Salinity [PSU]	Pot. Temp. [°C]	O2 [µmol/kg]	nitrite [mumol/kg]	nitrate [mumol/kg]	phosphate [mumol/kg]	silicate [mumol/kg]
99	ARKXXVII/1	67	2012	6	27	1.918	78.831	1776.123	1776.123	-0.719	34.916	-0.8	291.115	0.016	14.325	0.823	10.682
100	ARKXXVII/1	67	2012	6	27	1.918	78.831	1521.54	1521.54	-0.649	34.915	-0.716	292.391	0.017	14.097	0.804	9.978
101	ARKXXVII/1	67	2012	6	27	1.918	78.831	1266.565	1266.565	-0.548	34.912	-0.601	295.744	0.015	13.673	0.776	8.953
102	ARKXXVII/1	67	2012	6	27	1.918	78.831	1013.201	1013.201	-0.411	34.908	-0.453	300.656	0.021	13.282	0.776	7.694
103	ARKXXVII/1	67	2012	6	27	1.918	78.831	809.858	809.858	-0.029	34.921	-0.063	307.86	0.018	12.787	0.736	6.508
104	ARKXXVII/1	67	2012	6	27	1.918	78.831	607.326	607.326	0.723	34.957	0.695	314.355	0.041	12.431	0.724	5.721
105	ARKXXVII/1	67	2012	6	27	1.918	78.831	404.702	404.702	2.281	35.039	2.258	307.221	0.032	12.168	0.703	5.674
106	ARKXXVII/1	67	2012	6	27	1.918	78.831	303.276	303.276	3.033	35.083	3.014	311.853	0.026	11.767	0.657	4.745
107	ARKXXVII/1	67	2012	6	27	1.918	78.831	202.55	202.55	3.388	35.096	3.375	302.24	0.194	11.156	0.678	4.444
108	ARKXXVII/1	67	2012	6	27	1.918	78.831	100.976	100.976	3.879	35.124	3.872	301.182	0.162	10.956	0.618	4.392
109	ARKXXVII/1	67	2012	6	27	1.918	78.831	50.601	50.601	3.999	35.082	3.995	319.194	0.184	6.886	0.488	3.581
110	ARKXXVII/1	67	2012	6	27	1.918	78.831	50.601	50.601	3.999	35.082	3.995	319.611				
111	ARKXXVII/1	67	2012	6	27	1.918	78.831	10.423	10.423	1.451	33.724	1.45	397.786	0.037	0.071	0.095	2.125
112	ARKXXVII/1	69	2012	6	27	1.015	78.834	2503.435	2503.435	-0.759	34.925	-0.888	289.785	0.05	14.459	0.936	8.634
113	ARKXXVII/1	69	2012	6	28	1.015	78.834	2031.565	2031.565	-0.76	34.916	-0.857	289.605	0.042	14.427	0.889	10.684
114	ARKXXVII/1	69	2012	6	28	1.015	78.834	1776.904	1776.904	-0.737	34.914	-0.818	290.951	0.048	14.431	0.908	10.407
115	ARKXXVII/1	69	2012	6	28	1.015	78.834	1521.77	1521.77	-0.629	34.917	-0.696	291.382	0.041	13.721	0.91	9.052
116	ARKXXVII/1	69	2012	6	28	1.015	78.834	1267.459	1267.459	-0.577	34.911	-0.631	297.249	0.044	13.716	0.907	8.438
117	ARKXXVII/1	69	2012	6	28	1.015	78.834	1013.164	1013.164	-0.469	34.909	-0.51	302.987	0.046	13.473	0.894	7.476
118	ARKXXVII/1	69	2012	6	28	1.015	78.834	809.83	809.83	-0.229	34.914	-0.262	303.041	0.05	12.923	0.88	6.734
119	ARKXXVII/1	69	2012	6	28	1.015	78.834	607	607	0.142	34.924	0.116	304.876	0.051	12.692	0.846	5.818
120	ARKXXVII/1	69	2012	6	28	1.015	78.834	404.801	404.801	1.471	34.999	1.45	307.425	0.062	12.162	0.812	4.86
121	ARKXXVII/1	69	2012	6	28	1.015	78.834	303.418	303.418	2.462	35.052	2.444	304.395	0.059	12.073	0.806	4.821
122	ARKXXVII/1	69	2012	6	28	1.015	78.834	202.285	202.285	3.321	35.108	3.308	299.946	0.069	11.722	0.791	4.382
123	ARKXXVII/1	69	2012	6	28	1.015	78.834	101.375	101.375	3.508	35.097	3.501	304.343	0.24	10.591	0.745	4.127
124	ARKXXVII/1	69	2012	6	28	1.015	78.834	10.358	10.358	2	34.279	2		0.102	1.772	0.269	2.552
125	ARKXXVII/1	72	2012	6	28	0.095	78.836	2611.582	2611.582	-0.747	34.927	-0.884	290.958	0.029	14.22	0.844	10.708
126	ARKXXVII/1	72	2012	6	28	0.095	78.836	2541.379	2541.379	-0.753	34.927	-0.885	289.084	0.012	14.189	0.799	10.701
127	ARKXXVII/1	72	2012	6	28	0.095	78.836	2031.199	2031.199	-0.769	34.916	-0.865	290.432	0.004	14.263	0.84	11.055
128	ARKXXVII/1	72	2012	6	28	0.095	78.836	1776.406	1776.406	-0.73	34.916	-0.811	291.296	0.005	14.167	0.839	10.625
129	ARKXXVII/1	72	2012	6	28	0.095	78.836	1521.562	1521.562	-0.674	34.917	-0.74	291.274	0.018	14.019	0.876	10.247
130	ARKXXVII/1	72	2012	6	28	0.095	78.836	1267.365	1267.365	-0.627	34.913	-0.68	295.783	0.004	13.899	0.837	9.174
131	ARKXXVII/1	72	2012	6	28	0.095	78.836	1013.182	1013.182	-0.515	34.911	-0.556	296.257	0.014	13.326	0.769	8.526
132	ARKXXVII/1	72	2012	6	28	0.095	78.836	810.428	810.428	-0.406	34.908	-0.438	300.609	0.018	13.052	0.781	7.652
133	ARKXXVII/1	72	2012	6	28	0.095	78.836	607.711	607.711	-0.18	34.912	-0.204	303.641	0.016	12.748	0.739	7.012
134	ARKXXVII/1	72	2012	6	28	0.095	78.836	404.68	404.68	0.43	34.943	0.412	309.89	0.021	12.383	0.714	6.176
135	ARKXXVII/1	72	2012	6	28	0.095	78.836	303.696	303.696	0.662	34.948	0.649	305.353	0.023	12.152	0.722	5.891
136	ARKXXVII/1	72	2012	6	28	0.095	78.836	202.295	202.295	1.323	34.987	1.313	307.65	0.037	11.542	0.684	5.493
137	ARKXXVII/1	72	2012	6	28	0.095	78.836	101.073	101.073	2.311	35.044	2.306	310.951	0.118	10.727	0.579	4.997
138	ARKXXVII/1	72	2012	6	28	0.095	78.836	50.813	50.813	2.602	34.848	2.599	322.813	0.082	6.446	0.551	4.474
139	ARKXXVII/1	72	2012	6	28	0.095	78.836	10.009	10.009	1.569	33.614	1.568	357.42	0.067	0	0.019	0.681
140	ARKXXVII/1	76	2012	6	29	-1.083	78.835	2529.282	2529.282	-0.754	34.925	-0.885	289.785	0.023	14.182	0.699	14.442
141	ARKXXVII/1	76	2012	6	29	-1.083	78.835	2030.728	2030.728	-0.725	34.916	-0.822	290.026	0.023	14.165	0.711	13.683
142	ARKXXVII/1	76	2012	6	29	-1.083	78.835	1776.107	1776.107	-0.651	34.917	-0.733	290.529	0.013	14.028	0.734	13.818
143	ARKXXVII/1	76	2012	6	29	-1.083	78.835	1521.441	1521.441	-0.594	34.91	-0.662	298.941	0.018	13.493	0.674	11.694
144	ARKXXVII/1	76	2012	6	29	-1.083	78.835	1267.171	1267.171	-0.468	34.909	-0.522	301.876	0.013	13.498	0.675	10.325
145	ARKXXVII/1	76	2012	6	29	-1.083	78.835	1013.117	1013.117	-0.11	34.924	-0.155	319.354	0.014	12.42	0.621	8.329
146	ARKXXVII/1	76	2012	6	29	-1.083	78.835	809.896	809.896	-0.024	34.912	-0.059	301.366	0.028	12.53	0.652	8.452
147	ARKXXVII/1	76	2012	6	29	-1.083	78.835	607.152	607.152	0.822	34.946	0.792	301.514	0.018	12.118	0.605	6.328
148	ARKXXVII/1	76	2012	6	29	-1.083	78.835	404.514	404.514	2.399	35.039	2.375	299.523	0.026	11.609	0.57	6.082
149	ARKXXVII/1	76	2012	6	29	-1.083	78.835	354.016	354.016	2.544	35.035	2.522	299.285	0.034	11.569	0.58	6.417
150	ARKXXVII/1	76	2012	6	29	-1.083	78.835	303.435	303.435	2.847	35.056	2.828	299.105	0.07	11.432	0.627	5.966
151	ARKXXVII/1	76	2012	6	29	-1.083	78.835	252.758	252.758	2.918	35.041	2.903	299.309	0.076	11.165	0.565	6.053
152	ARKXXVII/1	76	2012	6	29	-1.083	78.835	201.925	201.925	3.564	35.11	3.551	305.52	0.325	10.221	0.544	4.794
153	ARKXXVII/1	76	2012	6	29	-1.083	78.835	151.484	151.484	3.463	35.075	3.453	302.94	0.251	10.186	0.526	5.513
154	ARKXXVII/1	76	2012	6	29	-1.083	78.835	101.076	101.076	3.594	35.05	3.588	310.872	0.282	8.261	0.484	4.938
155	ARKXXVII/1	76	2012	6	29	-1.083	78.835	75.497	75.497	3.201	34.958	3.196	329.794	0.154	5.193	0.387	5.161
156	ARKXXVII/1	76	2012	6	29	-1.083	78.835	50.303	50.303	0.686	34.467	0.684	325.081	0.085	6.187	0.415	5.754
157	ARKXXVII/1	76	2012	6	29	-1.083	78.835	25.325	25.325	-1.448	33.967	-1.448	332.01	0.096	6.602	0.431	3.779
158	ARKXXVII/1	76	2012	6	29	-1.083	78.835	10.249	10.249	-1.403	33.007	-1.403		0.082	4.752	0.331	3.573
159	ARKXXVII/1	79	2012	6	30	-2.362	78.826	2648.352	2648.352	-0.744	34.926	-0.885	290.013	0.042	14.372	0.969	9.853
160	ARKXXVII/1	79	2012	6	30	-2.362	78.826	2540.756	2540.756	-0.769	34.918	-0.9	289.775	0.043	14.556	0.992	11.367
161	ARKXXVII/1	79	2012	6	30	-2.362	78.826	2031.109	2031.109	-0.698	34.914	-0.796	290.292	0.034	14.226	1.003	9.955
162	ARKXXVII/1	79	2012	6	30	-2.362	78.826	1775.872	1775.872	-0.618	34.912	-0.701	294.311	0.042	13.811	0.911	8.238
163	ARKXXVII/1	79	2012	6	30	-2.362	78.826	1267.616	1267.616	-0.367	34.91	-0.423	305.931	0.041	13.139	0.865	5.673
164	ARKXXVII/1	79	2012	6	30	-2.362	78.826	1013.072	1013.072	0.126	34.93	0.079	310.044	0.038	12.325	0.808	6.017
165	ARKXXVII/1	79	2012	6	30	-2.362	78.826	810.426	810.426	0.024	34.879	-0.011	297.631	0.045	11.902	0.802	5.344
166	ARKXXVII/1	79	2012	6	30	-2.362	78.826	404.09	404.09	2.457	35.015	2.433	300.087	0.04	11.431	0.729	4.634
167	ARKXXVII/1	79	2012	6	30	-2.362	78.826	303.611	303.611	3.432	35.092	3.411	300.167	0.052	11.446	0.758	4.259
168	ARKXXVII/1	79	2012	6	30	-2.362	78.826	202.676	202.676	3.64	35.086	3.626	299.533	0.041	11.358	0.727	4.171
169	ARKXXVII/1	79	2012	6	30	-2.362	78.826	101.378	101.378	2.973	34.93	2.967	296.638	0.03	11.149	0.698	4.329
170	ARKXXVII/1	79	2012	6	30	-2.362	78.826	76.181	76.181	0.334	34.531	0.331	294.179	0.051	10.623	0.733	5.826
171	ARKXXVII/1	79	2012	6	30	-2.362	78.826	50.781	50.781	-0.999	34.168	-1	306.35	0.048	8.483	0.646	5.223
172	ARKXXVII/1	79	2012	6	30	-2.362	78.826	25.161	25.161	-1.768	33.992	-1.769	339.983	0.033	5.671	0.472	3.137
173	ARKXXVII/1	79	2012	6	30	-2.362	78.826	10.238	10.238	-1.743	33.904	-1.743	339.457	0.09	6.104	0.365	2.312
174	ARKXXVII/1	81	2012	6	30	-1.721	78.840	2643.913	2643.913	-0.786	34.916	-0.925	291.972	0.019	14.128	0.815	11.418
175	ARKXXVII/1	81	2012	6	30	-1.721	78.840	2541.815	2541.815	-0.782	34.916	-0.913	291.318	0	14.307	0.86	11.404
176	ARKXXVII/1	81	2012	6	30	-1.721	78.840	2031.059	2031.059	-0.716	34.914	-0.813	292.248	0.008	14.1	0.909	10.244
177	ARKXXVII/1	81	2012	6	30	-1.721	78.840	1776.162	1776.162	-0.613	34.916	-0.695	293.017	0.003	13.766	0.841	9.699
178	ARKXXVII/1	81	2012	6	30	-1.721	78.840	1521.597	1521.597	-0.557	34.91	-0.625	299.543	0.01	13.938	0.866	8.865
179	ARKXXVII/1	81	2012	6	30	-1.721	78.840	1267.127	1267.127	-0.434	34.909	-0.489	303.869	0.011	13.083	0.744	7.589
180	ARKXXVII/1	81	2012	6	30	-1.721	78.840	1013.291	1013.291	0.02	34.931	-0.025	316.145	0.013	12.355	0.721	6.101
181	ARKXXVII/1	81	2012	6	30	-1.721	78.840	809.901	809.901	0.382	34.95	0.345	318.813	0.015	12.004	0.631	5.529
182	ARKXXVII/1	81	2012	6	30	-1.721	78.840	607.497	607.497	0.953	34.96	0.923	304.464	0.014	12.231	0.735	5.677
183	ARKXXVII/1	81	2012	6	30	-1.721	78.840	404.481	404.481	2.673	35.06	2.648	303.326	0.008	11.906	0.705	5.058
184	ARKXXVII/1	81	2012	6	30	-1.721	78.840	302.836	302.836	3.049	35.072	3.029	300.52	0.012	11.432	0.679	4.647
185	ARKXXVII/1	81	2012	6	30	-1.721	78.840	202.183	202.183	3.387	35.082	3.373	303.14	0.124	10.598	0.617	4.46
186	ARKXXVII/1	81	2012	6	30	-1.721	78.840	101.239	101.239	2.989	34.978	2.982	303.898	0.121	9.193	0.644	4.285
187	ARKXXVII/1	81	2012	6	30	-1.721	78.840	75.236	75.236	3.415	34.975	3.41	336.605	0.064	3.194	0.273	3.342
188	ARKXXVII/1	81	2012	6	30	-1.721	78.840	48.672	48.672	1.104	34.473	1.102	344.474	0.038	3.607	0.323	3.295
189	ARKXXVII/1	81	2012	6	30	-1.721	78.840	20.061	20.061	-1.351	33.804	-1.351	347.894	0.042	4.646	0.441	2.862
190	ARKXXVII/1	81	2012	6	30	-1.721	78.840	10.795	10.795	-1.37	32.924	-1.37	383.582	0.031	1.726	0.249	2.417
191	ARKXXVII/1	92	2012	7	3	-12.004	79.833	150.53	150.53	-1.084	33.4	-1.088	323.259	0.062	7.661	0.784	7.296
192	ARKXXVII/1	92	2012	7	3	-12.004	79.833	150.53	150.53	-1.084	33.4	-1.088		0.065	4.97	0.793	8.42
193	ARKXXVII/1	92	2012	7	3	-12.004	79.833	150.53	150.53	-1.084	33.4	-1.088		0.089	2.428	0.754	5.207
194	ARKXXVII/1	92	2012	7	3	-12.004	79.833	150.53	150.53	-1.084	33.4	-1.088		0.094	1.771	0.742	4.227
195	ARKXXVII/1	92	2012	7	3	-12.004	79.833	150.53	150.53	-1.084	33.4	-1.088		0.086	1.405	0.687	3.641
196	ARKXXVII/1	92	2012	7	3	-12.004	79.833	150.53	150.53	-1.084	33.4	-1.088		0.068	0.866	0.664	2.928

Table A3, Chapter I: CTD and nutrient data (continued)

Nr.	Cruise	Station	Year	Month	Day	Longitude [°E]	Latitude [°N]	Depth [m]	Pressure [dB]	Temperature [°C]	Salinity [PSU]	Pot. Temp. [°C]	O2 [µmol/kg]	nitrite [mumol/kg]	nitrate [mumol/kg]	phosphate [mumol/kg]	silicate [mumol/kg]
197	ARKXXVII/1	92	2012	7	3	-12.004	79.833	150.53	150.53	-1.084	33.4	-1.088		0.056	0.414	0.615	2.555
198	ARKXXVII/1	92	2012	7	3	-12.004	79.833	150.53	150.53	-1.084	33.4	-1.088		0.046	0	0.549	2.091
199	ARKXXVII/1	92	2012	7	3	-12.004	79.833	150.53	150.53	-1.084	33.4	-1.088		0.057	0.096	0.512	1.123
200	ARKXXVII/1	92	2012	7	3	-12.004	79.833	150.53	150.53	-1.084	33.4	-1.088		0.071	0.013	0.525	1.155
201	ARKXXVII/1	94	2012	7	3	-12.006	79.669	252.819	252.819	-0.259	34.279	-0.268	294.431	0.024	10.485	0.599	9.005
202	ARKXXVII/1	94	2012	7	3	-12.006	79.669	242.924	242.924	-0.262	34.275	-0.271	294.184	0.021	10.566	0.586	8.736
203	ARKXXVII/1	94	2012	7	3	-12.006	79.669	202.322	202.322	-0.417	34.179	-0.423	299.276	0.017	10.03	0.595	9.077
204	ARKXXVII/1	94	2012	7	3	-12.006	79.669	161.785	161.785	-0.824	33.785	-0.828	312.857	0.024	8.782	0.57	6.999
205	ARKXXVII/1	94	2012	7	3	-12.006	79.669	121.206	121.206	-1.54	32.513	-1.542	352.578	0.043	4.998	0.656	9.066
206	ARKXXVII/1	94	2012	7	3	-12.006	79.669	80.803	80.803	-1.696	31.807	-1.697	374.908	0.061	2.661	0.562	6.006
207	ARKXXVII/1	94	2012	7	3	-12.006	79.669	60.55	60.55	-1.668	31.766	-1.669	381.571	0.087	1.872	0.544	4.977
208	ARKXXVII/1	94	2012	7	3	-12.006	79.669	50.314	50.314	-1.647	31.736	-1.647	382.413	0.071	1.332	0.533	3.964
209	ARKXXVII/1	94	2012	7	3	-12.006	79.669	40.569	40.569	-1.601	31.721	-1.601	383.795	0.056	1.035	0.501	3.65
210	ARKXXVII/1	94	2012	7	3	-12.006	79.669	29.696	29.696	-1.479	31.469	-1.479	408.327	0.01	0.088	0.437	1.122
211	ARKXXVII/1	94	2012	7	3	-12.006	79.669	20.3	20.3	-1.389	31.402	-1.389	414.877	0.005	0.006	0.417	0.794
212	ARKXXVII/1	94	2012	7	3	-12.006	79.669	10.128	10.128	-0.044	31.105	-0.044	396.102	0.006	0.019	0.433	1.097
213	ARKXXVII/1	94	2012	7	3	-12.006	79.669	2.543	2.543	-0.027	31.091	-0.027	399.326	0.01	0.032	0.369	1.231
214	ARKXXVII/1	96	2012	7	3	-11.920	79.503	237.691	237.691	-0.267	34.27	-0.275	285.948	0.021	10.505	0.716	8.638
215	ARKXXVII/1	96	2012	7	3	-11.920	79.503	202.243	202.243	-0.418	34.17	-0.424	300.902	0.034	10.159	0.675	8.461
216	ARKXXVII/1	96	2012	7	3	-11.920	79.503	161.575	161.575	-0.912	33.684	-0.916	316.41	0.036	8.658	0.685	7.598
217	ARKXXVII/1	96	2012	7	3	-11.920	79.503	121.523	121.523	-1.626	32.411	-1.628	347.229	0.046	5.808	0.794	9.987
218	ARKXXVII/1	96	2012	7	3	-11.920	79.503	80.6	80.6	-1.688	31.8	-1.69	375.022	0.071	2.778	0.687	6.311
219	ARKXXVII/1	96	2012	7	3	-11.920	79.503	61.055	61.055	-1.643	31.745	-1.644	381.689	0.075	1.552	0.602	4.397
220	ARKXXVII/1	96	2012	7	3	-11.920	79.503	50.67	50.67	-1.565	31.717	-1.566	383.16	0.074	1.151	0.604	3.816
221	ARKXXVII/1	96	2012	7	3	-11.920	79.503	40.306	40.306	-1.443	31.68	-1.444	389.999	0.036	0.514	0.581	2.69
222	ARKXXVII/1	96	2012	7	3	-11.920	79.503	30.489	30.489	-1.152	31.476	-1.152	411.372	0.001	0.016	0.497	0.927
223	ARKXXVII/1	96	2012	7	3	-11.920	79.503	20.036	20.036	0.646	31.272	0.645	399.564	0	0	0.451	0.83
224	ARKXXVII/1	96	2012	7	3	-11.920	79.503	10.201	10.201	0.351	31.046	0.35	378.129	0.01	0.025	0.427	1.173
225	ARKXXVII/1	96	2012	7	3	-11.920	79.503	1.543	1.543	0.013	30.782	0.013	378.117	0.008	0.016	0.457	1.437
226	ARKXXVII/1	98	2012	7	4	-11.438	79.382	238.517	238.517	-0.13	34.352	-0.138	288.562	0.059	11.013	0.763	9.17
227	ARKXXVII/1	98	2012	7	4	-11.438	79.382	203.127	203.127	-0.348	34.225	-0.355	297.534	0.039	10.314	0.763	8.424
228	ARKXXVII/1	98	2012	7	4	-11.438	79.382	162.223	162.223	-0.946	33.611	-0.951	313.499	0.056	8.603	0.709	7.826
229	ARKXXVII/1	98	2012	7	4	-11.438	79.382	121.696	121.696	-1.599	32.484	-1.601	342.013	0.071	5.97	0.837	9.819
230	ARKXXVII/1	98	2012	7	4	-11.438	79.382	81.36	81.36	-1.689	31.826	-1.69	374.22	0.095	2.375	0.736	5.222
231	ARKXXVII/1	98	2012	7	4	-11.438	79.382	61.094	61.094	-1.615	31.741	-1.615	378.042	0.101	1.681	0.687	4.219
232	ARKXXVII/1	98	2012	7	4	-11.438	79.382	50.701	50.701	-1.549	31.725	-1.55	379.757	0.08	1.395	0.651	3.745
233	ARKXXVII/1	98	2012	7	4	-11.438	79.382	40.788	40.788	-1.463	31.712	-1.464	390.802	0.054	0.328	0.603	1.9
234	ARKXXVII/1	98	2012	7	4	-11.438	79.382	30.998	30.998	-1.289	31.698	-1.29	401.716	0.025	0.015	0.561	1.47
235	ARKXXVII/1	98	2012	7	4	-11.438	79.382	20.893	20.893	0.316	31.442	0.315	401.858	0.045	0.022	0.508	0.997
236	ARKXXVII/1	98	2012	7	4	-11.438	79.382	10.745	10.745	0.359	31.185	0.359	387.626	0.047	0.029	0.519	0.028
237	ARKXXVII/1	98	2012	7	4	-11.438	79.382	1.23	1.23	0.355	31.093	0.355	378.84	0.02	0.06	0.502	0.863
238	ARKXXVII/1	112	2012	7	6	-11.998	78.833	197.882	197.882	-0.58	34.112	-0.586	308.153	0.022	9.529	0.579	7.703
239	ARKXXVII/1	112	2012	7	6	-11.998	78.833	160.454	160.454	-1.347	33.526	-1.35	327.738	0.033	7.319	0.615	10.317
240	ARKXXVII/1	112	2012	7	6	-11.998	78.833	141.523	141.523	-1.451	33.256	-1.454	332.575	0.048	7.021	0.667	10.134
241	ARKXXVII/1	112	2012	7	6	-11.998	78.833	122.285	122.285	-1.599	32.618	-1.601	341.119	0.047	6.294	0.732	12.75
242	ARKXXVII/1	112	2012	7	6	-11.998	78.833	81.303	81.303	-1.693	31.959	-1.695	371.86	0.097	3.008	0.616	7.4
243	ARKXXVII/1	112	2012	7	6	-11.998	78.833	61.221	61.221	-1.637	31.801	-1.638	376.145	0.262	2.6	0.61	5.585
244	ARKXXVII/1	112	2012	7	6	-11.998	78.833	50.928	50.928	-1.585	31.756	-1.586	379.929	0.087	1.826	0.565	5.184
245	ARKXXVII/1	112	2012	7	6	-11.998	78.833	40.793	40.793	-1.578	31.73	-1.578	382.782	0.077	1.138	0.536	4.237
246	ARKXXVII/1	112	2012	7	6	-11.998	78.833	30.538	30.538	-1.426	31.698	-1.427	395.091	0.015	0.117	0.473	2.134
247	ARKXXVII/1	112	2012	7	6	-11.998	78.833	19.923	19.923	-1.384	31.337	-1.385	407.134	0.024	0.068	0.438	1.383
248	ARKXXVII/1	112	2012	7	6	-11.998	78.833	10.497	10.497	-1.41	31.137	-1.41	410.029	0.017	0.026	0.428	1.262
249	ARKXXVII/1	112	2012	7	6	-11.998	78.833	1.745	1.745	-1.439	30.804	-1.439	413.476	0.015	0.047	0.402	1.199
250	ARKXXVII/1	115	2012	7	6	-10.996	78.832	321.037	321.037	0.223	34.524	0.21	289.994	0.023	11.405	0.726	7.789
251	ARKXXVII/1	115	2012	7	6	-10.996	78.832	283.959	283.959	0.121	34.467	0.11	296.312	0.027	10.83	0.73	7.765
252	ARKXXVII/1	115	2012	7	6	-10.996	78.832	243.385	243.385	-0.048	34.389	-0.057	296.892	0.028	10.831	0.723	7.739
253	ARKXXVII/1	115	2012	7	6	-10.996	78.832	202.763	202.763	-0.463	34.181	-0.469	301.497	0.021	10.2	0.722	7.516
254	ARKXXVII/1	115	2012	7	6	-10.996	78.832	162.207	162.207	-1.227	33.64	-1.231	318.539	0.036	8.233	0.681	7.593
255	ARKXXVII/1	115	2012	7	6	-10.996	78.832	141.942	141.942	-1.529	33.09	-1.532	328.666	0.035	7.077	0.693	8.388
256	ARKXXVII/1	115	2012	7	6	-10.996	78.832	122	122	-1.611	32.48	-1.613	345.846	0.05	5.893	0.848	10.432
257	ARKXXVII/1	115	2012	7	6	-10.996	78.832	101.383	101.383	-1.689	31.998	-1.691	366.635	0.061	3.672	0.78	7.448
258	ARKXXVII/1	115	2012	7	6	-10.996	78.832	81.511	81.511	-1.655	31.819	-1.657	372.925	0.08	2.724	0.699	6.06
259	ARKXXVII/1	115	2012	7	6	-10.996	78.832	40.2	40.2	-1.474	31.705	-1.474	385.982	0.044	0.65	0.594	2.775
260	ARKXXVII/1	115	2012	7	6	-10.996	78.832	30.749	30.749	-1.371	31.68	-1.371	398.824	0.01	0	0.532	1.294
261	ARKXXVII/1	115	2012	7	6	-10.996	78.832	20.904	20.904	-1.148	31.637	-1.149	405.808	0.01	0.014	0.532	1.108
262	ARKXXVII/1	115	2012	7	6	-10.996	78.832	10.643	10.643	-1.04	31.241	-1.04	410.589	0.013	0.015	0.477	0.925
263	ARKXXVII/1	115	2012	7	6	-10.996	78.832	1.409	1.409	-0.203	30.62	-0.203	385.781	0.019	0.002	0.447	0.942
264	ARKXXVII/1	117	2012	7	6	-10.000	78.832	305.101	305.101	0.095	34.452	0.084	292.827	0.05	11.236	0.89	8.273
265	ARKXXVII/1	117	2012	7	6	-10.000	78.832	282.965	282.965	0.068	34.442	0.058	295.867	0.038	11.192	0.93	8.181
266	ARKXXVII/1	117	2012	7	6	-10.000	78.832	242.711	242.711	-0.05	34.388	-0.059	294.351	0.058	11.038	0.89	8.089
267	ARKXXVII/1	117	2012	7	6	-10.000	78.832	202.322	202.322	-0.382	34.224	-0.388	300.473	0.031	10.389	0.873	7.888
268	ARKXXVII/1	117	2012	7	6	-10.000	78.832	161.729	161.729	-1.142	33.821	-1.146	317.374	0.039	8.5	0.821	7.182
269	ARKXXVII/1	117	2012	7	6	-10.000	78.832	141.107	141.107	-1.322	33.236	-1.325	324.291	0.056	7.643	0.928	7.817
270	ARKXXVII/1	117	2012	7	6	-10.000	78.832	121.164	121.164	-1.608	32.538	-1.61	343.372	0.037	5.874	0.934	9.731
271	ARKXXVII/1	117	2012	7	6	-10.000	78.832	100.835	100.835	-1.698	32.06	-1.7	357.371	0.058	4.683	0.995	8.923
272	ARKXXVII/1	117	2012	7	6	-10.000	78.832	80.818	80.818	-1.684	31.88	-1.686	366.585	0.084	3.709	0.96	6.832
273	ARKXXVII/1	117	2012	7	6	-10.000	78.832	40.184	40.184	-1.585	31.732	-1.585	381.034	0.087	1.281	0.762	3.765
274	ARKXXVII/1	117	2012	7	6	-10.000	78.832	30.105	30.105	-1.428	31.708	-1.428	389.412	0.057	0.636	0.713	2.631
275	ARKXXVII/1	117	2012	7	6	-10.000	78.832	20.292	20.292	-0.689	31.425	-0.69	411.609	0.048	0.007	0.64	1.033
276	ARKXXVII/1	117	2012	7	6	-10.000	78.832	10.451	10.451	-0.494	30.612	-0.494	400.846	0.051	0.031	0.927	0.705
277	ARKXXVII/1	117	2012	7	6	-10.000	78.832	1.563	1.563	-0.502	30.614	-0.502	389.798	0.06	0.069	0.578	0.656
278	ARKXXVII/1	119	2012	7	7	-9.001	78.834	218.403	218.403	-0.442	34.199	-0.449	302.094	0.02	9.88	0.577	7.901
279	ARKXXVII/1	119	2012	7	7	-9.001	78.834	201.999	201.999	-0.448	34.196	-0.455	302.213	0.024	9.869	0.565	7.656
280	ARKXXVII/1	119	2012	7	7	-9.001	78.834	161.478	161.478	-1.07	33.826	-1.074	313.2	0.025	8.847	0.558	7.67
281	ARKXXVII/1	119	2012	7	7	-9.001	78.834	141.371	141.371	-1.349	33.483	-1.352	325.082	0.027	7.343	0.525	7.778
282	ARKXXVII/1	119	2012	7	7	-9.001	78.834	121.248	121.248	-1.632	32.477	-1.634	344.365	0.019	5.87	0.737	11.682
283	ARKXXVII/1	119	2012	7	7	-9.001	78.834	100.959	100.959	-1.718	32.056	-1.72	364.856	0.014	4.045	0.669	9.423
284	ARKXXVII/1	119	2012	7	7	-9.001	78.834	80.828	80.828	-1.716	31.884	-1.717	374.595	0.022	2.936	0.611	7.175
285	ARKXXVII/1	119	2012	7	7	-9.001	78.834	40.309	40.309	-1.549	31.784	-1.55	402.602	0.021	0.26	0.49	2.292
286	ARKXXVII/1	119	2012	7	7	-9.001	78.834	30.469	30.469	-1.07	31.691	-1.07	406.888	0.016	0.131	0.482	1.931
287	ARKXXVII/1	119	2012	7	7	-9.001	78.834	20.24	20.24	-1.007	31.524	-1.008	409.338	0.017	0.016	0.453	1.675
288	ARKXXVII/1	119	2012	7	7	-9.001	78.834	9.943	9.943	-0.635	31.07	-0.636	408.446	0.011	0.002	0.428	0.839
289	ARKXXVII/1	119	2012	7	7	-9.001	78.834	1.589	1.589	-0.352	30.915	-0.352	375.579	0.019	0.1	0.424	0.893
290	ARKXXVII/1	121	2012	7	7	-7.996	78.833	184.038	184.038	-0.5	34.268	-0.506	306.624	0.02	9.742	0.647	6.872
291	ARKXXVII/1	121	2012	7	7	-7.996	78.833	162.414	162.414	-0.702	34.221	-0.707	308.079	0.019	9.538	0.618	6.635
292	ARKXXVII/1	121	2012	7	7	-7.996	78.833	142.045	142.045	-0.968	34.048	-0.972	319.419	0.018	8.524	0.637	6.146
293	ARKXXVII/1	121	2012	7	7	-7.996	78.833	121.275	121.275	-1.183	33.449	-1.186	323.961	0.056	7.718	0.739	7.537
294	ARKXXVII/1	121	2012	7	7	-7.996	78.833	101.404	101.404	-1.565	32.519	-1.567	338.045	0.019	6.451	0.793	10.568

Table A3, Chapter I: CTD and nutrient data (continued)

Nr.	Cruise	Station	Year	Month	Day	Longitude [°E]	Latitude [°N]	Depth [m]	Pressure [dB]	Temperature [°C]	Salinity [PSU]	Pot. Temp. [°C]	O2 [µmol/kg]	nitrite [mumol/kg]	nitrate [mumol/kg]	phosphate [mumol/kg]	silicate [mumol/kg]
295	ARKXXVII/1	121	2012	7	7	-7.996	78.833	81.254	81.254	-1.706	31.967	-1.707	359.682	0.067	4.516	0.825	8.45
296	ARKXXVII/1	121	2012	7	7	-7.996	78.833	41.005	41.005	-1.665	31.754	-1.665	382.329	0.092	1.756	0.643	4.557
297	ARKXXVII/1	121	2012	7	7	-7.996	78.833	30.79	30.79	-1.54	31.726	-1.54	386.592	0.06	1.02	0.593	3.37
298	ARKXXVII/1	121	2012	7	7	-7.996	78.833	20.365	20.365	-1.165	31.461	-1.165	399.322	0.021	0.332	0.579	2.094
299	ARKXXVII/1	121	2012	7	7	-7.996	78.833	10.546	10.546	-0.625	31.012	-0.625	405.943	0.014	0.02	0.508	0.979
300	ARKXXVII/1	121	2012	7	7	-7.996	78.833	2.685	2.685	-0.614	31.01	-0.614	324.665	0.02	0.047	0.492	1.039
301	ARKXXVII/1	123	2012	7	7	-7.009	78.709	225.76	225.76	1.072	34.821	1.061	305.521	0.024	12.042	0.752	6.833
302	ARKXXVII/1	123	2012	7	7	-7.009	78.709	202.639	202.639	0.978	34.785	0.969	292.851	0.027	11.937	0.748	6.93
303	ARKXXVII/1	123	2012	7	7	-7.009	78.709	161.837	161.837	-0.148	34.405	-0.154	297.987	0.008	10.638	0.687	6.691
304	ARKXXVII/1	123	2012	7	7	-7.009	78.709	141.648	141.648	-0.622	34.263	-0.627	304.523	0.016	9.678	0.658	6.441
305	ARKXXVII/1	123	2012	7	7	-7.009	78.709	121.384	121.384	-1.513	34.033	-1.516	328.859	0.01	6.75	0.516	4.512
306	ARKXXVII/1	123	2012	7	7	-7.009	78.709	101.34	101.34	-1.738	33.936	-1.74	334.425	0.012	6.535	0.508	3.898
307	ARKXXVII/1	123	2012	7	7	-7.009	78.709	80.906	80.906	-1.728	33.832	-1.729	336.534	0.047	6.445	0.494	4.372
308	ARKXXVII/1	123	2012	7	7	-7.009	78.709	40.84	40.84	-1.647	33.189	-1.648	333.704	0.049	6.643	0.695	8.878
309	ARKXXVII/1	123	2012	7	7	-7.009	78.709	30.108	30.108	-1.582	32.762	-1.582	339.199	0.054	6.454	0.854	12.361
310	ARKXXVII/1	123	2012	7	7	-7.009	78.709	20.21	20.21	-1.515	31.988	-1.515	359.832	0.033	4.001	0.821	10.685
311	ARKXXVII/1	123	2012	7	7	-7.009	78.709	10.285	10.285	-1.554	31.665	-1.554	363.437	0.041	3.737	0.813	10.894
312	ARKXXVII/1	123	2012	7	7	-7.009	78.709	1.317	1.317	-1.549	31.674	-1.549	365.04	0.049	3.679	0.793	11.043
313	ARKXXVII/1	125	2012	7	8	-6.017	78.843	331.832	331.832	1.477	34.918	1.46	294.562	0.044	11.962	0.903	5.624
314	ARKXXVII/1	125	2012	7	8	-6.017	78.843	303.675	303.675	1.813	34.913	1.797	294.729	0.042	11.572	0.77	5.453
315	ARKXXVII/1	125	2012	7	8	-6.017	78.843	253.178	253.178	1.442	34.794	1.429	295.688	0.063	11.256	0.833	5.5
316	ARKXXVII/1	125	2012	7	8	-6.017	78.843	202.797	202.797	-0.437	34.353	-0.444	299.803	0.038	9.522	0.794	4.786
317	ARKXXVII/1	125	2012	7	8	-6.017	78.843	151.642	151.642	-1.785	33.943	-1.788	338.091	0.028	5.963	0.55	3.45
318	ARKXXVII/1	125	2012	7	8	-6.017	78.843	101.245	101.245	-1.601	33.434	-1.603	331.029	0.057	6.652	0.753	7.445
319	ARKXXVII/1	125	2012	7	8	-6.017	78.843	75.713	75.713	-1.63	33.083	-1.631	329.062	0.047	7.294	0.989	12.914
320	ARKXXVII/1	125	2012	7	8	-6.017	78.843	50.712	50.712	-1.663	32.214	-1.664	348.967	0.089	5.514	1.029	12.337
321	ARKXXVII/1	125	2012	7	8	-6.017	78.843	25.302	25.302	-1.53	31.528	-1.53	376.381	0.148	5.613	1.048	11.61
322	ARKXXVII/1	125	2012	7	8	-6.017	78.843	10.171	10.171	-1.502	31.446	-1.502	372.164	0.089	2.86	0.884	8.835
323	ARKXXVII/1	128	2012	7	8	-4.939	78.834	1049.697	1049.697	-0.181	34.893	-0.227	296.849	0.039	12.561	0.781	7.03
324	ARKXXVII/1	128	2012	7	8	-4.939	78.834	811.012	811.012	0.043	34.88	0.008	295.765	0.045	12.388	0.79	6.567
325	ARKXXVII/1	128	2012	7	8	-4.939	78.834	607.041	607.041	0.336	34.871	0.309	294.245	0.03	12.378	0.785	6.375
326	ARKXXVII/1	128	2012	7	8	-4.939	78.834	406.312	406.312	1.188	34.89	1.168	292.977	0.025	12.199	0.729	6.015
327	ARKXXVII/1	128	2012	7	8	-4.939	78.834	304.81	304.81	2.134	34.936	2.116	295.848	0.031	11.8	0.738	5.144
328	ARKXXVII/1	128	2012	7	8	-4.939	78.834	253.57	253.57	2.594	34.955	2.579	0	0.036	11.621	0.689	4.827
329	ARKXXVII/1	128	2012	7	8	-4.939	78.834	202.565	202.565	1.152	34.685	1.143	293.923	0.033	11.314	0.706	5.378
330	ARKXXVII/1	128	2012	7	8	-4.939	78.834	151.87	151.87	-1.081	34.216	-1.085	307.092	0.027	8.967	0.611	5.028
331	ARKXXVII/1	128	2012	7	8	-4.939	78.834	101.359	101.359	-1.806	34.011	-1.808	344.032	0.035	5.438	0.423	2.609
332	ARKXXVII/1	128	2012	7	8	-4.939	78.834	76.079	76.079	-1.779	33.954	-1.781	340.04	0.026	5.806	0.484	3.589
333	ARKXXVII/1	128	2012	7	8	-4.939	78.834	50.82	50.82	-1.672	33.326	-1.672	336.045	0.037	6.172	0.678	8.348
334	ARKXXVII/1	128	2012	7	8	-4.939	78.834	25.24	25.24	-1.688	32.332	-1.689	340.093	0.055	6.779	1.063	14.657
335	ARKXXVII/1	128	2012	7	8	-4.939	78.834	10.367	10.367	-1.637	32.078	-1.637	351.195	0.053	5.272	0.946	12.219
336	ARKXXVII/1	128	2012	7	8	-4.939	78.834	1.478	1.478	-1.63	32.072	-1.63	352.16	0.057	5.289	0.916	12.58
337	ARKXXVII/1	132	2012	7	9	-3.920	78.833	1908.402	1908.402	-0.614	34.922	-0.705	291.469	0.023	14.017	0.956	10.212
338	ARKXXVII/1	132	2012	7	9	-3.920	78.833	1908.39	1908.39	-0.612	34.922	-0.703	292.463	0.006	13.987	0.886	10.179
339	ARKXXVII/1	132	2012	7	9	-3.920	78.833	1572.594	1572.594	-0.551	34.913	-0.622	290.93	0.018	13.867	0.896	9.852
340	ARKXXVII/1	132	2012	7	9	-3.920	78.833	1572.686	1572.686	-0.551	34.913	-0.622	297.443	0.013	13.532	0.856	8.949
341	ARKXXVII/1	132	2012	7	9	-3.920	78.833	1013.39	1013.39	-0.223	34.895	-0.266	295.402	0.008	13.038	0.789	8.186
342	ARKXXVII/1	132	2012	7	9	-3.920	78.833	1013.716	1013.716	-0.222	34.895	-0.266	298.526	0.018	12.499	0.842	7.107
343	ARKXXVII/1	132	2012	7	9	-3.920	78.833	607.691	607.691	0.245	34.872	0.219	297.974	0.01	12.269	0.78	6.723
344	ARKXXVII/1	132	2012	7	9	-3.920	78.833	608.157	608.157	0.242	34.872	0.216	296.692	0.013	12.163	0.807	6.425
345	ARKXXVII/1	132	2012	7	9	-3.920	78.833	405.016	405.016	0.815	34.878	0.796	297.641	0.007	12.143	0.737	6.144
346	ARKXXVII/1	132	2012	7	9	-3.920	78.833	405.372	405.372	0.813	34.878	0.795	303.764	0.02	11.616	0.696	4.831
347	ARKXXVII/1	132	2012	7	9	-3.920	78.833	202.37	202.37	2.875	35.029	2.863	306.353	0.019	11.335	0.676	4.492
348	ARKXXVII/1	132	2012	7	9	-3.920	78.833	202.601	202.601	2.886	35.03	2.874	305.699	0.067	11.226	0.685	4.485
349	ARKXXVII/1	132	2012	7	9	-3.920	78.833	100.555	100.555	2.818	34.93	2.812	304.409	0.098	10.968	0.676	4.489
350	ARKXXVII/1	132	2012	7	9	-3.920	78.833	76.105	76.105	0.886	34.491	0.883	312.308	0.114	8.303	0.574	4.533
351	ARKXXVII/1	132	2012	7	9	-3.920	78.833	50.636	50.636	-1.7	34.01	-1.701	317.208	0.096	7.785	0.599	4.343
352	ARKXXVII/1	132	2012	7	9	-3.920	78.833	50.677	50.677	-1.727	34.002	-1.728	325.953	0.076	7.009	0.547	3.383
353	ARKXXVII/1	132	2012	7	9	-3.920	78.833	37.808	37.808	-1.686	33.933	-1.686	366.78	0.059	3.536	0.375	3.414
354	ARKXXVII/1	132	2012	7	9	-3.920	78.833	12.4	12.4	-1.525	32.827	-1.525	376.963	0.05	2.026	0.369	4.923
355	ARKXXVII/1	132	2012	7	9	-3.920	78.833	5.128	5.128	-1.512	32.701	-1.512	393.815	0.055	0.091	0.285	6.175
356	ARKXXVII/1	135	2012	7	9	-3.019	78.835	2499.723	2499.723	-0.755	34.924	-0.884	293.695	0.05	14.542	0.879	10.789
357	ARKXXVII/1	135	2012	7	9	-3.019	78.835	2030.748	2030.748	-0.698	34.915	-0.796	293.149	0.039	14.415	0.837	10.498
358	ARKXXVII/1	135	2012	7	9	-3.019	78.835	1776.41	1776.41	-0.574	34.919	-0.657	293.927	0.065	14.033	0.855	9.746
359	ARKXXVII/1	135	2012	7	9	-3.019	78.835	1521.606	1521.606	-0.552	34.908	-0.62	305.828	0.041	13.448	0.795	8.022
360	ARKXXVII/1	135	2012	7	9	-3.019	78.835	1267.12	1267.12	-0.369	34.909	-0.425	305.255	0.038	13.279	0.81	7.389
361	ARKXXVII/1	135	2012	7	9	-3.019	78.835	1010.199	1010.199	0.137	34.925	0.091	310.488	0.043	12.568	0.761	6.133
362	ARKXXVII/1	135	2012	7	9	-3.019	78.835	810.249	810.249	0.043	34.874	0.008	300.151	0.04	12.142	0.756	5.959
363	ARKXXVII/1	135	2012	7	9	-3.019	78.835	607.759	607.759	0.331	34.866	0.304	293.665	0.044	12.411	0.752	6.608
364	ARKXXVII/1	135	2012	7	9	-3.019	78.835	404.778	404.778	1.342	34.913	1.322	295.963	0.041	12.168	0.735	5.7
365	ARKXXVII/1	135	2012	7	9	-3.019	78.835	303.19	303.19	2.855	35.044	2.836	301.066	0.079	11.746	0.675	4.749
366	ARKXXVII/1	135	2012	7	9	-3.019	78.835	202.175	202.175	3.207	35.042	3.194	301.176	0.113	11.453	0.696	4.549
367	ARKXXVII/1	135	2012	7	9	-3.019	78.835	101.417	101.417	-0.021	34.488	-0.024	296.893	0.037	10.439	0.649	5.686
368	ARKXXVII/1	135	2012	7	9	-3.019	78.835	75.741	75.741	-0.839	34.285	-0.841	313.732	0.04	8.528	0.564	4.731
369	ARKXXVII/1	135	2012	7	9	-3.019	78.835	50.794	50.794	-1.711	34.062	-1.712	342.497	0.072	5.817	0.455	2.733
370	ARKXXVII/1	135	2012	7	9	-3.019	78.835	25.786	25.786	-1.477	33.704	-1.477	330.835	0.055	6.726	0.588	7.346
371	ARKXXVII/1	135	2012	7	9	-3.019	78.835	10.42	10.42	-0.895	32.331	-0.895	379.156	0.604	0.589	0.18	3.683

Table A4, Chapter I: Nd isotope compositions of NE Greenland rocks

Nr.	*Location*	*Std./Sample*	*Rock name*	*Lat*	*Long*	*143/144 corr.*	*εNd*	*Reference*
1	NE Greenlan	363183	eclogite			0.511647	-19.3	Brueckner et al. (1998)
2	NE Greenlan	363020	coarse garnet websterite			0.512266	-7.3	Brueckner et al. (1998)
3	NE Greenlan	407542	garnet websterite			0.512006	-12.3	Brueckner et al. (1998)
4	NE Greenlan	272855	not given	79.715	-18.550	0.511291	-26.3	Kalsbeek et al. (1993)
5	NE Greenlan	273405	basalt	81.000	-26.000	0.511899	-14.4	Upton et al. (2005)
6	NE Greenlan	273451	basalt	81.000	-26.000	0.512341	-5.8	Upton et al. (2005)
7	NE Greenlan	335774	dolerite	80.000	-24.000	0.512154	-9.4	Upton et al. (2005)
8	NE Greenlan	273251	dolerite	80.000	-24.000	0.512411	-4.4	Upton et al. (2005)
9	NE Greenlan	273493	dolerite	80.000	-24.000	0.511724	-17.8	Upton et al. (2005)
10	NE Greenlan	273241	dolerite	81.922	-31.860	0.512391	-4.8	Kalsbeek & Frei (2006)
11	NE Greenlan	273247	dolerite	81.922	-31.860	0.512377	-5.1	Kalsbeek & Frei (2006)
12	NE Greenlan	273228	dolerite	81.915	-32.088	0.511811	-16.1	Kalsbeek & Frei (2006)
13	NE Greenlan	273230	dolerite	81.915	-32.088	0.511878	-14.8	Kalsbeek & Frei (2006)
14	NE Greenlan	273236	dolerite	81.915	-32.088	0.511797	-16.4	Kalsbeek & Frei (2006)
15	NE Greenlan	273390	dolerite	81.718	-32.830	0.511829	-15.8	Kalsbeek & Frei (2006)
16	NE Greenlan	273392	dolerite	81.718	-32.830	0.511728	-17.8	Kalsbeek & Frei (2006)
17	NE Greenlan	273398	dolerite	81.718	-32.830	0.511717	-18.0	Kalsbeek & Frei (2006)
18	NE Greenlan	273482	dolerite	80.943	-26.332	0.511805	-16.2	Kalsbeek & Frei (2006)
19	NE Greenlan	273487	dolerite	80.943	-26.332	0.511812	-16.1	Kalsbeek & Frei (2006)
20	NE Greenlan	273495	dolerite	80.943	-26.332	0.511714	-18.0	Kalsbeek & Frei (2006)
21	NE Greenlan	273214	dolerite	81.932	-31.893	0.510862	-34.6	Kalsbeek & Frei (2006)
22	NE Greenlan	273219	dolerite	81.932	-31.893	0.510933	-33.3	Kalsbeek & Frei (2006)
23	NE Greenlan	197405	dolerite	81.780	-29.490	0.511716	-18.0	Kalsbeek & Frei (2006)
24	NE Greenlan	197406	dolerite	81.780	-29.490	0.511588	-20.5	Kalsbeek & Frei (2006)
25	NE Greenlan	197408	psammite	81.780	-29.490	0.511383	-24.5	Kalsbeek & Frei (2006)
26	NE Greenlan	273364	dolerite	81.725	-32.677	0.511834	-15.7	Kalsbeek & Frei (2006)
27	NE Greenlan	273525	Psammite	80.952	-26.292	0.511136	-29.3	Kalsbeek & Frei (2006)
28	NE Greenlan	273532	psammite	80.952	-26.292	0.511121	-29.6	Kalsbeek & Frei (2006)
29	NE Greenlan	197429	not given	81.000	-26.000	0.510712	-37.6	Kalsbeek et al. (1984)
30	NE Greenlan	197439	not given	81.000	-26.000	0.51096	-32.7	Kalsbeek et al. (1984)
31	NE Greenlan	197440	not given	81.000	-26.000	0.510511	-41.5	Kalsbeek et al. (1984)
32	NE Greenlan	273260	sandstone	81.000	-26.000	0.511236	-27.3	Kalsbeek et al. (1984)
33	NE Greenlan	273262	sandstone	81.000	-26.000	0.511401	-24.1	Kalsbeek et al. (1984)
34	NE Greenlan	273293	sandstone	81.000	-26.000	0.511273	-26.6	Kalsbeek et al. (1984)
35	NE Greenlan	273402	sandstone	81.000	-26.000	0.511406	-24.0	Kalsbeek et al. (1984)
36	NE Greenlan	273410	basalt	81.000	-26.000	0.511872	-14.9	Kalsbeek et al. (1984)
37	NE Greenlan	273419	basalt	81.000	-26.000	0.511889	-14.6	Kalsbeek et al. (1984)
38	NE Greenlan	273427	basalt	81.000	-26.000	0.511775	-16.8	Kalsbeek et al. (1984)
39	NE Greenlan	273434	basalt	81.000	-26.000	0.512125	-10.0	Kalsbeek et al. (1984)
40	NE Greenlan	273436	basalt	81.000	-26.000	0.511937	-13.7	Kalsbeek et al. (1984)
41	NE Greenlan	273442	basalt	81.000	-26.000	0.512238	-7.8	Kalsbeek et al. (1984)
42	NE Greenlan	273447	basalt	81.000	-26.000	0.512485	-3.0	Kalsbeek et al. (1984)
43	NE Greenlan	273470	basalt	81.000	-26.000	0.512534	-2.0	Kalsbeek et al. (1984)
44	NE Greenlan	197402	dolerite	81.780	-29.490	0.512083	-10.8	Kalsbeek et al. (1984)
45	NE Greenlan	273367	psammite	81.725	-32.677	0.51136	-24.9	Kalsbeek et al. (1984)

Brueckner, H. K., Gilotti, J. A., & Nutman, A. P. (1998). Caledonian eclogite-facies metamorphism of early Proterozoic protoliths from the North-East Greenland eclogite province. Contributions to Mineralogy and Petrology, 130(2), 103-120.

Kalsbeek, F., & Frei, R. (2006). The Mesoproterozoic Midsommersø dolerites and associated high-silica intrusions, North Greenland: crustal melting, contamination and hydrothermal alteration. Contributions to Mineralogy and Petrology, 152(1), 89-110.

Kalsbeek, F., & Jepsen, H. F. (1984). The late Proterozoic Zig-Zag Dal Basalt Formation of eastern North Greenland. Journal of Petrology, 25(3), 644-664.

Kalsbeek, F., Nutman, A. P., & Taylor, P. N. (1993). Palaeoproterozoic basement province in the Caledonian fold belt of North-East Greenland. Precambrian Research, 63(1-2), 163-178.

Upton, B. G. J., Rämö, O. T., Heaman, L. M., Blichert-Toft, J., Kalsbeek, F., Barry, T. L., & Jepsen, H. F. (2005). The Mesoproterozoic Zig-Zag Dal basalts and associated intrusions of eastern North Greenland: mantle plume–lithosphere interaction. Contributions to Mineralogy and Petrology, 149(1), 40-56.

Table A4, Chapter I (continued): Nd isotope compositions of Svalbard rocks

Nr.	*Location*	*Std./Sample*	*Rock name*	*Lat*	*Long*	*143/144 corr.*	*εNd*	*Reference*
1	Svalbard	L 90:13	granite	79.775	15.825	0.5116085	-20.1	Gee et al (1995)
2	Svalbard	LP91:16	granodiorite	79.069	16.306	0.5116865	-18.6	Gee et al (1995)
3	Svalbard	J 91:006	granite	79.011	16.282	0.5115454	-21.3	Gee et al (1995)
4	Svalbard	J 91:013	granite	79.200	16.858	0.5113765	-24.6	Gee et al (1995)
5	Svalbard	J 91:017	granite	79.225	16.186	0.5114306	-23.6	Gee et al (1995)
6	Svalbard	J 92:011	aplite from a	79.865	15.650	0.5113377	-25.4	Gee et al (1995)
7	Svalbard	J92:001	granite	80.414	20.325	0.512006	-12.3	Johansson et al. (1999)
8	Svalbard	J92:004	granite	80.414	20.325	0.512003	-12.4	Johansson et al. (1999)
9	Svalbard	27+1	granite			0.512034	-11.8	Johansson et al. (1999)
10	Svalbard	23+2	granite			0.512258	-7.4	Johansson et al. (1999)
11	Svalbard	J92:006	gneiss	80.000	25.680	0.511964	-13.1	Johansson et al. (1999)
12	Svalbard	J92:007	gneiss	80.000	25.680	0.511959	-13.2	Johansson et al. (1999)
13	Svalbard	G92:023	gneiss	79.841	26.718	0.51201	-12.3	Johansson et al. (1999)
14	Svalbard	24+1	porphyry	80.233	19.170	0.51209	-10.7	Johansson et al. (1999)
15	Svalbard	24+2	porphyry	80.211	19.188	0.512106	-10.4	Johansson et al. (1999)
16	Svalbard	25+1	andesite	80.211	19.188	0.512018	-12.1	Johansson et al. (1999)
17	Svalbard	25+2	andesite	80.288	19.066	0.512059	-11.3	Johansson et al. (1999)
18	Svalbard	94046	volcanite	79.598	24.982	0.512093	-10.6	Johansson et al. (1999)
19	Svalbard	J91:001	granite	78.968	16.596	0.511639	-19.5	Johansson & Gee (1999)
20	Svalbard	J91:002	gneiss	78.968	16.596	0.511609	-20.1	Johansson & Gee (1999)
21	Svalbard	J91:003	gneiss	78.915	16.633	0.511508	-22.0	Johansson & Gee (1999)
22	Svalbard	LP91:19	migmatite	79.047	16.610	0.511548	-21.3	Johansson & Gee (1999)
23	Svalbard	J91:004	syenite	78.911	16.540	0.511491	-22.4	Johansson & Gee (1999)
24	Svalbard	94048	granite			0.512024	-12.0	Johansson et al. (2002)
25	Svalbard	28+1	granite			0.512067	-11.1	Johansson et al. (2002)
26	Svalbard	28+4	granite			0.512068	-11.1	Johansson et al. (2002)
27	Svalbard	G92:022	dyke			0.51207	-11.1	Johansson et al. (2002)
28	Svalbard	G94:044	granite			0.512042	-11.6	Johansson et al. (2002)
29	Svalbard	G95:038	syenite			0.512025	-12.0	Johansson et al. (2002)
30	Svalbard	G95:039	granite			0.512099	-10.5	Johansson et al. (2002)
31	Svalbard	G95:040	syenite			0.512071	-11.1	Johansson et al. (2002)
32	Svalbard	8405	pyroxenite			0.511603	-20.2	Bernard-Griffiths et al. (1993)
33	Svalbard	8406	eclogite			0.511589	-20.5	Bernard-Griffiths et al. (1993)
34	Svalbard	8397	metagabbro			0.512622	-0.3	Bernard-Griffiths et al. (1993)
35	Svalbard	8404	metagabbro			0.512873	4.6	Bernard-Griffiths et al. (1993)
36	Svalbard	8399	schist			0.512736	1.9	Bernard-Griffiths et al. (1993)
37	Svalbard	8402	schist			0.51272	1.6	Bernard-Griffiths et al. (1993)
38	Svalbard	8403	metaquartzite			0.512689	1.0	Bernard-Griffiths et al. (1993)
39	Svalbard	WoA	beach deposi	78.963	11.405	0.511732	-17.7	Schmitt (2007)
40	Svalbard	WoF	beach deposi	79.009	11.954	0.511876	-14.9	Schmitt (2007)
41	Svalbard	WoG	beach deposi	79.145	11.595	0.51184	-15.6	Schmitt (2007)
42	Svalbard	WoC	beach deposi	78.276	13.923	0.511987	-12.7	Schmitt (2007)
43	Svalbard	WoD	beach deposi	78.384	14.416	0.511929	-13.8	Schmitt (2007)
44	Svalbard	WoE	beach deposi	78.081	14.003	0.511966	-13.1	Schmitt (2007)
45	Svalbard	Sp03/11	greenschist	77.297	14.423	0.512324	-6.1	Gołuchowska et al. (in preparation)
46	Svalbard	Sp05/11	greenschist	77.280	14.505	0.511930	-13.8	Gołuchowska et al. (in preparation)
47	Svalbard	Sp07/11	greenschist	77.279	14.503	0.512039	-11.7	Gołuchowska et al. (in preparation)
48	Svalbard	Sp08/11	greenschist	77.279	14.500	0.512359	-5.4	Gołuchowska et al. (in preparation)
49	Svalbard	Sp10/11	greenschist	77.279	14.496	0.512030	-11.9	Gołuchowska et al. (in preparation)
50	Svalbard	Sp11/11	greenschist	77.278	14.494	0.511870	-15.0	Gołuchowska et al. (in preparation)
51	Svalbard	Sp26/11	greenstone	77.777	13.911	0.513013	7.3	Gołuchowska et al. (in preparation)
52	Svalbard	Sp31/11B	greenstone	77.808	13.886	0.512930	5.7	Gołuchowska et al. (in preparation)
53	Svalbard	Sp34/11	greenstone	77.806	13.886	0.512941	5.9	Gołuchowska et al. (in preparation)
54	Svalbard	Sp37/11A	greenstone	77.780	13.919	0.513018	7.4	Gołuchowska et al. (in preparation)
55	Svalbard	Sp38/11	greenstone	77.776	13.931	0.512962	6.3	Gołuchowska et al. (in preparation)
56	Svalbard	Sp39/11	greenstone	77.775	13.954	0.512982	6.7	Gołuchowska et al. (in preparation)
57	Svalbard	Sp40/11C	greenstone	77.769	13.940	0.513014	7.3	Gołuchowska et al. (in preparation)
58	Svalbard	Sp46/11	greenstone	77.846	13.659	0.512934	5.8	Gołuchowska et al. (in preparation)
59	Svalbard	Sp57/11	greenstone	77.813	14.060	0.512957	6.2	Gołuchowska et al. (in preparation)

Bernard-Griffiths, J., Peucat, J. J., & Ohta, Y. (1993). Age and nature of protoliths in the Caledonian blueschist-eclogite complex of western Spitsbergen: a combined approach using U Pb, Sm Nd and REE whole-rock systems. Lithos, 30(1), 81-90.

Gee, D. G., Johansson, Å., Ohta, Y., Tebenkov, A. M., Balashov, Y. A., Larionov, A. N., ... & Ryungenen, G. I. (1995). Grenvillian basement and a major unconformity within the Caledonides of Nordaustlandet, Svalbard. Precambrian Research, 70(3), 215-234.

Goluchowska, K., Barker, A.K. , Czerny, J., Manecki, M., Majka, J., Ellam, R., Bazarnik J., (in preparation). The role of crustal contamination in magma evolution; metaigneous Neoproterozoic rocks from SW coast of Svalbard . Contribution to Mineralogy and Petrology

Johansson, Å., & Gee, D. G. (1999). The late Palaeoproterozoic Eskolabreen granitoids of southern Ny Friesland, Svalbard Caledonides-geochemistry, age, and origin. GFF, 121(2), 113-126.

Johansson, Å., Larionov, A. N., Tebenkov, A. M., Gee, D. G., Whitehouse, M. J., & Vestin, J. (1999). Grenvillian magmatism of western and central Nordaustlandet, northeastern Svalbard. Transactions of the Royal Society of Edinburgh: Earth Sciences, 90(03), 221-254.

Johansson, Å., Larionov, A. N., Tebenkov, A. M., Ohta, Y., & Gee, D. G. (2002). Caledonian granites of western and central Nordaustlandet, northeast Svalbard. GFF, 124(3), 135-148.

Schmitt, W. (2007). Application of the Sm-Nd Isotope System to the Late Quaternary Paleoceanography of the Yermak Plateau (Arctic Ocean) (Doctoral dissertation, lmu).

Table A1, Chapter II: CTD, Nd itotope, REE and stable oxygen isotope data

Nr.	Sample ID	Cruise	Station	Year	Month	Day	Longitude [¬E]	Latitude [¬N]	Bot. Depth [m]	Depth [m]	Pressure [dB]	Temperature [°C]
1	VB13/01/05/5	VB13/TDXXI	1	2013	9	5	113.00	77.00	47	5.2	5.2	1.24
2	VB13/01/06/39	VB13/TDXXI	1	2013	9	5	113.00	77.00	47	38.6	39.0	-1.61
3	VB13/03/05/300	VB13/TDXXI	3	2013	9	6	112.80	78.52	363	293.2	296.5	-0.75
4	VB13/03/06/190	VB13/TDXXI	3	2013	9	6	112.80	78.52	363	186.8	188.8	0.18
5	VB13/03/07/3	VB13/TDXXI	3	2013	9	6	112.80	78.52	363	6.3	6.4	0.52
6	VB13/05/08/250	VB13/TDXXI	5	2013	9	7	112.85	77.97	297	243.4	246.1	-0.21
7	VB13/05/09/6	VB13/TDXXI	5	2013	9	7	112.85	77.97	297	6.1	6.1	0.60
8	VB13/07/04/10	VB13/TDXXI	7	2013	9	9	115.99	77.28	62	13.7	13.8	3.43
9	VB13/07/05/50	VB13/TDXXI	7	2013	9	9	115.99	77.28	62	50.8	51.4	-1.69
10	VB13/08/03/5	VB13/TDXXI	8	2013	9	9	115.37	76.27	40	6.5	6.5	4.00
11	VB13/08/04/35	VB13/TDXXI	8	2013	9	9	115.37	76.27	40	35.5	35.9	0.12
12	VB13/09/03/5	VB13/TDXXI	9	2013	9	10	114.51	74.50	37	5.0	5.1	4.74
13	VB13/09/04/33	VB13/TDXXI	9	2013	9	10	114.51	74.50	37	33.3	33.7	-0.42
14	VB13/10/03/5	VB13/TDXXI	10	2013	9	10	114.99	75.52	45	5.1	5.1	4.09
15	VB13/10/04/38	VB13/TDXXI	10	2013	9	10	114.99	75.52	45	33.1	38.7	0.56
16	VB13/12/02/5	VB13/TDXXI	12	2013	9	11	122.50	75.50	49	5.0	5.1	4.40
17	VB13/12/03/45	VB13/TDXXI	12	2013	9	11	122.50	75.50	49	45.0	45.5	-1.34
18	VB13/14/03/5	VB13/TDXXI	14	2013	9	12	135.00	75.50	39	5.1	5.1	3.22
19	VB13/14/04/36	VB13/TDXXI	14	2013	9	12	135.00	75.50	39	35.7	36.1	-1.23
20	VB13/15/04/7	VB13/TDXXI	15	2013	9	13	131.01	77.53	68	7.1	7.1	3.72
21	VB13/15/05/63	VB13/TDXXI	15	2013	9	13	131.01	77.53	68	63.7	64.4	-1.41
22	VB13/16/04/4	VB13/TDXXI	16	2013	9	15	125.99	76.00	47	4.1	4.1	4.25
23	VB13/16/05/41	VB13/TDXXI	16	2013	9	15	125.99	76.00	47	41.5	41.9	-1.11
24	VB13/17/03/4	VB13/TDXXI	17	2013	9	15	125.28	74.71	42	4.0	4.0	3.63
25	VB13/17/04/38	VB13/TDXXI	17	2013	9	15	125.28	74.71	42	38.9	39.3	-1.09
26	VB13/18/03/4	VB13/TDXXI	18	2013	9	16	127.99	74.33	32	4.2	4.2	1.42
27	VB13/18/04/28	VB13/TDXXI	18	2013	9	16	127.99	74.33	32	28.7	29.0	-1.20
28	VB13/19/03/4	VB13/TDXXI	19	2013	9	16	130.99	74.00	21	4.1	4.1	3.96
29	VB13/19/04/17	VB13/TDXXI	19	2013	9	16	130.99	74.00	21	15.5	15.7	-0.02
30	VB13/20/03/4	VB13/TDXXI	20	2013	9	17	130.99	72.50	18	4.9	4.9	3.23
31	VB14/02/1/3	VB14/TDXXII	2	2014	9	14	110.87	78.37	83	74.1	74.6	-1.64
32	VB14/02/1/4	VB14/TDXXII	2	2014	9	14	110.84	78.37	83	6.0	6.1	0.88
33	VB14/02/MUC	VB14/TDXXII	2	2014	9	14	110.84	78.37	83	75.1	75.13	-1.64
34	VB14/04/1/4	VB14/TDXXII	4	2014	9	14	111.81	78.16	325	4.6	4.6	1.42
35	VB14/04/1/6	VB14/TDXXII	4	2014	9	14	111.79	78.16	325	59.3	59.7	-1.42
36	VB14/04/1/7	VB14/TDXXII	4	2014	9	14	111.78	78.16	325	218.1	219.8	-0.79
37	VB14/04/1/8	VB14/TDXXII	4	2014	9	14	111.76	78.16	325	310.7	313.2	-0.89
38	VB14/05/1/4	VB14/TDXXII	5	2014	9	15	113.06	77.95	310	128.0	129.4	-1.63
39	VB14/05/1/5	VB14/TDXXII	5	2014	9	15	113.07	77.95	310	3.8	3.8	-0.24
40	VB14/06/1/3	VB14/TDXXII	6	2014	9	15	115.87	77.28	61	55.1	55.7	-1.45
41	VB14/06/1/4	VB14/TDXXII	6	2014	9	15	115.86	77.29	61	4.5	4.5	1.06
42	VB14/07/1/3	VB14/TDXXII	7	2014	9	15	115.33	76.25	39	33.7	34.1	-0.87
43	VB14/07/1/4	VB14/TDXXII	7	2014	9	16	115.32	76.25	39	3.3	3.3	1.24
44	VB14/08/1/3	VB14/TDXXII	8	2014	9	16	114.50	74.50	37	33.3	33.7	1.02
45	VB14/08/1/4	VB14/TDXXII	8	2014	9	16	114.50	74.50	37	2.4	2.5	3.26
46	VB14/08/MUC	VB14/TDXXII	8	2014	9	16	114.50	74.50	37	36.5	36.8	1.01
47	VB14/11/1/4	VB14/TDXXII	11	2014	9	17	114.98	75.49	43	40.2	40.6	1.11
48	VB14/11/1/5	VB14/TDXXII	11	2014	9	17	114.97	75.48	43	2.6	2.7	3.16
49	VB14/12/1/3	VB14/TDXXII	12	2014	9	18	118.49	75.49	32	27.8	28.1	-0.11
50	VB14/12/1/4	VB14/TDXXII	12	2014	9	18	118.48	75.49	32	2.7	2.8	3.16
51	VB14/13/1/3	VB14/TDXXII	13	2014	9	18	122.50	75.49	50	43.5	43.9	-1.50
52	VB14/13/1/5	VB14/TDXXII	13	2014	9	18	122.49	75.48	50	3.0	3.0	3.76
53	VB14/15/7/3	VB14/TDXXII	15	2014	9	19	126.00	76.01	44	39.7	40.2	-1.75
54	VB14/15/7/4	VB14/TDXXII	15	2014	9	19	126.00	76.01	44	3.1	3.1	4.09
55	VB14/15/MUC	VB14/TDXXII	15	2014	9	19	126.00	76.01	44	41.0	41.5	-1.75
56	VB14/16/1/3	VB14/TDXXII	16	2014	9	19	125.94	76.83	67	62.0	62.7	-1.74
57	VB14/16/1/4	VB14/TDXXII	16	2014	9	19	125.92	76.83	67	3.6	3.6	4.09
58	VB14/17/1/4	VB14/TDXXII	17	2014	9	20	125.92	77.50	222	4.2	4.2	1.61
59	VB14/17/1/5	VB14/TDXXII	17	2014	9	20	125.91	77.50	222	200.0	202.2	1.15
60	VB14/17/1/6	VB14/TDXXII	17	2014	9	20	125.87	77.50	222	52.6	53.2	-1.70
61	VB14/18/1/3	VB14/TDXXII	18	2014	9	22	135.41	75.50	30	27.0	27.3	2.62
62	VB14/18/1/5	VB14/TDXXII	18	2014	9	22	135.41	75.50	30	2.6	2.59	3.23
63	VB14/18/MUC	VB14/TDXXII	18	2014	9	22	135.41	75.50	30	30.4	30.8	-0.70
64	VB14/19/2/4	VB14/TDXXII	19	2014	9	23	130.86	77.49	67	5.2	5.3	2.46
65	VB14/19/2/5	VB14/TDXXII	19	2014	9	23	130.85	77.49	67	60.0	60.6	-1.49
66	VB14/21/1/3	VB14/TDXXII	21	2014	9	23	130.99	75.33	25	22.4	22.6	-1.58
67	VB14/21/1/6	VB14/TDXXII	21	2014	9	23	130.98	75.33	25	2.2	2.2	2.34
68	VB14/23/1/4	VB14/TDXXII	23	2014	9	24	125.97	74.67	33	1.9	1.9	2.42
69	VB14/26/5/2	VB14/TDXXII	26	2014	9	25	130.58	73.50	25	2.8	2.8	2.79
70	VB14/26/5/3	VB14/TDXXII	26	2014	9	25	130.58	73.50	25	21.6	21.8	-1.18
71	TI12/02/05	TI12/TDXX	2	2012	3	27	130.67	73.34	24	5		-0.88
72	TI12/02/20	TI12/TDXX	2	2012	3	27	130.67	73.34	24	20		-1.04
73	TI12/05/05	TI12/TDXX	5	2012	4	4	130.15	71.69	11	5		-0.57
74	TI12/10/03	TI12/TDXX	5	2012	4	19	130.15	71.69	11	3		-0.65
75	TI12/06/02	TI12/TDXX	6	2012	4	10	128.73	73.64	18	2		-0.79
76	TI12/06/17	TI12/TDXX	6	2012	4	10	128.73	73.64	18	17		-1.45
77	TI12/07/02	TI12/TDXX	7	2012	4	12	130.67	73.34	24	2		-0.97
78	TI12/07/20	TI12/TDXX	7	2012	4	12	130.67	73.34	24	20		-1.22

Table A1, Chapter II (continued): CTD, Nd itotope, REE and stable oxygen isotope data

Nr.	Conductivity [mS/cm]	Bottle Salinity [PSU]	Pot. Temp. [°C]	Sigma-theta [kg/m3]	d18O	fa 3 frac	fi 3 frac	fr 3 frac	143/144	Epsilon Nd
1	2.5	29.820	1.24	23.87	-2.05	85.15	3.63	11.22	0.512301	-6.58
2	2.6	33.806	-1.61	27.21	-0.78	97.24	-2.05	4.81	0.512294	-6.70
3	2.7	34.835	-0.76	28.01	0.12	100.01	-0.40	0.40	0.512160	-9.32
4	2.9	34.849	0.17	27.98	0.18	100.01	-0.09	0.08	0.512139	-9.73
5	2.3	27.748	0.52	22.24	-1.85	78.32	11.32	10.36	0.512276	-7.06
6	2.9	34.837	-0.22	27.99	0.14	100.00	-0.27	0.27	0.512169	-9.16
7	2.5	29.210	0.60	23.41	-2.51	83.47	3.08	13.46	0.512294	-6.71
8	3.0	31.929	3.43	25.40	-1.88	91.86	-2.10	10.24	0.512285	-6.88
9	2.7	34.140	-1.69	27.48	-0.44	98.11	-1.26	3.15	0.512265	-7.28
10	2.8	29.504	4.00	23.42	-3.51	85.05	-3.37	18.32	0.512217	-8.21
11	2.8	33.271	0.11	26.70	-1.39	95.90	-3.70	7.80	0.512258	-7.42
12	2.4	23.980	4.74	18.97	-6.49	69.06	-2.13	33.07	0.512135	-9.81
13	2.7	31.200	-0.42	25.06	-1.90	89.52	0.09	10.39	0.512206	-8.42
14	2.4	24.783	4.09	19.66	-5.74	71.18	-0.60	29.42	0.512229	-7.98
15	2.8	33.200	0.56	26.62	-1.47	95.72	-3.91	8.20	0.512237	-7.82
16	2.4	23.208	4.40	18.39	-7.25	67.04	-3.87	36.83	0.511899	-14.41
17	2.7	33.697	-1.34	27.11	-0.65	96.81	-1.00	4.20	0.512067	-11.13
18	1.4	14.450	3.22	11.51	-10.87	40.99	4.15	54.86	0.511884	-14.71
19	2.7	33.232	-1.23	26.73	-1.08	95.57	-1.86	6.29	0.511985	-12.75
20	2.5	26.140	3.72	20.77	-6.10	75.80	-6.87	31.07	0.511924	-13.93
21	2.7	34.294	-1.41	27.60	-0.28	98.51	-0.87	2.36	0.512166	-9.21
22	2.1	20.664	4.25	16.39	-8.70	59.72	-3.72	44.00	0.511841	-15.56
23	2.7	32.857	-1.12	26.42	-1.69	94.74	-4.01	9.26	0.512028	-11.90
24	2.3	24.166	3.63	19.21	-7.54	70.32	-8.46	38.15	0.511829	-15.77
25	2.6	32.643	-1.09	26.25	-2.06	94.28	-5.35	11.07	0.511987	-12.70
26	2.1	23.298	1.42	18.63	-7.62	67.56	-6.17	38.61	0.511820	-15.95
27	2.6	32.698	-1.20	26.29	-1.67	94.22	-3.41	9.19	0.511906	-14.28
28	0.8	6.870	3.96	5.46	-14.76	18.92	6.89	74.19	0.511834	-15.68
29	2.2	25.438	-0.02	20.39	-6.97	74.07	-9.36	35.29	0.511879	-14.80
30	1.1	11.056	3.23	8.81	-13.24	31.51	1.90	66.59	0.511897	-14.46
31	2.7	34.626	-1.64	27.87	-0.02	99.42	-0.49	1.07	0.512197	-8.60
32	2.8	32.371	0.88	25.94	-1.02	92.75	1.18	6.06	0.512240	-7.77
33	2.7	34.597	-1.64	27.85	-0.04	99.34	-0.52	1.18	0.512182	-8.89
34	2.8	32.294	1.42	25.84	-1.01	92.50	1.47	6.03	0.512234	-7.88
35	2.8	34.583	-1.42	27.83	0.02	99.25	-0.15	0.90	0.512198	-8.58
36	2.8	34.785	-0.79	27.97	0.18	99.80	0.11	0.09	0.512161	-9.31
37	2.8	34.802	-0.90	27.99	0.18	99.86	0.04	0.10	0.512155	-9.42
38	2.7	34.617	-1.63	27.86	-0.02	99.39	-0.45	1.07	0.512204	-8.47
39	2.2	25.802	-0.24	20.69	-3.71	73.20	7.30	19.50	0.512315	-6.30
40	2.7	33.935	-1.45	27.31	-0.51	97.49	-1.00	3.51	0.512263	-7.31
41	2.6	29.750	1.06	23.82	-2.31	85.09	2.43	12.48	0.512280	-6.99
42	2.7	32.568	-0.87	26.18	-1.51	93.70	-2.15	8.45	0.512281	-6.96
43	2.6	29.245	1.24	23.41	-2.58	83.63	2.54	13.83	0.512278	-7.03
44	2.9	33.662	1.02	26.97	-2.54	97.88	-11.21	13.33	0.512196	-8.61
45	2.7	28.582	3.26	22.75	-3.53	82.08	-0.55	18.47	0.512230	-7.95
46	2.9	33.663	1.01	26.97	-2.54	97.89	-11.23	13.35	0.512192	-8.70
47	2.9	33.885	1.11	27.14	-1.76	98.11	-7.64	9.53	0.512217	-8.22
48	2.8	30.696	3.16	24.44	-2.53	88.29	-1.76	13.48	0.512235	-7.86
49	2.8	34.174	-0.11	27.44	-1.06	98.61	-4.74	6.13	0.512206	-8.42
50	3.0	32.521	3.16	25.89	-1.37	93.46	-1.22	7.76	0.512253	-7.51
51	2.8	34.792	-1.50	28.00	-0.85	100.48	-5.57	5.10	0.512141	-9.69
52	2.8	30.048	3.76	23.87	-3.62	86.88	-5.70	18.82	0.512048	-11.52
53	2.7	34.669	-1.75	27.91	-0.89	100.10	-5.41	5.30	0.512115	-10.21
54	2.5	26.003	4.09	20.63	-6.64	75.69	-9.36	33.67	0.511952	-13.39
55	2.7	34.598	-1.75	27.85	-0.87	99.86	-5.07	5.21	0.512097	-10.55
56	2.7	34.502	-1.74	27.77	-0.46	99.29	-2.50	3.21	0.512181	-8.91
57	2.8	29.265	4.09	23.22	-4.51	84.90	-8.06	23.16	0.512001	-12.44
58	2.7	31.148	1.61	24.91	-1.80	89.29	0.81	9.90	0.512222	-8.12
59	3.0	34.849	1.14	27.91	0.22	99.99	0.09	-0.08	0.512126	-9.99
60	2.7	34.383	-1.70	27.68	-0.16	98.72	-0.47	1.75	0.512207	-8.41
61	2.1	22.293	2.62	17.78	-8.39	64.79	-7.16	42.37	0.512002	-12.40
62	1.9	19.794	3.23	15.76	-9.38	57.33	-4.67	47.33	0.511986	-12.73
63	2.5	31.243	-0.71	25.10	-3.44	90.62	-8.46	17.83	0.512011	-12.22
64	2.7	29.687	2.46	23.69	-3.83	85.84	-5.67	19.83	0.511982	-12.80
65	2.7	34.370	-1.50	27.66	-0.35	98.80	-1.48	2.69	0.512160	-9.32
66	2.7	33.613	-1.58	27.05	-1.39	97.00	-4.76	7.76	0.511997	-12.50
67	2.4	26.220	2.34	20.93	-6.55	76.34	-9.56	33.22	0.511893	-14.53
68	2.6	28.981	2.42	23.13	-5.39	84.54	-11.97	27.44	0.511959	-13.25
69	2.0	20.823	2.79	16.60	-9.10	60.49	-6.40	45.91	0.511890	-14.60
70	2.7	32.966	-1.18	26.51	-2.01	95.30	-6.15	10.84	0.511900	-14.39
71		16.490			-12.06	48.34	-8.87	60.53	0.511794	-16.46
72		29.338			-4.19	84.94	-6.53	21.59	0.511882	-14.75
73		15.079			-12.67	44.15	-7.70	63.55	0.511775	-16.84
74		7.710			-16.72	22.87	-6.48	83.61	0.511783	-16.68
75		18.400			-11.08	53.90	-9.55	55.66	0.511942	-13.57
76		30.483			-3.91	88.47	-8.66	20.19	0.511804	-16.28
77		17.999			-11.43	52.82	-10.21	57.39	0.511815	-16.05
78		29.711			-4.24	86.18	-8.01	21.83	0.511902	-14.36

Table A1, Chapter II (continued): CTD, Nd itotope, REE and stable oxygen isotope data

Nr.	143/144 [2sig]	Epsilon Nd [2sig]	143/144 repeat	Epsilon Nd repeat	143/144 repeat [2sig]	Epsilon Ndrepeat [2sig]	Y [pmol/kg]	La [pmol/kg]	Ce [pmol/kg]	Pr [pmol/kg]
1	0.000018	0.36					335.06	48.05	21.03	8.20
2	0.000012	0.23					255.88	34.61	5.08	4.91
3	0.000012	0.23					158.32	23.93	6.34	4.41
4	0.000016	0.31					148.90	22.28	6.47	3.75
5	0.000012	0.23					213.62	32.39	19.10	5.41
6	0.000014	0.28					158.11	23.25	6.05	4.25
7	0.000018	0.36					343.42	52.59	23.80	8.89
8	0.000014	0.27					326.05	43.31	14.31	7.33
9	0.000013	0.26					241.56	29.22	4.43	4.30
10	0.000011	0.21					444.72	65.97	39.75	11.38
11	0.000012	0.23					338.13	43.60	12.08	7.42
12	0.000011	0.21					521.22	90.26	63.79	15.74
13	0.000012	0.23					427.78	69.76	19.69	11.46
14	0.000012	0.23					479.94	73.70	44.96	12.59
15	0.000012	0.23					348.27	51.42	16.56	8.32
16	0.000018	0.36					570.23	153.70	101.02	26.97
17	0.000011	0.21					316.99	65.01	19.67	10.57
18	0.000010	0.19					493.53	124.71	80.80	26.60
19	0.000011	0.21					477.72	106.96	21.06	15.72
20	0.000012	0.23					530.97	126.67	64.25	22.87
21	0.000012	0.24					234.57	37.85	7.34	6.65
22	0.000010	0.19					663.27	211.66	164.43	41.78
23	0.000012	0.23					337.02	76.98	12.11	10.83
24	0.000010	0.19					619.11	202.96	155.00	37.45
25	0.000011	0.21					464.87	167.93	43.23	20.68
26	0.000018	0.36					704.75	336.58	285.40	56.29
27	0.000008	0.15					490.41	157.66	73.70	22.78
28	0.000010	0.19					1153.18	517.98	589.84	133.64
29	0.000010	0.19					589.56	232.64	87.54	34.55
30	0.000010	0.19					763.18	267.60	229.97	65.10
31	0.000012	0.23					155.65	24.29	5.95	4.08
32	0.000007	0.14					191.68	30.72	14.98	6.18
33	0.000012	0.23					156.14	29.54	8.24	4.87
34	0.000007	0.14					217.74	32.10	13.67	6.24
35	0.000007	0.14					147.86	22.83	7.01	4.09
36	0.000007	0.14					123.77	18.43	5.25	3.40
37	0.000007	0.14					154.50	22.32	6.09	4.07
38	0.000007	0.14					162.64	25.54	6.36	4.46
39	0.000007	0.14					350.59	58.70	38.86	10.79
40	0.000008	0.16					215.62	28.77	5.23	4.89
41	0.000007	0.14	0.512280	-6.98	0.000023	0.44	273.12	43.29	21.88	8.49
42	0.000012	0.23					306.78	42.16	10.88	7.86
43	0.000007	0.14					329.01	53.56	29.57	9.90
44	0.000007	0.14					581.48	93.72	29.57	15.04
45	0.000016	0.32					428.50	68.79	47.70	12.18
46	0.000016	0.32					557.37	95.41	41.08	15.82
47	0.000009	0.17	0.512218	-8.20	0.000023	0.44	479.72	77.47	22.71	13.08
48	0.000016	0.32					402.54	62.18	34.60	10.69
49	0.000012	0.23					379.32	54.18	19.50	9.08
50	0.000012	0.23					302.93	48.51	20.98	9.00
51	0.000012	0.23					359.90	55.53	18.18	9.36
52	0.000016	0.32					374.91	74.37	41.73	12.58
53	0.000007	0.14					370.02	62.19	16.31	10.31
54	0.000016	0.32					481.59	115.84	65.20	19.43
55	0.000012	0.23					348.78	58.47	18.06	9.22
56	0.000012	0.23					234.73	38.50	7.44	6.24
57	0.000016	0.32					438.06	88.38	47.34	14.94
58	0.000007	0.14	0.512211	-8.32	0.000023	0.44	230.10	35.76	17.19	7.07
59	0.000007	0.14					145.65	21.75	6.14	3.69
60	0.000012	0.23					193.54	36.08	27.20	6.97
61	0.000016	0.32					583.63	114.15	27.36	17.47
62	0.000016	0.32					361.96	66.75	29.72	12.64
63	0.000016	0.32					569.19	114.11	31.17	16.87
64	0.000007	0.14					362.20	74.17	29.15	13.49
65	0.000012	0.23					228.78	38.15	8.11	6.96
66	0.000007	0.14	0.511991	-12.63	0.000023	0.44	424.72	85.31	14.73	12.03
67	0.000016	0.32					442.71	117.83	45.80	18.62
68	0.000016	0.32					518.15	122.75	82.76	20.76
69	0.000016	0.32					456.82	151.30	102.10	24.50
70	0.000016	0.32					444.33	125.52	20.50	15.94
71	0.000007	0.14	0.511805	-16.25	0.000023	0.44	592.31	214.57	133.66	47.85
72	0.000007	0.14					460.37	148.43	48.12	20.88
73	0.000016	0.32					944.93	444.52	364.53	109.30
74	0.000016	0.32					1123.65	523.35	477.59	134.61
75	0.000012	0.23					490.20	239.40	294.72	47.83
76	0.000016	0.32					629.21	239.03	178.05	51.00
77	0.000007	0.14	0.511821	-15.93	0.000023	0.44	611.06	257.63	171.93	54.10
78	0.000012	0.23					473.31	160.52	77.76	24.15

Table A1, Chapter II (continued): CTD, Nd itotope, REE and stable oxygen isotope data

Nr.	Nd	Sm	Eu	Gd	Tb	Dy	Ho	Er	Tm	Yb	Lu
	[pmol/kg]	[pmol/kg]	[pmol/kg]	[pmol/kg]	[pmol/kg]	[pmol/kg]	[pmol/kg]	[pmol/kg]	[pmol/kg]	[pmol/kg]	[pmol/kg]
1	40.26	7.85	1.94	11.08	1.91	14.39	3.97	12.82	1.85	11.59	1.92
2	21.87	4.36	1.19	7.69	1.10	9.52	2.71	8.52	1.20	8.34	1.55
3	18.99	3.62	0.99	5.58	0.91	6.68	1.74	5.42	0.83	5.17	0.84
4	16.92	3.29	0.82	4.86	0.78	6.29	1.59	5.30	0.72	4.59	0.77
5	25.33	4.84	1.21	7.94	1.23	8.54	2.27	7.95	1.08	6.98	1.20
6	20.27	3.29	0.90	5.59	0.91	6.73	1.66	5.64	0.88	5.14	0.91
7	42.70	8.28	2.03	11.92	1.92	14.58	3.84	13.42	1.88	11.13	2.07
8	34.81	7.55	2.08	10.15	1.86	12.95	3.56	11.32	1.57	10.79	1.82
9	21.42	4.76	1.13	7.36	1.11	9.61	2.68	8.87	1.24	8.17	1.44
10	53.11	10.93	2.75	15.30	2.56	18.72	4.86	15.39	2.44	14.62	2.60
11	34.12	6.91	1.92	10.65	1.73	14.13	3.63	12.00	1.79	11.21	1.92
12	75.79	14.49	3.84	19.88	3.22	23.37	5.96	19.67	2.84	18.35	3.35
13	52.56	11.30	2.43	15.84	2.45	19.06	4.93	15.04	2.24	14.38	2.34
14	62.80	12.94	2.86	17.07	2.81	21.35	5.31	18.08	2.43	16.92	2.98
15	38.90	8.01	2.14	11.49	1.87	15.40	3.97	13.29	1.82	12.32	2.10
16	124.18	24.71	5.47	28.34	4.12	29.04	6.97	21.39	3.12	19.68	3.59
17	46.84	9.29	2.45	12.55	2.07	15.35	3.73	11.49	1.77	10.32	1.75
18	125.64	26.09	5.75	30.98	4.37	29.39	6.63	20.31	2.84	18.18	3.21
19	71.26	13.66	3.34	19.64	3.10	22.40	5.44	17.73	2.45	15.10	2.53
20	102.77	21.33	4.35	24.88	3.60	26.10	6.38	20.30	2.82	18.85	3.46
21	28.49	5.96	1.50	8.76	1.46	10.60	2.88	8.55	1.19	8.24	1.30
22	183.83	34.95	7.38	41.57	5.83	38.69	9.04	27.17	3.71	25.22	4.09
23	45.12	9.24	2.21	12.51	1.85	14.21	3.60	11.97	1.63	11.13	1.95
24	160.70	33.13	7.01	35.52	5.01	34.35	8.08	23.51	3.59	22.14	3.92
25	90.66	15.97	3.65	22.45	3.20	21.95	5.13	15.57	2.35	13.96	2.41
26	235.81	41.57	8.31	46.63	6.48	41.68	9.28	27.81	3.92	24.60	4.22
27	97.16	17.90	3.85	22.89	3.24	22.98	5.81	18.02	2.41	16.14	2.81
28	556.12	114.61	22.58	111.00	15.69	92.75	19.87	55.92	7.60	49.95	7.92
29	145.36	27.76	6.13	32.14	4.61	29.63	6.86	21.44	2.94	18.47	3.25
30	296.49	63.41	12.62	65.54	9.08	55.76	12.14	34.77	4.60	30.02	5.42
31	20.07	3.86	1.18	5.79	0.91	7.11	1.77	6.02	0.82	5.58	1.00
32	27.99	6.23	1.24	8.25	1.11	8.17	2.21	7.44	0.99	6.69	1.20
33	21.05	5.04	1.08	6.67	0.91	6.96	1.77	5.80	0.74	5.76	0.95
34	30.17	5.81	1.38	8.78	1.19	9.39	2.31	8.04	1.18	7.21	1.18
35	20.44	4.42	0.85	5.15	0.81	6.47	1.64	5.66	0.74	5.15	0.85
36	15.79	3.60	0.71	4.38	0.63	5.01	1.35	4.45	0.66	4.06	0.76
37	18.56	3.76	1.02	5.26	0.82	6.50	1.62	5.39	0.67	4.79	0.84
38	20.95	4.55	1.07	5.78	0.99	7.25	1.80	5.86	0.92	5.76	0.97
39	51.05	10.33	2.73	14.00	2.29	16.91	4.41	14.22	2.05	13.61	2.33
40	24.87	5.01	1.14	7.58	1.11	8.84	2.39	8.25	1.18	8.06	1.31
41	39.46	9.22	1.88	9.74	1.74	12.52	3.40	10.49	1.54	10.64	1.75
42	35.39	8.30	1.93	10.56	1.64	12.82	3.62	11.42	1.60	11.51	1.98
43	44.69	9.43	2.67	12.72	1.83	15.17	3.82	12.65	1.96	11.61	2.10
44	68.74	14.32	3.62	20.19	3.30	23.70	6.20	20.25	2.87	18.30	3.11
45	55.89	12.17	3.22	16.30	2.74	19.56	4.90	16.33	2.32	14.64	2.58
46	69.05	13.95	3.72	20.62	3.28	22.34	5.85	20.93	2.78	18.67	3.17
47	59.87	11.59	3.07	18.28	2.78	21.65	5.20	17.04	2.53	15.70	2.57
48	52.54	11.06	2.83	16.01	2.32	18.64	4.49	15.18	2.16	14.66	2.42
49	44.28	8.20	2.31	13.83	2.21	16.38	4.22	14.43	1.83	13.13	2.13
50	40.98	7.96	2.08	12.27	1.82	14.62	3.50	10.74	1.59	10.39	1.88
51	45.12	8.88	2.40	13.90	2.10	17.16	4.02	13.24	1.93	12.00	2.03
52	58.65	10.72	2.73	15.28	2.35	17.63	4.45	15.00	1.97	12.38	2.25
53	45.29	9.18	2.34	14.05	2.19	16.08	4.12	13.41	1.85	12.59	2.01
54	86.00	14.40	3.93	22.00	3.23	22.06	5.90	18.49	2.78	15.83	3.02
55	42.74	8.49	2.12	12.92	2.02	15.05	3.95	12.53	1.82	11.73	2.11
56	29.30	4.83	1.41	7.46	1.27	9.91	2.70	8.91	1.36	8.78	1.44
57	71.53	13.61	3.17	17.64	2.81	20.46	4.95	15.71	2.51	15.12	2.60
58	33.45	7.20	1.69	9.23	1.41	10.55	2.81	9.55	1.26	8.56	1.38
59	16.43	3.15	0.80	4.84	0.76	6.13	1.57	5.42	0.67	4.59	0.77
60	31.18	6.56	1.65	8.45	1.37	9.50	2.39	7.64	1.04	6.90	1.15
61	80.11	15.44	3.91	22.94	3.43	24.75	6.07	19.88	2.72	18.00	2.85
62	55.18	12.51	2.93	17.86	2.50	17.17	4.12	13.75	1.93	13.17	2.19
63	79.03	14.33	3.57	21.88	3.14	23.69	6.05	19.45	2.58	17.66	2.86
64	57.07	12.03	2.97	15.37	2.47	16.33	4.47	13.80	2.02	15.03	2.28
65	31.65	6.38	1.50	8.81	1.44	9.90	2.64	8.83	1.26	8.19	1.40
66	54.69	10.04	2.59	15.60	2.26	17.35	4.29	14.52	2.05	13.97	2.36
67	83.80	15.61	3.54	21.87	2.97	20.56	5.34	16.96	2.46	15.43	2.96
68	88.15	17.03	3.95	20.36	3.45	24.62	5.81	18.84	2.56	17.69	2.87
69	108.14	17.92	4.13	23.69	3.18	24.54	5.64	18.78	2.37	18.05	3.21
70	69.39	11.30	2.58	14.97	2.33	17.78	4.73	14.67	2.12	14.36	2.53
71	215.52	44.30	8.55	45.38	6.36	41.04	9.06	27.27	3.90	26.15	4.34
72	85.13	15.19	2.99	19.08	2.89	18.66	4.91	14.84	2.13	13.44	2.41
73	463.55	92.68	17.15	90.98	12.48	75.54	15.35	47.42	6.18	41.84	7.10
74	570.53	116.81	22.08	109.62	14.87	90.78	19.71	55.95	7.88	51.02	8.77
75	190.83	35.65	7.40	36.01	4.86	29.65	6.39	18.00	2.32	16.09	2.56
76	215.34	40.63	8.44	45.68	6.25	39.95	8.93	27.81	3.71	25.16	4.31
77	227.51	46.23	8.79	46.63	6.25	40.68	8.86	25.03	3.71	23.70	3.97
78	100.28	17.12	3.83	22.15	3.22	21.08	5.37	15.47	2.16	14.69	2.53

Table A1, Chapter II: REE standard data

Nr.	Sample ID	Y [pmol/kg]	La [pmol/kg]	Ce [pmol/kg]	Pr [pmol/kg]	Nd [pmol/kg]	Sm [pmol/kg]	Eu [pmol/kg]	Gd [pmol/kg]	Tb [pmol/kg]
1	BATS 15m	132.47	13.67	9.54	2.90	13.49	3.27	0.81	4.55	0.73
2	BATS 15m	142.39	14.37	10.43	3.04	14.79	3.15	0.80	4.63	0.77
3	BATS 15m	136.12	13.96	9.97	2.97	14.14	2.77	0.67	4.34	0.77
4	BATS 15m	133.22	13.58	9.43	2.86	13.86	2.89	0.73	4.47	0.72
5	BATS 15m	141.94	14.50	10.42	3.00	14.39	3.47	0.82	4.93	0.76
6	BATS 15m	147.94	15.23	10.82	3.27	14.73	3.32	0.84	4.59	0.78
7	BATS 15m	139.21	13.97	10.28	3.15	14.04	3.40	0.84	4.43	0.76
8	BATS 15m	129.38	14.48	9.70	2.97	14.48	3.39	0.74	4.65	0.81
9	BATS 15m	121.30	13.62	9.76	2.90	12.90	3.46	0.88	4.40	0.78
10	BATS 15m	128.74	14.17	10.06	3.04	13.48	2.76	0.75	4.65	0.75
11	BATS 15m	126.72	13.88	9.58	2.99	13.83	3.49	0.75	4.68	0.76
12	BATS 15m	130.59	13.85	10.18	3.01	14.63	3.16	0.83	4.85	0.78
13	BATS 15m	124.98	13.46	9.68	2.70	13.80	3.02	0.75	4.02	0.70
14	BATS 15m	125.25	13.59	9.89	3.05	15.12	3.11	0.91	4.22	0.68
15	BATS 15m	121.33	12.58	9.10	2.88	13.64	2.78	0.74	3.99	0.77
16	BATS 15m	134.67	14.09	10.80	2.94	14.40	2.89	0.80	4.67	0.82
17	BATS 15m	137.78	15.01	10.94	3.17	15.05	3.00	0.78	4.83	0.81
18	BATS 15m	135.17	14.81	11.18	3.26	14.82	3.25	0.76	4.87	0.82

Nr.	Sample ID	Dy [pmol/kg]	Ho [pmol/kg]	Er [pmol/kg]	Tm [pmol/kg]	Yb [pmol/kg]	Lu [pmol/kg]
1	BATS 15m	5.66	1.37	4.74	0.63	3.99	0.65
2	BATS 15m	5.67	1.50	4.67	0.65	4.13	0.73
3	BATS 15m	5.51	1.47	4.78	0.61	4.36	0.68
4	BATS 15m	5.72	1.35	4.65	0.64	3.67	0.62
5	BATS 15m	5.90	1.47	4.66	0.69	4.48	0.63
6	BATS 15m	5.94	1.59	4.97	0.68	4.05	0.65
7	BATS 15m	6.29	1.42	4.71	0.69	3.94	0.68
8	BATS 15m	5.50	1.53	4.71	0.59	4.37	0.72
9	BATS 15m	5.64	1.42	4.70	0.61	4.23	0.63
10	BATS 15m	5.41	1.37	4.73	0.65	4.28	0.67
11	BATS 15m	5.48	1.32	4.78	0.70	4.21	0.65
12	BATS 15m	5.42	1.50	5.06	0.71	4.26	0.71
13	BATS 15m	5.32	1.31	4.59	0.68	4.03	0.63
14	BATS 15m	5.36	1.42	4.57	0.56	3.90	0.63
15	BATS 15m	5.29	1.36	4.38	0.62	3.78	0.60
16	BATS 15m	5.82	1.53	4.57	0.70	3.83	0.59
17	BATS 15m	6.07	1.62	4.83	0.71	4.20	0.69
18	BATS 15m	6.20	1.62	5.04	0.76	4.30	0.65

Table A1, Chapter III: CTD and Nd isotope data

Nr	Sample ID	Cruise	Station	Year	Month	Day	Longitude [°E]	Latitude [°N]	Bot. Depth [m]	Depth [m]	Pressure [dB]
1	28/413/5	ARKXXVIII/2	413	2014	6	14	-15.1852	77.772	380	5	5
2	28/413/25	ARKXXVIII/2	413	2014	6	14	-15.1852	77.772	380	25	26
3	28/413/51	ARKXXVIII/2	413	2014	6	14	-15.1852	77.772	380	51	51
4	28/413/100	ARKXXVIII/2	413	2014	6	14	-15.1852	77.772	380	100	101
5	28/413/150	ARKXXVIII/2	413	2014	6	14	-15.1852	77.772	380	150	152
6	28/413/200	ARKXXVIII/2	413	2014	6	14	-15.1852	77.772	380	200	202
7	28/413/320	ARKXXVIII/2	413	2014	6	14	-15.1852	77.772	380	320	324
8	28/417/10	ARKXXVIII/2	417	2014	6	15	-16.0465	77.4262	272	6	6
9	28/417/25	ARKXXVIII/2	417	2014	6	15	-16.0465	77.4262	272	25	26
10	28/417/75	ARKXXVIII/2	417	2014	6	15	-16.0465	77.4262	272	75	76
11	28/417/150	ARKXXVIII/2	417	2014	6	15	-16.0465	77.4262	272	150	152
12	28/417/264	ARKXXVIII/2	417	2014	6	15	-16.0465	77.4262	272	263	266
13	28/435/5	ARKXXVIII/2	435	2014	6	17	-5.7485	78.8325	396	6	6
14	28/435/100	ARKXXVIII/2	435	2014	6	17	-5.7485	78.8325	396	101	102
15	28/435/200	ARKXXVIII/2	435	2014	6	17	-5.7485	78.8325	396	201	203
16	28/435/384	ARKXXVIII/2	435	2014	6	17	-5.7485	78.8325	396	384	388
17	28/448/5	ARKXXVIII/2	448	2014	6	19	-3.2585	78.7218	2256	5	5
18	28/448/100	ARKXXVIII/2	448	2014	6	19	-3.2585	78.7218	2256	100	101
19	28/448/300	ARKXXVIII/2	448	2014	6	19	-3.2585	78.7218	2256	300	304
20	28/448/450	ARKXXVIII/2	448	2014	6	19	-3.2585	78.7218	2256	450	455
21	28/448/550	ARKXXVIII/2	448	2014	6	19	-3.2585	78.7218	2256	550	556
22	28/448/800	ARKXXVIII/2	448	2014	6	19	-3.2585	78.7218	2256	799	810
23	28/448/1800	ARKXXVIII/2	448	2014	6	19	-3.2585	78.7218	2256	1800	1827
24	28/448/2210	ARKXXVIII/2	448	2014	6	19	-3.2585	78.7218	2256	2210	2245
25	28/465/10	ARKXXVIII/2	465	2014	6	23	2.7908	79.1487	5537	11	11
26	28/465/150	ARKXXVIII/2	465	2014	6	23	2.7908	79.1487	5537	151	152
27	28/465/700	ARKXXVIII/2	465	2014	6	23	2.7908	79.1487	5537	701	709
28	28/465/3000	ARKXXVIII/2	465	2014	6	23	2.7908	79.1487	5537	3001	3055
29	28/465/5535	ARKXXVIII/2	465	2014	6	23	2.7908	79.1487	5537	5546	5679
30	28/469/5	ARKXXVIII/2	469	2014	6	24	4.8952	79.1305	1515	5	5
31	28/469/25	ARKXXVIII/2	469	2014	6	24	4.8952	79.1305	1515	25	25
32	28/469/175	ARKXXVIII/2	469	2014	6	24	4.8952	79.1305	1515	175	177
33	28/469/450	ARKXXVIII/2	469	2014	6	24	4.8952	79.1305	1515	450	456
34	28/469/1000	ARKXXVIII/2	469	2014	6	24	4.8952	79.1305	1515	1000	1013
35	28/469/1511	ARKXXVIII/2	469	2014	6	24	4.8952	79.1305	1515	1512	1533
36	28/481/5	ARKXXVIII/2	481	2014	6	27	-2.0145	78.8023	2660	5	5
37	28/481/25	ARKXXVIII/2	481	2014	6	27	-2.0145	78.8023	2660	25	25
38	28/481/300	ARKXXVIII/2	481	2014	6	27	-2.0145	78.8023	2660	300	304
39	28/481/500	ARKXXVIII/2	481	2014	6	27	-2.0145	78.8023	2660	500	506
40	28/481/580	ARKXXVIII/2	481	2014	6	27	-2.0145	78.8023	2660	580	587
41	28/481/1600	ARKXXVIII/2	481	2014	6	27	-2.0145	78.8023	2660	1600	1624
42	28/481/2665	ARKXXVIII/2	481	2014	6	27	-2.0145	78.8023	2660	2665	2711
43	29/11/10	ARKXXIX/2.1	11	2015	7	2	-6.9972	80.376	255	10	11
44	29/11/100	ARKXXIX/2.1	11	2015	7	2	-6.9972	80.376	255	100	102
45	29/11/150	ARKXXIX/2.1	11	2015	7	2	-6.9972	80.376	255	150	152
46	29/11/244	ARKXXIX/2.1	11	2015	7	2	-6.9972	80.376	255	244	247
47	29/16/10	ARKXXIX/2.1	16	2015	7	3	-7.3422	81.2173	1549	10	10
48	29/16/51	ARKXXIX/2.1	16	2015	7	3	-7.3422	81.2173	1549	51	51
49	29/16/100	ARKXXIX/2.1	16	2015	7	3	-7.3422	81.2173	1549	100	102
50	29/16/200	ARKXXIX/2.1	16	2015	7	3	-7.3422	81.2173	1549	200	203
51	29/16/300	ARKXXIX/2.1	16	2015	7	3	-7.3422	81.2173	1549	300	304
52	29/20/36	ARKXXIX/2.1	20	2015	7	5	-8.9315	82.1003	2859	36	36
53	29/20/100	ARKXXIX/2.1	20	2015	7	5	-8.9315	82.1003	2859	100	101
54	29/20/200	ARKXXIX/2.1	20	2015	7	5	-8.9315	82.1003	2859	200	203
55	29/20/300	ARKXXIX/2.1	20	2015	7	5	-8.9315	82.1003	2859	300	304
56	29/24/10	ARKXXIX/2.1	24	2015	7	7	-6.3725	80.9147	1314	10	10
57	29/24/53	ARKXXIX/2.1	24	2015	7	7	-6.3725	80.9147	1314	52	53

Table A1, Chapter III (continued): CTD and Nd isotope data

Nr	Temperature [°C]	Conductivity [mS/cm]	Salinity [PSU]	Pot. Temp. [°C]	Sigma-theta [kg/m3]	O2 [µmol/l]	O2 sat [%]	143/144	Epsilon Nd	143/144 [2sig]	Epsilon Nd [2sig]
1	-1.26	25.50	31.62	-1.26	25.42	381.11	100.19	0.512056	-11.36	0.000012	0.23
2	-1.67	25.33	31.82	-1.67	25.59	375.14	97.64	0.512026	-11.94	0.000006	0.14
3	-1.72	25.55	32.16	-1.72	25.87	370.09	96.41	0.512041	-11.64	0.000016	0.32
4	-1.25	26.96	33.56	-1.26	27.00	338.10	90.09	0.512067	-11.14	0.000012	0.23
5	-0.92	27.65	34.09	-0.92	27.41	325.54	87.85	0.512078	-10.92	0.000005	0.14
6	-0.22	28.49	34.40	-0.23	27.63	312.09	85.99	0.512065	-11.17	0.000005	0.23
7	1.51	30.42	34.90	1.50	27.93	303.73	87.89	0.512053	-11.41	0.000007	0.14
8	-1.16	25.54	31.57	-1.16	25.38	380.04	100.14	0.512052	-11.44	0.000012	0.23
9	-1.27	25.69	31.88	-1.27	25.63	393.44	103.58	0.512040	-11.67	0.000016	0.32
10	-1.68	25.76	32.39	-1.69	26.06	365.01	95.34	0.512088	-10.73	0.000016	0.32
11	-0.96	27.57	34.04	-0.97	27.37	327.00	88.11	0.512072	-11.05	0.000012	0.23
12	1.05	29.88	34.75	1.04	27.84	303.17	86.60	0.512071	-11.06	0.000005	0.23
13	-1.17	25.20	31.12	-1.17	25.01	377.98	99.26	0.512108	-10.35	0.000006	0.14
14	-1.66	26.80	33.78	-1.66	27.19	345.99	91.32	0.512162	-9.28	0.000012	0.23
15	-1.16	27.62	34.29	-1.17	27.58	335.88	90.17	0.512134	-9.83	0.000008	0.14
16	0.75	29.75	34.85	0.73	27.94	307.72	87.26	0.512097	-10.54	0.000004	0.23
17	-1.67	26.71	33.74	-1.67	27.15	349.98	92.30	0.512129	-9.92	0.000007	0.14
18	1.19	29.90	34.73	1.19	27.81	313.69	89.92	0.512095	-10.59	0.000006	0.14
19	2.75	31.62	35.06	2.73	27.96	319.31	95.45	0.512058	-11.32	0.000005	0.14
20	1.79	30.79	34.99	1.77	27.98	317.01	92.44	0.512074	-10.99	0.000005	0.14
21	0.86	29.97	34.91	0.84	27.99	314.32	89.44	0.512104	-10.42	0.000006	0.14
22	0.09	29.40	34.89	0.06	28.02	314.00	87.54	0.512116	-10.17	0.000008	0.14
23	-0.56	29.30	34.92	-0.65	28.08	306.20	83.92	0.512119	-10.12	0.000005	0.23
24	-0.73	29.33	34.92	-0.84	28.09	305.93	83.46	0.512123	-10.04	0.000006	0.23
25	1.84	29.91	34.07	1.84	27.24	357.36	103.70	0.512040	-11.67	0.000008	0.23
26	3.50	32.27	35.11	3.49	27.93	319.39	97.32	0.512045	-11.57	0.000007	0.23
27	0.94	30.15	34.97	0.90	28.03	320.06	91.29	0.512091	-10.68	0.000008	0.14
28	-0.71	29.66	34.93	-0.88	28.09	302.64	82.61	0.512115	-10.20	0.000006	0.14
29	-0.43	30.78	34.93	-0.88	28.09	303.56	83.48	0.512112	-10.26	0.000007	0.14
30	1.25	29.06	33.63	1.25	26.93	361.77	103.09	0.512042	-11.62	0.000006	0.14
31	2.61	31.15	34.79	2.60	27.75	357.71	106.36	0.512035	-11.77	0.000007	0.14
32	2.16	31.05	35.06	2.15	28.01	323.66	95.32	0.512058	-11.31	0.000007	0.14
33	0.22	29.39	34.94	0.20	28.04	321.19	89.88	0.512101	-10.47	0.000004	0.23
34	-0.58	28.93	34.91	-0.62	28.07	317.23	86.88	0.512119	-10.11	0.000006	0.23
35	-0.81	28.96	34.91	-0.88	28.08	305.12	83.05	0.512121	-10.08	0.000006	0.23
36	-1.24	26.70	33.24	-1.24	26.73	385.61	102.56	0.512067	-11.14	0.000006	0.14
37	-0.74	27.52	33.79	-0.74	27.16	369.08	99.87	0.512082	-10.84	0.000005	0.23
38	2.25	31.15	35.02	2.23	27.97	317.85	93.80	0.512077	-10.95	0.000005	0.23
39	1.17	30.25	34.96	1.15	28.00	318.25	91.32	0.512098	-10.53	0.000005	0.14
40	0.66	29.82	34.93	0.63	28.01	317.42	89.86	0.512098	-10.54	0.000005	0.23
41	-0.64	29.14	34.91	-0.72	28.07	311.47	85.16	0.512125	-10.01	0.000006	0.23
42	-0.76	29.48	34.92	-0.91	28.08	303.78	82.80	0.512115	-10.20	0.000006	0.23
43	-1.53	25.07	31.32	-1.53	25.18	398.04	103.65	0.512049	-11.48	0.000019	0.38
44	0.08	28.59	34.26	0.07	27.51	311.88	86.55	0.512033	-11.80	0.000019	0.38
45	0.83	29.59	34.70	0.82	27.81	300.81	85.40	0.512002	-12.40	0.000019	0.38
46	0.62	29.57	34.85	0.61	27.95	304.11	85.95	0.512081	-10.86	0.000019	0.38
47	-1.53	25.15	31.43	-1.53	25.28	394.54	102.80	0.512061	-11.25	0.000019	0.38
48	-1.71	26.05	32.85	-1.72	26.43	360.52	94.39	0.512159	-9.34	0.000019	0.38
49	-1.68	26.78	33.79	-1.69	27.19	351.59	92.73	0.512145	-9.63	0.000019	0.38
50	0.32	29.12	34.63	0.31	27.79	305.27	85.46	0.512091	-10.67	0.000019	0.38
51	1.00	29.92	34.84	0.98	27.92	304.90	87.02	0.512080	-10.89	0.000019	0.38
52	-1.66	26.34	33.19	-1.66	26.71	353.82	92.99	0.512169	-9.15	0.000019	0.38
53	-1.42	27.29	34.20	-1.42	27.52	335.71	89.44	0.512128	-9.94	0.000019	0.38
54	0.70	29.55	34.76	0.69	27.87	302.38	85.59	0.512108	-10.35	0.000019	0.38
55	0.87	29.81	34.84	0.86	27.93	304.87	86.73	0.512083	-10.82	0.000019	0.38
56	0.99	26.30	30.39	0.99	24.34	415.15	114.93	0.512000	-12.45	0.000019	0.38
57	-1.38	26.57	33.20	-1.38	26.70	351.36	93.06	0.512106	-10.37	0.000019	0.38

Table A1, Chapter III (continued): REE data

Nr	Sample ID	Y [pmol/kg]	La [pmol/kg]	Ce [pmol/kg]	Pr [pmol/kg]	Nd [pmol/kg]	Sm [pmol/kg]	Eu [pmol/kg]	Gd [pmol/kg]	Tb [pmol/kg]
1	28/413/5	318.1	56.4	14.9	9.0	41.4	8.2	2.1	11.4	1.8
2	28/413/25	290.8	55.4	17.5	9.0	40.0	7.9	1.9	10.9	1.8
3	28/413/51	293.7	51.3	14.1	8.7	38.8	6.8	1.9	10.7	1.6
4	28/413/100	230.4	36.5	10.0	6.0	28.1	5.7	1.5	8.1	1.2
5	28/413/150	182.9	29.8	8.5	5.1	22.6	4.7	1.1	6.7	0.9
6	28/413/200	161.5	18.5	5.4	3.8	18.1	3.5	1.0	4.9	0.8
7	28/413/320	144.6	19.7	5.8	4.0	18.4	3.7	0.9	4.9	0.7
8	28/417/10	314.9	54.5	13.7	9.1	43.5	7.8	1.9	12.2	1.8
9	28/417/25	302.6	54.1	15.1	9.2	42.2	7.9	2.1	12.2	1.6
10	28/417/75	293.5	49.1	12.9	8.4	39.0	7.7	1.9	10.8	1.6
11	28/417/150	180.1	29.2	8.5	5.2	21.6	4.2	1.0	6.4	0.9
12	28/417/264	158.7	24.9	6.4	4.4	19.7	4.0	1.0	5.7	0.9
13	28/435/5	305.9	49.8	10.8	8.2	38.7	7.7	2.0	10.8	1.7
14	28/435/100	225.4	34.4	9.0	6.1	28.5	5.7	1.5	8.3	1.2
15	28/435/200	172.5	25.7	7.3	4.3	20.4	3.7	1.1	5.8	0.9
16	28/435/384	135.7	20.4	4.7	3.7	17.0	3.9	0.9	4.9	0.7
17	28/448/5	175.9	26.3	7.3	4.4	21.2	4.1	1.1	5.7	0.9
18	28/448/100	160.6	22.1	6.2	4.0	17.5	3.8	0.9	4.8	0.8
19	28/448/300	134.4	19.5	5.7	3.4	15.4	2.8	0.8	4.3	0.7
20	28/448/450	138.1	19.4	5.0	3.3	15.1	3.3	0.7	4.1	0.7
21	28/448/550	135.0	19.5	4.6	3.1	14.9	3.0	0.8	4.1	0.7
22	28/448/800	139.2	19.1	3.8	3.2	14.7	2.6	0.8	4.0	0.7
23	28/448/1800	131.9	18.3	2.8	3.3	15.3	3.0	0.6	4.0	0.6
24	28/448/2210	139.5	20.7	3.0	3.4	15.7	3.0	0.7	3.9	0.6
25	28/465/10	129.3	18.1	5.5	3.4	15.0	3.2	0.7	3.3	0.6
26	28/465/150	136.1	19.2	6.5	3.4	15.9	2.6	0.7	4.5	0.7
27	28/465/700	146.1	22.7	6.0	3.6	15.5	2.8	0.7	5.0	0.7
28	28/465/3000	133.3	19.4	2.7	3.0	15.4	2.5	0.6	3.8	0.6
29	28/465/5535	131.9	19.1	2.5	3.1	15.2	2.8	0.7	3.7	0.7
30	28/469/5	134.0	20.1	5.9	3.4	15.6	3.1	0.8	3.9	0.6
31	28/469/25	130.6	19.7	4.9	3.3	15.2	2.6	0.8	4.0	0.6
32	28/469/175	140.3	20.6	6.3	3.5	16.0	3.0	0.7	4.6	0.6
33	28/469/450	137.6	19.5	4.8	3.3	15.3	2.9	0.8	4.1	0.7
34	28/469/1000	135.2	19.6	4.1	3.3	14.6	2.9	0.7	3.9	0.7
35	28/469/1511	148.0	20.4	3.4	3.3	15.8	3.1	0.7	4.0	0.6
36	28/481/5	150.0	22.5	4.9	3.8	16.9	3.1	0.9	4.6	0.8
37	28/481/25	146.3	21.1	6.3	3.8	16.9	4.2	0.8	4.6	0.8
38	28/481/300	143.3	20.8	5.3	3.5	16.3	2.6	0.7	4.4	0.7
39	28/481/500	139.8	21.0	5.4	3.4	16.0	3.0	0.7	4.3	0.7
40	28/481/580	132.3	19.4	4.8	3.4	15.5	3.2	0.7	4.3	0.7
41	28/481/1600	140.4	19.5	3.6	3.4	14.9	3.0	0.8	4.2	0.7
42	28/481/2665	140.7	21.3	3.3	3.5	15.6	3.2	0.7	4.1	0.7

Table A1, Chapter III (continued): REE data

Nr	Sample ID	Dy [pmol/kg]	Ho [pmol/kg]	Er [pmol/kg]	Tm [pmol/kg]	Yb [pmol/kg]	Lu [pmol/kg]
1	28/413/5	13.1	3.3	10.8	1.6	10.2	1.7
2	28/413/25	12.6	3.2	10.1	1.5	10.0	1.6
3	28/413/51	12.2	3.3	10.0	1.5	9.6	1.6
4	28/413/100	9.1	2.3	7.7	1.1	7.4	1.3
5	28/413/150	7.9	1.9	6.5	0.9	6.2	1.0
6	28/413/200	6.7	1.7	5.6	0.7	5.0	0.9
7	28/413/320	6.1	1.5	4.9	0.7	4.7	0.7
8	28/417/10	13.3	3.3	10.9	1.5	10.6	1.7
9	28/417/25	13.3	3.2	10.6	1.4	10.2	1.7
10	28/417/75	12.3	3.2	10.5	1.4	9.8	1.6
11	28/417/150	7.2	1.8	6.0	0.8	5.2	1.0
12	28/417/264	6.4	1.6	5.3	0.8	5.4	0.9
13	28/435/5	13.1	3.2	10.7	1.5	10.6	1.7
14	28/435/100	9.2	2.4	8.1	1.2	7.3	1.2
15	28/435/200	6.9	1.7	5.5	0.8	5.2	0.8
16	28/435/384	5.6	1.4	5.0	0.7	4.3	0.6
17	28/448/5	7.0	1.7	5.9	0.9	6.1	0.9
18	28/448/100	5.6	1.5	4.8	0.7	5.4	0.8
19	28/448/300	5.2	1.3	4.4	0.6	4.1	0.7
20	28/448/450	5.2	1.3	4.6	0.6	4.2	0.7
21	28/448/550	5.4	1.4	4.5	0.6	4.6	0.7
22	28/448/800	5.4	1.4	4.8	0.7	4.7	0.7
23	28/448/1800	5.1	1.2	4.3	0.6	3.9	0.7
24	28/448/2210	5.4	1.3	4.7	0.6	4.4	0.7
25	28/465/10	4.8	1.2	3.8	0.5	3.8	0.6
26	28/465/150	4.8	1.3	4.7	0.7	4.0	0.6
27	28/465/700	5.7	1.4	4.8	0.6	4.5	0.7
28	28/465/3000	5.0	1.3	4.3	0.6	4.1	0.7
29	28/465/5535	4.8	1.3	4.3	0.7	4.1	0.7
30	28/469/5	5.2	1.3	4.6	0.6	3.8	0.7
31	28/469/25	5.1	1.2	4.1	0.6	3.6	0.6
32	28/469/175	5.2	1.4	4.5	0.6	4.3	0.8
33	28/469/450	5.1	1.4	4.7	0.7	4.2	0.7
34	28/469/1000	4.9	1.3	4.4	0.7	3.9	0.7
35	28/469/1511	5.4	1.3	4.5	0.6	4.1	0.7
36	28/481/5	5.9	1.5	4.9	0.7	4.3	0.7
37	28/481/25	5.6	1.5	4.9	0.7	4.4	0.8
38	28/481/300	5.3	1.4	4.7	0.6	4.1	0.7
39	28/481/500	5.4	1.4	4.7	0.6	4.1	0.6
40	28/481/580	5.2	1.3	4.8	0.7	4.4	0.7
41	28/481/1600	5.1	1.4	4.4	0.6	4.3	0.8
42	28/481/2665	5.5	1.4	4.4	0.7	4.7	0.7

Table A1, Chapter III: REE standard data

Nr	Sample ID	Y [pmol/kg]	La [pmol/kg]	Ce [pmol/kg]	Pr [pmol/kg]	Nd [pmol/kg]	Sm [pmol/kg]	Eu [pmol/kg]	Gd [pmol/kg]	Tb [pmol/kg]
1	BATS15m	132.5	13.7	9.5	2.9	13.5	3.3	0.8	4.6	0.7
2	BATS15m	142.4	14.4	10.4	3.0	14.8	3.2	0.8	4.6	0.8
3	BATS15m	136.1	14.0	10.0	3.0	14.1	2.8	0.7	4.3	0.8
4	BATS15m	133.2	13.6	9.4	2.9	13.9	2.9	0.7	4.5	0.7
5	BATS15m	141.9	14.5	10.4	3.0	14.4	3.5	0.8	4.9	0.8
6	BATS15m	147.9	15.2	10.8	3.3	14.7	3.3	0.8	4.6	0.8
7	BATS15m	139.2	14.0	10.3	3.1	14.0	3.4	0.8	4.4	0.8
8	BATS15m	129.4	14.5	9.7	3.0	14.5	3.4	0.7	4.7	0.8
9	BATS15m	121.3	13.6	9.8	2.9	12.9	3.5	0.9	4.4	0.8
10	BATS15m	128.7	14.2	10.1	3.0	13.5	2.8	0.7	4.7	0.8
11	BATS15m	126.7	13.9	9.6	3.0	13.8	3.5	0.7	4.7	0.8
12	BATS15m	130.6	13.9	10.2	3.0	14.6	3.2	0.8	4.9	0.8
13	BATS15m	125.0	13.5	9.7	2.7	13.8	3.0	0.7	4.0	0.7
14	BATS15m	125.3	13.6	9.9	3.1	15.1	3.1	0.9	4.2	0.7
15	BATS15m	121.3	12.6	9.1	2.9	13.6	2.8	0.7	4.0	0.8

Nr	Sample ID	Dy [pmol/kg]	Ho [pmol/kg]	Er [pmol/kg]	Tm [pmol/kg]	Yb [pmol/kg]	Lu [pmol/kg]
1	BATS15m	5.7	1.4	4.7	0.6	4.1	0.7
2	BATS15m	5.7	1.5	4.7	0.6	4.4	0.7
3	BATS15m	5.5	1.5	4.8	0.6	4.1	0.7
4	BATS15m	5.7	1.3	4.7	0.6	3.7	0.6
5	BATS15m	5.9	1.5	4.7	0.7	4.5	0.6
6	BATS15m	5.9	1.6	5.0	0.7	4.3	0.6
7	BATS15m	6.3	1.4	4.7	0.7	4.4	0.7
8	BATS15m	5.5	1.5	4.7	0.6	4.2	0.7
9	BATS15m	5.6	1.4	4.7	0.6	4.0	0.6
10	BATS15m	5.4	1.4	4.7	0.6	4.2	0.7
11	BATS15m	5.5	1.3	4.8	0.7	4.1	0.6
12	BATS15m	5.4	1.5	5.1	0.7	4.1	0.7
13	BATS15m	5.3	1.3	4.6	0.7	4.2	0.6
14	BATS15m	5.4	1.4	4.6	0.6	4.0	0.6
15	BATS15m	5.3	1.4	4.4	0.6	3.8	0.6